



저작자표시-비영리-변경금지 2.0 대한민국

이용자는 아래의 조건을 따르는 경우에 한하여 자유롭게

- 이 저작물을 복제, 배포, 전송, 전시, 공연 및 방송할 수 있습니다.

다음과 같은 조건을 따라야 합니다:



저작자표시. 귀하는 원저작자를 표시하여야 합니다.



비영리. 귀하는 이 저작물을 영리 목적으로 이용할 수 없습니다.



변경금지. 귀하는 이 저작물을 개작, 변형 또는 가공할 수 없습니다.

- 귀하는, 이 저작물의 재이용이나 배포의 경우, 이 저작물에 적용된 이용허락조건을 명확하게 나타내어야 합니다.
- 저작권자로부터 별도의 허가를 받으면 이러한 조건들은 적용되지 않습니다.

저작권법에 따른 이용자의 권리는 위의 내용에 의하여 영향을 받지 않습니다.

이것은 [이용허락규약\(Legal Code\)](#)을 이해하기 쉽게 요약한 것입니다.

[Disclaimer](#)

A Thesis for the Degree of Doctor of Philosophy in Pharmacy

**Discovery of Bioactive Secondary Metabolites
Produced by Gut Bacteria from
Lepidopteran and Coleopteran Insects**

August 2020

Yern-Hyerk Shin

Natural Products Science Major, College of Pharmacy

Doctoral Course in the Graduate School

Seoul National University

Abstract

Discovery of Bioactive Secondary Metabolites Produced by Gut Bacteria from Lepidopteran and Coleopteran Insects

Yern-Hyerk Shin

Natural Products Science Major

College of Pharmacy

Doctoral Course in the Graduate School

Seoul National University

For the past decades, investigation of natural products has played significant role in drug development. Following the paper in 2020, 23.5% of globally approved drugs have been covered by natural product drugs, which also include botanical drugs and natural product-derived drugs. In addition, synthetic drugs provided their pharmacophore from natural products composed 14.2% of pharmaceutical drugs. In the case of antibacterial and anticancer drugs, the proportions of natural products/natural products-derived drugs were over 55% and 48%, respectively. These high percentages of natural product-based drugs in worldwide validated drugs indicated that discovering unreported natural products still has become a significant part of development of new drugs.

The proportion of natural products produced by bacteria (kingdom: Bacteria) in total compounds from living organisms is smaller than that of other kingdoms such as Plantae (67.4%), Animalia (12.6%), and Fungi (10.0%). However, 47% of bacteria-derived natural products showed bioactivities and 5.7% was reported to be bioactive compounds based on their potent biological activities. These results indicated that investigating bacterial secondary metabolites could be an efficient approach for discovering bioactive natural

products. In addition, William C. Campbell and Satoshi Omura were awarded the 2015 Nobel Prize in Physiology or Medicine for discovering of avermectins, a series of pesticides and drugs from territorial actinobacteria *Streptomyces avermitilis*, which showed the importance of studies on bacterial bioactive small molecules in drug development. Following these reasons, bioactive secondary metabolites of bacteria, mainly insect-associated bacteria, were investigated during my research times.

1. Bombyxamycins A–C and Piceamycin, Cytotoxic Macrocyclic Lactams from the Gut *Streptomyces* sp. of the Silkworm *Bombyx mori*

Bombyxamycins A–C (**1–3**) and piceamycin (**4**) producing bacterial strain, *Streptomyces* sp. SD53, was isolated from a gut of silkworm *Bombyx mori*. Combinational spectroscopic analysis revealed the planar structures of bombyxamycins A–C (**1–3**) and piceamycin (**4**) as 26-membered cyclic macrolactams with polyene features. The absolute configurations of bombyxamycins A–C (**1–3**) and piceamycin (**4**) were determined by multiple-step chemical derivatizations, spectroscopic analysis, chromatographic methods, and computational calculations. Additionally, a new chromatography-based experimental method for determining the configurations of stereogenic centers β to nitrogen atoms in macrolactams was established and successfully applied in this work. The bombyxamycins and piceamycin biosynthetic gene cluster was identified by genomic analysis of the actinobacteria strain. Bombyxamycin A (**1**) and piceamycin (**4**) displayed potent antibacterial activity against human pathogenic Gram-positive and Gram-negative bacteria. Furthermore, piceamycin (**4**) also inhibited growth of silkworm pathogen *Bacillus thuringiensis*. Bombyxamycins A & C (**1** and **3**) and piceamycin (**4**) showed antiproliferative activities against human cancer cell lines.

2. Nicrophorusamides A and B, Antibacterial Chlorinated Cyclic Peptides from the Gut *Microbacterium* sp. of the Carrion Beetle *Nicrophorus concolor*

Nicrophorusamides A and B (**10** and **11**) were obtained during cultivation of a rare actinomycete *Microbacterium* sp. UTG9, which was isolated from the intestine of the carrion beetle *Nicrophorus concolor*. Based on the combinational analysis of their 1D & 2D NMR spectroscopic data, the structures of nicrophorusamides A and B (**10** and **11**) were established as a series of new chlorinated cyclic hexapeptides incorporating nonproteinogenic amino acid units such as 5-chloro-tryptophane and β -hydroxyasparagine. The absolute configurations of the amino acid residues in nicrophorusamide A (**10**) were determined by acid hydrolysis and L- and D- form of 1-fluoro-2,4-dinitrophenyl-5-alanine amide (FDAA) derivatizations followed by chromatographic analysis. In the case of nicrophorusamide B (**11**), the absolute configurations were deduced to be identical to those in nicrophorusamide A (**10**) based on identity between circular dichroism (CD) spectra and the common biosynthetic origin. Nicrophorusamide A (**10**) displayed antibacterial activities against several human pathogenic bacterial strains.

3. Coprisamides C and D, Cinnamic Acid Containing Cyclic Peptides from the Gut *Micromonospora* sp. of Carrion Beetle *Silpha perforata*

Coprisamides C and D (**14** and **15**), unreported cinnamic acid containing non-ribosomal peptides, were discovered from an intestinal *Micromonospora* sp. UTJ3, which was isolated from a gut of carrion beetle *Silpha perforata*. Based on the UV, MS, and NMR spectroscopic data, the planar structures of coprisamides C and D (**14** and **15**) were elucidated as heptacyclic depsipeptides bearing highly modified amino acid units such as β -methylaspartic acid (β -Me-Asp) and 2,3-diaminopropionic acid (2,3-Dap). The absolute configurations of coprisamides C and D (**14** and **15**) were identified by advanced Marfey's method and phenylglycine methyl ester (PGME) derivatization followed by NMR spectroscopic analysis. The biosynthetic gene cluster and pathways were predicted based on

genomic analysis of the whole genome sequence data of the producing strain. Coprisamide C (**14**) exhibited mild growth inhibition activity against human tuberculosis causing bacteria *Mycobacterium tuberculosis* mc² 6230.

Keywords: Actinobacteria, Insect-associated bacteria, Secondary metabolites, Structure determination, Bioactivity, Biosynthesis

Student number: 2014-21975

List of Contents

Abstract	I
List of Contents	V
List of Figures	VII
List of Tables	IX
Introduction	1
Introduction	2
General Experimental Procedures	6
Bombyxamycins A–C and Piceamycin, Cytotoxic Macrocyclic Lactams from the Gut	
<i>Streptomyces</i> sp. of the Silkworm <i>Bombyx mori</i>	7
Results and Discussion	8
Experimental Section	24
Nicrophorusamides A and B, Antibacterial Chlorinated Cyclic Peptides from the Gut	
<i>Microbacterium</i> sp. of the Carrion Beetle <i>Nicrophorus concolor</i>	41
Results and Discussion	42
Experimental Section	49
Coprisamides C and D, Antituberculosis Cinnamic Acid Containing Cyclic Peptides	
from the Gut <i>Micromonospora</i> sp. of the Carrion Beetle <i>Silpha perforata</i>	57
Results and Discussion	58
Experimental Section	67

Summary	73
References	76
Appendix: Supporting Information	82
List of Figures	83
List of Tables	91
Abstract in Korean	182
Publication List	194
Papers	195
Patents	197
Permissions for Republication of the Published Paper in Thesis	198
Acknowledgements	202

List of Figures

Figure 1.	Previously reported secondary metabolites produced by intestinal bacteria of insects.	2
Figure 2.	Key COSY and HMBC correlations for constructing the planar structures of bombyxamycins A–C (1–3) and piceamycin (4).	9
Figure 3.	$\Delta\delta_{S-R}$ values of <i>S</i> - and <i>R</i> -MTPA esters of bombyxamycins A–C (1–3).	10
Figure 4.	Chemical reactions for the identification of the absolute configuration at C-24 of bombyxamycin A (1).	10
Figure 5.	^{13}C NMR spectra of bombyxamycin B (2) in CD_3OD and $\text{CD}_3\text{OD}:\text{CD}_3\text{OH} = 1:1$	12
Figure 6.	Preparing <i>S</i> - and <i>R</i> -PGME amides products from piceamycin (4).	15
Figure 7.	Chromatographic analysis for the determination of the absolute configuration of the β -amino acid unit of piceamycin (4) by PGME derivatization.	17
Figure 8.	Energy-minimized structures of <i>S</i> - and <i>R</i> -PGME amides of 3-amino-2- methylpropanoic acids (6–9).	18
Figure 9.	Comparison of the experimental ECD data of piceamycin (4) with the calculated ECD data.	18
Figure 10.	Biosynthetic gene cluster and pathways for bombyxamycins A–C (1–3) and piceamycin (4).	23
Figure 11.	Chemical structures of nicrophorusamides A and B (10 and 11).	43

Figure 12.	Structure determination of the uncommon amino acid units in microphorusamide A (10) based on COSY and HMBC correlations.	43
Figure 13.	Identification of the amino acid sequence in microphorusamide A (10) based on HMBC and ROESY NMR spectra.	44
Figure 14.	Energy minimized conformations of microphorusamides A and B (10 and 11).	48
Figure 15.	Chemical structures of coprisamides C and D (14 and 15).	59
Figure 16.	Key COSY and HMBC correlations for structural determining of coprisamide C (14).	60
Figure 17.	Determining amino acid sequence of coprisamide C (14) based on HMBC and ROESY correlations.....	62
Figure 18.	Identification of the absolute configuration at C-3 based on the $\Delta\delta_{S-R}$ values in ppm of the <i>S</i> - and <i>R</i> -PGME amides of coprisamide C (14a and 14b).	62
Figure 19.	Dose response curve of coprisamides C and D (14 and 15) against <i>Mycobacterium tuberculosis</i> mc ² 6230.	63
Figure 20.	Biosynthetic gene cluster and pathways for coprisamides C and D (14 and 15).	66

List of Tables

Table 1.	^1H and ^{13}C NMR data for bombyxamycins A and B (1 and 2).	38
Table 2.	^1H and ^{13}C NMR data for bombyxamycin C and piceamycin (3 and 4).	39
Table 3.	Antibacterial activities of bombyxamycins A–C (1–3) and piceamycin (4) against human and silkworm pathogenic strains.	40
Table 4.	Antiproliferative activities of bombyxamycins A–C (1–3) and piceamycin (4) against various human cancer cell lines.	40
Table 5.	^1H and ^{13}C NMR Data for microphorusamides A and B (10 and 11) in DMSO- d_6	55
Table 6.	Inhibitory activities of microphorusamides A and B (10 and 11) against bacterial strains.	56
Table 7.	^1H and ^{13}C NMR spectra data for coprisamides C and D (14 and 15) in DMSO- d_6	72

Introduction

Introduction

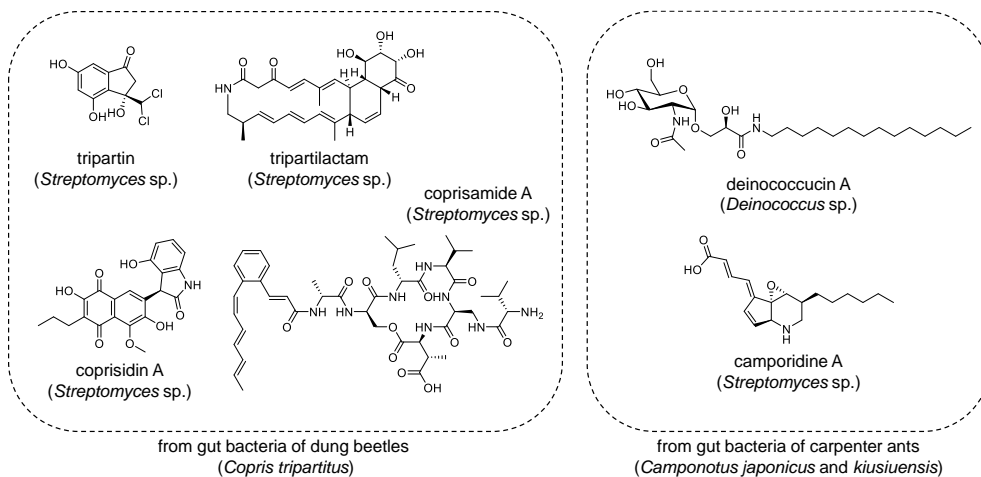


Figure 1. Previously reported secondary metabolites produced by intestinal bacteria of insects.

Insects are the largest animal clade on Earth based on their diversity in species and entire biomass.¹ The total number of their species are estimated to be around 1 million, which means that over half of all reported eukaryotes (~1.8 million) belong to insects.² Insects are also ubiquitous because they are one of the oldest animals on our planet, so they have adapted to a number of different environments for survive. Based on these kinds of diversity, insects could provide exponentially various habitats for their gut bacteria communities increasing their genetic diversity. As a result, investigating secondary metabolites from insect's gut bacteria lead me to discover unprecedented and diverse bioactive small molecules. For example, several kinds of secondary metabolites produced by dung beetles' (*Coprins tripartitus*) gut *Streptomyces* strains have been reported (Figure 1) such as tripartin,³ histone demethylase inhibiting dechlorinated indanone, tripartilactam,⁴ cytotoxic tricyclic macrolactam, coprisidins,⁵ naphthoquinone-oxindole alkaloids, and coprisamides,⁶ branched cyclic heptapeptides. Deinococcucins, which exhibited quinone reductase inducing activity, were

also discovered from a gut *Deinococcus* strain of queen carpenter ants, *Camponotus japonicus* (Figure 1).⁷ Furthermore, another study on intestinal bacteria of other species of carpenter ants, *Camponotus kiusiuensis*, discovered two unreported alkaloids with anti-inflammatory activity, camporidines A and B (Figure 1).⁸

During my research, intestinal bacterial strains were isolated from Coleoptera and Lepidoptera, which are two of the hugest orders among insect. At first, intestinal bacteria of Lepidopteran insects were isolated and chemically investigated. Though Lepidoptera is the second largest order after Coleoptera,⁹ the chemistry of microbes associated with Lepidopteran insects was rarely studied. Only a proteinaceous toxin, identified as an antibiotic modulating the gut microbiota from a symbiotic bacterium, *Enterococcus mundtii*, in the cotton leafworm *Spodoptera littoralis* was discovered in 2017.¹⁰ The silkworm *Bombyx mori*, including its microbiota, is the most heavily studied Lepidopteran insect because of its industrial and medicinal importance.¹¹ The paucity of chemical investigations of microbes in *B. mori* led me to focus on silkworm gut bacteria. In chemical examination of gut microorganisms of *B. mori* larvae, a bacterial strain, *Streptomyces* sp. SD53, was thought to produce a new series of polyene compounds based on their ultraviolet (UV) spectroscopic data and mass spectrometry (MS) data. Large-scale culture of the *Streptomyces* strain and subsequent chromatographic purification allowed the discovery of previously unreported macrocyclic lactams, bombyxamycins A–C, as the first small molecules from Lepidopteran insect-associated microbes. In addition, further investigations based on chemical profiling of the bacterial strain during cultivation in various culture media allowed me to detect additional macrocyclic lactams from the strain SD53. Large-scale cultivation of the strain in a specific medium enabled the production of piceamycin, which was discovered from *Streptomyces* sp. GB4-2 isolated from the mycorrhizosphere of *Picea abies*.¹² Although the planar structure of piceamycin was reported previously, the configurations of its two stereogenic centers remained unassigned. One of the centers is at the β -position of the amide nitrogen and has a branching methyl substituent, and the other is at the junction of the cyclopentenone and

originates from a secondary cyclization after the biosynthesis of the 26-membered macrocycle. In this work, a convenient chromatography-based method to determine the chirality of a carbon possessing a branching methyl group β to the amide nitrogen, which is a motif commonly found in macrolactams prepared from a β -amino acid, was developed and electronic circular dichroism (ECD) calculations were used to elucidate the stereogenic center in the cyclopentenone of piceamycin. The biological evaluation of piceamycin and bombyxamycins A–C in antibacterial and antiproliferative assays were also reported in this paper as well as the predicted post-PKS modification biosynthetic steps leading to bombyxamycin B and piceamycin from bombyxamycins A and C, respectively.

Gut bacteria isolated from Coleopteran insects were also chemically investigated. Especially, carrion beetles (Coleoptera, Silphidae) are ecologically interesting because they utilize vertebrate carrion to rear their offspring.¹³ Carrion beetles are, thus, exposed to carrion-borne bacteria, which may be pathogenic to them during development.¹⁴ Carrion beetles could be classified into two subfamilies, Nicrophorinae and Siphinae.¹⁵ A recent analysis of the gut microbiome of six carrion beetle species belonging to the genus *Nicrophorus* (subfamily Nicrophorinae) indicated that these carrion-feeding beetles harbor gut microbial communities that are distinctively different from those of herbivorous, xylophagous, humivorous, omnivorous, and predatory beetles.¹³ Although that study proposed hypothetical roles of carrion beetles' gut symbionts, such as carcass degradation, detoxification, and defense,¹³ the mechanisms by which carrion beetles defend themselves against entomopathogenic bacteria originating from carrion have not yet been clearly elucidated. In this context, I assumed that the gut symbiotic bacteria of the carrion beetle *Nicrophorus concolor* may be a potential source of antimicrobial compounds. Therefore, the intestinal parts were extracted from a *N. concolor* specimen and the bacterial strains were isolated, targeting chemically prolific actinobacteria. The isolated actinobacterial strains were cultivated and chemically analyzed. During the chemical analysis, a rare actinomycete strain (UTG9) belonging to the genus *Microbacterium* was found to produce a series of previously unreported compounds based

on UV and MS data with a characteristic isotopic pattern corresponding to chlorination. This initial chemical evaluation prompted a large-scale cultivation and deeper chemical investigation by chromatographic purification and spectroscopic analysis of the two major compounds, microphorusamides A and B.

On the other hand, gut bacteria of *Silpha perforata*, a flightless roving carrion beetle species classified as a species of the other subfamily Siphinae¹⁶ were also subjected because microbes associated even in the genus *Silpha* have not been chemically investigated yet as only chemical reports about the genus were defensive steroids produced from rectal glands in *S. novaboracensis* and *S. americana*.^{17, 18} Chemically profiling of gut bacterial isolates of *S. perforata* based on their LC/MS chromatogram data detected the production of unidentified secondary metabolites in the culture of *Micromonospora* sp. UTJ3 strain. Based on the UV spectra of these two compounds and the mass spectrometric data along with accumulated UV library (~2,000 compounds) indicated that they were recognized as undiscovered bacterial small molecules, leading me to further investigation. Finally, large-scale culture, chromatographic purification, and spectroscopic analysis revealed the planar structures of the unknown compounds, coprisamides C and D, which structurally related to coprisamides A and B, which were isolated from the gut bacterium *Streptomyces* sp. SNU533 of the dung beetle *Copris tripartitus*.⁶ Coprisamides bear 2-alkenyl-cinnamic acid unit as an acyl chain and modified amino acids with a distinct branched amino acid chain, indicating an interesting but unreported biosynthetic pathway.

General Experimental Procedures

Optical rotations were measured on a JASCO P-2000 polarimeter with a 1-cm cell at 20 °C and 25 °C. Ultraviolet (UV) spectral data and circular dichroism (CD) data were recorded on an Applied Photophysics ChirscanTM plus circular dichroism detector at 25 °C using a 1-cm quartz cell. Infrared (IR) spectral data were collected on a JASCO FT/IR-4200 FT-IR spectrometer. ¹H, ¹³C, and 2D NMR experiments were conducted by using Bruker Avance III 500 MHz, 600 MHz, 800 MHz, and 850 MHz spectrometers. Low-resolution electrospray ionization mass spectrometry (LR-ESI-MS) and UV chromatogram data were acquired using an Agilent Technologies 6130 quadrupole mass spectrometer coupled with an Agilent Technologies 1200-series HPLC using a reversed-phase C₁₈(2) column (Phenomenex Luna, 5 μm, 100 × 4.6 mm). HR-FAB (fast atom bombardment)-MS data and HR-ESI-MS data were acquired by using a JEOL JMS-700 HR-MS and AB Sciex 5600 QTOF HR-MS, respectively. The NMR spectrometers (500 MHz, 600 MHz, and 850 MHz) and HR-FAB-MS were located at the National Center for Interuniversity Research Facilities (NCIRF) in Seoul National University. The HR-ESI-MS was located at the National Instrumentation Center for Environmental Management (NICEM) in Seoul National University.

**1. Bombyxamycins A–C and Piceamycin, Cytotoxic
Macrocyclic Lactams from the Gut *Streptomyces* sp.
of the Silkworm *Bombyx mori***

1.1. Results and Discussion

Bombyxamycin A (**1**) was isolated as yellow powder. A molecular formula of $C_{27}H_{33}NO_3$ was identified by high-resolution fast atom bombardment mass spectrometry (HR-FAB-MS). Based on the molecular formula, the unsaturation number of **1** was deduced as 12. Combined analysis of 1H and HSQC NMR data of **1** showed the existence of one amide proton (δ_H 7.97) and 17 olefinic methine protons in the downfield region (δ_H 7.45–5.23) (Table 1). One oxygen-bound methine proton (δ_H 4.04), one hydroxy proton (δ_H 4.77), six protons (δ_H 3.46, 2.86, 2.46, 2.31 [2H], and 2.30) belonging to three methylene groups, one aliphatic methine proton (δ_H 3.12), and two methyl group protons (δ_H 1.64 and 0.94) were also identified by 1H and HSQC NMR data. The ^{13}C NMR spectral data (Table 1) revealed that **1** bears two carbonyl carbons (δ_C 199.8 and 166.3), eighteen olefinic carbons (δ_C 140–120), one oxygen-bound carbon (δ_C 68.5), and six aliphatic carbons, including two methyl groups (δ_C 17.9 and 12.5). Based on the NMR and UV spectroscopic data, **1** was deduced to possess a couple of conjugated chromophores with double bonds in its structure.

By interpretation of COSY NMR correlations of **1**, three discrete spin systems were identified. One of the spin systems from C-2 could be successfully traced to C-7 by a series of COSY correlations from H-2 (δ_H 5.55) to H-7 (δ_H 6.41). Consecutive 1H – 1H couplings from H-9 (δ_H 5.52) to H₂-12 (δ_H 2.86 and 2.46) through H-10 (δ_H 2.31) and H-11 (δ_H 4.04) established the C-9–C-10–C-11–C-12 connectivity. The last spin system was assigned based on an array of COSY signals from H-14 (δ_H 6.15) to 25-NH (δ_H 7.97). H₃-2' (δ_H 0.94) was connected to C-24 by H₃-2'/H-24 (δ_H 3.12) COSY correlations.

An HMBC correlation from H-2 to C-1 (δ_C 166.3) established the connectivity between the olefinic carbon C-2 (δ_C 121.3) and the carbonyl carbon C-1. Analysis of HMBC correlations from the methyl protons H₃-1' (δ_H 1.64) to C-7 (δ_C 140.1), C-8 (δ_C 135.1), and C-9 (δ_C 131.4) connected the first and the second spin systems through the fully substituted olefinic carbon C-8. Furthermore, the 2-bond HMBC signals from H₂-12 and H-14 to C-13 (δ_C 199.8) indicated that the carbonyl carbon C-13 was between the second and the third spin systems,

resulting in a pentaenone-bearing structure. Because two carbonyl groups and nine double bonds explained 11 unsaturation equivalents out of 12, **1** was deduced to possess a ring. Finally, a 25-NH/C-1 HMBC correlation established the 26-membered monocyclic structure of **1** (Figure 2a). The double bond geometries in **1** were clarified as 2*Z*, 4*Z*, 6*E*, 14*E*, 16*Z*, 18*Z*, 20*E*, and 22*Z* by measuring $^3J_{\text{HH}}$ values of the olefinic protons (Table 1 and Figure S2). The 8*Z* geometry was established by H-9/H₃-1' NOESY correlation.

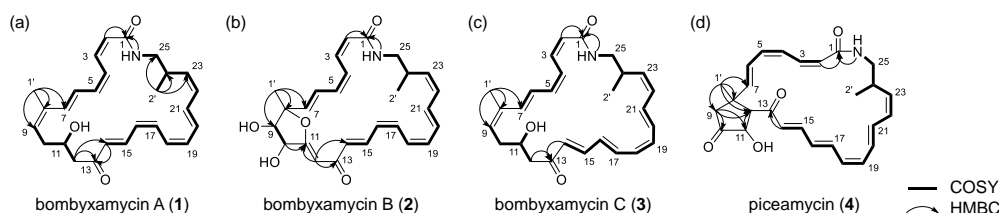


Figure 2. Key COSY and HMBC correlations for constructing the planar structures of (a) bombyxamycin A (**1**), (b) bombyxamycin B (**2**), (c) bombyxamycin C (**3**), and (d) piceamycin (**4**).

The absolute configuration of C-11 of **1** was established by the modified Mosher's method.¹⁹ The secondary alcohol at C-11 was derivatized with *R*- and *S*- α -methoxy-(trifluoromethyl) phenyl acetyl chloride (MTPA-Cl) to yield *S*- and *R*-MTPA esters (**1a** and **1b**) (Figure 3a). $\Delta\delta_{S-R}$ values were calculated by analysis of ^1H and COSY NMR spectra of **1a** and **1b**. The signs of $\Delta\delta_{S-R}$ values were consistently distributed, assigning the 11*R* configuration (Figure 3a).

To determine the absolute configuration of C-24 in **1**, ozonolysis and acid hydrolysis of **1** were conducted (Figure 4).⁴ After the sequential chemical reactions, the desired β -amino acid (3-amino-2-methyl-propanoic acid) was derivatized with Sanger's reagent (1-fluoro-2,4-dinitrobenzene). The product, 3-(2,4-dinitro-phenylamino)-2-methyl-propanoic acid (**5**), was additionally derivatized with *S*- and *R*-phenylglycine methyl ester (PGME) to yield *S*- and *R*-PGME amides of **5** (**5a** and **5b**).²⁰ Discrete analysis of ^1H NMR spectral data of these PGME

products (**5a** and **5b**) enabled the determination of the absolute configuration of **5** as 2*S* based on $\Delta\delta_{S-R}$ values, thus establishing the 24*R* configuration of **1** (Figure 4).

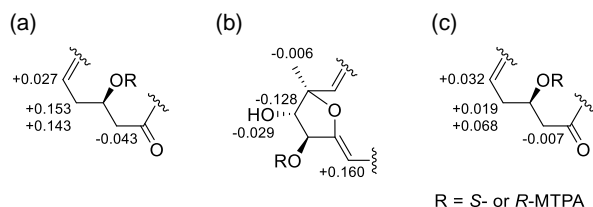


Figure 3. $\Delta\delta_{S-R}$ values of S- and R-MTPA esters of (a) bombyxamycin A (**1**), (b) bombyxamycin B (**2**), and (c) bombyxamycin C (**3**).

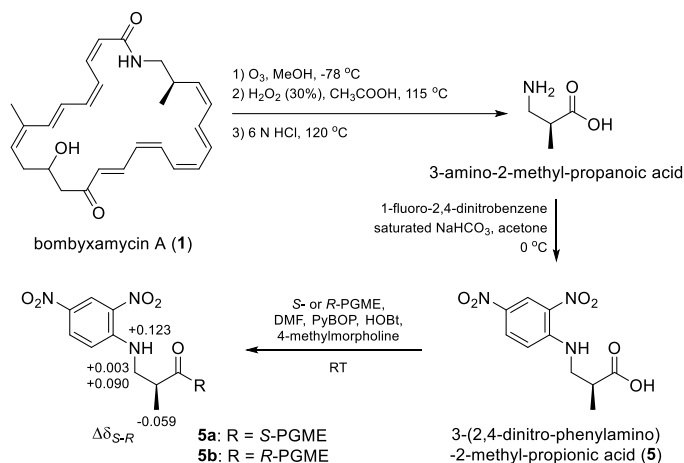


Figure 4. Chemical reactions for the identification of the absolute configuration at C-24 of bombyxamycin A (**1**). $\Delta\delta_{S-R}$ values in ppm are noted for **5a** and **5b**.

Bombyxamycin B (**2**) was obtained as pale-yellow powder by consecutive chromatographic isolation. The molecular formula of **2** could be assigned as $\text{C}_{27}\text{H}_{31}\text{NO}_5$ with an unsaturation number of 13 by using HR-FAB-MS data. Analysis of 1D and 2D NMR data of **2** (Table 1) revealed that it possesses two carbonyl carbons, nine double bonds, three oxygen-bearing sp^3 carbons, and four aliphatic carbons, including two methyl groups. Because **2** has one more unsaturation equivalent than and the same numbers of carbonyl carbons and double bonds as

1, it was deduced that **2** must bear an additional ring. Examination of the COSY NMR spectrum elucidated the two polyene spin systems (C-1 to C-7 and C-14 to 25-NH) that were consistently found in **1** (Figure 2b). The other spin system was composed of two oxygen-bearing methine groups, and two hydroxyl groups were identified by H-9/H-10, H-9/9-OH, and H-10/10-OH COSY correlations. The HMBC correlation signals from H₃-1' to C-7, C-8, and C-9 demonstrated C-7–C-8–C-9 connectivity. In addition, ¹H–¹³C correlations from H-10 to C-11 and from H-12 to C-11, C-13, and C-14 allowed for the construction of a long polyketide chain from C-1 to 25-NH. As shown in **1**, a 26-membered ring structure of **2** could be secured by HMBC correlation between 25-NH and C-1 (Figure 2b).

The planar structure of **2** was then proposed by connecting the last oxygen-bearing *sp*³ carbon, C-8 (δ_{C} 89.1), and the fully substituted, highly deshielded olefinic carbon C-11 (δ_{C} 167.6) through an ether linkage to make one more ring based on the molecular formula even though HMBC correlations indicating the five-membered ether ring could not be observed because C-8 and C-11 do not have a proton (Figure 2b). However, the ether bond was further supported by ¹³C NMR experiments for **2** in CD₃OD and a 1:1 mixture of CD₃OD–CD₃OH (Figure 5). Carbon signals that are located at the β -position of exchangeable protons are doubled or broadened in a 1:1 mixture of CD₃OD and CD₃OH by a β -isotope effect.²¹ The carbon peaks of C-9 and C-10 of **2** were broadened, whereas C-8 and C-11 peaks were not affected by the mixed solvent, indicating that C-8 and C-11 are oxygen bearing but not bound to –OH (Figure 5). This result strongly supported the elucidated structure of **2**.

The relative configuration of the tetrahydrofuran (THF) moiety was assigned by analysis of NOESY NMR data. H-7/H-9, and H₃-1'/H-10 NOESY correlations indicated that H-7 and H-9 are in the same phase. In contrast, H₃-1' displayed a NOESY correlation with H-10, indicating that these protons are on the other side of the molecule. Therefore, the relative configurations of the THF in **2** were established as 8*R**, 9*S**, and 10*S**. The geometries of the double bonds were assigned mainly by ¹H–¹H coupling constants (Table 1 and Figure S16). The H-12/H-10 NOESY correlation allowed for the 12*Z* configuration (Figure S56).

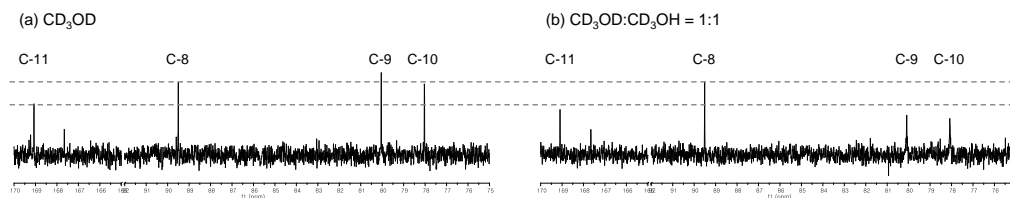


Figure 5. ^{13}C NMR spectra of bombyxamycin B (**2**) in (a) CD_3OD and (b) $\text{CD}_3\text{OD}:\text{CD}_3\text{OH} = 1:1$.

The absolute configurations at C-8, C-9, and C-10 of **2** were determined by the application of the modified Mosher's method.¹⁹ With a short derivatization time (5 min) and using *R*- and *S*-MTPA-Cl, mono-*S*- and *R*-MTPA esters of **2** (**2a** and **2b**) were predominantly obtained rather than bis-MTPA esters. Analysis of ^1H and COSY NMR spectral data of **2a** and **2b** revealed that 10-OH in **2** was esterified. Calculation of $\Delta\delta_{S-R}$ values enabled the determination of the 10*S* configuration. Based on the relative configurations, the absolute configurations of C-8 and C-9 were assigned as 8*R* and 9*S* (Figure 3b). The absolute configuration of C-24 was determined as *R* by the same procedure mentioned above for **1**.

Bombyxamycin C (**3**), purified as a dark yellow powder, was found to have a formula of $\text{C}_{27}\text{H}_{33}\text{NO}_3$, corresponding to 12 degrees of unsaturation, by HR-FAB-MS. Analysis of its ^1H and HSQC NMR spectroscopic data (Table 2) indicated that **3** possessed one amide proton (δ_{H} 7.71), 17 olefinic protons (δ_{H} 7.00–5.19), and one carbinol proton (δ_{H} 4.09) in the deshielded region. In addition, six methylene protons (δ_{H} 3.36, 3.08, 2.74, 2.19 (2H), and 2.18), one aliphatic methine proton (δ_{H} 2.71), and two methyl groups (δ_{H} 1.49 and 0.96) were identified in the shielded region. Interpretation of the ^{13}C and HSQC NMR spectra of **3** indicated the presence of two carbonyl carbons (δ_{C} 199.1 and 165.9) and 18 olefinic methine carbons (δ_{C} 144.3, 140.3, 137.8, 136.6, 135.7, 134.6, 133.3, 132.3, 132.3, 131.2, 130.6, 130.5, 129.7, 127.5, 127.0, 124.4, 123.3, and 120.9) in the structure. In addition, one oxygen-bound carbon (δ_{C} 67.3) and six aliphatic carbons (δ_{C} 44.0, 43.0, 34.4, 33.7, 17.7, and 12.3) were identified (Table 2). Initial analysis of its 1D and HSQC NMR spectra suggested that

bombyxamycin C (**3**) should possess two carbonyl groups and nine double bonds, explaining 11 out of the 12 unsaturations inherent in the molecular formula. Therefore, **3** must have one ring.

The discrete spin systems were elucidated by analysis of the COSY NMR correlations. Consecutive COSY correlations of the olefinic methine protons, from H-2 (δ_{H} 5.58) to H-7 (δ_{H} 6.50), revealed the connectivity from C-2 (δ_{C} 123.3) to C-7 (δ_{C} 140.3). Another spin system (C-9–C-12 linkage) was constructed via three-bond ^1H – ^1H couplings among H-9 (δ_{H} 5.84), H₂-10 (δ_{H} 2.19), H-11 (δ_{H} 4.09), and H₂-12 (δ_{H} 3.08 and 2.18). A long spin system from H-14 (δ_{H} 5.99) to 25-NH (δ_{H} 7.71) was established based on the COSY signals of the protons belonging to this system. CH₃-2' could be assigned at C-24 by the ^1H – ^1H COSY correlation between H₃-2' (δ_{H} 0.96) and H-24 (δ_{H} 2.71). An HMBC correlation between H-2 and the amide carbon C-1 (δ_{C} 165.9) indicated that C-1 is adjacent to C-2. ^1H – ^{13}C HMBC signals from H-1' (δ_{H} 1.49) to C-7, C-8 (δ_{C} 135.7), and C-9 (δ_{C} 129.7) connected the first and the second spin systems, forming the tetraenone chromophore of **3**. This partial structure could be combined with the long spin system bearing the pentaene through the C-13 ketone carbon based on the HMBC correlations from H₂-12 and H-14 to C-13 (δ_{C} 199.1). Furthermore, the 25-NH/C-1 ^1H – ^{13}C correlation connected 25-NH to C-1, generating the 26-membered macrocyclic structure of **3** (Figure 2c). The geometries of the double bonds in bombyxamycin C (**3**) could be assigned as 2*Z*, 4*Z*, 6*E*, 14*E*, 16*E*, 18*Z*, 20*E*, and 22*Z* from the $^3J_{\text{HH}}$ values between olefinic protons (Table 2). In addition, the NOESY correlation between H₃-1' and H-9 enabled the identification of the 8*Z* geometry.

Bombyxamycin C (**3**) has two stereogenic centers: C-11 bearing a secondary alcohol and C-24 at the β -position of the amide nitrogen. The secondary hydroxy group at C-11 was esterified with *R*- and *S*-MTPA-Cl, yielding *S*- and *R*-MTPA esters of **3** (**3a** and **3b**), respectively. Detailed analyses of the ^1H and COSY NMR spectra of **3a** and **3b** confirmed that the absolute configuration at C-11 was *R* based on the distribution of the signs of the $\Delta\delta_{\text{S}}$ *R* values by the modified Mosher's method (Figure 3c).¹⁹

During the cultivation of *Streptomyces* sp. SD53 in YPM medium, a metabolite with a polyene UV signature (λ_{max} values of 296 and 410 nm), which is unlike those of bombyxamycins A–C (**1–3**), was detected by LC/MS analysis. Subsequent chromatographic separation yielded a pure orange powder, enabling spectroscopic analysis of the metabolite (**4**). The molecular formula of **4** was identified as $\text{C}_{27}\text{H}_{29}\text{NO}_4$, corresponding to 14 double bond equivalents, by HR-FAB-MS data. The planar structure of **4** was deduced as that of piceamycin, which was previously reported from *Streptomyces* sp. GB 4-2 isolated from the mycorrhizosphere of *Picea abies*, by comparing its ^1H and ^{13}C NMR chemical shifts in $\text{DMSO}-d_6$ (Table 2) with those in the literature.¹² Its was further confirmed to be piceamycin by COSY, HSQC, and HMBC spectroscopic analyses (Figure 2d). Careful comparison of the NMR data of **4** with the literature data of piceamycin revealed that the chemical shifts and coupling constants of the methylene protons at C-9 must be revised. In the original report, $\text{H}_2\text{-9}$ was assigned as δ_{H} 2.42 (d, $J = 5.53$ Hz). However, if the methylene protons are magnetically equivalent, these protons should appear as a singlet because this methylene group is flanked by a ketone group and an aliphatic quaternary carbon. In fact, these two protons are not magnetically equivalent and should be considered separate signals at δ_{H} 2.43 and 2.39 with 19.0 Hz geminal coupling (Table 2), which is characteristic of a five-membered ring.

The two stereogenic centers of piceamycin (**4**) remain unassigned, prompting me to take on this challenge. Indeed, the stereogenic center at the β -position of the amide nitrogen is derived from the β -amino acid starting material (3-amino-2-methylpropanoic acid) and is a common motif to all macrocyclic lactams in this class, as shown in cyclamenol A,²² macrotermycins A–D,²³ sceliphrolactam,²⁴ niizalactam C,²⁵ and vicienistatin.²⁶ However, the absolute configurations of the chiral carbons at this position can be either *R* or *S* depending on the natural product, indicating that L-glutamic acid is being converted to 3-amino-2-methylpropanoic acid stereo-selectively by an unknown mechanism in the biosynthesis of the starting material. The unambiguous determination of this β -amino acid starting material-

derived stereogenic center has been time consuming and inefficient as a total synthesis or at least a 4-step degradation process of a macrocyclic lactam followed by product purification and ^1H NMR spectroscopic analysis were required.⁴

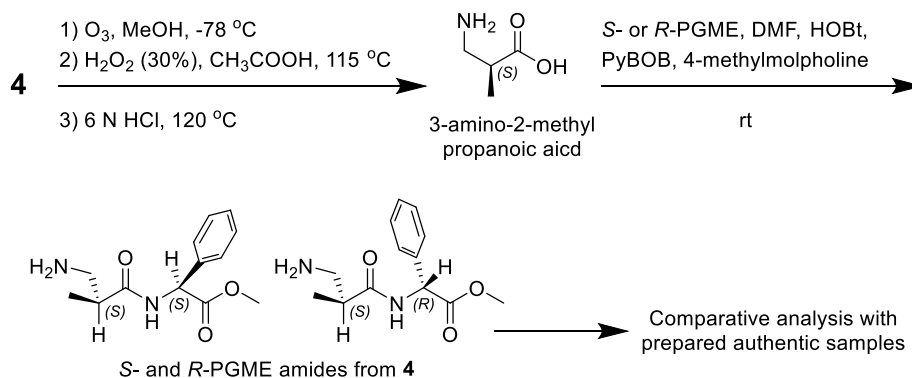


Figure 6. Preparing *S*- and *R*-PGME amides products from piceamycin (**4**).

Therefore, a new method for elucidating this common but problematic stereogenic center by combining simple chemical derivatization and chromatographic analysis without preparative purification and ^1H NMR spectroscopic analysis of the products (Figure 6) was developed. First, to obtain a β -amino acid unit bearing the C-24 stereogenic center, piceamycin (**4**) was sequentially subjected to ozonolysis and acid hydrolysis. Then, portions of the hydrolysate were separately derivatized with *S*- or *R*-phenylglycine methyl ester (PGME).²⁰ The *S*- and *R*-PGME products were analyzed via LC/MS, and their retention times were compared with those of the PGME amides (**6–9**) prepared with authentic 2*S*- and 2*R*-3-amino-2-methylpropanoic acids (Figure 7). The *S*-PGME adduct (**6**) of 2*S*-3-amino-2-methylpropanoic acid eluted later (8.3 min) than the *R*-PGME derivative (**7**) (6.4 min) (Figure 7). LC/MS analysis of the PGME adducts of 2*R*-3-amino-2-methylpropanoic acid showed that its *R*-PGME adduct (**9**) eluted later than the *S*-PGME derivative (**8**), as expected. The elution order could be deduced based on the conformations determined by density functional theory (DFT) calculations (Figure 8). The *S–S* (or *R–R*) PGME amide has a hydrophobic

methyl group from the β -amino acid and the phenyl group of PGME on the same side, which allows the formation of more hydrophobic interaction with the reversed-phase stationary phase, resulting in a higher retention time (Figures 7a and 7b). On the other hand, these hydrophobic functional groups are oriented in opposite directions in the *S*–*R* (or *R*–*S*) PGME amide, resulting in weaker interactions with the reversed-phase stationary phase and thus faster elution (Figures 7a and 7b). The PGME derivatives originating from **4** showed retention times consistent with those of the PGME amides of 2*S*-3-amino-2-methylpropanoic acid (Figure 7c), confirming the absolute configuration of 3-amino-2-methylpropanoic acid derived from piceamycin (**4**) as 2*S* and thus 24*R* in **4**. This convenient procedure provides an empirical rule: if the *S*-PGME amide of the 3-amino-2-methylpropanoic acid unit derived from a macrocyclic lactam elutes slower than its *R*-PGME amide, this β -amino acid must possess a 2*S*-configuration. Conversely, the 2*R* configuration can be assigned when the *R*-PGME amide elutes later than its *S*-PGME adduct. This method was also conducted with a small quantity of piceamycin (**4**, 0.2 mg), which provided the identical experimental results, indicating its validity on the 0.2 mg scale (Figure S65). The absolute configuration of the asymmetric carbon at C-24 of **3** was also determined as *R* by the same three-step reaction followed by LC/MS analysis as used for **4**, and this process did not require NMR experiments. As a proof of the versatility of the method developed in this work, this chiral center was successfully established using only 1 mg of **3**.

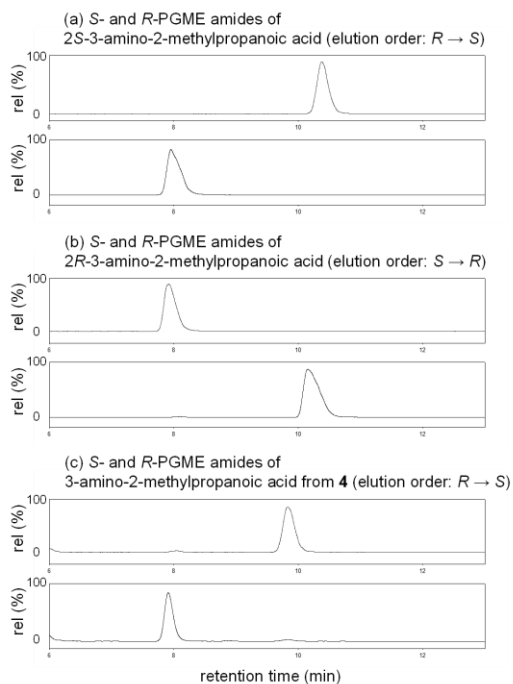


Figure 7. Chromatographic analysis for the determination of the absolute configuration of the β -amino acid unit (3-amino-2-methylpropanoic acid) of **4** by PGME derivatization. LC/MS chromatograms of the *S*- and *R*-PGME derivatives of (a) 2*S*-3-amino-2-methylpropanoic acid (**6** and **8**), (b) 2*R*-3-amino-2-methylpropanoic acid (**7** and **9**), and (c) 3-amino-2-methylpropanoic acid from **4** (Phenomenex, Luna, C₁₈(2), 100 × 4.6 mm; 10%–25% CH₃CN–H₂O over 30 min with 0.1% formic acid; flow rate: 0.7 mL/min; ion extraction for [M + H]⁺ *m/z* at 251).

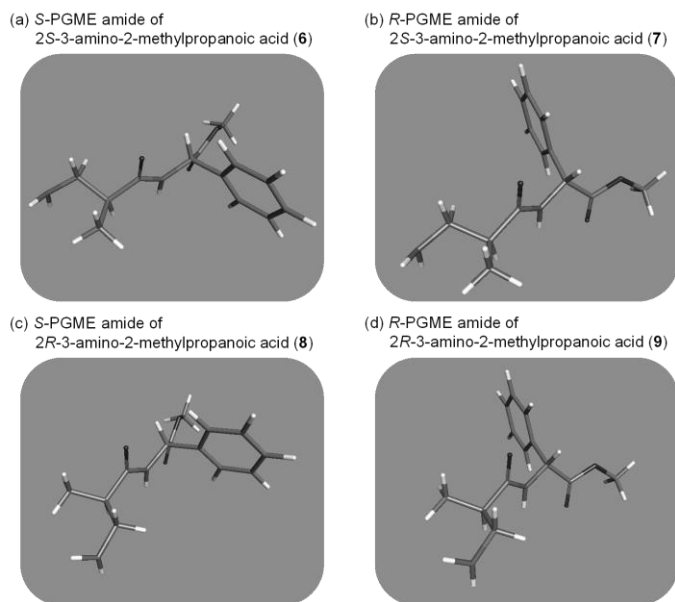


Figure 8. Energy-minimized structures of *S*- and *R*-PGME amides of 3-amino-2-methylpropanoic acids (**6–9**).

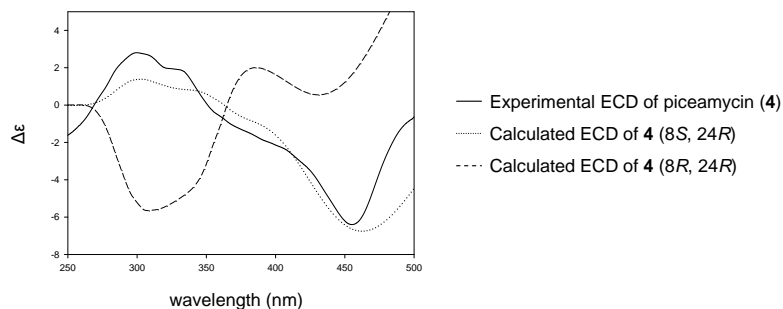


Figure 9. Comparison of the experimental ECD data of piceamycin (**4**) with the calculated ECD data; solid line: experimental ECD data; dotted line: calculated ECD data (8*S*, 24*R*); dashed line: calculated ECD data (8*R*, 24*R*).

The other asymmetric carbon in piceamycin (**4**) is the unprotonated C-8 moiety of the cyclopentenone. Because chemical derivatization of this chiral center for stereochemical analysis is not possible, electronic circular dichroism (ECD) calculations were utilized.²⁷ Three-dimensional models of two possible diastereomers of **4** (8*S*/24*R* and 8*R*/24*R*) were

constructed, and ECD calculations were conducted for each diastereomer. The experimental ECD spectrum of **4** showed a positive Cotton effect at 300 nm and a negative Cotton effect at 455 nm. The calculated spectrum of the 8*S*,24*R* diastereomer was similar to the ECD spectrum calculated for that diastereomer (positive Cotton effect at 305 nm and negative Cotton effect at 460 nm) (Figure 9), indicating that the configuration of C-8 of **4** is 8*S*.

Compounds **1–4** were biologically evaluated for antibacterial activity (Table 3) against several human pathogenic bacterial strains (*Staphylococcus aureus* ATCC 25923, *Enterococcus faecalis* ATCC 19433, *Enterococcus faecium* ATCC 19434, *Proteus hauseri* NBRC 3851, *Klebsiella pneumoniae* ATCC 10031, *Salmonella enterica* ATCC 14028, and *Escherichia coli* ATCC 25922) and silkworm pathogenic bacterial strain *Bacillus thuringiensis* KACC 10168. Bombyxamycin A (**1**) showed significant inhibitory activity against *P. hauseri* (MIC = 0.5 µg/mL) and *S. enterica* (MIC = 1 µg/mL) and *S. aureus* (MIC = 8 µg/mL), whereas bombyxamycin B (**2**) moderately inhibited only *S. aureus* (MIC = 64 µg/mL). Bombyxamycin C (**3**) exhibited only weak activity against Gram-negative pathogens *P. hauseri* and *S. enterica* with an MIC value of 128 µg/mL, and Gram-positive pathogen *E. faecium* (MIC = 128 µg/mL) but did not suppress the growth of *S. aureus* and *E. faecalis*. Piceamycin (**4**), which was previously reported inactive against Gram-negative bacteria,¹² displayed potent activity against Gram-negative pathogens *P. hauseri* NBRC 3851 (MIC = 0.025 µg/mL) and *S. enterica* ATCC 14028 (MIC = 0.083 µg/mL). Piceamycin also inhibited Gram-positive pathogenic bacteria *S. aureus* ATCC 25923, *E. faecalis* ATCC 19433, and *E. faecium* ATCC 19434 (MIC = 0.025–32 µg/mL). In addition, piceamycin (**4**) strongly inhibited *B. thuringiensis* KACC 10168 with an MIC value of 3.2 µg/mL, whereas bombyxamycin C (**3**) displayed weak activity (MIC = 380 µg/mL). Bombyxamycin A (**1**) showed even weaker inhibitory activity (MIC = 2.1 mg/mL). These results indicated the additional cyclization in piceamycin (**1**) play a significant role in their antibacterial activity mechanism.

The antiproliferation activities of **1–4** were also evaluated in a panel of human cancer cell lines representing lung cancer (A549), colon cancer (HCT116), stomach cancer (SNU638), liver cancer (SK-HEP-1), breast cancer (MDA-MB-231), and leukemia (K562) (Table 4). Bombyxamycin A (**1**) displayed remarkable antiproliferation activities against most of the tested cancer cell lines (IC_{50} = 0.93–4.20 μ M). However, **2** exhibited weak activity against only K562 cells, with an IC_{50} value of 82.93 μ M. Bombyxamycin C (**3**) also inhibited the proliferation of the tested cancer cells (IC_{50} = 0.78–1.87 μ M). Piceamycin (**4**) exhibited potent cytotoxicity comparable to that of the positive control (etoposide) against these cancer cell lines, with IC_{50} values between 0.22 and 0.74 μ M.

Bombyxamycins A–C and piceamycin exhibited no significant inhibitory effect ($MIC \geq 128$ μ g/mL) against the tested pathogenic fungi (*Candida albicans* ATCC 10231, *Aspergillus fumigatus* HIC 6094, *Trichophyton rubrum* NBRC 9185, and *Trichophyton mentagrophytes* IFM 40996).

Approximately 8.1 Mb of draft genome sequence was obtained from the bombyxamycin producer strain *Streptomyces* sp. SD53. Analysis of the sequences with antiSMASH 4.0²⁸ revealed that the bombyxamycin biosynthetic gene clusters (GenBank accession No. MK433001) contained six genes encoding polyketide synthases (PKSs), eight characteristic enzymes involved in β -amino acid synthesis, and several putative post-PKS tailoring enzymes (Figure 10a and Table S8). The core macrolactam ring of bombyxamycin is biosynthesized by a type I modular PKS, BomP1–BomP6, which comprises a loading and 11 elongation modules. These modules are consistent with the 26-membered structure of **1** except for the presence of the ketoreductase (KR) domain in module 6. However, a detailed sequence analysis of the modules revealed that the ketoreductase domain in module 6 is nonfunctional due to the absence of the highly conserved KR active site motif and an NADP(H) binding motif, which explains the ketone group at C-13 (Figure S67).²⁹ In addition, the KR domain of module 7 is an A-type KR, which contains a conserved tryptophan residue (“W” motif) instead of the LDD motif in B-type KRs (Figure S67).³⁰ This sequence analysis

is consistent with the chemically determined 11*R* configuration of **1**. A β -amino acid starter unit (3-amino-2-methyl-propanoic acid) is predicted to be synthesized from glutamic acid by glutamate mutase BomG/BomH, decarboxylase BomI, acyl carrier protein (ACP) BomD, two ATP-dependent ligases (BomE and BomJ), and acyltransferase BomM in a similar way as the starter unit biosynthesis of vicenistatin.³¹ After the polyketide chain is fully processed, I propose that the terminal acyl group (alanine) is removed by the L-amino acid amidase BomC before macrolactam formation by the thioesterase domain of BomP1 (Figure 10b).³²

Compound **1** appeared to be modified by post-PKS modification enzymes to produce **2**. Although the detailed post-PKS modification route is unresolved, I propose a pathway for **2** biosynthesis based on sequence analysis and the deletion of one of the genes involved (Figure 10c). First, a cytochrome P450 hydroxylase (BomK, BomN, or BomO) catalyzes the hydroxylation at C-10 of **1**. With the action of a monooxygenase (BomA and BomB), the intermediate is hydrated, and nonbonding electrons of C-11 hydroxyl group could attack C-8, forming a THF ring structure. To identify the gene responsible for the C-10 hydroxylation step, each gene encoding *bomK*, *bomN* and *bomO* was inactivated by in-frame deletion (Figures S68–S70). Compound **2** production was not changed in the knockout mutants Δ bomN and Δ bomO (Figures S71 and S72). However, the Δ bomK mutant led to the selective loss of **2** production and the contrasting accumulation of **1**, confirming that this gene is involved in **2** biosynthesis (Figure S73).

Piceamycin (**4**) appear to be biosynthesized through the bombyxamycin biosynthetic pathway. The post-PKS modification pathways involved in the transformation of bombyxamycin C (**3**) into piceamycin (**4**) seem to be similar to the proposed post-PKS tailoring steps in the synthesis of hitachimycin, which also possesses a penta-carbocyclic moiety in its structure.³³ Although the mechanism of the formation of the cyclopentenone moiety in hitachimycin was not experimentally elucidated, the post-PKS pathway leading to piceamycin could be proposed based on the presence of three highly homologous enzymes in the bombyxamycin gene cluster (BomK, BomL, and BomP) and hitachimycin cluster. First,

the hydroxy group at C-11 of bombyxamycin C is likely converted to a ketone by BomP (GenBank accession No. MN095224), a putative short-chain dehydrogenase/reductase. Then, BomK (putative cytochrome P450) catalyzes a hydroxylation at C-10 and further oxidation to a carbonyl. With the catalytic action of sugar phosphate isomerase/epimerase (BomL), this α , β -unsaturated ketone moiety in the intermediate could be transformed into a cyclopentenone by a Michael addition (Figure 10d), as proposed in the biosynthesis of hitachimycin.³³

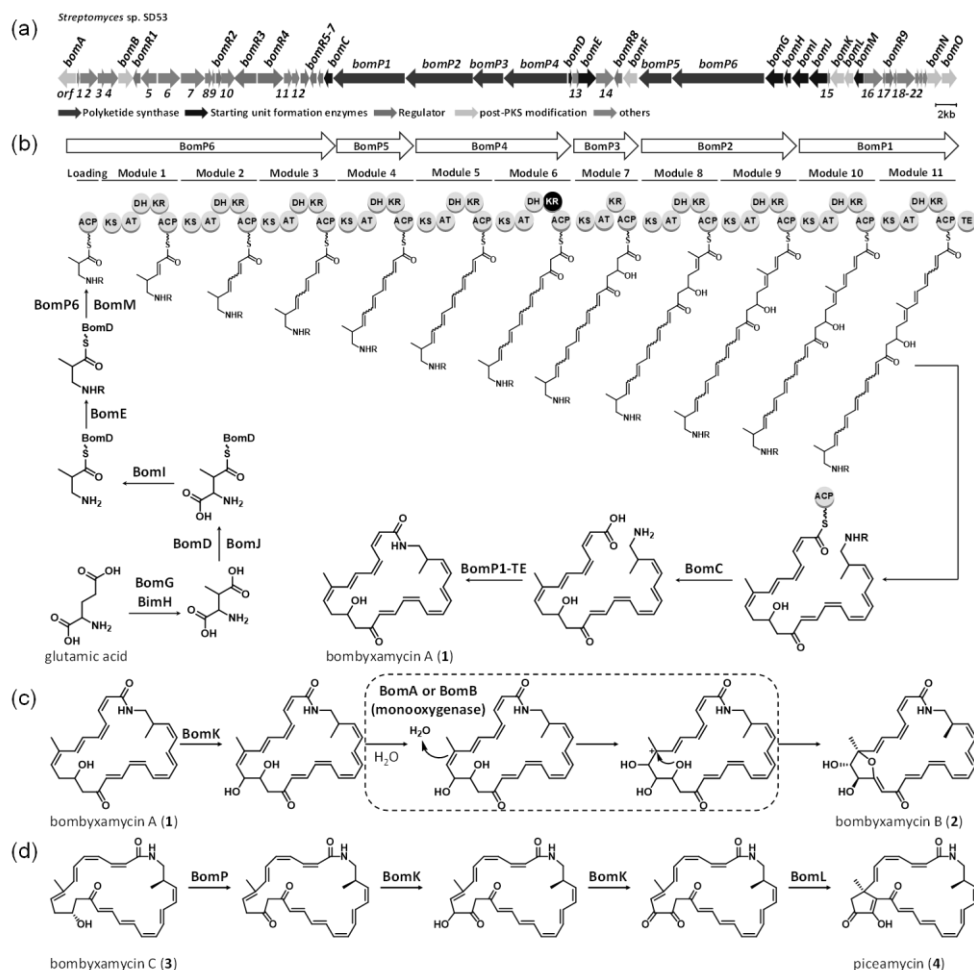


Figure 10. (a) Biosynthetic gene cluster for bombyxamycins A–C (1–3) and piceamycin (4). (b) Schematic representation of predicted biosynthetic procedure for bombyxamycin A (1). Domains within each module are represented by circles. The black circle indicates a domain that is predicted from the final structure and deletions in the active sites to not be active. KS, ketoacyl synthase; AT, acyl transferase; DH, dehydratase; KR, keto reductase; ACP, acyl carrier protein; TE, thioesterase. (c) The proposed biosynthetic pathway for producing bombyxamycin B (2) from bombyxamycin A (1). (d) Predicted post-PKS modification pathway for piceamycin (4) from bombyxamycin C (3).

1.2. Experimental Section

Bacterial isolation. Silkworm specimens (*Bombyx mori*, 4th–5th instar) used for bacterial isolation were collected from Boeun-eup, Boeun-gun, Chungcheongbuk-do, Republic of Korea, in 2014. Suspensions of intestinal bacteria of *Bombyx mori* were obtained from the samples and spread onto the surfaces of diverse solid media for bacterial isolation. The plates were incubated at 25 °C for 3 weeks. An actinobacterial strain was isolated from A1 + C medium (10 g of starch, 4 g of yeast extract, 2 g of peptone, 1 g of CaCO₃, 18 g of agar powder, and 100 mg of cycloheximide per 1 L of sterilized water) and inoculated onto fresh YEME solid medium (4 g of yeast extract, 10 g of malt extract, 4 g of glucose, and 18 g of agar powder per 1 L of sterilized water) to obtain a single strain. The bacterial strain SD53 was identified as a *Streptomyces* sp. (99% identity with *Streptomyces drozdowiczii*) by comparative analysis of the 16S rDNA sequence (GenBank accession No. KY249557).

Cultivation and extraction. For preparing **1** and **3**, spores of *Streptomyces* sp. SD53 were inoculated into 50 mL of YPM liquid medium (2 g of yeast extract, 4 g of mannitol, and 2 g of peptone per 1 L of sterilized water) and cultured with 200 rpm shaking at 30 °C for 2 days. A portion of the seed culture (5 mL) was transferred to 125 mL of K liquid medium (2 g of yeast extract, 15 g of soybean peptone, and 25 g of starch per 1 L of sterilized water) and cultivated for 5 days under the same conditions as the seed culture. The whole culture (24 L) was extracted with an equal volume of ethyl acetate and concentrated *in vacuo*, finally yielding 5 g of K medium extract. The production of **2** and **4** was achieved through the following procedure. Five milliliters of the SD53 YPM seed culture was transferred to 180 mL of YPM liquid media and cultivated (180 rpm, 30 °C). After 2 days, 25 mL of the bacterial culture was inoculated into 1 L of YPM liquid medium and shaken at 160 rpm and 30 °C for 5 days. The entire large-scale culture (24 L in total) was extracted with ethyl acetate by using a separation funnel. The whole extract was concentrated under low pressure. As a result, 3.5 g of dry YPM media extract was acquired.

Purification. The bacterial crude extract was directly injected into HPLC for purification to minimize the degradation of the polyene metabolites **1–4** by light exposure. The dried K medium extract was dissolved in HPLC-grade methanol (MeOH) and strained through a hydrophilic syringe filter (ADVANTEC, 25HP045AN) to remove small particles. The filtered extract was directly injected into semipreparative reversed-phase HPLC. The purification was conducted under an isocratic solvent system (58% CH₃CN–H₂O, flow rate: 2 mL/min, detection: UV 280 nm) using a YMC column (C₁₈(2), 5 μ m, 250 \times 10 mm). Compound **1** and **3** eluted at 24 min and 14 min, respectively. Bombyxamycin C (**3**) was further purified by HPLC with a gradient solvent system (YMC C₁₈(2) column, 5 μ m, 250 \times 10 mm, 65%–90% CH₃OH–H₂O over 60 min with 0.1% formic acid, UV 280 nm, flow rate: 2 mL/min) (retention time: 21 min).

Compound **2** and **4** were also directly purified without other fractionation steps. The YPM medium extract was filtered as mentioned above and directly purified under isocratic solvent conditions using semipreparative HPLC (reversed-phase C₁₈(2) YMC column, 5 μ m, 250 \times 10 mm, 58% CH₃CN–H₂O, flow rate: 2 mL/min, detection: UV 280 nm). Compound **2** and **4** eluted at 11 min and 24 min, respectively, and compound **2** was further purified under gradient solvent conditions (35%–60% CH₃CN–H₂O over 50 min, flow rate: 2 mL/min, detection: UV 280 nm). Pure **2** was obtained 28 min after injection.

Bombyxamycin A (1): yellow powder; UV (MeOH) λ_{max} (log ϵ) 323 (2.38), 383 (1.93) nm; ECD (c 0.2 \times 10⁻⁴ M, MeOH) λ_{max} ($\Delta\epsilon$) 215 (-1.26), 268 (1.63), 320 (-2.26), 380 (2.26) nm; IR (neat) ν_{max} 2922, 2864, 1641, 1053, 1032, 1010 cm⁻¹; For NMR spectral data, see Table 1; HR-FAB-MS m/z at 420.2540 [M+H]⁺ (calcd for C₂₇H₃₄NO₃, 420.2539). $[\alpha]_{\text{D}}^{20}$ was not exactly measurable (+73 \sim +167).

Bombyxamycin B (2): pale-yellow powder; UV (MeOH) λ_{max} (log ϵ) 290 (2.77), 387 (2.34) nm; ECD (c 0.2 \times 10⁻⁴ M, MeOH) λ_{max} ($\Delta\epsilon$) 228 (-1.51), 271 (1.80), 309 (-1.87), 369 (3.21) nm; IR (neat) ν_{max} 2971, 2868, 1350, 1053, 1023, 1010 cm⁻¹; For NMR spectral data, see

Table 1; HR-FAB-MS m/z at 450.2284 $[M+H]^+$ (calcd for $C_{27}H_{32}NO_5$, 450.2280). $[\alpha]_D^{20}$ was not exactly measurable ($-826 \sim -410$).

Bombyxamycin C (3): dark yellow powder; UV (MeOH) λ_{\max} ($\log \epsilon$) 320 (2.42), 396 (1.95) nm; ECD ($c\ 0.1 \times 10^{-4}$ M, MeOH) λ_{\max} ($\Delta\epsilon$) 216 (-1.01), 244 (2.72), 290 (0.44), 320 (1.74), 376 (-1.50) nm; IR (neat) ν_{\max} 2920, 2860, 1639, 1052, 1032, 1010 cm^{-1} ; For NMR spectral data, see Table 2; HR-FAB-MS m/z at 420.2534 $[M+H]^+$ (calcd for $C_{27}H_{34}NO_3$, 420.2539). $[\alpha]_D^{20}$ was not exactly measurable ($+86 \sim +140$).

Piceamycin (4): orange powder; UV (MeOH) λ_{\max} ($\log \epsilon$) 296 (2.52), 410 (1.89) nm; ECD ($c\ 0.7 \times 10^{-4}$ M, MeOH) λ_{\max} ($\Delta\epsilon$) 228 (-1.25), 300 (1.31), 455 (-2.99) nm; IR (neat) ν_{\max} 2970, 2870, 1349, 1051, 1022, 1010 cm^{-1} ; For NMR spectral data, see Table 2; HR-FAB-MS m/z at 432.2174 $[M+H]^+$ (calcd for $C_{27}H_{30}NO_4$, 432.2175). $[\alpha]_D^{20}$ was not exactly measurable ($-619 \sim -487$).

Preparing MTPA esters. Four milligrams of **1** was split into two amber vials and dried under high vacuum to eliminate residual water. The compound in each vial was dissolved in 1 mL of distilled anhydrous pyridine. Then, 15 μL of *R*-MTPA-Cl reactant was added to one of the vials, and the same volume of an *S*-MTPA-Cl mixture was added to the other reaction vial. The reactions were maintained at rt for 1 h, and 30 μL of MeOH was added to each reaction vial to quench the reaction. The mixtures were concentrated under low pressure. To prepare pure state *S*- and *R*-MTPA ester products of **1**, the reaction products were purified by using HPLC (YMC, 5 μm , C_{18} (2), 250×10 mm) with gradient solvent conditions (0–20 min: 40%–100% CH_3OH – H_2O ; 20–40 min: 100% CH_3OH – H_2O). The molecular formulas of *S*- and *R*-MTPA esters of **1** (**1a** and **1b**) were determined to be $C_{37}H_{40}F_3NO_5$ by LR-ESI-MS ($[M+H]^+$ m/z at 636, $[M+Na]^+$ m/z at 658). *S*- and *R*-MTPA esters of **2** (**2a** and **2b**) were prepared in a similar manner. The MTPA esters **2a** and **2b** were purified under gradient solvent conditions (YMC, 5 μm , C_{18} (2), 250×10 mm, 0–20 min: 20%–85% CH_3CN – H_2O , 20–40 min: 85% CH_3CN – H_2O , flow rate: 2 mL/min, detection: UV 280 nm) at retention

times of 37 min (**2a**) and 36 min (**2b**), respectively. The molecular formula of **2a** and **2b** was confirmed as $C_{37}H_{38}F_3NO_7$ with LR-ESI-MS ($[M+H]^+$ m/z at 666, $[M+Na]^+$ m/z at 688). Careful analysis of 1H and COSY NMR spectral data indicated that **2a** and **2b** have an MTPA ester at C-10. Bombyxamycin C (**3**, 1 mg) was also transferred into an amber vial and completely dried under high vacuum. Then, the compound was dissolved in 1 mL of distilled pyridine, and 15 μ L of *R*-MTPA-Cl was added into the vial. The reaction mixture was stirred at rt for 30 min and then quenched with 30 μ L of MeOH. The mixture was dried *in vacuo* and resuspended in MeOH for purification by reversed phase HPLC (Kromasil, $C_{18}(2)$, 5 μ m, 250 \times 10 mm). The desired product, *S*-MTPA-ester of **3** (**3a**, 0.5 mg), was observed at t_R 26.3 min under gradient solvent conditions (0–20 min: 40%–100% CH_3OH-H_2O ; 20–40 min: 100% CH_3OH ; detection: UV 280 nm; flow rate: 2 mL/min). The *R*-MTPA-ester of **3** (**3b**) was also prepared through the same procedure used for **3a**. *R*-MTPA-ester (**3b**, 0.4 mg) eluted at 26.7 min under the same gradient conditions.

***S*-MTPA ester of 1 (**1a**):** 1H NMR (DMSO- d_6 , 500 MHz) δ_H 7.974 (1H, dd, $J = 6.0, 6.0$ Hz), 7.487 (1H, m), 7.481–7.450 (5H, m), 7.286 (1H, dd, $J = 15.0, 11.5$ Hz), 6.827 (1H, dd, $J = 11.5, 11.5$ Hz), 6.816 (1H, dd, $J = 11.5, 11.5$ Hz), 6.681 (1H, dd, $J = 13.5, 11.5$ Hz), 6.647 (1H, dd, $J = 15.0, 11.0$ Hz), 6.444 (1H, d, $J = 15.0$ Hz), 6.363 (1H, dd, $J = 11.0, 11.0$ Hz), 6.288 (1H, dd, $J = 13.5, 11.0$ Hz), 6.207–6.135 (2H, m), 6.093 (1H, d, $J = 15.0$ Hz), 6.060 (1H, dd, $J = 11.5, 11.5$ Hz), 5.954 (1H, dd, $J = 11.5, 11.0$ Hz), 5.564 (1H, d, $J = 11.5$ Hz), 5.556 (1H, m), 5.475 (1H, m), 5.241 (1H, dd, $J = 10.5, 10.5$ Hz), 3.476 (1H, m), 3.456 (3H, s), 3.143 (1H, m), 3.077 (1H, dd, $J = 15.5, 5.0$ Hz), 2.771 (1H, dd, $J = 15.5, 7.5$ Hz), 2.695–2.611 (2H, m), 2.310 (1H, m), 1.658 (3H, s), 0.945 (3H, d, $J = 6.5$ Hz)

***R*-MTPA ester of 1 (**1b**):** 1H NMR (DMSO- d_6 , 500 MHz) δ_H 7.970 (1H, dd, $J = 6.0, 6.0$ Hz), 7.513 (1H, dd, $J = 11.5, 11.5$ Hz), 7.501–7.468 (5H, m), 7.302 (1H, dd, $J = 15.5, 11.5$ Hz), 6.841 (1H, dd, $J = 11.5, 11.5$ Hz), 6.819 (1H, dd, $J = 11.5, 11.5$ Hz), 6.691 (1H, dd, $J = 14.0, 11.5$ Hz), 6.636 (1H, dd, $J = 15.0, 11.5$ Hz), 6.431 (1H, d, $J = 15.0$ Hz), 6.361 (1H, dd, $J =$

11.5, 11.5 Hz), 6.281 (1H, dd, $J = 14.0, 11.5$ Hz), 6.176 (1H, d, $J = 15.5$ Hz), 6.175–6.143 (2H, m), 6.133 (1H, dd, $J = 11.5, 11.5$ Hz), 5.944 (1H, dd, $J = 11.5, 11.5$ Hz), 5.565 (1H, d, $J = 11.5$ Hz), 5.528 (1H, dd, $J = 10.5, 5.0$ Hz), 5.460 (1H, m), 5.244 (1H, dd, $J = 10.5, 10.5$ Hz), 3.531 (3H, s), 3.468 (1H, ddd, $J = 13.0, 6.0, 4.0$ Hz), 3.143 (1H, m), 3.121 (1H, dd, $J = 15.5, 5.0$ Hz), 2.872 (1H, dd, $J = 15.5, 6.5$ Hz), 2.500 (1H, m), 2.374 (1H, m), 2.311 (1H, ddd, $J = 13.0, 11.5, 6.0$ Hz), 1.612 (3H, s), 0.947 (3H, d, $J = 6.5$ Hz)

mono-S-MTPA ester of 2 (2a): ^1H NMR (DMSO- d_6 , 500 MHz) δ_{H} 8.005 (1H, dd, $J = 6.0, 6.0$ Hz), 7.551–7.496 (5H, m), 7.438 (1H, dd, $J = 11.5, 11.5$ Hz), 7.348 (1H, dd, $J = 15.5, 11.5$ Hz), 6.818 (1H, dd, $J = 15.0, 11.5$ Hz), 6.794 (1H, dd, $J = 11.5, 11.5$ Hz), 6.788 (1H, dd, $J = 11.5, 11.5$ Hz), 6.685 (1H, dd, $J = 14.5, 11.5$ Hz), 6.342 (1H, dd, $J = 14.5, 11.5$ Hz), 6.247 (1H, d, $J = 5.0$ Hz), 6.214 (1H, d, $J = 15.5$ Hz), 6.134 (1H, dd, $J = 11.5, 11.5$ Hz), 6.132 (1H, dd, $J = 11.5, 11.5$ Hz), 6.032 (1H, dd, $J = 11.5, 11.5$ Hz), 5.974 (1H, dd, $J = 11.5, 11.5$ Hz), 5.852 (1H, d, $J = 1.5$ Hz), 5.740 (1H, dd, $J = 11.5, 11.5$ Hz), 5.708 (1H, d, $J = 15.0$ Hz), 5.626 (1H, d, $J = 11.5$ Hz), 5.263 (1H, s), 5.232 (1H, dd, $J = 11.5, 11.5$ Hz), 3.963 (1H, dd, $J = 5.0, 1.5$ Hz), 3.542 (3H, s), 3.397 (1H, ddd, $J = 13.0, 6.0, 4.0$ Hz), 3.139 (1H, m), 2.425 (1H, ddd, $J = 13.0, 11.5, 6.0$ Hz), 1.424 (3H, s), 0.945 (3H, d, $J = 6.5$ Hz)

mono-R-MTPA ester of 2 (2b): ^1H NMR (DMSO- d_6 , 500 MHz) δ_{H} 7.997 (1H, dd, $J = 6.0, 6.0$ Hz), 7.540–7.463 (5H, m), 7.436 (1H, dd, $J = 11.5, 11.5$ Hz), 7.193 (1H, dd, $J = 15.5, 11.5$ Hz), 6.808 (1H, dd, $J = 15.0, 11.5$ Hz), 6.791 (1H, dd, $J = 11.5, 11.5$ Hz), 6.775 (1H, dd, $J = 11.5, 11.5$ Hz), 6.687 (1H, dd, $J = 14.5, 11.5$ Hz), 6.370 (1H, dd, $J = 14.5, 11.5$ Hz), 6.207 (1H, br s), 6.182 (1H, d, $J = 15.5$ Hz), 6.138 (1H, dd, $J = 11.5, 11.5$ Hz), 6.102 (1H, dd, $J = 11.5, 11.5$ Hz), 5.996 (1H, dd, $J = 11.5, 11.5$ Hz), 5.921 (1H, dd, $J = 11.5, 11.5$ Hz), 5.882 (1H, s), 5.860 (1H, dd, $J = 11.5, 11.5$ Hz), 5.755 (1H, d, $J = 15.0$ Hz), 5.635 (1H, d, $J = 11.5$ Hz), 5.230 (1H, dd, $J = 11.5, 11.5$ Hz), 5.103 (1H, s), 4.090 (1H, br s), 3.598 (3H, s), 3.393 (1H, m), 3.154 (1H, m), 2.438 (1H, m), 1.418 (3H, s), 0.949 (3H, d, $J = 6.5$ Hz)

S-MTPA ester of 3 (3a): ^1H NMR (CD $_3$ OD, 850 MHz) δ_{H} 7.4821–7.4370 (5H, m), 7.1267 (1H, dd, $J = 15.5, 11.0$ Hz), 6.9389 (1H, dd, $J = 14.5, 12.0$ Hz), 6.8294 (1H, dd, $J = 12.0,$

12.0 Hz), 6.6985 (1H, dd, $J = 12.0, 12.0$ Hz), 6.5952 (1H, dd, $J = 15.0, 12.0$ Hz), 6.5446 (1H, dd, $J = 14.5, 11.0$ Hz), 6.4977 (1H, dd, $J = 14.5, 11.5$ Hz), 6.4649 (1H, d, $J = 15.0$ Hz), 6.3875 (1H, dd, $J = 14.0, 11.0$ Hz), 6.3069 (1H, dd, $J = 11.0, 11.0$ Hz), 6.2275 (1H, dd, $J = 11.5, 11.5$ Hz), 6.1100 (1H, dd, $J = 11.0, 11.0$ Hz), 6.0653 (1H, d, $J = 15.5$ Hz), 6.0442 (1H, dd, $J = 11.0, 11.0$ Hz), 5.6646 (1H, m), 5.6472 (1H, d, $J = 11.5$ Hz), 5.6239 (1H, m), 5.2657 (1H, dd, $J = 10.5, 10.5$ Hz), 3.5742 (3H, s), 3.4086 (1H, dd, $J = 12.5, 11.5$ Hz), 3.3727 (1H, dd, $J = 13.5, 11.5$ Hz), 3.3300 (1H, m), 2.9219 (1H, dd, $J = 13.0, 4.0$ Hz), 2.5851 (1H, m), 2.5130 (1H, m), 2.4082 (1H, dd, $J = 14.0, 5.0$ Hz), 1.6077 (3H, s), 1.0508 (3H, d, $J = 6.5$ Hz)

R-MTPA ester of 3 (3b): ^1H NMR (CD_3OD , 850 MHz) δ_{H} 7.4789–7.4252 (5H, m), 7.1466 (1H, dd, $J = 15.5, 11.0$ Hz), 6.9383 (1H, dd, $J = 14.5, 12.0$ Hz), 6.8329 (1H, dd, $J = 12.0, 12.0$ Hz), 6.6968 (1H, dd, $J = 12.0, 12.0$ Hz), 6.5806 (1H, dd, $J = 15.0, 12.0$ Hz), 6.5472 (1H, dd, $J = 14.5, 11.0$ Hz), 6.4925 (1H, dd, $J = 14.5, 11.5$ Hz), 6.3949 (1H, dd, $J = 14.5, 11.0$ Hz), 6.3633 (1H, d, $J = 14.5$ Hz), 6.2843 (1H, dd, $J = 11.0, 11.0$ Hz), 6.2311 (1H, dd, $J = 11.5, 11.5$ Hz), 6.2306 (1H, dd, $J = 11.0, 11.0$ Hz), 6.1047 (1H, dd, $J = 11.0, 11.0$ Hz), 6.0693 (1H, d, $J = 15.5$ Hz), 6.0472 (1H, dd, $J = 11.0, 11.0$ Hz), 5.6442 (1H, d, $J = 11.5$ Hz), 5.5951 (1H, m), 5.4438 (1H, dd, $J = 10.5, 3.5$ Hz), 5.2649 (1H, dd, $J = 10.5, 10.5$ Hz), 3.5947H, s), 3.4666 (1H, dd, $J = 12.5, 11.5$ Hz), 3.4118 (1H, dd, $J = 13.5, 11.5$ Hz), 3.3287 (1H, m), 2.9206 (1H, dd, $J = 13.0, 4.0$ Hz), 2.8281 (1H, m), 2.4962 (1H, m), 2.4148 (1H, dd, $J = 14.0, 5.0$ Hz), 1.5872 (3H, s), 1.0504 (3H, d, $J = 6.5$ Hz)

Ozonolysis and acid hydrolysis. Compound **1** (10 mg) was dissolved in 2 mL of MeOH and cooled to $-78\text{ }^\circ\text{C}$ in a deep freezer. Ozone was then passed through the solution of **1** for 5 min using a microozonizer for ozonolysis. The residual ozone was eliminated by purging with argon gas, and the solvent was evaporated *in vacuo*. The dried mixture was dissolved in 7 mL of $\text{CH}_3\text{COOH-H}_2\text{O}_2$ (30%) solution and refluxed at $115\text{ }^\circ\text{C}$ for 6 h. After drying the reaction mixture under low pressure, 1.5 mL of 6 N HCl solution was added for acid hydrolysis ($120\text{ }^\circ\text{C}$, 15 h). HCl was then removed by evaporation *in vacuo*. To remove

residual HCl completely, 1 mL of deionized water was added to the reaction vial and vaporized with a rotary evaporator three times.

Preparing 3-(2,4-dinitro-phenylamino)-2-methyl-propanoic acid (5). The ozonolysis–acid hydrolysis product 3-amino-2-methyl-propanoic acid was dissolved in saturated sodium bicarbonate solution (300 μ L) and cooled to 0 $^{\circ}$ C. Sanger’s reagent (1-fluoro-2,4-dinitrobenzene) was prepared in acetone solution (15 mg/mL). Then, 300 μ L of Sanger’s reagent solution was added to the reaction vial with 3-amino-2-methyl-propanoic acid. The reaction was proceeded at 0 $^{\circ}$ C for 18 h and quenched by adding 150 μ L of 2 N HCl solution. The reaction mixture was then concentrated under low pressure and chromatographed by reversed-phase HPLC (YMC, 5 μ m, C₁₈(2), 250 \times 10 mm) using a gradient solvent system (55%–75% CH₃OH–H₂O over 50 min, flow rate: 2 mL/min, detection: UV 360 nm). The target product, 3-(2,4-dinitro-phenylamino)-2-methyl-propanoic acid (**5**), eluted at 28 min. The molecular formula (C₁₀H₁₁N₃O₆) and δ_{H} values (in ppm) of **5** were determined by using LR-ESI-MS ([M+H]⁺ at m/z 270, [M+Na]⁺ at m/z 292) and ¹H NMR spectrum data.

3-(2,4-dinitro-phenylamino)-2-methyl-propanoic acid (5): ¹H NMR (CD₃OD, 600 MHz) δ_{H} 9.02 (1H, d, J = 2.7 Hz), 8.27 (1H, dd, J = 9.5, 2.7 Hz), 7.21 (1H, d, J = 9.5 Hz), 3.67 (1H, dd, J = 13.3, 8.3 Hz), 3.53 (1H, dd, J = 13.3, 5.3 Hz), 2.81 (1H, m), 1.23 (3H, d, J = 7.0 Hz)

Preparing *S*- and *R*-PGME amides of 5 (5a and 5b). Two milligrams of 3-(2,4-dinitro-phenylamino)-2-methyl-propanoic acid (**5**) was divided into two vials and dissolved in 1 mL of THF in each vial. Then, 1-ethyl-3-(3-dimethylaminopropyl)carbodiimide (EDC, 10 mg) and a catalytic amount of 4-dimethylaminopyridine (DMAP) were added to each vial. One of the vials was treated with *S*-PGME (10 mg), and the other was treated with *R*-PGME (10 mg). The reaction vials were stirred at rt for 24 h. The solvent in the reaction vials was evaporated *in vacuo*, and the mixture was injected into HPLC for purification of PGME amide products under an isocratic solvent system (64% CH₃OH–H₂O, flow rate: 2 mL/min,

detection: UV 360 nm) with a reversed-phase HPLC column (YMC, 5 μ m, C₁₈(2), 250 \times 10 mm). *S*- and *R*-PGME amide products of **5** (**5a** and **5b**) eluted at 32 min and 30 min, respectively. The molecular formula of **5a** and **5b** was confirmed as C₁₉H₂₀N₄O₇ by LR-ESI-MS ([M-H]⁻ at *m/z* 415 and [M+Cl]⁻ at *m/z* 451). $\Delta\delta_{S-R}$ values of **5a** and **5b** were identified with ¹H and COSY NMR spectrum data.

***S*-PGME amide of 5 (5a):** ¹H NMR (CD₃OD, 600 MHz) δ_H 9.062 (1H, d, *J* = 2.8 Hz), 8.294 (1H, dd, *J* = 9.7, 2.8 Hz), 7.360–7.320 (5H, m) 7.227 (1H, d, *J* = 9.7 Hz), 5.435 (1H, s), 3.708 (1H, dd, *J* = 13.7, 8.7 Hz), 3.619 (3H, s), 3.602 (1H, dd, *J* = 13.7, 5.3 Hz), 2.961 (1H, m), 1.197 (3H, d, *J* = 7.0 Hz)

***R*-PGME amide of 5 (5b):** ¹H NMR (CD₃OD, 600 MHz) δ_H 8.896 (1H, d, *J* = 2.8 Hz), 8.147 (1H, dd, *J* = 9.6, 2.8 Hz), 7.360–7.320 (5H, m) 7.104 (1H, d, *J* = 9.6 Hz), 5.434 (1H, s), 3.705 (1H, dd, *J* = 13.7, 9.0 Hz), 3.685 (3H, s), 3.512 (1H, dd, *J* = 13.7, 5.0 Hz), 2.944 (1H, m), 1.256 (3H, d, *J* = 7.0 Hz)

Preparing PGME amides of 2*S*- and 2*R*-3-amino-2-methylpropanoic acid (6–9). A commercial racemic mixture of 3-amino-2-methylpropanoic acid (CAS no. 144-90-1, Sigma-Aldrich) was purchased and derivatized with *S*- and *R*-PGME. To prepare the *S*-PGME amides, 30 mg of the β -amino acid was dissolved in anhydrous dimethylformamide (DMF, 1.5 mL) and treated with *S*-PGME (20 mg), hydroxybenzotriazole hydrate (HOBt, 20 mg), benzotriazole-1-yl-oxytrispyrrolidinophosphonium hexafluorophosphate (PyBOP, 10 mg), and 4-methylmorpholine (300 μ L). The reaction mixture was stirred for 3 h at rt, quenched by adding 5% HCl solution (3 mL), and concentrated *in vacuo*. The dried products were injected onto a preparative HPLC column (Phenomenex Luna, C₁₈(2), 10 μ m, 250 \times 21.2 mm) and purified under a gradient solvent system (10%–30% CH₃CN–H₂O over 20 min with 0.1% formic acid, detection: UV 210 nm, flow rate: 10 mL/min). As a result, two different *S*-PGME amides (**6** and **8**) eluted at different retention times (**8** at 19.5 min and **6** at 20.5 min,

respectively), and the molecular formula of each product was determined to be $C_{13}H_{18}N_2O_3$ by HR-FAB-MS ($[M+H]^+$ m/z at 251). By comparing the LC/MS retention times of the two *S*-PGME amides with that of the *S*-PGME amide derived from authentic 2*S*-3-amino-2-methylpropanoic acid (CAS no. 4249-19-8, Sigma-Aldrich), *S*-PGME product **6** was assigned as the *S*-PGME amide of 2*S*-3-amino-2-methylpropanoic acid, whereas **8** was revealed as the *S*-PGME amide of 2*R*-3-amino-2-methylpropanoic acid (Figure S58). Through the same derivatization, purification, and analysis procedures with *R*-PGME and the racemic mixture of 3-amino-2-methylpropanoic acid (CAS no. 144-90-1, Sigma-Aldrich), *R*-PGME products (**7** and **9**) were acquired and assigned as the *R*-PGME amide of 2*S*-3-amino-2-methylpropanoic acid and the *R*-PGME amide of 2*R*-3-amino-2-methylpropanoic acid, respectively (Figure S59).

***S*-PGME amide of 2*S*-3-amino-2-methylpropanoic acid (6):** $[\alpha]_D^{20} +46$ (c 0.1, MeOH); UV (MeOH) λ_{\max} (log ϵ) 202 (2.70) nm; ECD (c 0.4×10^{-4} M, MeOH) λ_{\max} ($\Delta\epsilon$) 219 (3.97) nm; IR (neat) ν_{\max} 3703, 3671, 2972, 2867, 1058, 1011 cm^{-1} ; ^1H NMR (CD_3OD , 850 MHz) δ_{H} 7.4025–7.3477 (5H), 5.5217 (1H, s), 3.7186 (3H, s), 3.1548 (1H, dd, $J = 12.8, 8.2$ Hz), 3.0158 (1H, dd, $J = 12.8, 4.6$ Hz), 2.8757 (1H, m), and 1.1987 (3H, d, $J = 7.1$ Hz); ^{13}C NMR (CD_3OD , 212.5 MHz) δ_{C} 175.4, 172.9, 137.2, 130.0, 130.0, 129.8, 128.8, 128.8, 58.2, 53.2, 42.9, 38.5, and 16.2; HR-FAB-MS m/z at 251.1397 $[M+H]^+$ (calcd for $C_{13}H_{19}N_2O_3$, 251.1396).

***R*-PGME amide of 2*S*-3-amino-2-methylpropanoic acid (7):** $[\alpha]_D^{20} -103$ (c 0.1, MeOH); UV (MeOH) λ_{\max} (log ϵ) 205 (2.71) nm; ECD (c 0.4×10^{-4} M, MeOH) λ_{\max} ($\Delta\epsilon$) 219 (-4.31) nm; IR (neat) ν_{\max} 3703, 3671, 2972, 2868, 1058, 1011 cm^{-1} ; ^1H NMR (CD_3OD , 850 MHz) δ_{H} 7.4090–7.3501 (5H), 5.4939 (1H, s), 3.7078 (3H, s), 3.1472 (1H, dd, $J = 12.8, 8.2$ Hz), 2.9796 (1H, dd, $J = 12.8, 4.6$ Hz), 2.8344 (1H, m), and 1.3128 (3H, d, $J = 7.1$ Hz); ^{13}C NMR (CD_3OD , 212.5 MHz) δ_{C} 175.6, 172.5, 137.0, 130.0, 130.0, 129.8, 129.0, 129.0, 58.3, 53.0, 42.7, 38.4, and 16.4; HR-FAB-MS m/z at 251.1396 $[M+H]^+$ (calcd for $C_{13}H_{19}N_2O_3$, 251.1396).

S-PGME amide of 2R-3-amino-2-methylpropanoic acid (8): $[\alpha]_{\text{D}}^{20} +106$ (c 0.1, MeOH); UV (MeOH) λ_{max} (log ϵ) 203 (2.71) nm; ECD (c 0.4×10^{-4} M, MeOH) λ_{max} ($\Delta\epsilon$) 219 (4.06) nm; IR (neat) ν_{max} 3703, 3671, 2972, 2867, 1055, 1011 cm^{-1} ; ^1H NMR (CD_3OD , 850 MHz) δ_{H} 7.4077–7.3494 (5H), 5.4931 (1H, s), 3.7075 (3H, s), 3.1480 (1H, dd, $J = 12.8, 8.2$ Hz), 2.9779 (1H, dd, $J = 12.8, 4.6$ Hz), 2.8363 (1H, m), and 1.3114 (3H, d, $J = 7.1$ Hz); ^{13}C NMR (CD_3OD , 212.5 MHz) δ_{C} 175.6, 172.5, 137.0, 130.0, 130.0, 129.8, 129.0, 129.0, 58.3, 53.0, 42.7, 38.4, and 16.4; HR-FAB-MS m/z at 251.1399 $[\text{M}+\text{H}]^+$ (calcd for $\text{C}_{13}\text{H}_{19}\text{N}_2\text{O}_3$, 251.1396).

R-PGME amide of 2R-3-amino-2-methylpropanoic acid (9): $[\alpha]_{\text{D}}^{20} -46$ (c 0.1, MeOH); UV (MeOH) λ_{max} (log ϵ) 202 (2.70) nm; ECD (c 0.4×10^{-4} M, MeOH) λ_{max} ($\Delta\epsilon$) 219 (-4.31) nm; IR (neat) ν_{max} 3703, 3671, 2972, 2868, 1058, 1011 cm^{-1} ; ^1H NMR (CD_3OD , 850 MHz) δ_{H} 7.4241–7.3442 (5H), 5.5213 (1H, s), 3.7187 (3H, s), 3.1549 (1H, dd, $J = 12.8, 8.2$ Hz), 3.0183 (1H, dd, $J = 12.8, 4.6$ Hz), 2.8745 (1H, m), and 1.1992 (3H, d, $J = 7.1$ Hz); ^{13}C NMR (CD_3OD , 212.5 MHz) δ_{C} 175.4, 172.9, 137.2, 130.0, 130.0, 129.8, 128.8, 128.8, 58.2, 53.2, 42.9, 38.5, and 16.2; HR-FAB-MS m/z at 251.1394 $[\text{M}+\text{H}]^+$ (calcd for $\text{C}_{13}\text{H}_{19}\text{N}_2\text{O}_3$, 251.1396).

Determination of the stereogenic center at the β -position of the amide nitrogen in piceamycin (4). Piceamycin (4, 5 mg) was dissolved in 2 mL of MeOH and frozen at -80°C . The chilled solution was treated with ozone gas generated from a microozonizer for 5 min, and the residual ozone was removed by purging with argon. The ozonolysis products were dried *in vacuo*, re-dissolved in 7 mL of 1:1 $\text{CH}_3\text{COOH-H}_2\text{O}_2$ (30%) and refluxed at 115°C for 6 h. The mixture was concentrated under low pressure, and 1.5 mL of 6 N HCl was added into the vial for acid hydrolysis (120°C , 15 h). After hydrolysis, the HCl was evaporated on a rotary evaporator. To eliminate residual HCl, the hydrolysate was dissolved in 1 mL of deionized water, and the HCl was quickly evaporated three times. The hydrolysate was dissolved in 2 mL of DMF and divided equally into two vials. The vials were treated with

PyBOP (5 mg), HOBt (3 mg), 4-methylmorpholine (200 μ L), and *S*- or *R*- PGME (10 mg). The reaction mixtures were stirred at rt for 3 h. The reactions were quenched by adding 5% HCl solution (2 mL) and analyzed by using LC/MS (Phenomenex, C₁₈(2), 100 \times 4.6 mm, gradient solvent system: 10%–25% CH₃CN–H₂O over 30 min with 0.1% formic acid, detection: UV 210 nm, flow rate: 0.7 mL/min). For bombyxamycin C (**3**), the same procedure was performed with 1 mg of **3**.

Molecular modeling of PGME products (6–9) and ECD calculations for piceamycin (4). The first structural energy minimizations of **6–9** was conducted using Avogadro 1.2.0 with the MMFF94. Then, density functional theory (DFT) calculations were conducted via Tmolex 3.4 with the DFT settings (functional B3-LYP / gridsize m3), 6-31G basis set for all atoms, and geometry optimization options (energy 10^{-6} Hartree, gradient norm $|dE/dxyz| = 10^{-3}$ Hartree/bohr). The initial energy-minimized structures of **4** were also obtained by using Avogadro 1.2.0 with MMFF94. The ground-state geometries were optimized via Tmolex 3.4 by using DFT with the 6-31G basis set for all atoms at the DFT level (functional B3-LYP / gridsize m3). The theoretical ECD data were calculated by TD-DFT with the 6-311++G** basis set for all atoms at the DFT level (functional B3-LYP / gridsize m3). The calculated ECD spectra were simulated by overlapping each transition, where σ is the width of the band at 1/e height. ΔE_i and R_i are the excitation energies and rotatory strengths, respectively, for transition *i*. In this study, the value of σ was fixed at 0.10 eV.

Antibacterial activity assay. Three species of Gram-positive bacteria (*Staphylococcus aureus* ATCC 25923, *Enterococcus faecalis* ATCC 19433, and *Enterococcus faecium* ATCC 19434) and four species of Gram-negative bacteria (*Proteus hauseri* NBRC 3851, *Klebsiella pneumoniae* ATCC 10031, *Salmonella enterica* ATCC 14028, and *Escherichia coli* ATCC 25922) as human pathogens and a silkworm pathogen (*Bacillus thuringiensis* KACC 10168) were selected as test strains and prepared for the antibacterial activity assays. The test bacterial strains were cultured overnight in Mueller–Hinton broth (MHB) at 37 °C for human pathogens and in tryptic soy broth (TSB) at 28 °C for *B. thuringiensis*. The grown strains

were harvested by using a centrifuge and washed twice with sterilized water. Ampicillin, tetracycline, and streptomycin were used as positive controls, and dimethyl sulfoxide (DMSO) was used as a negative control. Each compound, including **1–4**, was dissolved in DMSO and diluted with MHB or TSB to prepare serial two-fold dilutions (from 128 µg/mL to 0.015 µg/mL). For the antibacterial activity assay, 10 µL of suspensions containing 1×10^6 colony-forming units (cfu)/mL of the test bacteria and 190 µL of MHB or TSB, which included the positive control compounds or test compounds, were added into each well of a 96-well plate (final concentration of test bacteria was 5×10^4 cfu/mL). Then, the plate was incubated at 37 °C or 28 °C for 24 h. The MIC values of each compounds were defined as the lowest concentration at which the compound inhibited the growth of the test bacteria.

Cell culture. Human lung cancer (A549), colorectal cancer (HCT116), breast cancer (MDA-MB-231), liver cancer (SK-HEP-1), and leukemia (K-562) cells were obtained from the American Type Culture Collection (ATCC, Manassas, VA, USA), and stomach cancer (SNU-638) cells were obtained from the Korean Cell Line Bank (Seoul, Korea). The cells were cultured in an appropriate medium (Roswell Park Memorial Institute 1640 for A549, HCT116, SNU-638, and K562 cells; Dulbecco's modified Eagle's medium for MDA-MB-231 and SK-HEP-1 cells) supplemented with 10% heat-inactivated FBS, 100 units/mL penicillin, 100 µg/mL streptomycin, and 0.25 µg/mL amphotericin B. The cells were incubated at 37 °C with 5% CO₂ in a humidified atmosphere. All reagents were purchased from Gibco Invitrogen Corp. (Grand Island, NY, USA).

Cell proliferation assay. Cell proliferation was measured by the sulforhodamine B (SRB) assay.³⁴ Briefly, cells were seeded in 96-well plates and incubated for 30 min (for zero-day controls) or treated with **1–4** for the indicated times. After incubation, the cells were fixed, dried, and stained with 0.4% SRB in 1% acetic acid. The unbound dye was removed by washing, and the stained cells were suspended in 10 mM Tris (pH 10.0). The absorbance was measured at 515 nm, and the cell proliferation was determined. IC₅₀ values were calculated by nonlinear regression analysis using TableCurve 2D v5.01 software (Systant Software Inc.,

Richmond, CA, USA). All reagents were purchased from Sigma–Aldrich (St. Louis, MO, USA).

Antifungal activity assay. Potato dextrose agar (PDA) was used to cultivate *Candida albicans* ATCC 10231. After incubation for 48 h at 28 °C, the yeast cells were harvested by centrifugation and washed twice with sterile distilled water. *Aspergillus fumigatus* HIC 6094, *Trichophyton rubrum* NBRC 9185, and *Trichophyton mentagrophytes* IFM 40996 were also plated on PDA and incubated for 2 weeks at 28 °C. Spores were harvested and washed twice with sterile distilled water. Stock solutions of **1–4** were prepared in DMSO. Each stock solution was diluted with RPMI 1640 broth (Difco, Livonia, MI, USA) to give serial twofold dilutions in the range of 0.06–128 µg/mL. The final DMSO concentration was maintained at 1% by adding DMSO to the broth. Aliquots (10 µL) of the RPMI 1640 broth containing approximately 10⁴ cells/mL were mixed with the test compound solutions in each well of a 96-well plate. The plates were incubated for 24 h (for *C. albicans*), 48 h (for *A. fumigatus*), and 96 h (for *T. rubrum* and *T. mentagrophytes*) at 37 °C. A culture with DMSO (1%) was used as a solvent control, and a culture supplemented with amphotericin B was used as a positive control.

Sequencing and gene annotation of the *Streptomyces* sp. SD53. The genome of the bombyxamycin-producing strain *Streptomyces* sp. SD53 was sequenced by ChunLab, Inc. (Seoul, Republic of Korea), using single-molecule sequencing technology with the PacBio RS II system (Pacific Biosciences, Menlo Park, CA). The genome assembly was carried out using a hierarchical genome assembly process (HGAP) with SMRT analysis 2.3.0 (Pacific Bioscience, USA). These analyses resulted in 3 contigs with a total of 8,095,858 bases. This genome was annotated with EggNOG 4.5, Swissprot, KEGG, and SEED as ChunLab’s in-house pipeline. The genome of *Streptomyces* sp. SD53 consisted of 71.69% G + C content, 6,972 predicted coding sequences (CDS), 18 rRNA genes and 69 tRNA genes. AntiSMASH 4.0²⁸ was used to identify the biosynthetic gene clusters of bombyxamycins. Data obtained from sequences available at GenBank (GenBank accession No. MK433001) (Table S8).

Gene inactivation by in-frame deletion. For in-frame deletion, the construction of recombinant plasmids was carried out by PCR amplification of the left- and right-flanking fragments from genomic DNA derived from *Streptomyces* sp. SD53. The primer pairs bomK-LF/bomK-LR, bomN-LF/bomN-LR and bomO-LF/bomO-LR were designed for amplification of left-flanking fragments of target genes, whereas bomK-RF/bomK-RR, bomN-RF/bomN-RR, and bomO-RF/bomO-RR were used for amplification of right-flanking fragments (Table S9). A total of 6 PCR fragments were separately cloned into the pGEM-T Easy vector (Promega) and sequenced. *Escherichia coli* DH5 α was used for routine subcloning. After digestion with appropriate restriction enzymes, the fragments were cloned into *E. coli*-*Streptomyces* shuttle vector pKC1139 digested with NheI-XbaI or XbaI-HindIII to construct an in-frame deletion plasmid. This plasmid was transferred by conjugation from *E. coli* ET12567/pUZ8002 (nonmethylating plasmid donor strain) to wild-type *Streptomyces* sp. SD53, and then target genes were deleted by homologous recombination. The desired double crossover mutants, Δ bomK, Δ bomN, and Δ bomO, were selected by a thiostrepton-resistant phenotype and verified by PCR and sequence analysis (Figures S68–S70).

Table 1. ^1H and ^{13}C NMR data for bombyxamycins A and B (**1** and **2**).

no.	bombyxamycin A (1)				bombyxamycin B (2)			
	δ_{C}^a	type	δ_{H}^b	mult (J in Hz)	δ_{C}^a	type	δ_{H}^b	mult (J in Hz)
1	166.3	C			165.8	C		
2	121.3	CH	5.55	d (11.5)	123.3	CH	5.63	d (11.5)
3	133.7	CH	6.82	dd (11.5, 11.5)	132.3	CH	6.80	dd (11.5, 11.5)
4	124.4	CH	7.45	dd (11.5, 11.5)	126.4	CH	7.41	dd (11.5, 11.5)
5	135.2	CH	6.35	dd (11.5, 11.5)	133.5	CH	6.30	dd (11.5, 11.5)
6	121.7	CH	6.60	dd (15.0, 11.5)	124.6	CH	6.84	dd (15.0, 11.5)
7	140.1	CH	6.41	d (15.0)	138.2	CH	6.16	d (15.0)
8	135.1	C			89.1	C		
9	131.4	CH	5.52	dd (9.5, 4.5)	79.4	CH	3.83	br dd (5.5, 4.5)
10	37.2	CH	2.31	m	77.5	CH	4.50	br dd (5.5, 5.5)
11	68.5	CH	4.04	m	167.6	C		
12a	44.5	CH ₂	2.86	dd (14.5, 4.5)	100.1	CH	5.08	s
12b			2.46	dd (14.5, 6.5)				
13	199.8	C			189.6	C		
14	132.0	CH	6.15	d (15.0)	131.7	CH	6.48	d (15.5)
15	136.6	CH	7.26	dd (15.0, 11.5)	135.8	CH	7.38	dd (15.5, 11.0)
16	126.6	CH	6.13	dd (11.5, 11.5)	127.1	CH	6.09	dd (11.0, 11.0)
17	132.4	CH	6.81	dd (11.5, 11.5)	130.6	CH	6.78	dd (11.0, 11.0)
18	122.7	CH	6.16	m	123.3	CH	6.34	dd (11.0, 11.0)
19	135.1	CH	5.94	dd (11.5, 11.5)	134.3	CH	6.10	dd (11.0, 11.0)
20	127.1	CH	6.69	dd (14.0, 11.5)	127.6	CH	6.71	dd (14.5, 11.0)
21	132.7	CH	6.27	dd (14.0, 11.5)	131.8	CH	6.38	dd (14.5, 11.5)
22	130.1	CH	6.16	m	129.9	CH	6.14	dd (11.5, 10.5)
23	137.7	CH	5.23	dd (10.5, 10.5)	137.4	CH	5.22	dd (10.5, 10.5)
24	30.5	CH	3.12	m	31.3	CH	3.04	m
25a	44.8	CH ₂	3.46	ddd (12.5, 7.0, 4.0)	44.8	CH ₂	3.29	m
25b			2.30	m			2.60	m
1'	12.5	CH ₃	1.64	s	18.2	CH ₃	1.38	s
2'	17.9	CH ₃	0.94	d (6.5)	18.1	CH ₃	0.95	d (6.5)
1-NH			7.97	dd (6.5, 6.5)			7.99	dd (6.0, 6.0)
9-OH							5.88	br d (4.5)
10-OH							6.14 ^c	
11-OH			4.77	br s				

^a 125 MHz, ^b 500 MHz, ^c overlapped

Table 2. ^1H and ^{13}C NMR data for bombyxamycin C and piceamycin (**3** and **4**).

no.	bombyxamycin C (3)				piceamycin (4)			
	δ_{C}^a	type	δ_{H}^b	mult (J in Hz)	δ_{C}^a	type	δ_{H}^c	mult (J in Hz)
1	165.9	C			164.9	C		
2	123.3	CH	5.58	d (11.5)	122.4	CH	5.08	d (11.5)
3	130.6	CH	6.59	dd (11.5, 11.5)	132.1	CH	6.22	dd (11.5, 11.5)
4	124.4	CH	6.82	dd (11.5, 11.5)	124.2	CH	7.21	dd (11.5, 11.5)
5	133.3	CH	6.24	dd (11.5, 11.5)	133.7	CH	6.10	dd (11.5, 11.5)
6	120.9	CH	6.49	dd (15.0, 11.5)	121.3	CH	6.02	dd (15.0, 11.5)
7	140.3	CH	6.50	d (15.0)	143.8	CH	5.99	d (15.0)
8	135.7	C			49.6	C		
9a	129.7	CH	5.84	dd (7.0, 7.0)	49.2	CH ₂	2.43	d (19.0)
9b							2.39	d (19.0)
10	33.7	CH ₂	2.19	m	203.4	C		
11	67.3	CH	4.09	m	155.2	C		
12a	43.0	CH ₂	3.08	dd (13.0, 10.5)	138.9	C		
12b			2.18	dd (13.0, 4.5)				
13	199.1	C			192.3	C		
14	130.5	CH	5.99	d (15.5)	129.2	CH	7.24	d (15.0)
15	144.3	CH	7.00	dd (15.5, 11.0)	142.3	CH	7.06	dd (15.0, 11.0)
16	131.2	CH	6.42	dd (14.5, 11.0)	129.8	CH	6.52	dd (14.5, 11.0)
17	136.6	CH	6.84	dd (14.5, 11.5)	138.5	CH	7.22	dd (14.5, 11.0)
18	127.5	CH	6.04	dd (11.5, 11.5)	127.3	CH	6.20	dd (11.0, 10.5)
19	134.6	CH	6.19	dd (11.5, 11.5)	134.1	CH	6.29	dd (10.5, 10.5)
20	127.0	CH	6.39	dd (14.5, 11.5)	127.3	CH	6.66	dd (15.0, 10.5)
21	132.3	CH	6.58	dd (14.5, 11.0)	132.2	CH	6.59	dd (15.0, 10.0)
22	132.3	CH	5.97	dd (11.0, 10.5)	129.2	CH	6.06	dd (10.0, 10.0)
23	137.8	CH	5.19	dd (10.5, 10.5)	136.2	CH	5.13	dd (10.0, 10.0)
24	34.4	CH	2.71	m	33.3	CH	2.68	m
25a	44.0	CH ₂	3.36	m ^d	43.6	CH ₂	3.36	m
25b			2.74	m			2.65	m
1'	12.3	CH ₃	1.49	s	28.4	CH ₃	1.58	s
2'	17.7	CH ₃	0.96	d (6.5)	17.7	CH ₃	0.96	d (6.5)
11-OH							11.18	br s
25-NH			7.71	dd (10.0, 2.5)			7.52	dd (10.0, 2.0)

^a 212.5 MHz, ^b 850 MHz, ^c 500 MHz, ^d overlapped

Table 3. Antibacterial activities of bombyxamycins A–C (**1–3**) and piceamycin (**4**) against human and silkworm pathogenic strains.

	MICs ($\mu\text{g/mL}$)						
	Gram-positive				Gram-negative		
	<i>S. aureus</i>	<i>E. faecalis</i>	<i>E. faecium</i>	<i>B. thuringiensis</i>	<i>P. hauseri</i>	<i>K. pneumoniae</i>	<i>S. enterica</i>
1	8	128	>128	2,100	0.5	>128	1
2	64	>128	>128	>128	>128	>128	>128
3	>128	>128	128	380	128	>128	128
4	0.03	32	5.33	3.2	0.03	>128	0.08
ampicillin	0.17	0.5	1.00	-	0.03	>128	0.25
tetracycline	-	-	-	-	-	0.44	-
streptomycin	-	-	-	128	-	-	-

Table 4. Antiproliferative activities of bombyxamycins A–C (**1–3**) and piceamycin (**4**) against various human cancer cell lines.

	IC ₅₀ (μM)					
	A549	HCT116	SNU638	SK-HEP-1	MDA-MB-231	K562
1	0.94	1.14	0.93	4.20	2.09	1.08
2	>100	>100	>100	>100	>100	82.93
3	0.78	1.01	0.85	1.87	1.00	0.96
4	0.28	0.22	0.38	0.32	0.66	0.74
etoposide	0.60	1.36	0.52	0.38	3.32	0.98

*cell lines: A549 – lung cancer, HCT116 – colon cancer, SNU638 – stomach cancer, SK-HEP-1 – liver cancer, MDA-MB-231 – breast cancer, K562 – leukemia.

**2. Nicrophorusamides A and B,
Antibacterial Chlorinated Cyclic Peptides from
the Gut *Microbacterium* sp. of the Carrion Beetle
*Nicrophorus concolor***

2.1. Results and Discussion

Nicrophorusamide A (**10**) was purified as a white powder, and the molecular formula of **10** was deduced as $C_{37}H_{56}ClN_9O_8$, which has an unsaturation number of 14, based on high-resolution fast atom bombardment MS (HR-FAB-MS) data. The 1H and HSQC NMR spectra of **10** identified 11 exchangeable protons (δ_H 11.03, 8.43, 7.98, 7.87, 7.81, 7.66 (2H), 7.62, 7.45, 7.31, and 7.28) and four aromatic protons (δ_H 7.57, 7.32, 7.15, and 7.05) in the downfield region below δ_H 7.0. One more heteroatom-bound proton was detected at δ_H 5.85, and six α -amino proton resonances were observed at δ_H 4.7–3.5 (δ_H 4.62, 4.60, 4.24, 4.23, 4.01, and 3.75). These initial analyses indicated that nicrophorusamide A is likely a peptide-derived compound with an aromatic ring structure. In addition, the 1H NMR and HSQC spectra revealed the existence of a methine proton (δ_H 4.47) directly bonded to an oxygen-bearing carbon (δ_C 70.8). Further analysis of the 1H NMR and multiplicity-edited HSQC spectra of **10** identified six aliphatic methylene and three methine protons between 3.11 and 1.16 ppm and six methyl groups (δ_H 0.87, 0.86, 0.85, 0.83, 0.72, and 0.69).

The ^{13}C NMR spectrum of **10** (in DMSO- d_6 at 125 MHz) revealed seven carbonyl carbon signals (δ_C 173.2, 172.1, 171.7, 171.1, 170.6, 170.4, and 169.4), eight aromatic carbon resonances (δ_C 134.5, 128.4, 125.4, 122.9, 120.7, 117.5, 112.7, and 109.8), one oxygenated carbon (δ_C 70.8), and six amino acid α -carbon peaks (δ_C 60.4, 56.5, 55.8, 53.5, 53.1, and 51.5), reflecting the characteristic features of a peptide-class compound. The ^{13}C NMR spectrum of nicrophorusamide A (**10**) also displayed 15 aliphatic carbon resonances at δ_C 39.6–11.3, including six methyl carbons (δ_C 22.7, 21.8, 18.8, 18.5, 14.5, and 11.3). All the one-bond 1H – ^{13}C correlations were established by analyzing the 1H , ^{13}C and HSQC NMR spectral data together.

Because nicrophorusamide A (**10**) was revealed to be a peptide with several amino acid units, individual amino acid moieties were elucidated by interpreting COSY, TOCSY, and HMBC NMR spectra. A 2-NH (δ_H 7.98)/H-2 (δ_H 4.62) COSY correlation connected the nitrogen to the C-2 α -carbon (δ_C 53.5). The COSY correlations from H-2 to H₂-3 (δ_H 3.11 and 2.89)

showed connectivity between the α -carbon and β -carbon of the amino acid unit. The HMBC correlations from H₂-3 to C-4 (δ_C 109.8), C-5 (δ_C 125.4), and C-11 (δ_C 128.4) revealed that this amino acid has an aromatic ring structure in its side chain group.

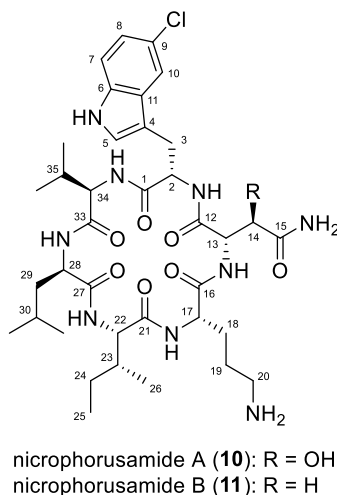


Figure 11. Chemical structures of nicrophorusamides A and B (**10** and **11**).

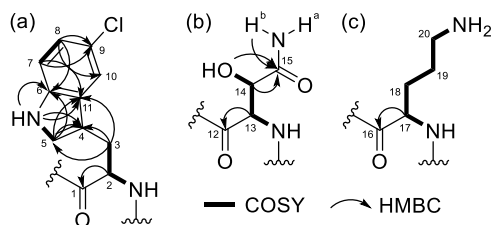


Figure 12. Structure determination of the uncommon amino acid units in nicrophorusamide A (**10**) based on COSY and HMBC correlations: (a) chloro-tryptophan, (b) β -hydroxyasparagine, and (c) ornithine.

The aromatic ring was constructed by analyzing COSY and HMBC NMR spectra. A ^1H – ^1H coupling between H-7 (δ_H 7.32 [d, J = 8.5 Hz]) and H-8 (δ_H 7.05 [dd, J = 8.5, 2.0 Hz]) established the C-7–C-8 connectivity. The $^3J_{\text{H}7\text{H}8}$ value (8.5 Hz) indicated that this spin system belongs to a six-membered aromatic ring. This six-membered aromatic ring was

assigned based on 3-bond HMBC correlations from H-7 to C-9 and C-11, from H-8 to C-6 and C-10, and from H-10 to C-6 and C-8. The other aromatic proton, H-5 (δ_{H} 7.15), correlated with 5-NH (δ_{H} 11.03) in the COSY NMR spectrum, allowing for C-5–5-N connectivity. The HMBC correlations from H-5 to C-4, C-6 (δ_{C} 134.5), and C-11 and from 5-NH to C-4, C-6, and C-11 indicated an indole ring structure, thereby identifying a tryptophan moiety (Figure 12a). An array of COSY correlations among 13-NH (δ_{H} 7.62), H-13 (δ_{H} 4.60), H-14 (δ_{H} 4.47), and 14-OH (δ_{H} 5.85) showed 13-NH–C-13–C-14–14-OH connectivity. This spin system was also confirmed by their TOCSY correlations. The 2-bond H-13/C-12 (δ_{C} 169.4) ^1H – ^{13}C coupling along with HMBC correlations from 15-NH₂b (δ_{H} 7.28) and H-14 to C-15 (δ_{C} 173.2) indicated β -hydroxyasparagine (Figure 12b). An ornithine unit was assigned based on the ^1H – ^1H couplings of 17-NH (δ_{H} 8.43), H-17 (δ_{H} 4.01), H₂-18 (δ_{H} 1.84 and 1.64), H₂-19 (δ_{H} 1.50), H₂-20 (δ_{H} 2.79), and 20-NH₂ (δ_{H} 7.66) in the COSY and TOCSY NMR spectra, along with an H-17/C-16 (δ_{C} 170.6) HMBC correlation (Figure 12c).

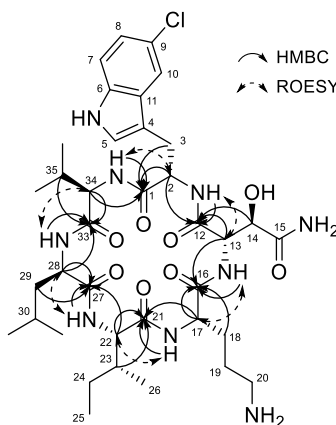


Figure 13. Identification of the amino acid sequence in microphorusamide A (**10**) based on HMBC and ROESY NMR spectra.

Other amino acid units, including valine, leucine, and isoleucine, were constructed by further analyzing COSY, TOCSY, HSQC and HMBC NMR spectra. Based on these results,

nicrophorusamide A is a peptide with six amino acid units. After elucidating the six amino acids, the chlorine atom was assigned at the quaternary carbon C-9 in the tryptophan unit based on the molecular formula and the ^{13}C chemical shift, corresponding to 5-chloro-tryptophan (Figure 12a).

The discrete structures of 5-chloro-tryptophan, β -hydroxyasparagine, ornithine, valine, leucine, and isoleucine bearing seven carbonyl carbons, four double bonds, and two rings explain 13 out of 14 double bond equivalents. Therefore, nicrophorusamide A (**10**) was deduced to possess an additional ring. The last ring was constructed by connecting these six amino acid partial structures based on HMBC and ROESY correlations (Figure 13). The two- or three-bond ^1H – ^{13}C correlations from α -proton of 5-chloro-tryptophan (H-2) to two different carbonyl carbons, C-1 and C-12, were determined based on the HMBC spectrum data. However, connectivity between C-1 and C-2 was confirmed by the HMBC correlation of H-3/C-1, the other carbonyl carbon C-12 should be connected to 2-NH establishing 5-chloro-tryptophan– β -hydroxyasparagine connectivity. This result could be crosschecked by two-bond ^1H – ^{13}C HMBC correlation from 2-NH to C-13 and ROESY ^1H – ^1H correlations between amide proton of 5-chloro-tryptophan (2-NH) and α -proton of β -hydroxyasparagine (H-13). By this method, the other amino acid units such as ornithine, isoleucine, leucine, and valine units could be connected sequentially, constructing the amino acids sequence as 5-Cl-Trp– β -OH-Asn–Orn–Ile–Leu–Val. A macrocyclic ring was also closed by same procedure. There were also two HMBC correlations from H-34 to two discrete carbonyl carbons, C-33 and C-1. Because C-33 was identified to be linked to C-34 based on the HMBC correlation of H-35/C-33, the other carbonyl carbon C-1, which was also carbonyl carbon of 5-chloro-tryptophan unit, should be connected to 34-NH, completing the cyclic hexapeptide structure of nicrophorusamide A (**10**). ROESY correlation of 34-NH/H-2 and HMBC correlation of 34-NH/C-1 furtherly confirmed the macrocyclic ring structure of **10** (Figure 13).

The absolute configurations at the α -carbons of the six amino acid units were determined by applying the advanced Marfey's method with the L- and D- forms of 1-fluoro-2,4-

dinitrophenyl-5-alanine amide (FDAA).³⁵ First, 1 mg of **10** was hydrolyzed with 6 N HCl for 1 h at 115 °C to obtain each free amino acid. The amino acid residues in the hydrolysate were chemically derivatized with L- and D-FDAA and analyzed by LC/MS under a gradient solvent system. Comparing the LC/MS analysis results revealed 5-chloro-L-tryptophan, D- β -hydroxyasparagine, L-ornithine, L-isoleucine, D-leucine, and D-valine (Table S11, Figures S88 and S89).

An additional chiral center at C-14 of D- β -hydroxyasparagine had to be subjected to further stereochemical analysis. Because β -hydroxyasparagine changes to β -hydroxyaspartic acid during acid hydrolysis, both authentic samples of *threo*- β -hydroxyaspartic acid and *erythro*- β -hydroxyaspartic acid were prepared. Then, the FDAA adducts of authentic *threo*- β -hydroxyaspartic acid and *erythro*- β -hydroxyaspartic acid were analyzed by LC/MS, which assigned D-*threo*- β -hydroxyaspartic acid, thus determining 14*R* configuration (Figure S91). To elucidate the absolute configuration at C-23 of the L-isoleucine unit, 2,3,4,6-tetra-*O*-acetyl- β -D-glucopyranosyl isothiocyanate (GITC) was used.³⁶ Derivatizing authentic L-isoleucine and L-*allo*-isoleucine with GITC and subsequently comparing their retention times with that of GITC revealed that this isoleucine in **10** is L-*allo*-isoleucine (Figure S92).

Nicrophorusamide B (**11**) was isolated as a white powder, the molecular formula of which was determined to be C₃₇H₅₆ClN₉O₇ by HR-FAB-MS and 1D ¹H and ¹³C NMR spectral data (Table 5). Based on its molecular formula, nicrophorusamide B (**11**) has one fewer oxygen atom than **10**. The NMR and UV spectra of **11** displayed high degrees of similarity to those of **10**, indicating that this compound is analogous to nicrophorusamide A (**10**). Careful comparison of 1D and 2D NMR spectroscopic data with those of **10** revealed that D-*threo*- β -hydroxyasparagine was replaced with D-asparagine, whereas the other amino acids were identical. The absolute configurations of the amino acid units in **11** were deduced to be identical to those in **10** based on their identical circular dichroism (CD) spectra (Figure S93) and common biosynthetic origin.

A few cyclic hexapeptides bearing some of the amino acid units in the nicrophorusamides were found by literature search. For example, desotamides A–D, discovered from deep sea-derived *Streptomyces scopuliridis*, have L-tryptophan, glycine, L-asparagine, L-*allo*-isoleucine/L-valine, D-leucine, and L-leucine in sequence.³⁷ Their biosynthetic gene cluster was also recently reported along with a new analogue by heterologous expression.³⁸ However, the desotamides and nicrophorusamide A share only L-*allo*-isoleucine and D-leucine in different positions in their hexapeptide sequences. Another series of cyclic hexapeptides, wollamides A–B, which were isolated from an Australian soil *Streptomyces*, are more similar to the desotamides rather than the nicrophorusamides because these antimycobacterial compounds only replaced glycine in the desotamides with D-ornithine.³⁹ The most closely related cyclic hexapeptide with the nicrophorusamides (**10** and **11**) could be longicatenamycin A, an antibacterial compound previously discovered from *Streptomyces diastaticus* strain S-520.^{40, 41} Longicatenamycin A is also a cyclic hexapeptide commonly bearing 5-chloro-tryptophan and ornithine in **10** and **11**. However, the other four amino acids (i.e., glycine, homohomoleucine, valine and β -hydroxyglutamic acid) in longicatenamycin A are different from those in **10** (i.e., valine, leucine, isoleucine, and β -hydroxyasparagine). Interestingly, the absolute configuration of the amino acids in **10** is opposite to that of the amino acids in longicatenamycin A, of which structure was confirmed by total synthesis.⁴¹ Nicrophorusamide A (**10**) ($[\alpha]_D^{25} = -18$) has the sequence L–D–D–L–L–D (5-chloro-L-tryptophan, D-valine, D-leucine, L-*allo*-isoleucine, L-ornithine, and D-*threo*- β -hydroxyasparagine), whereas longicatenamycin A ($[\alpha]_D^{25} = +13$) possesses the sequence D–NA–L–D–D–L (5-chloro-D-tryptophan, glycine, L-homohomoleucine, D-valine, D-ornithine, and L-*threo*- β -hydroxyglutamic acid).

The biological activities of the nicrophorusamides were evaluated against pathogenic bacterial strains (Table 6). Nicrophorusamide A (**10**) showed antibacterial bioactivity against *Staphylococcus aureus* ATCC 25923, *Enterococcus faecalis* ATCC 19433, *Enterococcus faecium* ATCC 19434, and *Salmonella enterica* ATCC 14028 with minimum inhibitory

concentration (MIC) values of 8–16 $\mu\text{g/mL}$. Nicrophorusamide B (**11**), which bears D-asparagine instead of D-*threo*- β -hydroxyasparagine, displayed 8 times lower activity against these bacteria than **10**, implying that D-*threo*- β -hydroxyasparagine could play a significant role in determining the antibacterial activity. The structural importance of the hydroxy group in nicrophorusamide A (**10**) can be rationalized by the conformational difference between nicrophorusamides A and B. Careful analysis of the ROESY NMR spectra and density functional theory (DFT) modeling for the energy minimization of nicrophorusamide A (**10**) clearly revealed a ROESY correlation between the hydroxy proton (14-OH) of D-*threo*- β -hydroxyasparagine and the terminal amine protons (20-NH₂) of L-ornithine, which enables an additional ring to form that is closed by a 14-O–20-NH hydrogen bond (Figure 14a). In contrast, nicrophorusamide B (**11**), which lacks the hydroxy group at C-14, is unable to make a rigid conformation with the corresponding hydrogen bond (Figure 14b).

Nicrophorusamides A and B did not inhibit the pathogenic fungi *Candida albicans* ATCC 10231, *Aspergillus fumigatus* HIC 6094, *Trichophyton rubrum* NBRC 9185, or *T. mentagrophytes* IFM 40996. In cytotoxicity tests against various human cancer cell lines, such as A-549, HCT-116, SNU-638, SK-HEP-1, MDA-MB-231, and K-562, nicrophorusamides A and B exhibited no significant cytotoxicity.

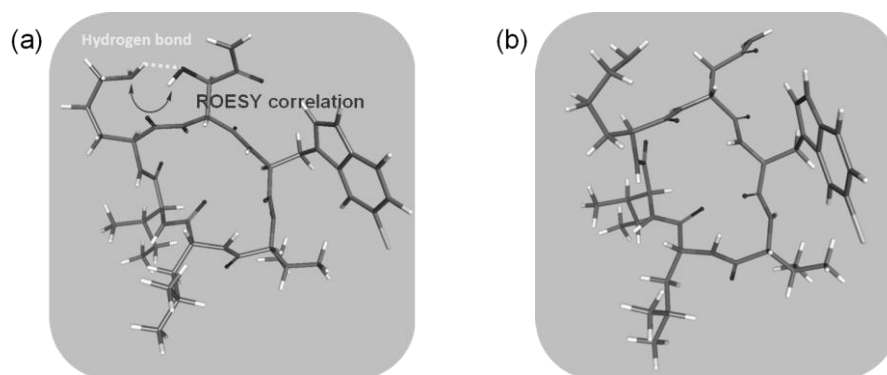


Figure 14. Energy minimized conformations of nicrophorusamides A and B (**10** and **11**): (a) nicrophorusamide A (**10**), (b) nicrophorusamide B (**11**).

2.2. Experimental Section

Bacterial isolation. Two identical burying beetles were collected using pitfall traps from Maebong Mountain, Seoul, Republic of Korea, in July 2015. The burying beetles were identified as *N. concolor* by morphological classification. The burying beetle samples were soaked in 70% aqueous ethanol (EtOH–H₂O) for 1 min and rinsed with sterilized distilled water to eliminate residual EtOH. The guts of the burying beetles were expelled with a sterilized surgical blade and diluted with 40 mL of sterilized water to extract the bacterial strains from the intestines. For bacterial isolation from the guts of the burying beetles, the bacterial suspension was spread on various isolation agar media (actinomycetes isolation agar medium, YPM agar medium, YPG agar medium, A1 agar medium, K agar medium, Czapek–Dox agar medium, ISP1 agar medium, ISP4 agar medium, starch–casein agar medium, chitin-based agar medium, and R2A agar medium), and the plates were cultivated at 25 °C for more than 14 days. The actinobacterial strain UTG9, which produces microphorusamides A and B (**10** and **11**), was separated on starch–casein agar medium (10 g of soluble starch, 1 g of casein, 0.5 g of K₂HPO₄, 18 g of agar, and 100 mg of cycloheximide per 1 L of sterilized water). The actinomycete strain was identified as *Microbacterium* sp. (97% identity) by analyzing its 16S rDNA sequence (GenBank accession number: MF000987).

Cultivation and extraction. To obtain microphorusamides A and B (**10** and **11**) produced by the *Microbacterium* sp. UTG9 strain, a spore of the bacterial strain was transferred and inoculated into a 500-mL flask containing 125 mL of YPM liquid medium (2 g of yeast extract, 2 g of peptone, and 4 g of mannitol per 1 L of sterilized water) and cultivated on rotary shaker at 200 rpm and 27 °C. After 2 days of fermentation, 10 mL of the liquid culture was moved to a 2.3-L large flask with 1 L of YPM liquid medium for scale-up and incubated on a rotary shaker at 160 rpm and 27 °C for 6 days. The entire culture (72 L) was extracted with an equivalent volume of ethyl acetate (EtOAc) in a separation funnel. The EtOAc layer was segregated from the water layer and dried by a rotary evaporator *in vacuo* to acquire 10 g of the crude extract.

Purification of nicrophorusamides A and B (10 and 11). The entire extraction was absorbed on Celite and loaded onto 20 g of C₁₈ resin for fractionation. Then, 200 mL aliquots of 20%, 40%, 60%, 80%, and 100% aqueous methanol (CH₃OH–H₂O) were collected, and a portion of each fraction was analyzed by LC/MS under a gradient solvent system (flow rate: 0.7 mL/min; UV detection: 210, 230, 254, 280, and 360 nm; 10%–100% aqueous acetonitrile [CH₃CN–H₂O] with 0.1% formic acid over 20 min) with a Phenomenex column (Luna, 100 × 4.6 mm, C₁₈(2), 5 μm). Analyzing the LC/MS data confirmed that nicrophorusamides A and B (**10** and **11**) were present in the 80% and 100% CH₃OH–H₂O fractions. To acquire the nicrophorusamides, the fractions were purified by semi-preparative reversed-phase HPLC with a YMC column (250 × 10 mm, C₁₈(2), 5 μm) under gradient solvent conditions (flow rate: 2 mL/min; UV detection: 280 nm; 35%–62% CH₃CN–H₂O with 0.2% trifluoroacetic acid over 50 min). Nicrophorusamides A (**10**, 12 mg) and B (**11**) eluted at 28.0 min and 28.5 min, respectively. Nicrophorusamide B (**11**) was purified again with another gradient solvent system (flow rate: 2 mL/min; UV detection: 280 nm; 30%–45% CH₃CN–H₂O with 0.2% trifluoroacetic acid over 50 min) for refinement. Finally, pure nicrophorusamide B (**11**, 4 mg) was obtained at 31.0 min after injection.

Nicrophorusamide A (10): white powder; $[\alpha]_D^{25} = -18$ (c 0.2, MeOH); UV (MeOH) λ_{\max} (log ϵ) 228 (3.85), 290 (3.02) nm; IR (neat) ν_{\max} 3693, 3262, 2923, 1679, 1633, 1540, 1206, 1140 cm⁻¹; For ¹H and ¹³C NMR spectral data, see Table 5; HR-FAB-MS m/z at 790.4022 [M + H]⁺ (calcd for C₃₇H₅₆ClN₉O₈, 790.4019).

Nicrophorusamide B (11): white powder; $[\alpha]_D^{25} = -20$ (c 0.2, MeOH); UV (MeOH) λ_{\max} (log ϵ) 228 (3.79), 290 (2.97) nm; IR (neat) ν_{\max} 3413, 2926, 1682, 1634, 1543, 1207, 1138 cm⁻¹; For ¹H and ¹³C NMR spectral data, see Table 5; HR-FAB-MS m/z at 774.4066 [M + H]⁺ (calcd for C₃₇H₅₆ClN₉O₇, 774.4069).

Determination of the absolute configurations at the α -carbons of the amino acid units in microphorusamide A (10). One milligram of **10** was dissolved in 1 mL of 6 N HCl and heated at 115 °C for 1 h. The heated suspension was cooled in a 0 °C ice bath for 5 min, and the HCl was vaporized *in vacuo*. To eliminate residual HCl in the vial, 1 mL of water was added to the vial and then evaporated under low pressure three times. Subsequently, the hydrolysate mixture was lyophilized for 24 h and divided into two vials. Each hydrolysate sample was dissolved in 200 μ L of 1 N NaHCO₃. Then, 100 μ L of 10 mg/mL L-FDAA in acetone was added to one of the two vials, and an equivalent proportion of D-FDAA in acetone was added to the other vial. The two reaction vials were heated at 80 °C for 3 min to accelerate the chemical derivatization. Then, 100 μ L of 2 N HCl was added to neutralize both vials, and the two reaction mixtures were diluted with 300 μ L of 50% CH₃CN–H₂O solution. Ten microliters of each reaction mixture was injected into the LC/MS under a gradient solvent system (flow rate: 0.7 mL/min; UV detection: 360 nm; 10%–60% CH₃CN–H₂O with 0.1% formic acid over 40 min) with a Phenomenex column (Luna, 100 \times 4.6 mm, C₁₈(2), 5 μ m) (Table S11). The retention times of the FDAA derivatives of the free amino acids were observed via LC/MS analysis.

Synthesis of L- β -hydroxyaspartic acid for determination of the absolute configuration at the β -carbon of D- β -hydroxyasparagine. Synthesis of L- β -hydroxyaspartic acid was conducted according to Tang *et al* (*J. Am. Chem. Soc.* **2005**, *127*, 9285–9289). A mixture of (+)-diethyl L-tartrate (1.0 g, 4.85 mmol) and anhydrous triethylamine (Et₃N, 1.6 mL, 9.70 mmol) in 10 mL of dry CH₂Cl₂ was stirred, and thionyl chloride (SOCl₂, 0.7 mL, 9.70 mmol) was added dropwise to the vial at 0 °C. The reaction vial was gradually heated at room temperature, and the reaction was quenched by adding water. The product was extracted with CH₂Cl₂. The combined organic layer was dried over MgSO₄ and concentrated *in vacuo* to acquire diethyl (2*R*, 3*R*)-2,3-*O*-sulfinyl-tartrate as a light-brown oil. The product was dissolved in 17 mL of dimethylformamide (DMF), and 347 mg of sodium azide (NaN₃, 5.34 mmol) was added to the suspension. After stirring for 13 h, the reaction mixture was

quenched with water, extracted with EtOAc, and washed with water and brine. The mixed organic layer was dried over MgSO₄ and condensed under low pressure. The reaction suspension was purified by flash column chromatography on silica gel (EtOAc:*n*-hexane = 1:3) to afford 785 mg (70%) of (2*S*, 3*R*)-diethyl 2-azido-3-hydroxysuccinate (**12**) as a colorless oil. Then, 352 mg of triphenylphosphine (PPh₃, 1.34 mmol) was added to the solution of **12** (239 mg, 1.03 mmol) in tetrahydrofuran (THF)–water (THF:H₂O = 5:1, 10 mL), and the reaction vial was heated at 70 °C and stirred for 1.5 h. The reaction mixture was then cooled to ambient temperature and concentrated *in vacuo*. The residue was purified by flash column chromatography (CH₂Cl₂:MeOH = 9:1) to obtain 181 mg (86%) of (2*S*,3*R*)-diethyl 2-amino-3-hydroxysuccinate (**13**) as a pale-yellow oil. Finally, *L*-erythro- β -hydroxyaspartic acid was obtained by acid hydrolysis of **13** with 6 N HCl at 115 °C.

(2*S*, 3*R*)-diethyl 2-azido-3-hydroxysuccinate (12**):** ¹H NMR (in CDCl₃ at 800 MHz) δ_{H} 4.60 (1H, dd, *J* = 5.4, 2.7 Hz), 4.29 (1H, d, *J* = 2.7 Hz), 4.26 (4H, m), 3.31 (1H, d, *J* = 5.4 Hz), 1.28 (3H, t, *J* = 7.2 Hz), 1.28 (3H, t, *J* = 7.2 Hz); ¹³C NMR (in CDCl₃ at 200 MHz) δ_{C} 170.7, 166.9, 72.0, 64.4, 62.7, 62.3, 14.0, 14.0; HR-ESI-MS *m/z* at 232.0932 [M + H]⁺ (calcd for C₈H₁₄N₃O₅, 232.0928).

(2*S*, 3*R*)-diethyl 2-amino-3-hydroxysuccinate (13**):** ¹H NMR (in CDCl₃ at 600 MHz) δ_{H} 4.47 (1H, d, *J* = 3.0 Hz), 4.22–4.14 (4H, m), 3.88 (1H, d, *J* = 3.0 Hz), 1.24 (3H, t, *J* = 7.3 Hz), 1.22 (3H, t, *J* = 7.3 Hz); ¹³C NMR (in CDCl₃ at 150 MHz) δ_{C} 171.9, 171.7, 72.7, 61.8, 61.3, 57.5, 14.0; HR-ESI-MS *m/z* at 206.1030 [M + H]⁺ (calcd for C₈H₁₆NO₅, 206.1028).

Determination of the absolute configuration at the β -carbon of D- β -hydroxyasparagine in nicrophorusamide A (10**).** Because *L*-threo- β -hydroxyaspartic acid [(2*S*,3*R*)-2-amino-3-hydroxysuccinic acid] was commercially available among four diastereomers of β -hydroxyaspartic acid, an authentic sample of *L*-threo- β -hydroxyaspartic acid was purchased (CAS No. 7298-99-9, Tocris). Then *L*-erythro- β -hydroxyaspartic acid [(2*S*,3*S*)-2-amino-3-

hydroxysuccinic acid] was synthesized via several reaction steps as described in the supporting information (Figure S90). These two synthetic amino acids were derivatized with L-FDAA and injected into LC/MS under a gradient solvent system (flow rate: 0.7 mL/min; detection: UV 360 nm; 10%–30% CH₃CN–H₂O with 0.1% formic acid over 40 min) to compare retention times. The retention times of the L-FDAA derivatives of *L-threo*- β -hydroxyaspartic acid (2*S*,3*S*-L) and *L-erythro*- β -hydroxyaspartic acid (2*S*,3*R*-L) were 19.3 min and 26.8 min, respectively. To elucidate the absolute configuration at the β -carbon of D- β -hydroxyasparagine in **10**, these L-FDAA derivatives were co-injected with the D-FDAA derivative of D- β -hydroxyaspartic acid in the hydrolysate of **10**. The LC/MS results revealed that D-FDAA derivative of D- β -hydroxyaspartic acid from the hydrolysate of **10** showed the identical retention time with L-FDAA derivative of authentic *L-threo*- β -hydroxyaspartic acid (Figure S91). This result demonstrated that the D-FDAA derivative of D- β -hydroxyaspartic acid (2*R*-2-amino-3-hydroxysuccinic acid) from the hydrolysate of **10** is an enantiomer of the L-FDAA derivative of authentic *L-threo*- β -hydroxyaspartic acid, thus possessing 3*R* configuration. Therefore, D- β -hydroxyasparagine in nicrophorusamide A (**10**) was elucidated as D-*threo*- β -hydroxyasparagine.

Determination of the absolute configuration of the β -carbon of L-isoleucine in nicrophorusamide A (10**).** The hydrolysate of **10** was obtained by the same procedures described above and dissolved in 1 mL of water. For the chemical derivatization of the L-isoleucine residue in **10**, 100 μ L of triethylamine and 100 μ L of 1% GITC solution in acetone were added to the reaction vial. The reaction was processed at room temperature (25 °C) for 15 min and quenched with 100 μ L of 5% acetic acid solution. Then, 20 μ L of the reaction mixture was analyzed by LC/MS under a gradient solvent system (flow rate: 0.3 mL/min; UV detection: 254 nm; 35%–50% CH₃CN–H₂O with 0.1% formic acid over 80 min) with a Phenomenex column (Gemini, 250 \times 4.6 mm, C₁₈(2), 5 μ m). The GITC derivative eluted at 60.1 min. GITC derivatives of authentic L-isoleucine (CAS No. 73-32-5, Sigma–Aldrich) and L-*allo*-isoleucine (CAS No. 1509-34-8, Sigma) were prepared via the same procedure and

injected into the LC/MS using the same analysis conditions. The GITC derivatives of authentic L-isoleucine and L-*allo*-isoleucine eluted at 60.7 min and 60.0 min, respectively. Finally, the amino acid residue in **10** was identified as L-*allo*-isoleucine.

Molecular modeling of nicrophorusamides A and B (10 and 11). To identify the conformational difference between nicrophorusamides A and B, computational DFT (density functional theory) calculation was performed. The initial structural energy minimizations of **10** and **11** were established by using Avogadro 1.2.0 with UFF force field.⁴² An array of energy optimization was processed via Tmolex 4.3.1 with the DFT settings (B3-LYP functional/ M3 gridsize) and geometry optimization options (energy 10^{-6} Hartree, gradient norm $|dE/dxyz| = 10^{-3}$ Hartree/bohr).

Antibacterial activity assay. The antibacterial activities of nicrophorusamides A and B (**10** and **11**) were determined by evaluating their MIC values; ampicillin was used as a reference compound. Three species of Gram-positive bacteria (*S. aureus* ATCC 25923, *E. faecalis* ATCC 19433, and *E. faecium* ATCC 19434) and two species of Gram-negative bacteria (*S. enterica* ATCC 14028 and *E. coli* ATCC 25922) were used in this study. The bacteria were grown overnight in Mueller–Hinton broth (MHB) at 37 °C, harvested by centrifugation, and washed twice with sterile distilled water. Each compound was dissolved in DMSO and diluted with MBH to prepare serial twofold dilutions of 128 to 0.03 µg/mL. The final DMSO concentration was maintained at 1% by adding DMSO to the medium. In each well of a 96-well plate, 190 µL of MBH containing **10**, **11** and ampicillin was mixed with 10 µL of broth containing approximately 10^7 colony-forming units (cfu)/mL of the test bacteria (final: 5×10^5 cfu/mL). The plates were incubated for 24 h at 37 °C, and the MIC value was defined as the lowest concentration of the test compound that inhibited bacterial growth.

Table 5. ^1H and ^{13}C NMR Data for microphorusamides A and B (**10** and **11**) in DMSO- d_6 .

no.	microphorusamide A (10)				microphorusamide B (11)			
	δ_{C}^a	type	δ_{H}^b	mult (J in Hz)	δ_{C}^a	type	δ_{H}^c	mult (J in Hz)
1	171.1	C			170.8	C		
2	53.5	CH	4.62	ddd (7.5, 7.5, 7.5)	53.4	CH	4.51	ddd (7.5, 7.5, 7.5)
2-NH			7.98	d (7.5)			7.80	d (7.5)
3a	26.7	CH ₂	3.11	dd (14.5, 7.5)	26.5	CH ₂	3.18	dd (14.5, 7.5)
3b			2.89	dd (14.5, 7.5)			2.88	dd (14.5, 7.5)
4	109.8	C			109.8	C		
5	125.4	CH	7.15	d (2.0)	125.7	CH	7.18	d (2.0)
5-NH			11.03	d (2.0)			11.06	d (2.0)
6	134.5	C			134.5	C		
7	112.7	CH	7.32	d (8.5)	112.8	CH	7.32	d (8.5)
8	120.7	CH	7.05	dd (8.5, 2.0)	120.7	CH	7.04	dd (8.5, 2.0)
9	122.9	C			123.0	C		
10	117.5	CH	7.57	d (2.0)	117.5	CH	7.54	d (2.0)
11	128.4	C			128.4	C		
12	169.4	C			170.6	C		
13	55.8	CH	4.60	dd (8.5, 2.5)	49.3	CH	4.55	dd (8.0, 6.0)
13-NH			7.62	d (8.5)			7.95	d (8.0)
14	70.8	CH	4.47	dd (6.0, 2.5)	36.0	CH ₂	2.56	d (6.0)
14-OH			5.85	d (6.0)				
15	173.2	C			171.8	C		
15-NH _{2a}			7.31	d (2.0)				
15-NH _{2b}			7.28	d (2.0)				
16	170.6	C			170.5	C		
17	53.1	CH	4.01	ddd (7.5, 7.5, 6.0)	52.3	CH	4.19	ddd (7.5, 7.5, 6.0)
17-NH			8.43	d (6.0)			7.81	d (7.5)
18a	26.8	CH ₂	1.84	m	28.0	CH ₂	1.85	m
18b			1.64	m			1.60	m
19	23.7	CH ₂	1.50	m	23.8	CH ₂	1.52	m
20	38.4	CH ₂	2.79	br s	38.5	CH ₂	2.79	m
20-NH ₂			7.66	br s			7.76	t (7.0)
21	171.7	C			171.2	C		
22	56.5	CH	4.24	dd (7.5, 6.0)	57.1	CH	4.11	dd (7.5, 7.0)
22-NH			7.87	d (7.5)			8.05	d (7.0)
23	36.3	CH	1.89	m	35.9	CH	1.92	m
24a	25.6	CH ₂	1.35	m	25.7	CH ₂	1.29	m
24b			1.16	m			1.19	m
25	11.3	CH ₃	0.86	d (7.5)	11.5	CH ₃	0.84	d (7.0)
26	14.5	CH ₃	0.85	d (7.5)	14.6	CH ₃	0.85	d (7.0)
27	172.1	C			172.8	C		
28	51.5	CH	4.23	dd (7.5, 7.5)	51.4	CH	4.43	dd (7.0, 6.5)
28-NH			7.45	d (7.5)			7.61	d (7.0)
29	39.6	CH ₂	1.57	dd (7.5, 7.5)	41.0	CH ₂	1.50	m
30	24.3	CH	1.47	m	24.2	CH	1.49	m
31	22.7	CH ₃	0.87	d (6.5)	22.5	CH ₃	0.90	d (6.0)
32	21.8	CH ₃	0.83	d (6.5)	22.6	CH ₃	0.85	d (7.0)
33	170.4	C			170.4	C		
34	60.4	CH	3.75	dd (7.0, 7.0)	59.8	CH	3.84	dd (8.0, 7.5)
34-NH			7.81	d (7.0)			7.92	d (8.0)
35	29.1	CH	1.84	m	29.8	CH	1.90	m
36	18.5	CH ₃	0.72	d (6.5)	19.0	CH ₃	0.70	d (6.5)
37	18.8	CH ₃	0.69	d (6.5)	18.1	CH ₃	0.64	d (6.5)

^a 125 MHz, ^b 600 MHz, ^c 500 MHz

Table 6. Inhibitory activities of nicrophorusamides A and B (**10** and **11**) against bacterial strains.

	MICs ($\mu\text{g/mL}$)				
	Gram-positive			Gram-negative	
	<i>S. aureus</i>	<i>E. faecalis</i>	<i>E. faecium</i>	<i>S. enterica</i>	<i>E. coli</i>
10	8	16	16	16	>128
11	64	128	128	>128	>128
ampicillin	0.13	0.5	0.25	0.13	8

3. Coprisamides C and D, Antituberculosis
Cinnamic Acid Containing Cyclic Peptides from
the Gut *Micromonospora* sp. of the Carrion Beetle
Silpha perforata

3.1. Results and Discussion

Coprisamide C (**14**) was acquired as a white powder during consecutive chromatographic purifications. The unsaturation number of **14** was deduced as 17 based on their molecular formula ($C_{47}H_{70}N_8O_{11}$), which was determined by high-resolution electrospray ionization mass spectrometry (HR-ESI-MS) data coupled with 1H and ^{13}C NMR spectroscopic data (Table 7). Further analysis of 1H NMR spectrum of coprisamide C (**14**) along with HSQC NMR spectroscopic data indicated the existence of nine amide protons (δ_H 8.73, 8.57, 8.51, 8.39, 8.15, 8.11 (2H), 8.01, and 7.32), six olefinic methine protons (δ_H 7.57, 6.91, 6.48, 6.40, 6.12, and 5.91), and four aromatic protons (δ_H 7.61, 7.38, 7.31, and 7.24) in the downfield region based on their chemical shifts and $^3J_{HH}$ values (olefinic protons: $^3J_{HH} = 11.5\text{--}15.0$ Hz; aromatic protons: $^3J_{HH} = 7.5$ Hz). Furthermore, seven α amino methine proton signals at δ_H 4.7–3.5 (δ_H 4.68, 4.50, 4.28, 4.27, 4.24, 3.82, and 3.56) were detected, which suggested that coprisamide C (**14**) incorporates seven amino acid units in the structure. The ^{13}C NMR spectrum of **14** showed signals of nine carbonyl carbons (δ_C 176.0, 172.7, 171.5, 170.3, 169.7, 169.5, 169.2, 169.0, and 164.5) and twelve sp^2 carbons (δ_C 137.0, 136.9, 136.8, 133.3, 131.9, 130.0, 129.0, 127.6, 126.9, 126.3, 125.6, and 122.8), which explained 15 out of 17 equivalent number of coprisamide C (**14**); this result revealed that coprisamide C (**14**) is a bicyclic compound. In addition, carbon signals of one oxygen-bound carbon (δ_C 63.2) and seven carbons at α -position of amino acids (δ_C 58.0, 57.6, 54.7, 52.9, 50.5, 49.9, and 49.4) were also detected.

All the one-bond $^1H\text{--}^{13}C$ correlations were assigned by interpreting HSQC NMR spectrum with 1H and ^{13}C NMR spectroscopic data (Table 7). Combinational analysis of COSY, HMBC, and TOCSY NMR data revealed that coprisamide C (**14**) possessed five common amino acids (alanine, serine, leucine, and two valines) and two non-proteinogenic amino acid units such as β -methyl-aspartic acid (β -Me-Asp) and 2,3-diaminopropionic acid (Dap). Initially, the spin system from H₃-4 (δ_H 0.98) to 2-NH (δ_H 8.51) was successfully identified based on the

sequential COSY/TOCSY correlations, constructing C-4–C-3–C-2–2-NH connectivity. HMBC correlations from H-2 (δ_{H} 3.82) to C-1 (δ_{C} 169.5) and from H₃-4/H-3 (δ_{H} 2.98) to C-5 (δ_{C} 176.0) indicated that the carbonyl carbon C-1 and C-5 should be connected to C-2 (δ_{C} 54.7) and C-3 (δ_{C} 38.6), respectively. As a result, this amino acid unit was elucidated as β -methylaspartic acid unit (Figure 16). The 2,3-diaminopropanoic acid (Dap) unit in **14** was also determined by interpreting COSY, TOCSY and HMBC correlations. TOCSY correlations of 7-NH (δ_{H} 8.15), H-7 (δ_{H} 4.68), H₂-8 (δ_{H} 4.01 and 2.89), and 8-NH (δ_{H} 8.57) revealed that these protons belong to a spin system. The connectivity among these protons was assigned by ¹H–¹H COSY correlations. Additionally, carbonyl carbon C-6 (δ_{C} 169.2) was linked to C-7 (δ_{C} 49.9) based on a three-bond ¹H–¹³C HMBC correlations from H-7 to C-6 showing this amino acid to be a Dap unit (Figure 16). The proteinogenic amino acid residues in **14** such as two valines (Val-1 and Val-2), leucine (Leu), serine (Ser), and alanine (Ala) were also confirmed in a straightforward manner by comprehensive analysis of the 1D and 2D NMR spectra data.

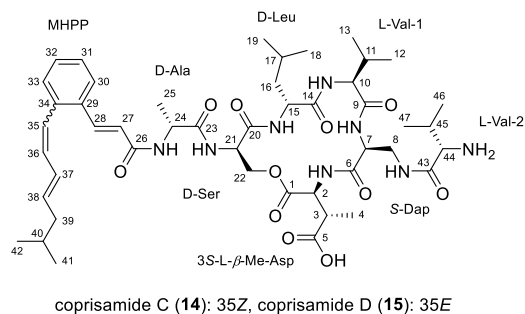


Figure 15. Chemical structures of coprisamides C and D (**14** and **15**).

The last moiety, which must explain the UV spectrum (λ_{max} 267, 288 nm), was also determined based on the COSY, TOCSY, and HMBC NMR spectra. TOCSY correlations indicated that there are three more discrete spin systems to be elucidated. One of the spin systems was identified as C-27–C-28 by COSY correlation between H-27 (δ_{H} 6.91) and H-

28 (δ_{H} 7.57). An array of ^1H – ^1H correlations of H-30, H-31, H-32, and H-33 (δ_{H} 7.24, 7.38, 7.31 and 7.61, respectively) and their ^1H – ^1H coupling constants (7.5 Hz) elucidated another spin system as a 6-membered aromatic ring. The fully substituted carbons composing the aromatic structure (C-29 and C-34) were assigned by HMBC NMR data. Based on HMBC correlations from H-30/H-32 to C-34 (δ_{C} 136.9) and from H-31/H-33 to C-29 (δ_{C} 133.3) along with C-30–C-31–C-32–C-33 spin system, the six-membered aromatic ring structure was established. The last spin system was successfully constructed from H-35 (δ_{H} 6.48) to H₃-42 (δ_{H} 0.83) based on the consecutive COSY correlations among these protons. HMBC correlations from H₃-42 (δ_{H} 0.83) to C-39 (δ_{C} 41.6), C-40 (δ_{C} 27.9), and C-41 (δ_{C} 22.1) constructed the terminal dimethyl structure. These three spin systems were assembled based on the ^1H – ^{13}C three-bond correlations. A HMBC signal from H-27 to C-26 (δ_{C} 164.5) elucidated the carbonyl carbon C-26 is linked to C-27 (δ_{C} 122.8). HMBC correlations from H-27/H-28 to C-29 and from H-35/H-36 (δ_{H} 6.40) to C-34 finally disclosed the last partial structure, 3-[2-(6-methyl-1,3-heptenyl)phenyl]-2-propenoic acid (MHPP), 2-alkenyl cinnamic acid (Figure 16).

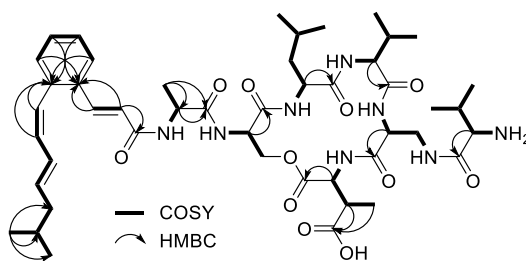


Figure 16. Key COSY and HMBC correlations for structural determining of coprisamide C (14).

The connections of the partial structures were elucidated based on 2,3-bond ^1H – ^{13}C couplings (Figure 17). HMBC correlations from α -proton of β -Me-Asp (H-2) to three discrete carbonyl carbons C-1, C-5, and C-6 were found. However, C-1 and C-5 should be connected

to C-2 and C-3 based on ^1H - ^{13}C HMBC correlations (H-3/C-1, H-3/C-5, and H-4/C-5), respectively, the other carbonyl carbon C-6 could be linked to 2-NH. In this way, the other amino acid units also could be connected to each other, resulting β -Me-Asp-Dap-Val-Leu-Ser-Ala sequence. This sequence was further crosschecked based on the ROESY correlations between amide protons and α -protons of the amino acid units. 2-alkenyl cinnamic acid unit (MHPP) was connected to 24-NH (δ_{H} 8.01) based on a HMBC correlation of 24-NH/C-26 and a ROESY correlation between 24-NH and H-27. The additional Val unit (Val-2) was located adjacent to Dap based on the three- and two-bond HMBC correlations of 8-NH/C-43 (δ_{C} 168.0). Although there was no more observed HMBC correlation, ROESY correlation from 8-NH to α - and β -amino protons, H-44 (δ_{H} 3.56) and H-45 (δ_{H} 2.03) of Val-2 supported this branched connectivity. In addition, an ester bond could be established based on three-bond ^1H - ^{13}C correlation from H-22 to C-1 constructing a macrocyclic ring structure of **14**. Finally, coprisamide C (**14**) was revealed as a cyclic depsipeptide containing 2-alkenyl cinnamic acid (MHPP) and a branched amino acid unit attached to 2,3-diaminopropanoic acid (Dap).

The geometric configurations of double bonds in MHPP were identified based on $^3J_{\text{HH}}$ coupling constant values. By careful analysis of ^1H NMR spectrum, $^3J_{\text{H}27\text{H}28}$ and $^3J_{\text{H}37\text{H}38}$ were measured as 15.5 Hz whereas $^3J_{\text{H}35\text{H}36}$ was 11.0 Hz. Therefore, the geometries in **14** could be identified as 27*E*, 35*Z*, and 37*E*, respectively. Finally, the cinnamoyl moiety of **14** was identified as 3-[2-(6-methyl-1-(*Z*)-3-(*E*)-heptenyl)phenyl]-2-(*E*)-propenoic acid.

The absolute configurations at α -carbons of the amino acids in **14** were determined by adopting advanced Marfey's method.³⁵ The acid hydrolysate of **14** was separately derivatized with L- and D-1-fluoro-2,4-dinitrophenyl-5-alanine amide (L- and D-FDAA) and subsequently analyzed by using LC/MS using a reversed-phase C₁₈ column (Figure S116). The elution orders of the FDAA derivatives established the amino acid residues in **14** as L- β -Me-Asp, *S*-Dap, L-Val-1, D-Leu, D-Ser, D-Ala, and L-Val-2, respectively (Table S14).

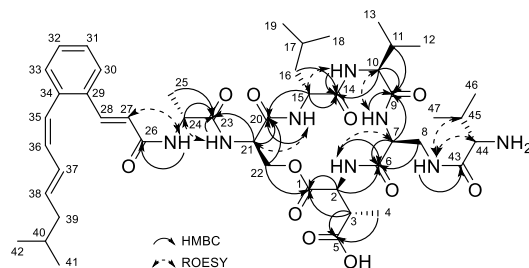


Figure 17. Determining amino acid sequence of coprisamide C (**14**) based on HMBC and ROESY correlations.

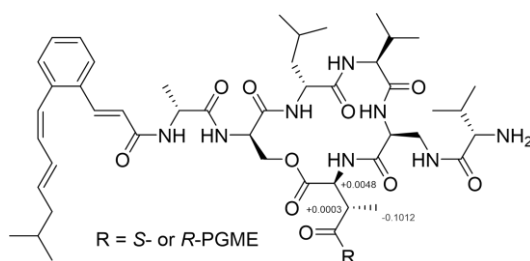


Figure 18. Identification of the absolute configuration at C-3 based on the $\Delta\delta_{S-R}$ values in ppm of the *S*- and *R*-PGME amides of coprisamide C (**14a** and **14b**).

The absolute configuration at C-3 stereogenic center, which located in β -Me-Asp unit, was assigned through *S*- and *R*-phenylglycine methyl ester (*S*- and *R*-PGME) derivatization²⁰ and subsequent analysis of ¹H and COSY NMR data of *S*- and *R*-PGME amides (**14a** and **14b**). The $\Delta\delta_{S-R}$ values established that C-3 of **14** has *S* configuration (Figure 18). This result was further confirmed by *J*-based configuration analysis. Because α - and β -amino protons of β -Me-Asp unit in **14**, H-2 and H-3, showed a large coupling constant ($^3J_{H2H3} = 10.5$ Hz), anti-relationship between C-2 and C-3 was deduced. Then the rotamer (Figure S117) was constructed based on H-2/H₃-4, H₃-4/2-NH, and 2-NH/H-3 REOSY correlations. Following the rotamer model, the absolute configuration at C-3 could be deduced as *S* again because of 2*S* configuration by advanced Marfey's method.

Coprisamide D (**15**) was also purified as amorphous white powdery form, and the HR-ESI-MS data indicated the molecular formula as $C_{47}H_{70}N_8O_{11}$ with 17 unsaturation number, which were identical to **14**. Because coprisamide D showed high similarity in its NMR spectra to those of **14** (Table 7), the NMR data of **14** and **15** were carefully compared. As a result, coprisamide D was revealed as a geometric isomer of **14**, which possesses 35*E* geometry based on the $^3J_{H_{35}H_{36}}$ value ($J = 15.5$ Hz) whereas **14** has 35*Z* configuration ($J_{H_{35}H_{36}} = 11.5$ Hz). Additionally, the circular dichroism (CD) spectra of **14** and **15** (Figure S118) are virtually identical and their common biosynthetic origin deduced that the absolute configurations of the amino acid units in **15** are the same as those in **14**.

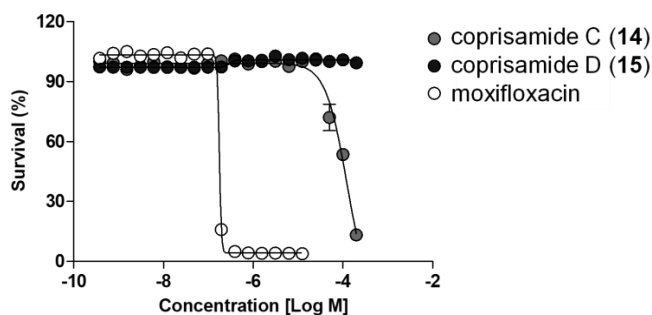


Figure 19. Dose response curve of coprisamides C and D (**14** and **15**) against *Mycobacterium tuberculosis* mc² 6230. Moxifloxacin was used for positive control.

Coprisamides C and D (**14** and **15**) were tested for anti-tuberculosis activity against *Mycobacterium tuberculosis* (Mtb) mc² 6230, by using the resazurin microtiter assay (REMA). The MIC₅₀ (the lowest concentration of antibiotics at which 50% of the isolates were inhibited) values of **14** and **15** were calculated based on the triplicated results and compared with those of moxifloxacin, which has been used for multidrug-resistant tuberculosis (MDR-TB) treatment. Following the results, only coprisamide C (**14**) showed mild growth inhibition activity against the test strain with MIC₅₀ value at 95.7 μ M. Coprisamide D (**15**) did not display any significant activity against Mtb strain (Figure 19).

The reference compound moxifloxacin was found to be effective against Mtb with low MIC₅₀ value (0.18 μ M), as described previously.⁴³

Antibacterial and antifungal activities of coprisamides C and D (**14** and **15**) against pathogenic bacteria and fungi were also evaluated. However, **14** and **15** did not display growth inhibition activity (MIC values: >128 μ g/mL) against the bacteria (*Staphylococcus aureus* ATCC 25923, *Enterococcus faecalis* ATDD 19433, *Enterococcus faecium* ATCC 19434, *Klebsiella pneumoniae* ATCC 10031, *Salmonella enterica* ATCC 14028, and *Escherichia coli* ATCC 25922) and fungi (*Aspergillus fumigatus* HIC 6094, *Trichophyton rubrum* NBRC 9185, *Trichophyton mentagrophytes* IFM 40996, and *Candida albicans* ATCC 10231).

Approximately 7.8 Mb of draft genome sequence data could be acquired from the coprisamides C and D producer strain *Micromonospora* sp. UTJ3. Analysis of the genomic data through antiSMASH 5.0⁴⁴ revealed that the coprisamides C and D biosynthetic gene cluster (BGC, *cpr*) consisted of two genes encoding modular non-ribosomal peptide synthases (NRPSs), and several characteristic genes involved in biosynthesis of nonproteinogenic amino acids and modified cinnamic acid unit (Figure 20a). Based on the antiSMASH result, the NRPSs were identified to be composed of six NRPS modules and predicted to produce six-membered cyclic non-ribosomal peptide, which was consistent with coprisamides. Additionally, three epimerase domains (E domain) could be found at downstream of modules for Ala, Ser, and Leu, which suggested identical result with chemically determined absolute configurations (Figure 20b).

Biosynthetic pathways of cinnamate units in coprisamides seemed to resemble those of atratumycin,⁴⁵ which also contained modified cinnamic acid unit, 3-(2-methyl phenyl)-2-(*E*)-propenoic acid, in the structure. Although the exact procedures and mechanisms in their biosynthesis were not determined experimentally, general biosynthetic pathways and enzyme candidates for formation of the cinnamates could be predicted based on the presence of several homologous enzymes between *cpr* and *atr* cluster. 10 genes, which showed high

similarity with cinnamate synthases of atratumycin, were found from *cpr* cluster. Those genes such as ketosynthase/chain length factor (*cprA–D*), ketoreductase (*cprJ*), dehydratase (*cprK* and *cprL*) and *cis–trans* isomerase (*cprE*) were speculated to compose cinnamoyl synthetic gene cassette, constructing cinnamic acid units during biosynthesis of coprisamides (Figure 20c).

2,3-Diaminopropionate unit in coprisamides was predicted to be synthesized from *O*-phosphoserine by CprF and CprG because those genes displayed homology with 2,3-diaminopropionate biosynthesis proteins SbnA and SbnB from staphyloferrin B gene cluster (*sbm* cluster), respectively.⁴⁶ In the case of *sbm*, SbnA produce *N*-(1-amino-1-carboxy-2-ethyl)-glutamic acid by using L-glutamic acid and *O*-phospho-L-serine, and then this intermediate is hydrolyzed as α -ketoglutarate and L-2,3-diaminopropionic acid by SbnB in biosynthetic pathway of staphyloferrin B. Therefore, Dap unit in coprisamides could be suggested to be synthesized in a similar way as like that of staphyloferrin B biosynthesis (Figure 20d).

During functional analysis of genes from *cpr* cluster, genes coding glutamate mutase (methylasspartate mutase) were found based on their translated amino acid sequences. Following previously reported investigation about the glutamate fermentation pathway in *Clostridium* spp.,⁴⁷ the enzyme catalyzed the reversible conversion of L-glutamic acid to 3*S*-L- β -aspartic acid (Figure 20e). In the case of *cpr* cluster, the methylasspartate mutase gene was coded in two genes discretely, large subunit (*cprO*) and small subunit (*cprN*).

Coprisamides A and B⁶ have the most similar structure with coprisamides C and D (**14** and **15**). They bear 3*S*-L- β -Me-Asp, *S*-Dap, two L-Val, D-Leu, D-Ser, and D-Ala in their structure, which were identical with **14** and **15**. They also possess modified cinnamic acid units in their structure, but not identical one with **14** and **15**: coprisamides C and D have 3-[2-(6-mehtyl-1-(*Z*)-3-(*E*)-heptenyl)phenyl]-2-(*E*)-propenoic acid whereas coprisamides A and B have 3-[2-(1-(*Z*)-3-(*E*)-5-(*E*)-heptenyl)phenyl]-2-(*E*)-propenoic acid. Atratumycin⁴⁵ and skyllamycin⁴⁸, which also possess modified cinnamate in the structure, showed difference

from **14** and **15** in the detailed structure of cinnamoyl moiety. Another branched Dap unit containing non-ribosomal peptide, GE23077,⁴⁹ the branch is not a kind of amino acid, so there should be distinction from coprisamides in biosynthetic level.

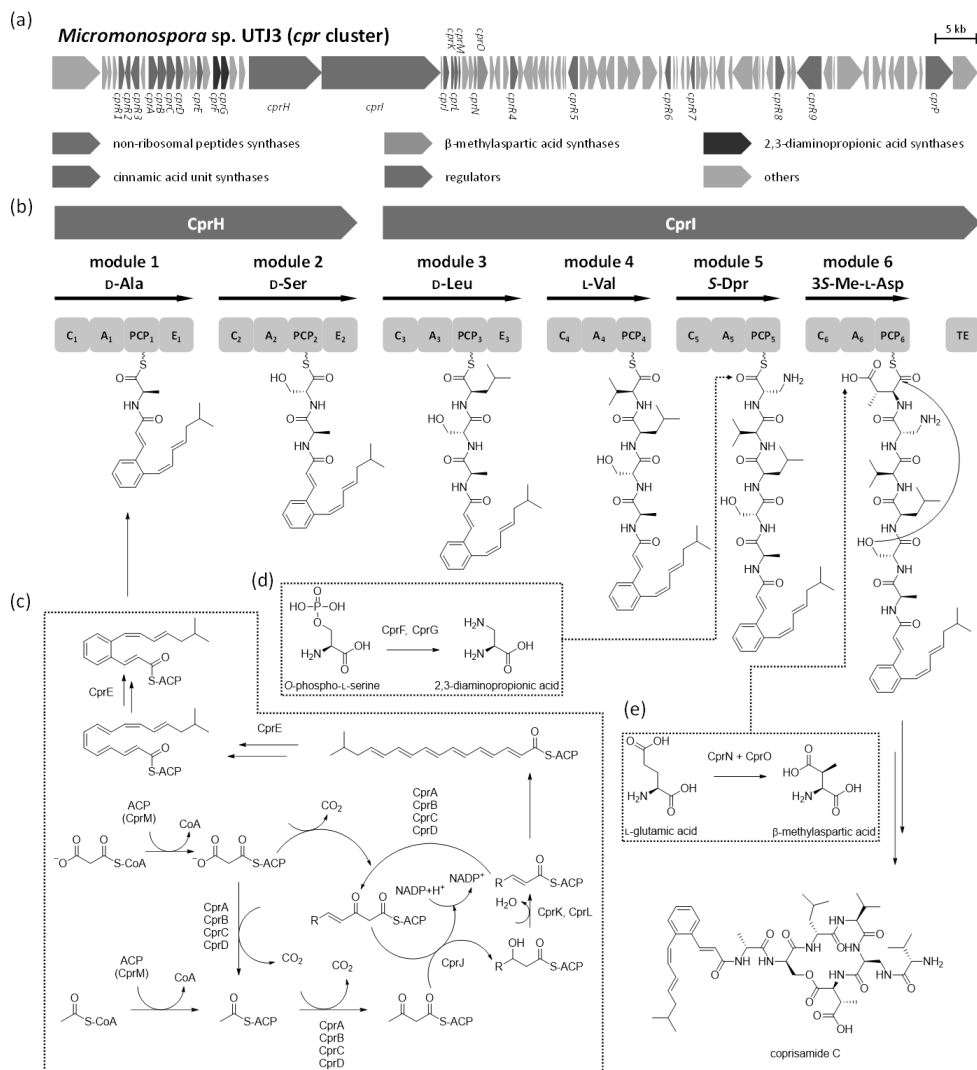


Figure 20. (a) Biosynthetic gene clusters and (b) biosynthetic procedures for coprisamides C and D (**14** and **15**). C, condensation domain; A, adenylation domain; PCP, peptide carrier protein; E, epimerase; TE, thioesterase. (c-e) Predicted biosynthetic pathway for cinnamic acid unit, 2,3-diaminopropionic acid unit, and β-methyl-aspartic acid unit.

3.2. Experimental Section

Bacterial isolation. Carrion beetle specimens, which were morphologically identified as *Silpha perforata*, were collected in Gwanak Mountain, Seoul, Republic of Korea in July 2017. To isolate actinobacterial strains from the beetle, the guts of the specimens were extracted, suspended with sterilized water, spread onto various kinds of bacterial isolation agar media, and incubated at 30 °C for 14 days. *Micromonospora* sp. UTJ3 was grown on potato dextrose agar (PDA) medium and isolated as a single strain. Analysis of 16S rDNA sequence of the strain UTJ3 indicated that this actinobacterial strain belongs to the genus *Micromonospora* (GenBank accession no. MT312832, 98% identity with *Micromonospora vridifaciens* GenBank accession no. LT607411)

Cultivation and extraction. *Micromonospora* sp. UTJ3 strain was initially inoculated in 200 mL of YEME liquid medium (4 g of yeast extract, 10 g of malt extract, and 4 g of glucose per 1 L of sterilized water) and incubated at 30 °C in a rotary shaker at 160 rpm. After 3 days, 15 mL of the bacterial culture was transferred into 1 L volume of modified K liquid medium (2 g of yeast extract, 2 g of peptone, 2 g of glucose, 3 g of mannitol, 5 g of malt extract, 5 g of soybean peptone, and 5 g of soluble starch per 1 L of sterilized water) for scale up. This culture stage was maintained for 7 days. The whole culture (18 L) was moved to a separation funnel and extracted with the equivalent volume of ethyl acetate (EtOAc). The EtOAc layer was separated from the water phase and concentrated by using a rotary evaporator *in vacuo* to acquire 10 g of dry extract.

Purification of coprisamides C and D (14 and 15). The entire extract was adsorbed on Celite and loaded onto a reversed-phase flash chromatography column (20 g of YMC C₁₈ resin, 60 × 40 mm). 200 mL of 20%, 40%, 60%, and 100% CH₃OH–H₂O were sequentially used for fractionation. 20 µL aliquot of each fraction was analyzed by LC/MS and the LC/MS data showed that **14** and **15** eluted in the 100% CH₃OH fraction. The fraction was subjected to semi-preparative reversed-phase HPLC composed of a reversed-phase column (250 × 10

mm, YMC C₁₈(2)) using a gradient solvent system (40%–65% CH₃CN–H₂O over 50 min with 0.1% trifluoroacetic acid, flow rate: 2 mL/min, detection: UV 280 nm). Coprisamides C and D (**14** and **15**) eluted at 34 min and 38 min, respectively. Coprisamide C (**14**) was re-injected into a reversed-phase HPLC coupled with C₁₈ column (Phenomenex, 250 × 4.6 mm) and further purified at the retention time at 39.5 min under gradient solvent conditions (30%–50% CH₃CN–H₂O over 40 min with 0.1% trifluoroacetic acid, flow rate: 1 mL/min, detection: UV 280 nm). Coprisamide D (**15**) was also purified (Phenomenex C₁₈(2) 250 × 4.6 mm; 33%–53% CH₃CN–H₂O over 40 min with 0.1% trifluoroacetic acid, flow rate: 1 mL/min, detection: UV 280) and obtained as pure state at 37.5 min.

Coprisamide C (14): white powder; $[\alpha]_{\text{D}}^{20} = -1.86$ (c 0.2, MeOH); UV (MeOH) λ_{max} (log ϵ) 267 (3.35), 288 (3.31) nm; IR (neat) ν_{max} 3670, 2970, 2868, 2359, 2317, 1679, 1518, 1205, 1143, 1054, 1043, 1024 cm⁻¹; For ¹H and ¹³C NMR spectral data, see Table 7; HR-ESI-MS m/z at 923.5242 [M+H]⁺ (calcd for C₄₇H₇₁N₈O₁₁, 923.5237).

Coprisamide D (15): white powder; $[\alpha]_{\text{D}}^{20} = -0.61$ (c 0.2, MeOH); UV (MeOH) λ_{max} (log ϵ) 267 (3.21), 288 (3.18) nm; IR (neat) ν_{max} 3655, 2930, 2864, 2358, 2317, 1686, 1518, 1207, 1139, 1054, 1042, 1024 cm⁻¹; For ¹H and ¹³C NMR spectral data, see Table 7; HR-ESI-MS m/z at 923.5242 [M+H]⁺ (calcd for C₄₇H₇₁N₈O₁₁, 923.5237).

Determination of the absolute configurations at the α -carbons of coprisamide C (14).

For acquiring free amino acid units, 2 mg of coprisamide C (**14**) was dissolved with 1 mL of 6 N HCl and heated at 100 °C for 2 hours. The hydrolysate was cooled in an ice bath (0 °C) for 5 min and vaporized *in vacuo* rapidly. For eliminating residual HCl, 1 mL of deionized water was added into the vial, dried completely under low pressure for three times. Then, the dried mixture was lyophilized for 24 h and divided into two vials. For acquiring L-FDAA derivatives of the amino acids, the hydrolysate in one of the vials was re-dissolved with 500 μ L of 1 N NaHCO₃ and treated with 100 μ L of L-FDAA solution (10 mg/mL in acetone). The

reaction mixture was stirred at 80 °C and quenched with 2 N HCl (250 μ L) after 10 min. In the same manner, D-FDAA derivatives were obtained. The products were diluted with 50% CH₃CN–H₂O solution for LC/MS analysis (Phenomenex, C₁₈(2), 100 \times 4.6 mm; 10%–60% CH₃CN–H₂O with 0.1% formic acid over 50 min; flow rate: 0.7 mL/min; UV detection: 340 nm). The retention times of each FDAA derivatives were confirmed by MS ion extraction (Figure S116).

Determination of the stereogenic center at the β -carbon of β -methyl-aspartic acid of coprisamide C (14). The absolute configuration at the β -carbon of β -Me-Asp in coprisamide C (14) was identified by PGME (phenylglycine methyl ester) derivatization. For preparing *S*-PGME amide product (14a), 2 mg of 14 was dissolved in 500 μ L of *N,N*-dimethylformamide (DMF) and treated with (benzotriazol-1-yloxy)tripyrrolidinophosphonium hexafluorophosphate (PyBOP, 3.3 mg), 1-hydroxybenzotriazole hydrate (HOBt, 1.5 mg), 4-methylmorpholine (100 μ L), and *S*-PGME (5.0 mg). The derivatization was proceeded at room temperature for 1 h and quenched by adding 5% HCl solution (1 mL). The reaction mixture was subjected to reversed-phase HPLC and purified with using C₁₈ column (YMC, 250 \times 10 mm) under gradient solvent conditions (45%–75% CH₃CN–H₂O with 0.1% trifluoroacetic acid over 60 min; flow rate: 2 mL/min; detect: UV 280 nm). The desired product, *S*-PGME amide of 14 (14a), eluted at 54 min. *R*-PGME amide of 14 (14b) was also prepared in the same method (retention time: 52.5 min under the identical HPLC conditions). The molecular formulae of 14a and 14b were deduced as C₅₆H₇₉N₉O₁₂ based on their LR-ESI-MS data ([M+H]⁺ *m/z* at 1070, [M+Na]⁺ *m/z* at 1092, and [M-H][−] *m/z* at 1068).

***S*-PGME amide of 14 (14a):** ¹H NMR (800 MHz, CD₃OD) δ_{H} 7.8907 (1H, d, *J* = 15.5 Hz), 7.4763 (1H, d, *J* = 7.5 Hz), 7.4665 (1H, d, *J* = 7.5 Hz), 7.3542–7.3177 (2H, m), 7.2377 (1H, dd, *J* = 7.5, 7.5 Hz), 7.2307–7.2045 (2H, m), 7.1488 (1H, dd, *J* = 7.5, 7.5 Hz), 6.7555 (1H, d, *J* = 15.5 Hz), 6.6386 (1H, dd, *J* = 15.5, 10.5 Hz), 6.4767 (1H, d, *J* = 11.0 Hz), 6.1910 (1H,

dd, $J = 15.0, 10.5$ Hz), 5.8108 (1H, s), 5.7903 (1H, td, $J = 15.0, 7.5$ Hz), 4.3948 (1H, dd, $J = 6.5, 5.5$ Hz), 4.3796–4.3382 (2H, m), 4.3233 (1H, m), 4.2275 (1H, d, $J = 6.5$ Hz), 4.0264 (1H, d, $J = 6.5$ Hz), 3.8313 (1H, d, $J = 11.0, 5.0$ Hz), 3.6738 (1H, dd, $J = 11.0, 5.5$ Hz), 3.6424 (3H, s), 3.5132 (1H, d, $J = 5.5$ Hz), 3.2367 (1H, m), 2.9375 (1H, m), 2.1271 (1H, m), 1.9630 (2H, dd, $J = 7.0, 7.0$ Hz), 1.8967 (1H, m), 1.6451–1.5761 (4H, m), 1.3433 (3H, d, $J = 7.5$ Hz), 1.2510 (3H, d, $J = 7.5$ Hz), 0.8918 (3H, d, $J = 7.0$ Hz), 0.8843 (3H, d, $J = 7.0$ Hz), 0.8648 (3H, d, $J = 7.0$ Hz), 0.8549 (3H, d, $J = 7.0$ Hz), 0.8451 (6H, d, $J = 6.5$ Hz), 0.8199 (3H, d, $J = 6.0$ Hz), 0.8058 (3H, d, $J = 6.5$ Hz)

R-PGME amide of 14 (14b): ^1H NMR (800 MHz, CD_3OD) δ_{H} 7.7386 (1H, d, $J = 16.0$ Hz), 7.5853 (1H, d, $J = 7.5$ Hz), 7.3998–7.3804 (2H, m), 7.3629–7.3150 (3H, m), 7.2995–7.2487 (3H, m), 6.8774 (1H, d, $J = 15.5$ Hz), 6.4325 (1H, d, $J = 11.0$ Hz), 6.3640 (1H, dd, $J = 11.0, 11.0$ Hz), 6.1565 (1H, dd, $J = 14.5, 11.0$ Hz), 5.8786 (1H, td, $J = 14.5, 7.5$ Hz), 5.4356 (1H, s), 5.2214 (1H, d, $J = 11.5$ Hz), 4.5485 (1H, br s), 4.4278–4.3913 (2H, m), 4.3153 (1H, dd, $J = 9.0, 7.5$ Hz), 4.2701 (1H, dd, $J = 13.5, 9.5$ Hz), 4.0316 (1H, m), 3.9437 (1H, d, $J = 11.5$ Hz), 3.6992 (3H, s), 3.6086 (1H, d, $J = 5.5$ Hz), 3.5736 (2H, br s), 3.0435 (1H, dd, $J = 13.5, 4.5$ Hz), 2.5181 (1H, m), 2.1719 (1H, m), 1.9346 (2H, dd, $J = 7.0, 7.0$ Hz), 1.6679 (1H, m), 1.6257 (1H, m), 1.5994 (1H, m), 1.5209 (1H, td, m), 1.4260 (3H, d, $J = 7.5$ Hz), 1.3833 (1H, m), 1.2903 (3H, m), 1.0967 (3H, d, $J = 7.5$ Hz), 1.0837 (3H, d, $J = 7.0$ Hz), 1.0449 (3H, d, $J = 7.0$ Hz), 0.9882 (3H, d, $J = 7.0$ Hz), 0.9698 (3H, d, $J = 7.0$ Hz), 0.9443 (3H, d, $J = 6.5$ Hz), 0.9157 (3H, d, $J = 7.0$ Hz), 0.8739 (6H, d, $J = 6.5$ Hz)

Resazurin microtiter assay against *Mycobacterium tuberculosis* mc² 6230 WT. The MIC₅₀ values of **14** and **15** against *M. tuberculosis* mc² 6230 strain were obtained by using the resazurin microtiter assay (REMA). The avirulent Mtb strain was grown at 37 °C in Middlebrook 7H9 liquid medium (Difco) supplemented with 0.5% albumin, 0.2% glucose, 0.085% NaCl, 0.2% glycerol, 0.05% Tween 80, 24 µg/mL pantothenate, and 0.2% casamino acid, and a 100 µL aliquot of the media was added to all the well of a 96-well microtiter plate

adjusting final bacteria's OD₆₀₀ at 0.005. Test compounds, including moxifloxacin as a positive control, were added into each well by using two-fold serial dilution method. The prepared 96-well plates were incubated at 37 °C. After 5 days culture, resazurin was added to each well (0.025% [wt./vol.]) and the fluorescence was read (560–590 nm) with using a SpectraMax M3 Multi-Mode Microplate Reader (Molecular Devices, CA, USA). The MIC₅₀ values of the compounds were calculated based on the triplicated results using Prism 6 (GraphPad Software, Inc., La Jolla, CA).

Sequencing and gene annotation of the coprisamides producing strain. The whole-genome sequence data of coprisamides producing *Micromonospora* sp. UTJ3 was acquired by ChunLab, Inc., using single-molecule sequencing technology with the PacBio RS II system. The genomic sequence data were assembled by using a hierarchical genome assembly process (HGAP) with SMRT analysis 2.3.0, resulting 7,757,889 bp (1 contig) size. The DNA sequence data were annotated with EggNOG 4.5, Swissprot, KEGG, and SEED as ChunLab's in-house pipeline. Further analysis revealed that the genome data of *Micromonospora* sp. UTJ3 was composed of 71.43 % of G + C content, 6,045 of CDS, and 51 of tRNA genes were identified. For determining the biosynthetic gene clusters of coprisamides, antiSMASH 5.0⁴⁴ was utilized.

Table 7. ^1H and ^{13}C NMR spectra data for coprisamides C and D (**14** and **15**) in $\text{DMSO}-d_6$.

no	coprisamide C (14)				coprisamide D (15)			
	δ_{C}^a	type	δ_{H}^b	mult (J in Hz)	δ_{C}^c	type	δ_{H}^d	mult (J in Hz)
1	169.5	C			169.5	C		
2	54.7	CH	3.82	dd (10.5, 7.5)	54.7	CH	3.81	dd (10.5, 7.5)
2-NH			8.51	d (7.5)			8.55	d (7.5)
3	38.6	CH	2.98	qd (10.5, 7.5)	38.6	CH	2.98	qd (10.5, 7.5)
4	14.9	CH_3	0.98	d (7.5)	14.9	CH_3	0.98	d (7.5)
5	176.0	C			176.0	C		
6	169.2	C			169.2	C		
7	49.9	CH	4.68	ddd (9.5, 9.5, 5.0)	49.9	CH	4.69	ddd (9.5, 9.5, 4.5)
7-NH			8.15	d (9.5)			8.16	d (9.5)
8a	39.2	CH_2	4.01	m	39.2	CH_2	4.02	m
8b			2.89	m			2.88	m
8-NH			8.57	dd (7.5, 4.0)			8.52	dd (6.5, 4.5)
9	170.3	C			170.3	C		
10	58.0	CH	4.24	dd (9.0, 4.0)	58.0	CH	4.24	dd (9.0, 4.0)
10-NH			8.39	d (9.0)			8.39	d (9.0)
11	28.1	CH	2.38	m	28.1	CH	2.38	m
12	16.8	CH_3	0.84	d (7.0)	16.8	CH_3	0.85	d (7.0)
13	16.8	CH_3	0.84	d (7.0)	16.8	CH_3	0.85	d (7.0)
14	172.7	C			172.7	C		
15	52.9	CH	4.28	m	52.9	CH	4.29	m ^e
15-NH			8.73	d (4.0)			8.73	d (4.0)
16a	38.8	CH_2	1.56	m	39.0	CH_2	1.56	m
16b			1.41	ddd (14.0, 7.0, 7.0)			1.41	ddd (13.0, 7.0, 7.0)
17	24.2	CH	1.50	m	24.2	CH	1.51	m
18	22.8	CH_3	0.92	d (7.0)	22.8	CH_3	0.87	d (6.5)
19	21.9	CH_3	0.86	d (7.0)	21.9	CH_3	0.87	d (6.5)
20	169.7	C			169.7	C		
21	50.5	CH	4.50	ddd (7.5, 3.0, 2.0)	50.7	CH	4.51	ddd (7.5, 2.5, 2.5)
21-NH			7.32	d (7.5)			7.34	d (7.5)
22a	63.2	CH_2	4.89	dd (11.0, 3.0)	63.4	CH_2	4.91	dd (11.0, 2.5)
22b			3.96	dd (11.0, 2.0)			3.97	dd (11.0, 2.5)
23	171.5	C			171.5	C		
24	49.4	CH	4.27	qd (7.0, 7.0)	49.5	CH	4.30	m ^e
24-NH			8.01	d (7.0)			8.03	d (7.0)
25	17.4	CH_3	1.31	d (7.0)	17.4	CH_3	1.33	d (7.0)
26	164.5	C			164.5	C		
27	122.8	CH	6.91	d (15.5)	123.5	CH	6.87	d (15.5)
28	137.0	CH	7.57	d (15.5)	136.5	CH	7.78	d (15.5)
29	133.3	C			132.4	C		
30	130.0	CH	7.24	d (7.5)	126.5	CH	7.52	d (7.5)
31	129.0	CH	7.38	dd (7.5, 7.5)	127.5	CH	7.25	dd (7.5, 7.5)
32	127.6	CH	7.31	dd (7.5, 7.5)	129.5	CH	7.35	dd (7.5, 7.5)
33	126.3	CH	7.61	d (7.5)	126.0	CH	7.59	d (7.5)
34	136.9	C			136.6	C		
35	125.6	CH	6.48	d (11.5)	126.1	CH	6.80	d (15.5)
36	131.9	CH	6.40	dd (11.5, 11.5)	132.6	CH	6.78	dd (15.5, 9.0)
37	126.9	CH	6.12	dd (15.0, 11.5)	131.8	CH	6.32	dd (15.0, 9.0)
38	137.1	CH	5.91	td (15.0, 7.5)	135.5	CH	5.91	td (15.0, 7.5)
39	41.6	CH_2	1.91	dd (7.5, 7.5)	41.6	CH_2	2.03	dd (7.5, 7.5)
40	27.9	CH	1.60	m	28.0	CH	1.67	m
41	22.1	CH_3	0.83	d (7.0)	22.2	CH_3	0.89	d (6.5)
42	22.1	CH_3	0.83	d (7.0)	22.2	CH_3	0.89	d (6.5)
43	168.0	C			167.9	C		
44	57.6	CH	3.56	m	57.6	CH	3.53	m
44-NH ₂			8.11	d (4.5)			8.07	d (4.5)
45	29.8	CH	2.03	m	29.8	CH	2.03	m ^e
46	18.4	CH_3	0.91	d (6.5)	18.4	CH_3	0.92	d (6.5)
47	17.2	CH_3	0.87	d (6.5)	17.2	CH_3	0.88	d (6.5)

^a 212.5 MHz, ^b 850 MHz, ^c 200 MHz, ^d 800 MHz, ^e overlapped

Summary

Bombyxamycin A (**1**) is a structurally unique 26-membered macrolactam bearing tetraenone and pentaenone. Sceliphrolactam from a mud dauber-associated *Streptomyces* is the most similar compound with a 26-membered lactam ring.²⁴ However, sceliphrolactam exhibits different C-methylation and hydroxylation patterns. Mirilactam B⁵⁰ and FW05328-1⁵¹ are previously-reported 26-membered macrocyclic lactams, but their carbon skeletons differ by possessing a methyl group at the α -position of the amide nitrogen, which indicates that their biosynthesis start with an α -amino acid unit rather than a β -amino acid unit as in **1**. Cyclamenol shares its β -amino acid starting block with the bombyxamycins,²² but it possesses a 20-membered cyclic lactam skeleton differently from the 26-membered framework of **1–3**. The structural novelty of **2** is even higher because of the incorporation of a secondary ring, THF, in the middle of the macrocycle. To the best of my knowledge, this is the first bicyclic macrolactam with substituted THF. Additionally, in the course of determining the absolute configuration of the center β to the amide bond of the macrocyclic lactams, a new chromatography-based method using PGME derivatization was developed. This method provides a convenient approach for elucidating the absolute configurations of commonly encountering macrolactams biosynthesized from 3-amino-2-methylpropanoic acid as a starting material. The bombyxamycins are the first organic molecules from Lepidopteran insect-associated microorganisms. This result indicates that expanding the chemical investigation of microbes inhabiting insects to Lepidoptera, could lead to additional successful discoveries of unexplored novel compounds with pharmaceutical potential.

The discovery of *Nicrophorus* amides with antibacterial activities from a gut bacterial strain of *N. concolor* might provide a significant clue regarding the defense mechanism of carrion beetles against carrion-borne bacterial infection. A recent study revealed that carrion beetles in the genus *Nicrophorus* transmit their gut symbionts to their offspring through the prenatal treatment of the carcass by parents, indicating the importance of the gut microbiome in the beetle's ecology. This culture-dependent research might have missed chemically prolific actinomycetes during strain isolation because actinobacteria tend to form colonies slowly.

This report should lead to additional studies about carrion beetles' gut microbiota and their molecular mechanisms for chemical defense utilizing gut actinobacteria. Indeed, this result indicates that actinomycetes exist in the gut microbiome of carrion beetles and could produce antibacterial metabolites possibly against potential bacterial pathogens.

Investigation of carrion beetle's gut bacterial strain *Micromonospora* sp. UTJ3 lead me to discover coprisamides C and D (**14** and **15**), which bear unprecedented cinnamoyl moiety and nonproteinogenic amino acids. Additionally, during genetic analysis of genomic sequence data of coprisamides producing strain, *Micromonospora* sp. UTJ3, general biosynthetic pathway of coprisamides involving cinnamoyl synthesis gene cassettes and unusual amino acids constructing genes could be suggested based on their putative functions. Because there are only few kinds of cinnamate-containing bacterial non-ribosomal peptides, discovery and investigating of coprisamides in biosynthetic level could provide foundation for development in bioinformatics.

References

References

1. Basset, Y.; Cizek, L.; Cuenoud, P.; Didham, R. K.; Guilhaumon, F.; Missa, O.; Novotny, V.; Odegaard, F.; Roslin, T.; Schmidl, J.; Tishechkin, A. K.; Winchester, N. N.; Roubik, D. W.; Aberlenc, H. P.; Bail, J.; Barrios, H.; Bridle, J. R.; Castano-Meneses, G.; Corbara, B.; Curletti, G.; Duarte da Rocha, W.; De Bakker, D.; Delabie, J. H.; Dejean, A.; Fagan, L. L.; Floren, A.; Kitching, R. L.; Medianero, E.; Miller, S. E.; Gama de Oliveira, E.; Orivel, J.; Pollet, M.; Rapp, M.; Ribeiro, S. P.; Roisin, Y.; Schmidt, J. B.; Sorensen, L.; Leponce, M., Arthropod diversity in a tropical forest. *Science* **2012**, *338*, 1481–1484.
2. Stork, N. E., How many species of insects and other terrestrial arthropods are there on Earth? *Annu. Rev. Entomol.* **2018**, *63*, 31–45.
3. Kim, S. H.; Kwon, S. H.; Park, S. H.; Lee, J. K.; Bang, H. S.; Nam, S. J.; Kwon, H. C.; Shin, J.; Oh, D. C., Tripartin, a histone demethylase inhibitor from a bacterium associated with a dung beetle larva. *Org. Lett.* **2013**, *15*, 1834–1837.
4. Park, S. H.; Moon, K.; Bang, H. S.; Kim, S. H.; Kim, D. G.; Oh, K. B.; Shin, J.; Oh, D. C., Tripartilactam, a cyclobutane-bearing tricyclic lactam from a *Streptomyces* sp. in a dung beetle's brood ball. *Org. Lett.* **2012**, *14*, 1258–1261.
5. Um, S.; Bach, D. H.; Shin, B.; Ahn, C. H.; Kim, S. H.; Bang, H. S.; Oh, K. B.; Lee, S. K.; Shin, J.; Oh, D. C., Naphthoquinone-oxindole alkaloids, coprisidins A and B, from a gut-associated bacterium in the dung beetle, *Copris tripartitus*. *Org. Lett.* **2016**, *18*, 5792–5795.
6. Um, S.; Park, S. H.; Kim, J.; Park, H. J.; Ko, K.; Bang, H. S.; Lee, S. K.; Shin, J.; Oh, D. C., Coprisamides A and B, new branched cyclic peptides from a gut bacterium of the dung beetle *Copris tripartitus*. *Org. Lett.* **2015**, *17*, 1272–1275.
7. Shin, B.; Park, S. H.; Kim, B. Y.; Jo, S. I.; Lee, S. K.; Shin, J.; Oh, D. C., Deinococcucins A–D, aminoglycolipids from *Deinococcus* sp., a gut bacterium of the carpenter ant *Camponotus japonicus*. *J. Nat. Prod.* **2017**, *80*, 2910–2916.
8. Hong, S. H.; Ban, Y. H.; Byun, W. S.; Kim, D.; Jang, Y. J.; An, J. S.; Shin, B.; Lee, S. K.; Shin, J.; Yoon, Y. J.; Oh, D. C., Camporidines A and B: antimetastatic and anti-inflammatory polyketide alkaloids from a gut bacterium of *Camponotus kiusiuensis*. *J. Nat. Prod.* **2019**, *82*, 903–910.
9. Xia, Q. Y.; Wang, J.; Zhou, Z. Y.; Li, R. Q.; Fan, W.; Cheng, D. J.; Cheng, T. C.; Qin, J. J.; Duan, J.; Xu, H. F.; Li, Q. B.; Li, N.; Wang, M. W.; Dai, F. Y.; Liu, C.; Lin, Y.; Zhao, P.; Zhang, H. J.; Liu, S. P.; Zha, X. F.; Li, C. F.; Zhao, A. C.; Pan, M. H.; Pan, G. Q.; Shen, Y. H.; Gao, Z. H.; Wang, Z. L.; Wang, G. H.; Wu, Z. L.; Hou, Y.; Chai, C. L.; Yu, Q. Y.; He, N. J.; Zhang, Z.; Li, S. G.; Yang, H. M.; Lu, C.; Wang, J.; Xiang, Z. H.; Mita, K.; Kasahara, M.; Nakatani, Y.; Yamamoto, K.; Abe, H.; Ahsan, B.; Dai-

Mon, T.; Doi, K.; Fujii, T.; Fujiwara, H.; Fujiyama, A.; Futahashi, R.; Hashimoto, S. I.; Ishibashi, J.; Iwami, M.; Kadono-Okuda, K.; Kanamori, H.; Kataoka, H.; Katsuma, S.; Kawaoka, S.; Kawasaki, H.; Kohara, Y.; Kozaki, T.; Kuroshu, R. M.; Kuwazaki, S.; Matsushima, K.; Minami, H.; Nagayasu, Y.; Nakagawa, T.; Narukawa, J.; Nohata, J.; Ohishi, K.; Ono, Y.; Osanai-Futahashi, M.; Ozaki, K. H.; Qu, W.; Roller, L.; Sasaki, S.; Sasaki, T.; Seino, A.; Shimomura, M.; Shimomura, M.; Shin-I, T.; Shinoda, T.; Shiotsuki, T.; Suetsugu, Y.; Sugano, S.; Suwa, M.; Suzuki, Y.; Takiya, S. H.; Tamura, T.; Tanaka, H.; Tanaka, Y.; Touhara, K.; Yamada, T.; Yamakawa, M.; Yamanaka, N.; Yoshikawa, H.; Zhong, Y. S.; Shima-Da, T.; Morishita, S.; Consortium, I. S. G., The genome of a lepidopteran model insect, the silkworm *Bombyx mori*. *Insect Biochem. Molec.* **2008**, *38*, 1036–1045.

10. Shao, Y.; Chen, B.; Sun, C.; Ishida, K.; Hertweck, C.; Boland, W., Symbiont-derived antimicrobials contribute to the control of the lepidopteran gut microbiota. *Cell Chem. Biol.* **2017**, *24*, 66–75.

11. Chen, B.; Du, K.; Sun, C.; Vimalanathan, A.; Liang, X.; Li, Y.; Wang, B.; Lu, X.; Li, L.; Shao, Y., Gut bacterial and fungal communities of the domesticated silkworm (*Bombyx mori*) and wild mulberry-feeding relatives. *ISME J.* **2018**, *12*, 2252–2262.

12. Schulz, D.; Nachtigall, J.; Riedlinger, J.; Schneider, K.; Poralla, K.; Imhoff, J. F.; Beil, W.; Nicholson, G.; Fiedler, H. P.; Sussmuth, R. D., Piceamycin and its *N*-acetylcysteine adduct is produced by *Streptomyces* sp. GB 4-2. *J. Antibiot.* **2009**, *62*, 513–518.

13. Kaltenpoth, M.; Steiger, S., Unearthing carrion beetles' microbiome: characterization of bacterial and fungal hindgut communities across the Silphidae. *Mol. Ecol.* **2014**, *23*, 1251–1267.

14. Wang, Y.; Rozen, D. E., Gut microbiota colonization and transmission in the burying beetle *Nicrophorus vespilloides* throughout development. *Appl. Environ. Microbiol.* **2017**, *83*, e03250-16.

15. Dekeirsschieter, J.; Verheggen, F.; Lognay, G.; Haubruge, E., Large carrion beetles (Coleoptera, Silphidae) in western Europe: a review. *Biotechnol. Agron. Soc.* **2011**, *15*, 435–447.

16. Ito, N.; Katoh, T.; Kobayashi, N.; Katakura, H., Effects of straits as dispersal barriers for the flightless roving carrion beetle, *Silpha perforata* (Coleoptera, Silphidae, Silphinae). *Zool. Sci.* **2010**, *27*, 313–319.

17. Meinwald, J.; Roach, B.; Hicks, K.; Alsop, D.; Eisner, T., Defensive steroids from a carrion beetle (*Silpha americana*). *Experientia* **1985**, *41*, 516–519.

18. Meinwald, J.; Roach, B.; Eisner, T., Defensive steroids from a carrion beetle (*Silpha novaboracensis*). *J. Chem. Ecol.* **1987**, *13*, 35–38.

19. Seco, J. M.; Quinoa, E.; Riguera, R., A practical guide for the assignment of the absolute configuration of alcohols, amines and carboxylic acids by NMR. *Tetrahedron: Asymmetry* **2001**, *12*, 2915–2925.
20. Yabuuchi, T.; Kusumi, T., Phenylglycine methyl ester, a useful tool for absolute configuration determination of various chiral carboxylic acids. *J. Org. Chem.* **2000**, *65*, 397–404.
21. Williams, P. G.; Asolkar, R. N.; Kondratyuk, T.; Pezzuto, J. M.; Jensen, P. R.; Fenical, W., Saliniketals A and B, bicyclic polyketides from the marine actinomycete *Salinispora arenicola*. *J. Nat. Prod.* **2007**, *70*, 83–88.
22. Shen, J.; Fan, Y.; Zhu, G.; Chen, H.; Zhu, W.; Fu, P., Polycyclic macrolactams generated via intramolecular Diels-Alder reactions from an antarctic *Streptomyces* species. *Org. Lett.* **2019**, *21*, 4816–4820.
23. Beemelmans, C.; Ramadhar, T. R.; Kim, K. H.; Klassen, J. L.; Cao, S.; Wyche, T. P.; Hou, Y.; Poulsen, M.; Bugni, T. S.; Currie, C. R.; Clardy, J., Macrotermycins A–D, glycosylated macrolactams from a termite-associated *Amycolatopsis* sp. M39. *Org. Lett.* **2017**, *19*, 1000–1003.
24. Oh, D. C.; Poulsen, M.; Currie, C. R.; Clardy, J., Sceliphrolactam, a polyene macrocyclic lactam from a wasp-associated *Streptomyces* sp. *Org. Lett.* **2011**, *13*, 752–755.
25. Hoshino, S.; Okada, M.; Wakimoto, T.; Zhang, H. P.; Hayashi, F.; Onaka, H.; Abe, I., Niizalactams A–C, multicyclic macrolactams isolated from combined culture of *Streptomyces* with mycolic acid-containing bacterium. *J. Nat. Prod.* **2015**, *78*, 3011–3017.
26. Shindo, K.; Kamishohara, M.; Odagawa, A.; Matsuoka, M.; Kawai, H., Vicenistatin, a novel 20-membered macrocyclic lactam antitumor antibiotic. *J. Antibiot.* **1993**, *46*, 1076–1081.
27. Bringmann, G.; Tasler, S.; Endress, H.; Kraus, J.; Messer, K.; Wohlfarth, M.; Lobin, W., Murrastifoline-F: first total synthesis, atropo-enantiomer resolution, and stereoanalysis of an axially chiral N,C-coupled biaryl alkaloid. *J. Am. Chem. Soc.* **2001**, *123*, 2703–2711.
28. Blin, K.; Wolf, T.; Chevrete, M. G.; Lu, X. W.; Schwalen, C. J.; Kautsar, S. A.; Duran, H. G. S.; Santos, E. L. C. D. L.; Kim, H. U.; Nave, M.; Dickschat, J. S.; Mitchell, D. A.; Shelest, E.; Breitling, R.; Takano, E.; Lee, S. Y.; Weber, T.; Medema, M. H., antiSMASH 4.0-improvements in chemistry prediction and gene cluster boundary identification. *Nucleic Acids Res.* **2017**, *45*, W36–W41.
29. Alt, S.; Wilkinson, B., Biosynthesis of the novel macrolide antibiotic anthracimycin. *ACS Chem. Biol.* **2015**, *10*, 2468–2479.

30. Hari, S. B.; Merritt, E. A.; Maly, D. J., Sequence determinants of a specific inactive protein kinase conformation. *Chem. Biol.* **2013**, *20*, 806–815.
31. Ogasawara, Y.; Katayama, K.; Minami, A.; Otsuka, M.; Eguchi, T.; Kakinuma, K., Cloning, sequencing, and functional analysis of the biosynthetic gene cluster of macrolactam antibiotic vicenistatin in *Streptomyces halstedii*. *Chem. Biol.* **2004**, *11*, 79–86.
32. Shinohara, Y.; Kudo, F.; Eguchi, T., A natural protecting group strategy to carry an amino acid starter unit in the biosynthesis of macrolactam polyketide antibiotics. *J. Am. Chem. Soc.* **2011**, *133*, 18134–18137.
33. Kudo, F.; Kawamura, K.; Uchino, A.; Miyana, A.; Numakura, M.; Takayanagi, R.; Eguchi, T., Genome mining of the hitachimycin biosynthetic gene cluster: involvement of a phenylalanine-2,3-aminomutase in biosynthesis. *Chembiochem* **2015**, *16*, 909–914.
34. Vichai, V.; Kirtikara, K., Sulforhodamine B colorimetric assay for cytotoxicity screening. *Nat. Protoc.* **2006**, *1*, 1112–1116.
35. Fujii, K.; Ikai, Y.; Oka, H.; Suzuki, M.; Harada, K., A nonempirical method using LC/MS for determination of the absolute configuration of constituent amino acids in a peptide: combination of Marfey's method with mass spectrometry and its practical application. *Anal. Chem.* **1997**, *69*, 5146–5151.
36. Hess, S.; Gustafson, K. R.; Milanowski, D. J.; Alvira, E.; Lipton, M. A.; Pannell, L. K., Chirality determination of unusual amino acids using precolumn derivatization and liquid chromatography-electrospray ionization mass spectrometry. *J. Chromatogr. A* **2004**, *1035*, 211–219.
37. Song, Y.; Li, Q.; Liu, X.; Chen, Y.; Zhang, Y.; Sun, A.; Zhang, W.; Zhang, J.; Ju, J., Cyclic hexapeptides from the deep south China sea-derived *Streptomyces scopuliridis* SCSIO ZJ46 active against pathogenic Gram-positive bacteria. *J. Nat. Prod.* **2014**, *77*, 1937–1941.
38. Li, Q.; Song, Y.; Qin, X.; Zhang, X.; Sun, A.; Ju, J., Identification of the biosynthetic gene cluster for the anti-infective desotamides and production of a new analogue in a heterologous host. *J. Nat. Prod.* **2015**, *78*, 944–948.
39. Khalil, Z. G.; Salim, A. A.; Lacey, E.; Blumenthal, A.; Capon, R. J., Wollamides: antimycobacterial cyclic hexapeptides from an Australian soil *Streptomyces*. *Org. Lett.* **2014**, *16*, 5120–5123.
40. Shiba, T.; Mukunoki, Y., The total structure of the antibiotic longicatenamycin. *J. Antibiot.* **1975**, *28*, 561–566.

41. von Nussbaum, F.; Anlauf, S.; Freiberg, C.; Benet-Buchholz, J.; Schamberger, J.; Henkel, T.; Schiffer, G.; Habich, D., Total synthesis and initial structure-activity relationships of longicatenamycin A. *ChemMedChem* **2008**, *3*, 619–626.
42. Hanwell, M. D.; Curtis, D. E.; Lonie, D. C.; Vandermeersch, T.; Zurek, E.; Hutchison, G. R., Avogadro: an advanced semantic chemical editor, visualization, and analysis platform. *J. Cheminform.* **2012**, *4*, 17.
43. Jang, J.; Kim, R.; Woo, M.; Jeong, J.; Park, D. E.; Kim, G.; Delorme, V., Efflux attenuates the antibacterial activity of Q203 in *Mycobacterium tuberculosis*. *Antimicrob. Agents Chemother.* **2017**, *61*, e02637-16.
44. Blin, K.; Shaw, S.; Steinke, K.; Villebro, R.; Ziemert, N.; Lee, S. Y.; Medema, M. H.; Weber, T., antiSMASH 5.0: updates to the secondary metabolite genome mining pipeline. *Nucleic Acids Res.* **2019**, *47*, W81–W87.
45. Sun, C.; Yang, Z.; Zhang, C.; Liu, Z.; He, J.; Liu, Q.; Zhang, T.; Ju, J.; Ma, J., Genome mining of *Streptomyces atratus* SCSIO ZH16: discovery of atratumycin and identification of its biosynthetic gene cluster. *Org. Lett.* **2019**, *21*, 1453–1457.
46. Kobylarz, M. J.; Grigg, J. C.; Takayama, S. J.; Rai, D. K.; Heinrichs, D. E.; Murphy, M. E., Synthesis of L-2,3-diaminopropionic acid, a siderophore and antibiotic precursor. *Chem. Biol.* **2014**, *21*, 379–388.
47. Barker, H. A.; Rooze, V.; Suzuki, F.; Iodice, A. A., The glutamate mutase system. Assays and properties. *J. Biol. Chem.* **1964**, *239*, 3260–3266.
48. Toki, S.; Agatsuma, T.; Ochiai, K.; Saitoh, Y.; Ando, K.; Nakanishi, S.; Lokker, N. A.; Giese, N. A.; Matsuda, Y., RP-1776, a novel cyclic peptide produced by *Streptomyces* sp., inhibits the binding of PDGF to the extracellular domain of its receptor. *J. Antibiot.* **2001**, *54*, 405–414.
49. Mariani, R.; Granata, G.; Maffioli, S. I.; Serina, S.; Brunati, C.; Sosio, M.; Marazzi, A.; Vannini, A.; Patel, D.; White, R.; Ciabatti, R., Antibiotics GE23077, novel inhibitors of bacterial RNA polymerase. Part 3: Chemical derivatization. *Bioorg. Med. Chem. Lett.* **2005**, *15*, 3748–3752.
50. Schulze, C. J.; Donia, M. S.; Siqueira-Neto, J. L.; Ray, D.; Raskatov, J. A.; Green, R. E.; McKerrow, J. H.; Fischbach, M. A.; Lington, R. G., Genome-directed lead discovery: biosynthesis, structure elucidation, and biological evaluation of two families of polyene macrolactams against *Trypanosoma brucei*. *ACS Chem. Biol.* **2015**, *10*, 2373–2381.
51. Nie, Y. L.; Wu, Y. D.; Wang, C. X.; Lin, R.; Xie, Y.; Fang, D. S.; Jiang, H.; Lian, Y. Y., Structure elucidation and antitumour activity of a new macrolactam produced by marine-derived actinomycete *Micromonospora* sp. FIM05328. *Nat. Prod. Res.* **2018**, *32*, 2133–2138.

Appendix:

Supporting Information

List of Figures

Figure S1.	^1H NMR spectrum data of bombyxamycin A (1) at 500 MHz in DMSO- d_6	92
Figure S2.	Expanded ^1H NMR spectrum of bombyxamycin A (1) at 500 MHz in DMSO- d_6 and measurement of ^1H - ^1H coupling constants of the olefinic protons.	93
Figure S3.	^{13}C NMR spectrum data of bombyxamycin A (1) at 125 MHz in DMSO- d_6	94
Figure S4.	COSY NMR spectrum data of bombyxamycin A (1) at 500 MHz in DMSO- d_6	95
Figure S5.	HSQC NMR spectrum data of bombyxamycin A (1) at 500 MHz in DMSO- d_6	95
Figure S6.	HMBC NMR spectrum data of bombyxamycin A (1) at 500 MHz in DMSO- d_6	96
Figure S7.	NOESY NMR spectrum data of bombyxamycin A (1) at 500 MHz in DMSO- d_6	96
Figure S8.	^1H NMR spectrum data of <i>S</i> -MTPA ester of 1 (1a) at 500 MHz in DMSO- d_6	97
Figure S9.	COSY NMR spectrum data of <i>S</i> -MTPA ester of 1 (1a) at 500 MHz in DMSO- d_6	97
Figure S10.	^1H NMR spectrum data of <i>R</i> -MTPA ester of 1 (1b) at 500 MHz in DMSO- d_6	98
Figure S11.	COSY NMR spectrum data of <i>R</i> -MTPA ester of 1 (1b) at 500 MHz in DMSO- d_6	98
Figure S12.	^1H NMR spectrum data of 3-(2,4-dinitro-phenylamino)-2-methyl-propanoic acid (5) at 600 MHz in CD $_3$ OD.	99
Figure S13.	^1H NMR spectrum data of <i>S</i> -PGME amide of 5 (5a) at 600 MHz in CD $_3$ OD.	100

Figure S14.	^1H NMR spectrum data of <i>R</i> -PGME amide of 5 (5b) at 600 MHz in CD_3OD	100
Figure S15.	^1H NMR spectrum data of bombyxamycin B (2) at 500 MHz in $\text{DMSO}-d_6$	101
Figure S16.	Expanded ^1H NMR spectrum of bombyxamycin B (2) at 500 MHz in $\text{DMSO}-d_6$ and measurement of $^1\text{H}-^1\text{H}$ coupling constants of the olefinic protons.	102
Figure S17.	^{13}C NMR spectrum data of bombyxamycin B (2) at 125 MHz in $\text{DMSO}-d_6$	103
Figure S18.	^{13}C NMR spectrum data of bombyxamycin B (2) at 212.5 MHz in CD_3OD	104
Figure S19.	^{13}C NMR spectrum data of bombyxamycin B (2) at 212.5 MHz in 1:1 $\text{CD}_3\text{OD}/\text{CD}_3\text{OH}$	104
Figure S20.	COSY NMR spectrum data of bombyxamycin B (2) at 500 MHz in $\text{DMSO}-d_6$	105
Figure S21.	HSQC NMR spectrum data of bombyxamycin B (2) at 500 MHz in $\text{DMSO}-d_6$	105
Figure S22.	HMBC NMR spectrum data of bombyxamycin B (2) at 500 MHz in $\text{DMSO}-d_6$	106
Figure S23.	NOESY NMR spectrum data of bombyxamycin B (2) at 500 MHz in $\text{DMSO}-d_6$	106
Figure S24.	^1H NMR spectrum data of <i>S</i> -MTPA ester of 2 (2a) at 500 MHz in $\text{DMSO}-d_6$	107
Figure S25.	COSY NMR spectrum data of <i>S</i> -MTPA ester of 2 (2a) at 500 MHz in $\text{DMSO}-d_6$	107
Figure S26.	^1H NMR spectrum data of <i>R</i> -MTPA ester of 2 (2b) at 500 MHz in $\text{DMSO}-d_6$	108
Figure S27.	COSY NMR spectrum data of <i>R</i> -MTPA ester of 2 (2b) at 500 MHz in $\text{DMSO}-d_6$	108

Figure S28.	^1H NMR spectrum of bombyxamycin 3 at 850 MHz in $\text{DMSO-}d_6$	109
Figure S29.	^{13}C NMR spectrum of bombyxamycin 3 at 212.5 MHz in $\text{DMSO-}d_6$	109
Figure S30.	COSY NMR spectrum of bombyxamycin 3 at 500 MHz in $\text{DMSO-}d_6$	110
Figure S31.	HSQC NMR spectrum of bombyxamycin 3 at 500 MHz in $\text{DMSO-}d_6$	110
Figure S32.	HMBC NMR spectrum of bombyxamycin 3 at 500 MHz in $\text{DMSO-}d_6$	111
Figure S33.	NOESY NMR spectrum of bombyxamycin 3 at 850 MHz in $\text{DMSO-}d_6$	111
Figure S34.	^1H NMR spectrum of <i>S</i> -MTPA ester of 3 (3a) at 850 MHz in CD_3OD	112
Figure S35.	COSY NMR spectrum of <i>S</i> -MTPA ester of 3 (3a) at 850 MHz in CD_3OD	112
Figure S36.	^1H NMR spectrum of <i>R</i> -MTPA ester of 3 (3b) at 850 MHz in CD_3OD	113
Figure S37.	COSY NMR spectrum of <i>R</i> -MTPA ester of 3 (3b) at 850 MHz in CD_3OD	113
Figure S38.	^1H NMR spectrum of piceamycin (4) at 500 MHz in $\text{DMSO-}d_6$	114
Figure S39.	^{13}C NMR spectrum of piceamycin (4) at 212.5 MHz in $\text{DMSO-}d_6$	114
Figure S40.	COSY NMR spectrum of piceamycin (4) at 500 MHz in $\text{DMSO-}d_6$	115
Figure S41.	HSQC NMR spectrum of piceamycin (4) at 500 MHz in $\text{DMSO-}d_6$	115
Figure S42.	HMBC NMR spectrum of piceamycin (4) at 500 MHz in $\text{DMSO-}d_6$	116
Figure S43.	NOESY NMR spectrum of piceamycin (4) at 850 MHz in $\text{DMSO-}d_6$	116
Figure S44.	^1H NMR spectrum of <i>S</i> -PGME amide of 2 <i>S</i> -3-amino-2-methylpropanoic acid (6) at 850 MHz in CD_3OD	117
Figure S45.	^{13}C NMR spectrum of <i>S</i> -PGME amide of 2 <i>S</i> -3-amino-2-methylpropanoic acid (6) at 212.5 MHz in CD_3OD	117

Figure S46.	^1H NMR spectrum of <i>R</i> -PGME amide of 2 <i>S</i> -3-amino-2-methylpropanoic acid (7) at 850 MHz in CD_3OD	118
Figure S47.	^{13}C NMR spectrum of <i>R</i> -PGME amide of 2 <i>S</i> -3-amino-2-methylpropanoic acid (7) at 212.5 MHz in CD_3OD	118
Figure S48.	^1H NMR spectrum of <i>S</i> -PGME amide of 2 <i>R</i> -3-amino-2-methylpropanoic acid (8) at 850 MHz in CD_3OD	119
Figure S49.	^{13}C NMR spectrum of <i>S</i> -PGME amide of 2 <i>R</i> -3-amino-2-methylpropanoic acid (8) at 212.5 MHz in CD_3OD	119
Figure S50.	^1H NMR spectrum of <i>R</i> -PGME amide of 2 <i>R</i> -3-amino-2-methylpropanoic acid (9) at 850 MHz in CD_3OD	120
Figure S51.	^{13}C NMR spectrum of <i>R</i> -PGME amide of 2 <i>R</i> -3-amino-2-methylpropanoic acid (9) at 212.5 MHz in CD_3OD	120
Figure S52.	HR-FAB-MS data of bombyxamycin A (1).	121
Figure S53.	HR-FAB-MS data of bombyxamycin B (2).	121
Figure S54.	HR-FAB-MS data of bombyxamycin C (3).	122
Figure S55.	HR-FAB-MS data of piceamycin (4).	122
Figure S56.	Determining relative configurations of bombyxamycin B (2) by interpretation of NOESY correlation data.	123
Figure S57.	^1H NMR chemical shifts of <i>S</i> - and <i>R</i> -PGME amides of 5 (5a and 5b) at 600 MHz in CD_3OD	123
Figure S58.	Comparing the retention times of 6 , 8 , and <i>S</i> -PGME amide of authentic 2 <i>S</i> -3-amino-2-methylpropanoic acid.	124
Figure S59.	Comparing the retention times of 7 , 9 , and <i>R</i> -PGME amide of authentic 2 <i>S</i> -3-amino-2-methylpropanoic acid.	124
Figure S60.	$\Delta\delta_{S-R}$ values in ppm between PGME amides of 3-amino-2-methylpropanoic acids (6–9).	125
Figure S61.	HR-FAB-MS data of 6	126

Figure S62.	HR-FAB-MS data of 7	126
Figure S63.	HR-FAB-MS data of 8	127
Figure S64.	HR-FAB-MS data of 9	127
Figure S65.	Chromatographic analysis of <i>S</i> -PGME and <i>R</i> -PGME amide products of 3-amino-2-methylpropanoic acid from 0.2 mg of 4	128
Figure S66.	NOESY correlations analysis and energy-minimized model of 4	128
Figure S67.	Multiple sequence alignment of KR domains.	129
Figure S68.	Constuction and verification of <i>bomK</i> in-frame deletion in <i>Streptomyces</i> sp. SD53.	130
Figure S69.	Constuction and verification of <i>bomN</i> in-frame deletion in <i>Streptomyces</i> sp. SD53.	131
Figure S70.	Constuction and verification of <i>bomO</i> in-frame deletion in <i>Streptomyces</i> sp. SD53.	132
Figure S71.	HPLC-ESI-MS/MS chromatograms obtained from the culture of Δ bomN strain.	133
Figure S72.	HPLC-ESI-MS/MS chromatograms obtained from the culture of Δ bomO strain.	133
Figure S73.	HPLC-ESI-MS/MS chromatograms obtained from the culture of Δ bomK strain.	134
Figure S74.	^1H NMR spectrum of nicrophorusamide A (10) at 600 MHz in DMSO- d_6	135
Figure S75.	^{13}C NMR spectrum of nicrophorusamide A (10) at 125 MHz in DMSO- d_6	135
Figure S76.	COSY NMR spectrum of nicrophorusamide A (10) at 600 MHz in DMSO- d_6	136
Figure S77.	TOCSY NMR spectrum of nicrophorusamide A (10) at 500 MHz in DMSO- d_6	136

Figure S78.	HSQC NMR spectrum of nicrophorusamide A (10) at 500 MHz in DMSO- <i>d</i> ₆	137
Figure S79.	HMBC NMR spectrum of nicrophorusamide A (10) at 500 MHz in DMSO- <i>d</i> ₆	137
Figure S80.	ROESY NMR spectrum of nicrophorusamide A (10) at 500 MHz in DMSO- <i>d</i> ₆	138
Figure S81.	¹ H NMR spectrum of nicrophorusamide B (11) at 500 MHz in DMSO- <i>d</i> ₆	139
Figure S82.	¹³ C NMR spectrum of nicrophorusamide B (11) at 125 MHz in DMSO- <i>d</i> ₆	139
Figure S83.	COSY NMR spectrum of nicrophorusamide B (11) at 500 MHz in DMSO- <i>d</i> ₆	140
Figure S84.	TOCSY NMR spectrum of nicrophorusamide B (11) at 500 MHz in DMSO- <i>d</i> ₆	140
Figure S85.	HSQC NMR spectrum of nicrophorusamide B (11) at 500 MHz in DMSO- <i>d</i> ₆	141
Figure S86.	HMBC NMR spectrum of nicrophorusamide B (11) at 500 MHz in DMSO- <i>d</i> ₆	141
Figure S87.	ROESY NMR spectrum of nicrophorusamide B (11) at 500 MHz in DMSO- <i>d</i> ₆	142
Figure S88.	LC/MS analysis of L-FDAA derivatives of amino acids in nicrophorusamide A (10).	143
Figure S89.	LC/MS analysis of D-FDAA derivatives of amino acids in nicrophorusamide A (10).	143
Figure S90.	Synthesis of L- <i>erythro</i> -β-hydroxyaspartic acid.	144
Figure S91.	Co-injection experiments to determinate the absolute configuration at the β- carbon of D-β-hydroxyasparagine.	144

Figure S92.	HPLC analysis of GITC derivatives of isoleucine unit in microphorusamide A (10) and authentic L- / L- <i>allo</i> -isoleucine.	144
Figure S93.	Circular dichroism spectra data of microphorusamides A and B (10 and 11).	145
Figure S94.	HR-FAB-MS data of microphorusamide A (10).	146
Figure S95.	HR-FAB-MS data of microphorusamide B (11).	148
Figure S96.	¹ H NMR spectrum data of coprisamide C (14) at 850 MHz in DMSO- <i>d</i> ₆	150
Figure S97.	¹³ C NMR spectrum data of coprisamide C (14) at 212.5 MHz in DMSO- <i>d</i> ₆	150
Figure S98.	COSY NMR spectrum data of coprisamide C (14) at 800 MHz in DMSO- <i>d</i> ₆	151
Figure S99.	HSQC NMR spectrum data of coprisamide C (14) at 800 MHz in DMSO- <i>d</i> ₆	151
Figure S100.	HMBC NMR spectrum data of coprisamide C (14) at 850 MHz in DMSO- <i>d</i> ₆	152
Figure S101.	TOCSY NMR spectrum data of coprisamide C (14) at 800 MHz in DMSO- <i>d</i> ₆	152
Figure S102.	ROESY NMR spectrum data of coprisamide C (14) at 800 MHz in DMSO- <i>d</i> ₆	153
Figure S103.	¹ H NMR spectrum data of <i>S</i> -PGME amide of 14 (14a) at 800 MHz in CD ₃ OD.	154
Figure S104.	COSY NMR spectrum data of <i>S</i> -PGME amide of 14 (14a) at 800 MHz in CD ₃ OD.	154
Figure S105.	¹ H NMR spectrum data of <i>R</i> -PGME amide of 14 (14b) at 800 MHz in CD ₃ OD.	155
Figure S106.	COSY NMR spectrum data of <i>R</i> -PGME amide of 14 (14b) at 800 MHz in CD ₃ OD.	155

Figure S107.	^1H NMR spectrum data of coprisamide D (15) at 800 MHz in DMSO- d_6	156
Figure S108.	^1H NMR spectrum data of coprisamide D (15) at 200 MHz in DMSO- d_6 . ..	156
Figure S109.	COSY NMR spectrum data of coprisamide D (15) at 800 MHz in DMSO- d_6	157
Figure S110.	HSQC NMR spectrum data of coprisamide D (15) at 800 MHz in DMSO- d_6	157
Figure S111.	HMBC NMR spectrum data of coprisamide D (15) at 800 MHz in DMSO- d_6	158
Figure S112.	TOCSY NMR spectrum data of coprisamide D (15) at 800 MHz in DMSO- d_6	158
Figure S113.	ROESY NMR spectrum data of coprisamide D (15) at 800 MHz in DMSO- d_6	159
Figure S114.	HR-ESI-MS data of coprisamide C (14).	160
Figure S115.	HR-ESI-MS data of coprisamide D (15).	160
Figure S116.	LC/MS chromatogram data of L- and D-FDAA derivatives of the amino acid units in coprisamide C (14).	161
Figure S117.	<i>J</i> -based configuration analysis of C-2 and C-3 of coprisamide C (14).	162
Figure S118.	Circular dichroism spectra data of coprisamides C and D (14 and 15).	162

List of Tables

Table S1.	^1H and ^{13}C NMR data for 6–9 in CD_3OD	163
Table S2.	Energy-minimized modeling of 6	164
Table S3.	Energy-minimized modeling of 7	165
Table S4.	Energy-minimized modeling of 8	166
Table S5.	Energy-minimized modeling of 9	167
Table S6.	ECD calculation of 4 (<i>8S</i> , <i>24R</i>).	168
Table S7.	ECD calculation of 4 (<i>8R</i> , <i>24R</i>).	169
Table S8.	Deduced function of ORFs in the bombyxamycin biosynthetic gene cluster from <i>Streptomyces</i> sp. SD53.	170
Table S9.	Bacterial strains and plasmids used in this study.	174
Table S10.	Primers used in this study.	175
Table S11.	LC/MS analysis of L- and D-FDAA derivatives of the amino acids in nicrophorusamide A (10).	175
Table S12.	Energy minimized coordinates of nicrophorusamide A (10) at the basis set def-SVP for all atoms (\AA).	176
Table S13.	Energy minimized coordinates of nicrophorusamide B (11) at the basis set def-SVP for all atoms (\AA).	177
Table S14.	LC/MS analysis of L- and D-FDAA derivatives of the amino acids in coprisamide C (14).	178
Table S15.	Deduced putative functions of ORFs in the coprisamides biosynthetic gene cluster (<i>cpr</i> cluster) from <i>Micromonospora</i> sp. UTJ3.	179

Figure S1. ^1H NMR spectrum data of bombyxamycin A (**1**) at 500 MHz in $\text{DMSO}-d_6$.

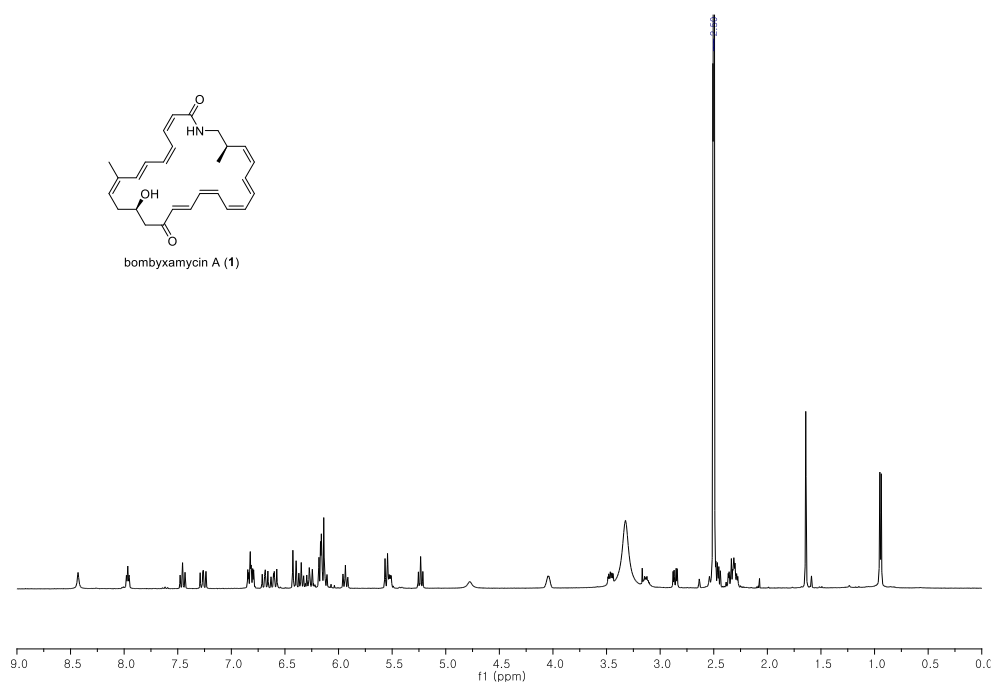
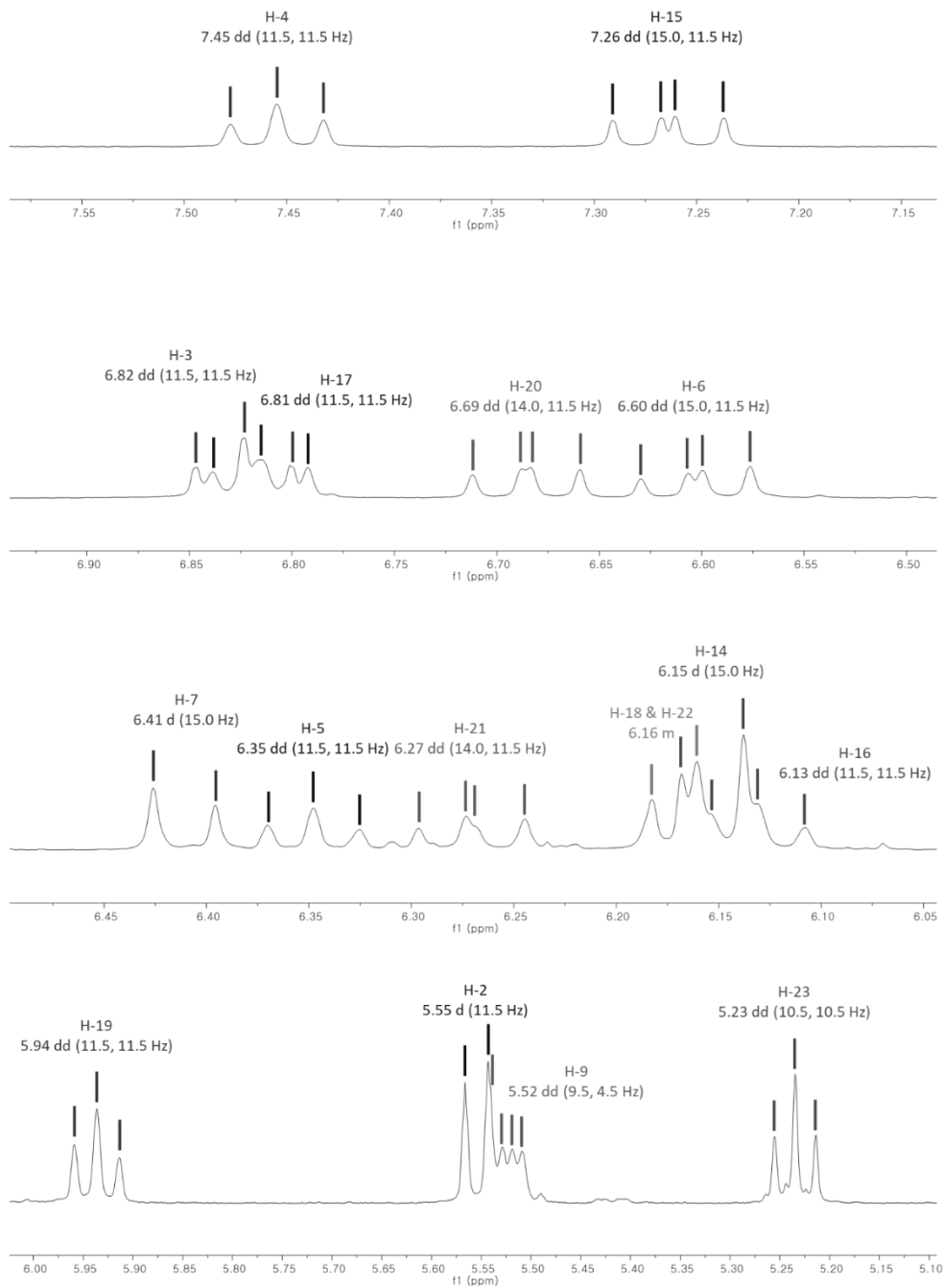



Figure S2. Expanded ^1H NMR spectrum of bombyxamycin A (**1**) at 500 MHz in $\text{DMSO-}d_6$ and measurement of ^1H - ^1H coupling constants of the olefinic protons.





 The chemical structure of bombyxamycin A (1) is shown above its ^1H NMR spectrum. The molecule is a complex macrocyclic lactone with multiple double bonds and a hydroxyl group. The NMR spectrum displays peaks from 0 to 10 ppm, with a prominent peak at approximately 4.2 ppm corresponding to the hydroxyl group.

Figure S4. COSY NMR spectrum data of bombyxamycin A (**1**) at 500 MHz in DMSO-*d*₆.

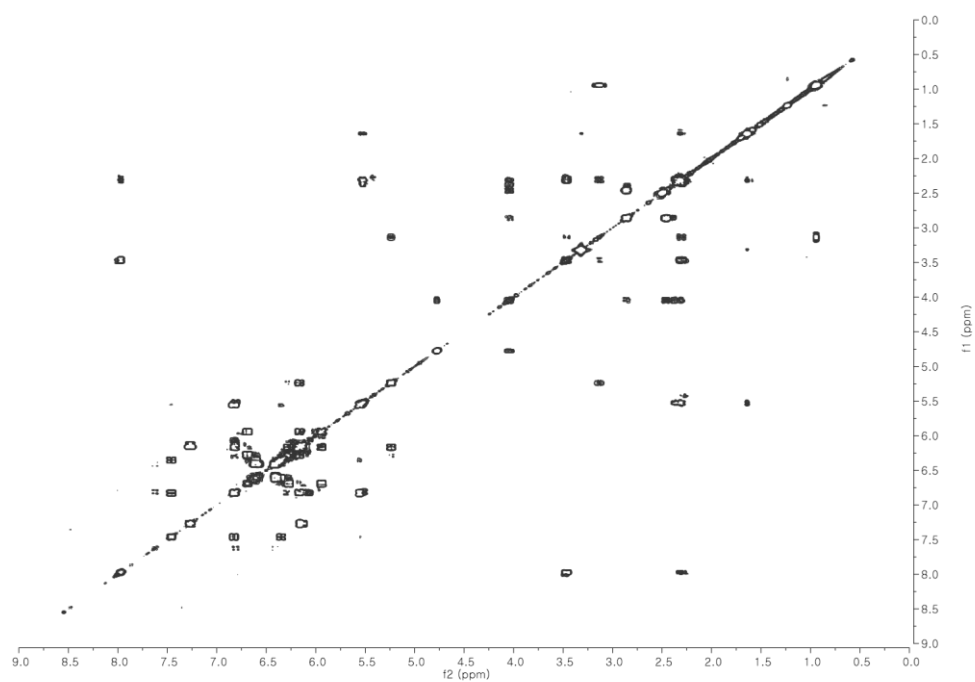


Figure S5. HSQC NMR spectrum data of bombyxamycin A (**1**) at 500 MHz in DMSO-*d*₆.

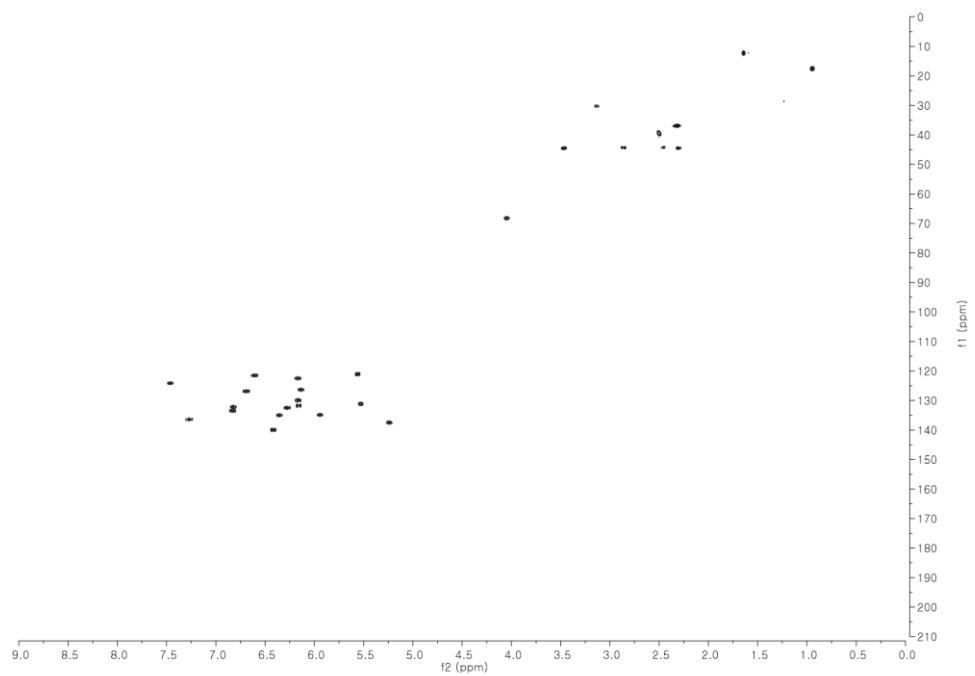


Figure S6. HMBC NMR spectrum data of bombyxamycin A (**1**) at 500 MHz in DMSO-*d*₆.

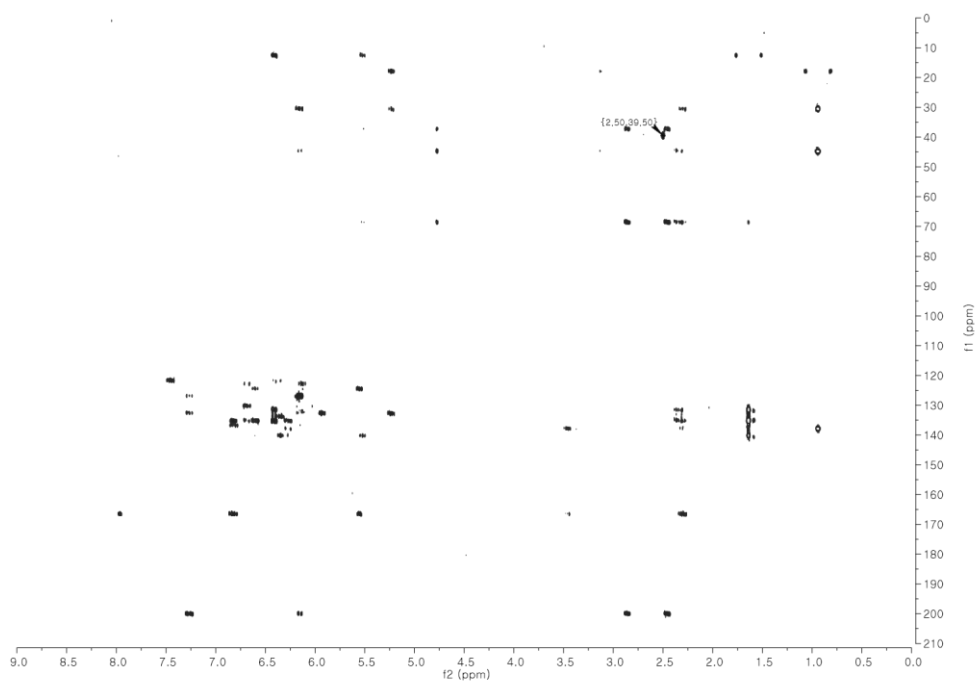


Figure S7. NOESY NMR spectrum data of bombyxamycin A (**1**) at 500 MHz in DMSO-*d*₆.

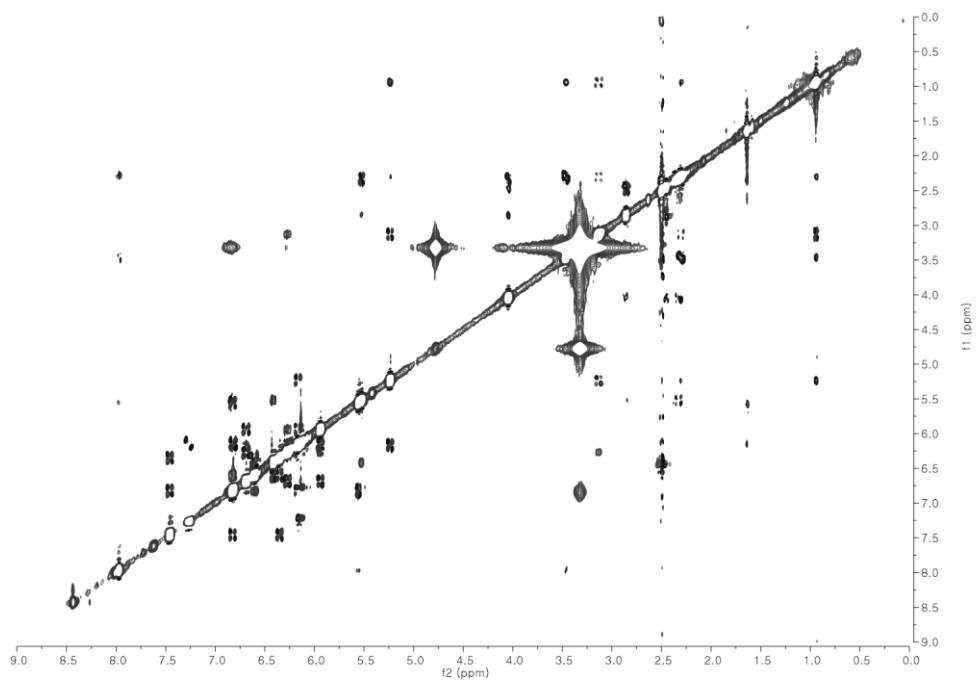


Figure S8. ^1H NMR spectrum data of *S*-MTPA ester of **1** (**1a**) at 500 MHz in $\text{DMSO}-d_6$.

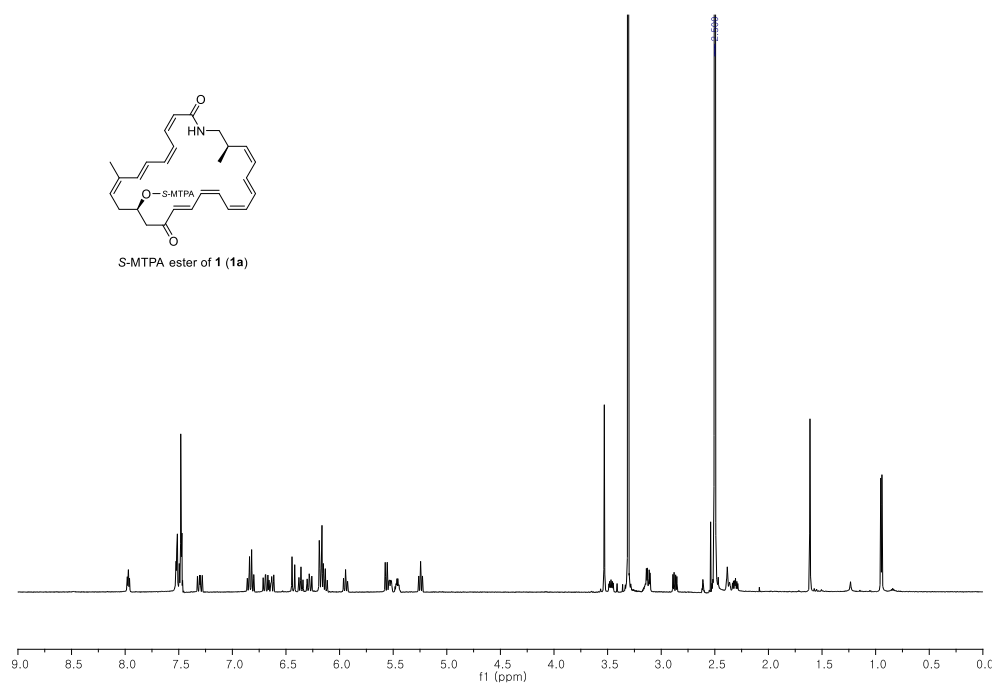


Figure S9. COSY NMR spectrum data of *S*-MTPA ester of **1** (**1a**) at 500 MHz in $\text{DMSO}-d_6$.

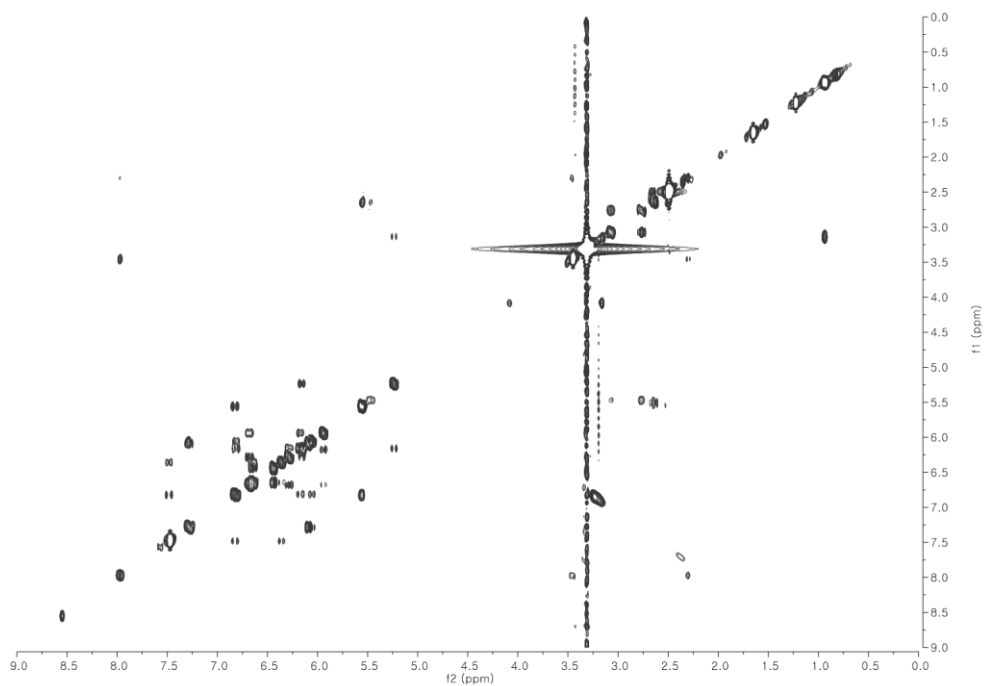


Figure S12. ^1H NMR spectrum data of 3-(2,4-dinitro-phenylamino)-2-methyl-propanoic acid (**5**) at 600 MHz in CD_3OD .

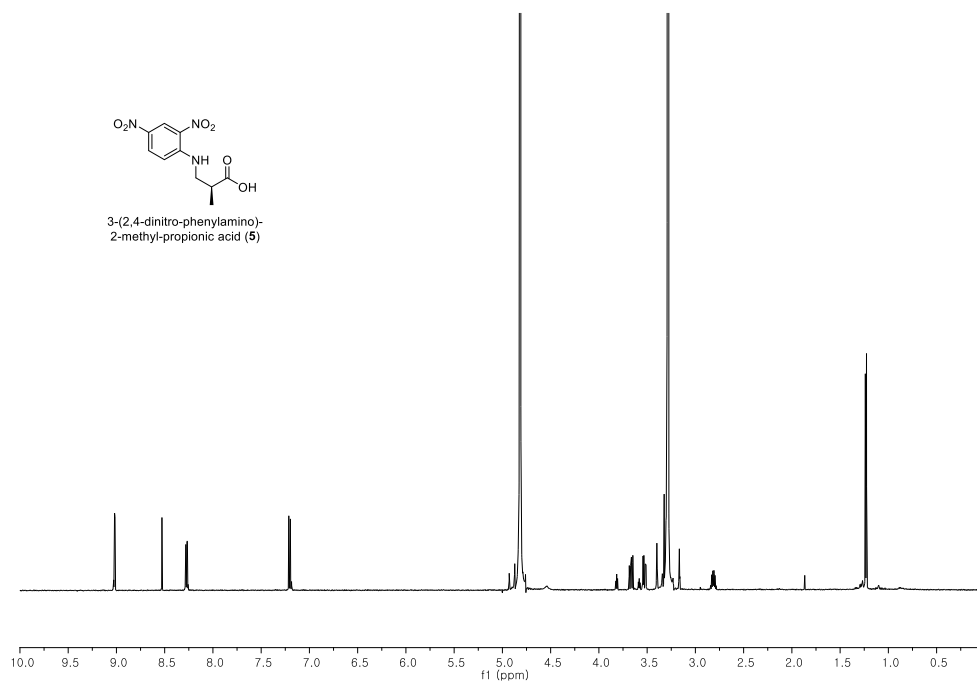


Figure S13. ^1H NMR spectrum data of *S*-PGME amide of **5** (**5a**) at 600 MHz in CD_3OD .

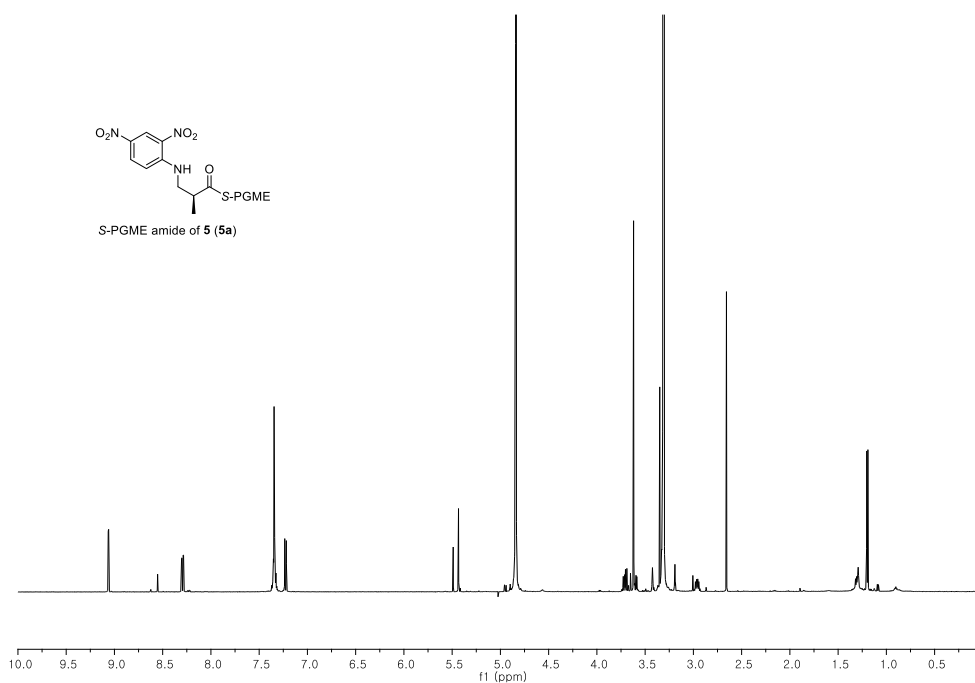


Figure S14. ^1H NMR spectrum data of *R*-PGME amide of **5** (**5b**) at 600 MHz in CD_3OD .

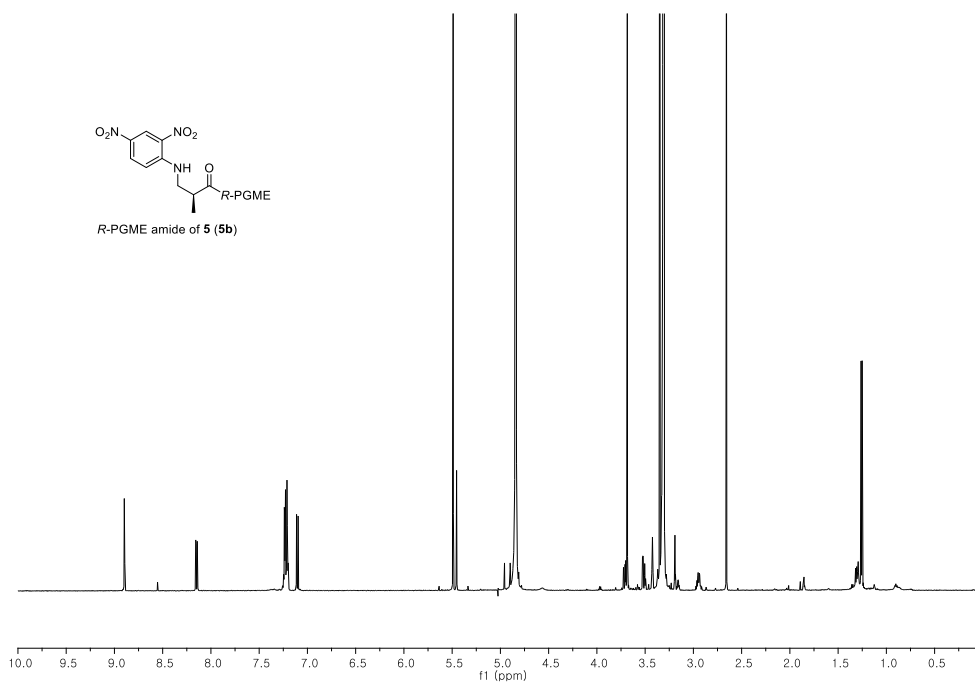


Figure S16. Expanded ^1H NMR spectrum of bombyxamycin B (**2**) at 500 MHz in DMSO- d_6 and measurement of ^1H - ^1H coupling constants of the olefinic protons.

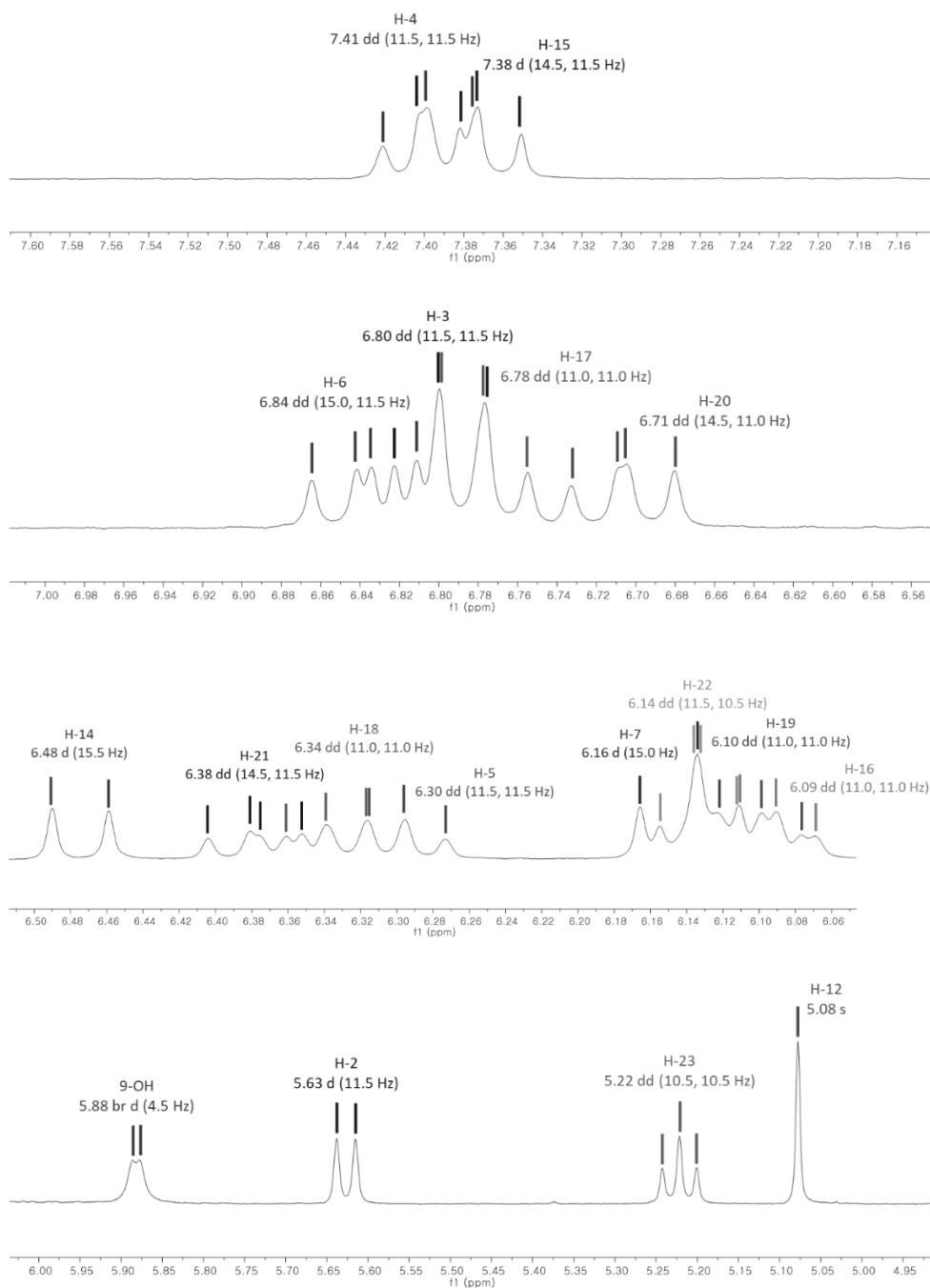


Figure S17. ^{13}C NMR spectrum data of bombyxamycin B (**2**) at 125 MHz in $\text{DMSO-}d_6$.

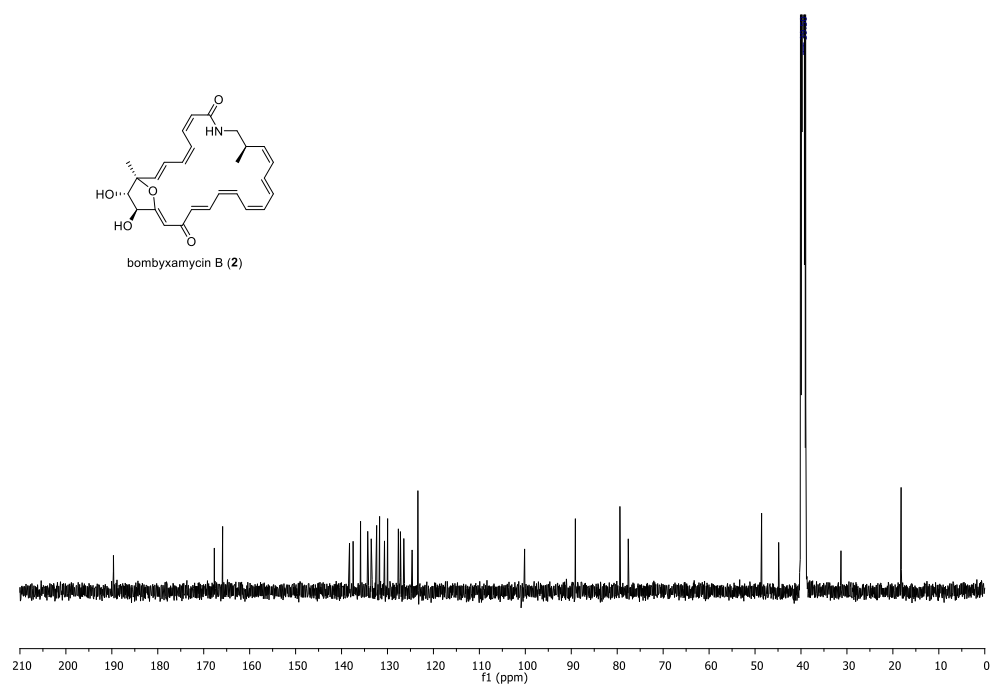


Figure S18. ^{13}C NMR spectrum data of bombyxamycin B (**2**) at 212.5 MHz in CD_3OD .

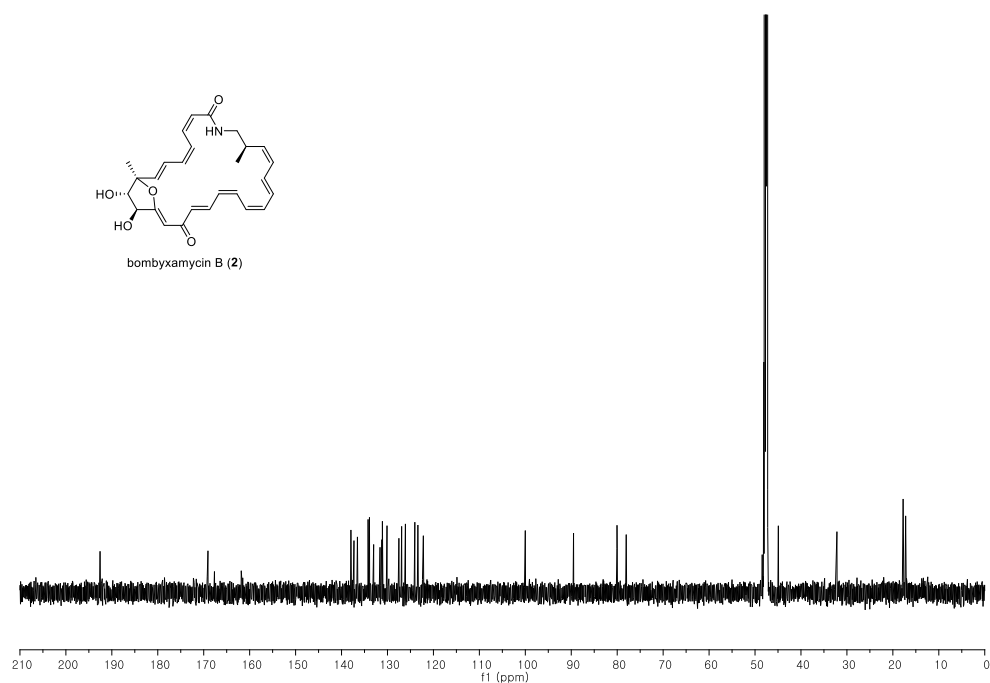


Figure S19. ^{13}C NMR spectrum data of bombyxamycin B (**2**) at 212.5 MHz in 1:1 $\text{CD}_3\text{OD}/\text{CD}_3\text{OH}$.

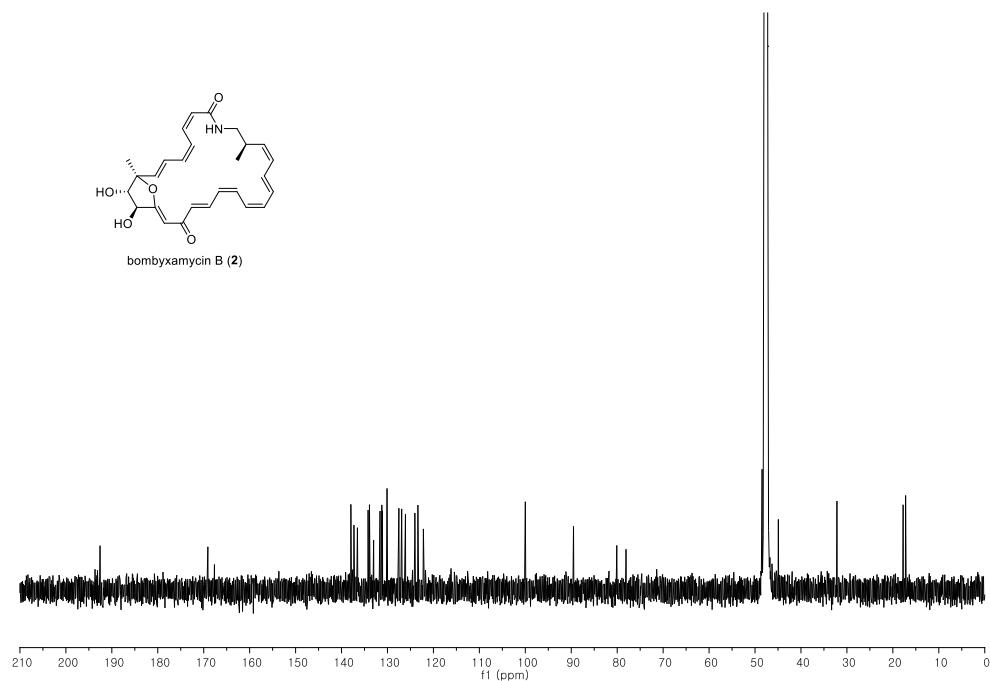


Figure S20. COSY NMR spectrum data of bombyxamycin B (**2**) at 500 MHz in DMSO- d_6 .

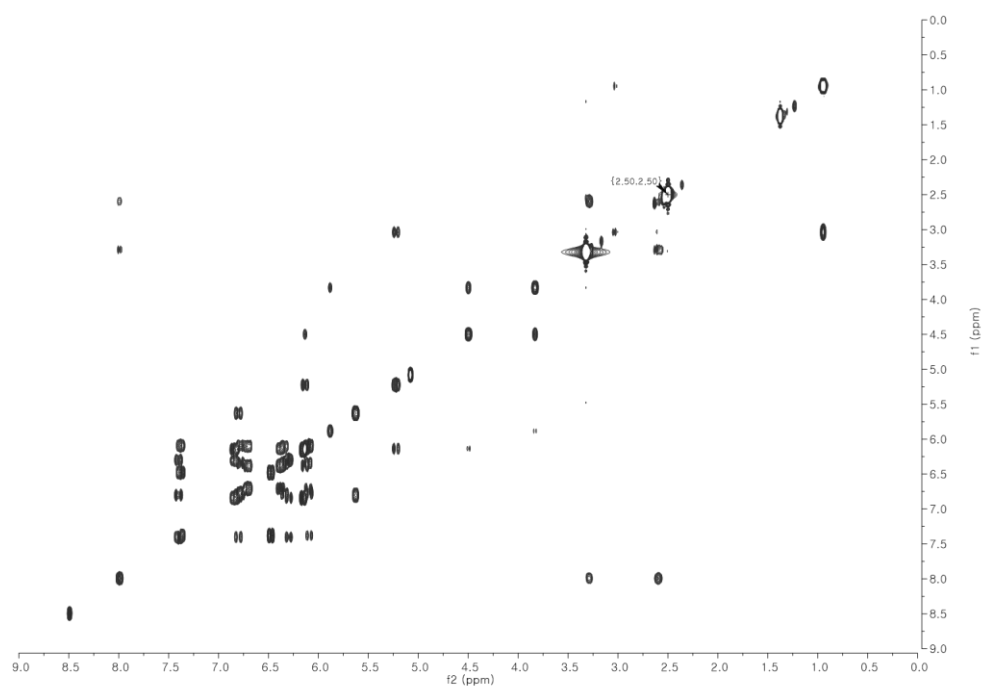


Figure S21. HSQC NMR spectrum data of bombyxamycin B (**2**) at 500 MHz in DMSO- d_6 .

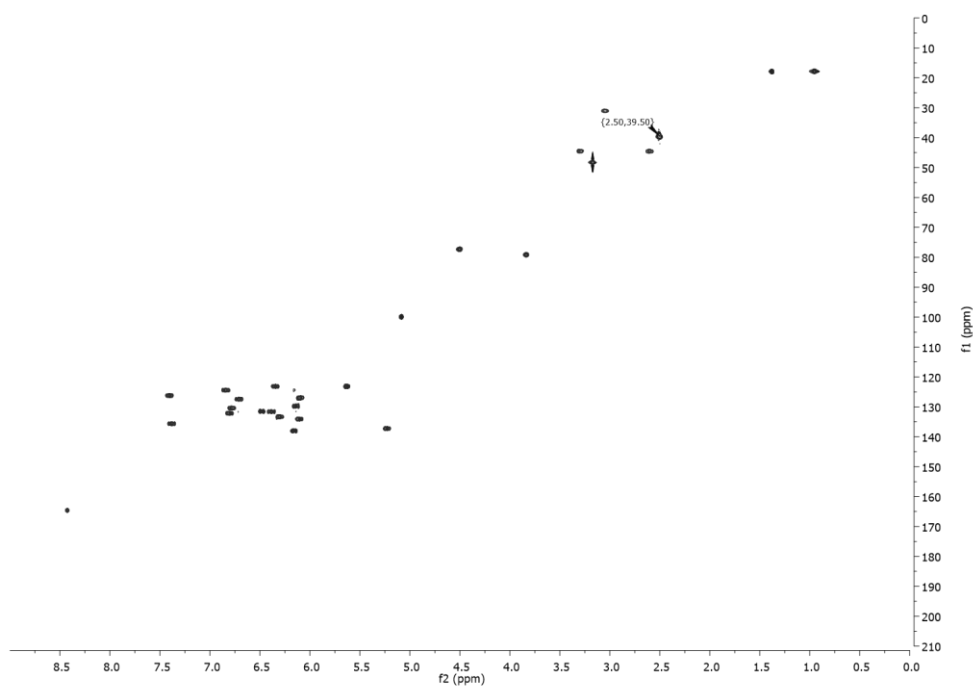


Figure S22. HMBC NMR spectrum data of bombyxamycin B (**2**) at 500 MHz in DMSO-*d*₆.

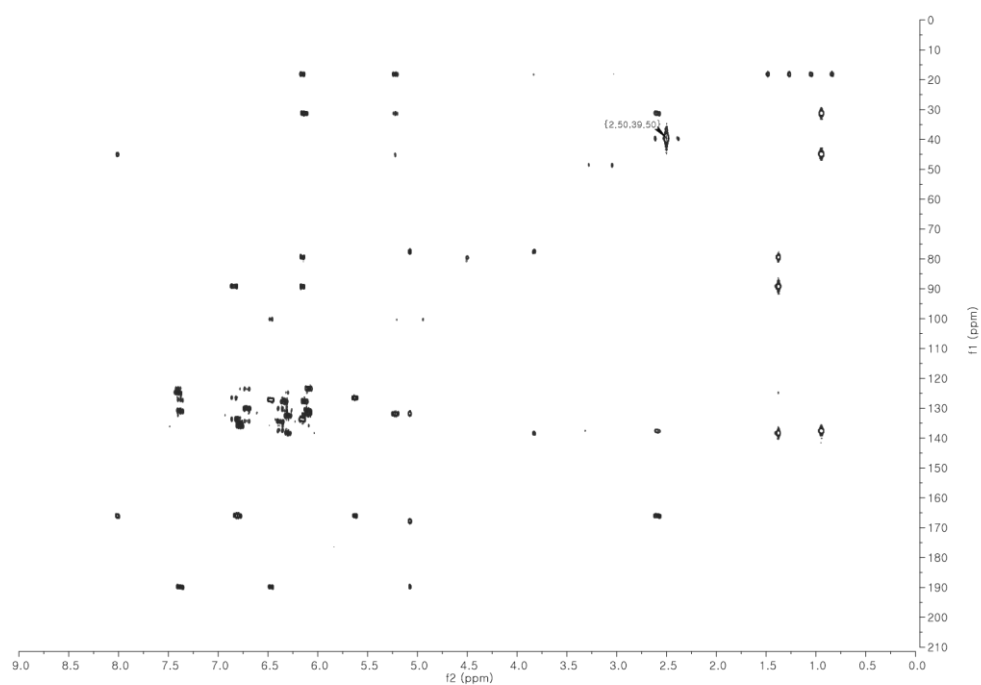


Figure S23. NOESY NMR spectrum data of bombyxamycin B (**2**) at 500 MHz in DMSO-*d*₆.

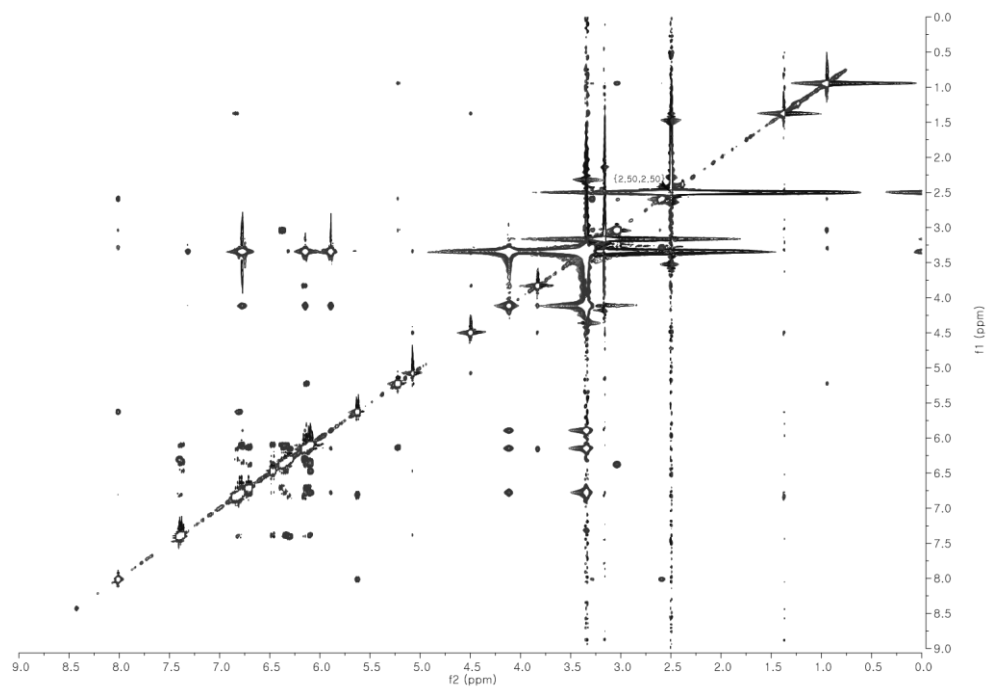


Figure S24. ^1H NMR spectrum data of *S*-MTPA ester of **2** (**2a**) at 500 MHz in $\text{DMSO}-d_6$.

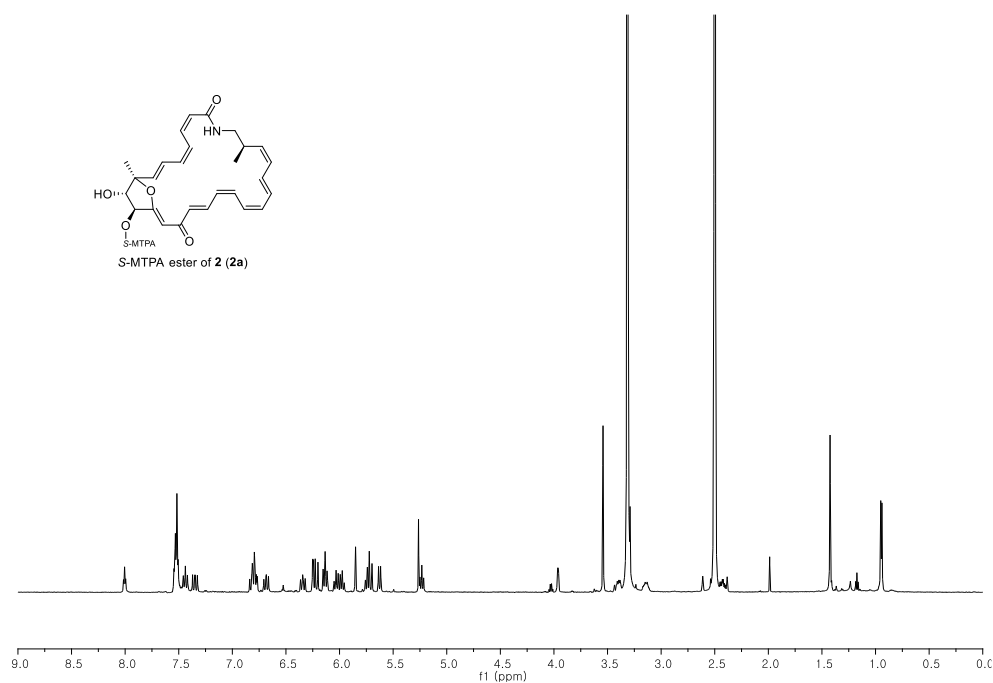


Figure S25. COSY NMR spectrum data of *S*-MTPA ester of **2** (**2a**) at 500 MHz in $\text{DMSO}-d_6$.

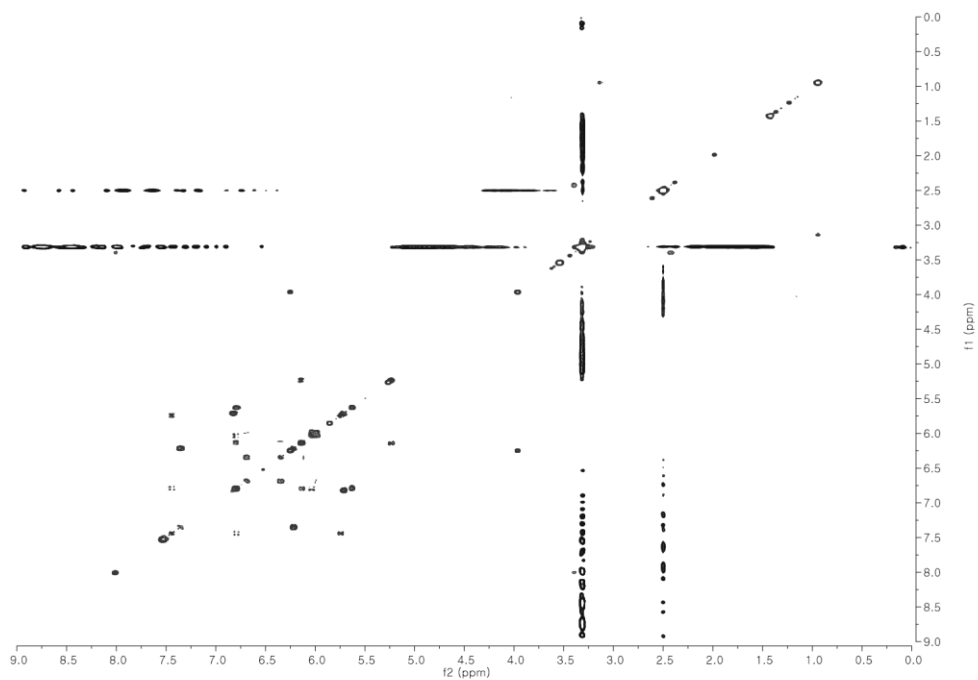


Figure S26. ^1H NMR spectrum data of *R*-MTPA ester of **2** (**2b**) at 500 MHz in $\text{DMSO}-d_6$.

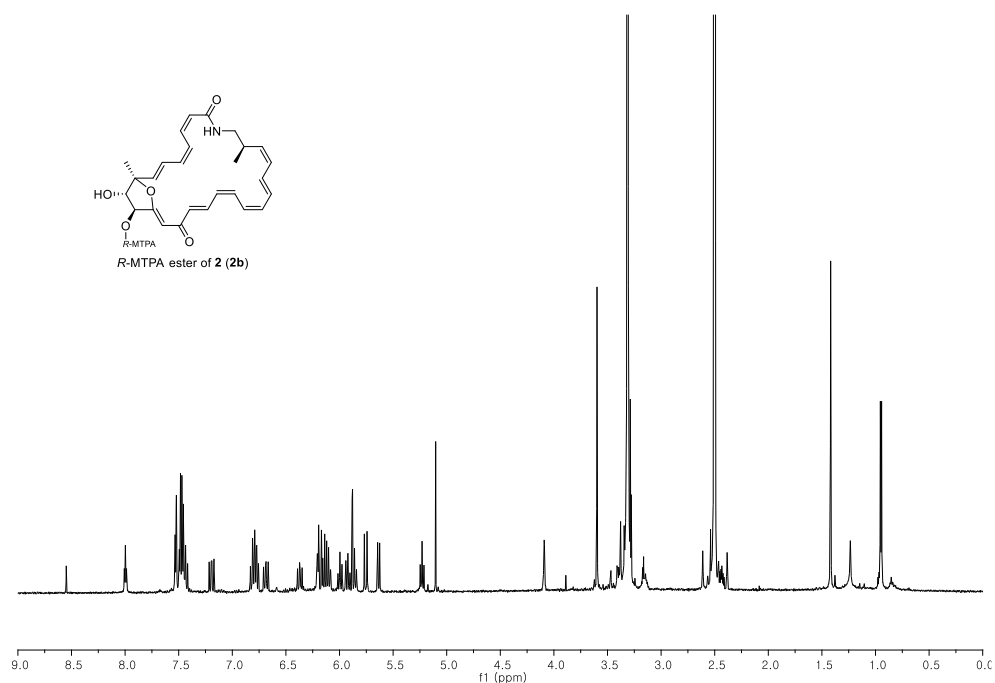


Figure S27. COSY NMR spectrum data of *R*-MTPA ester of **2** (**2b**) at 500 MHz in $\text{DMSO}-d_6$.

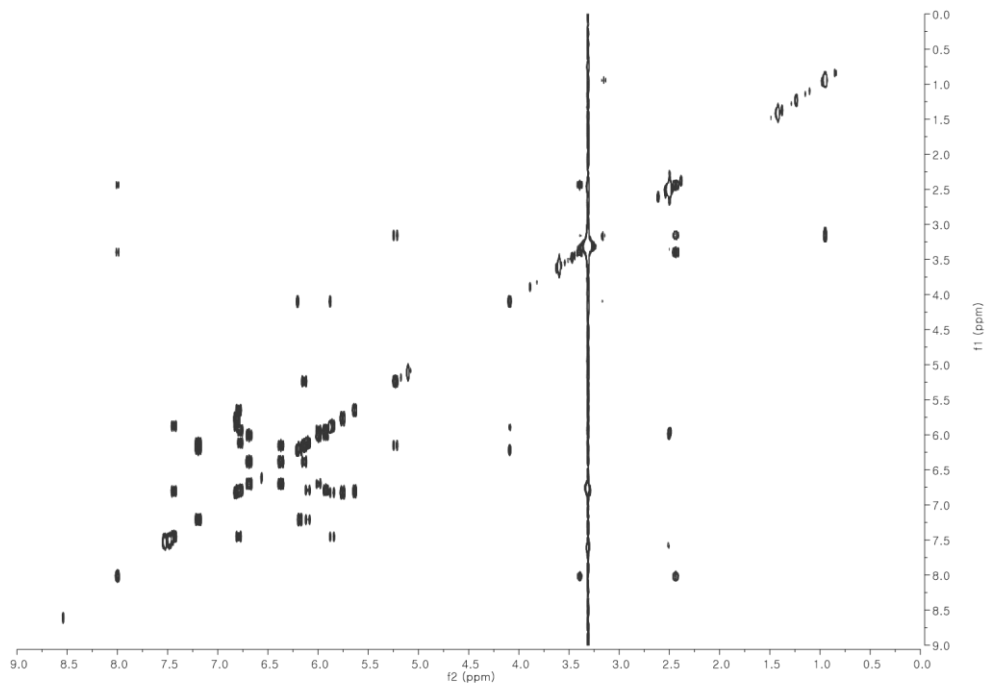


Figure S28. ^1H NMR spectrum of bombyxamycin C (**3**) at 850 MHz in $\text{DMSO}-d_6$.

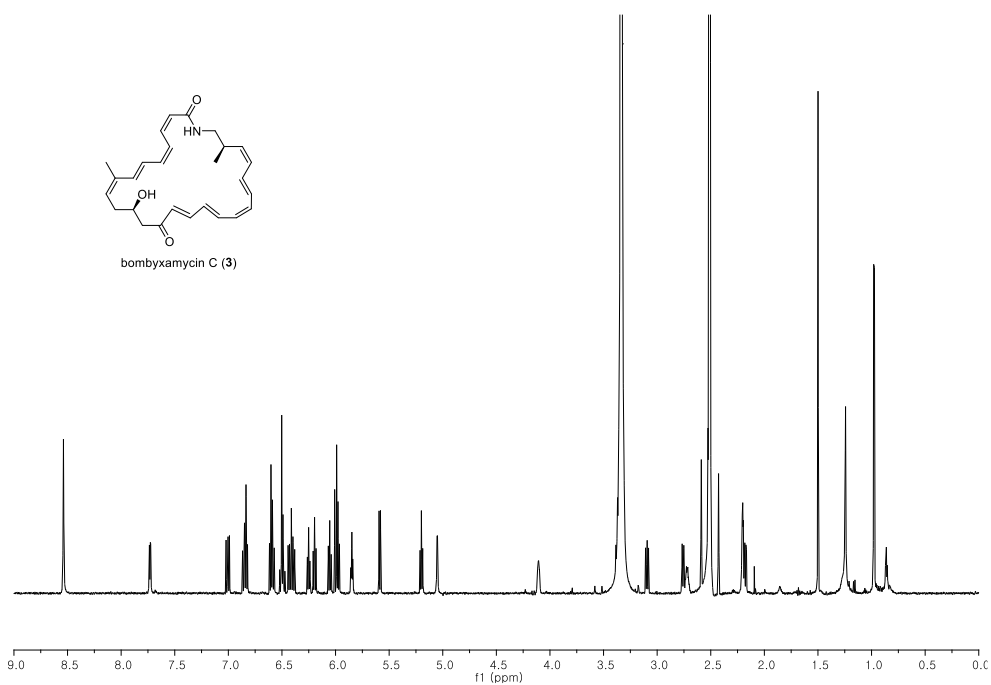


Figure S29. ^{13}C NMR spectrum of bombyxamycin C (**3**) at 212.5 MHz in $\text{DMSO}-d_6$.

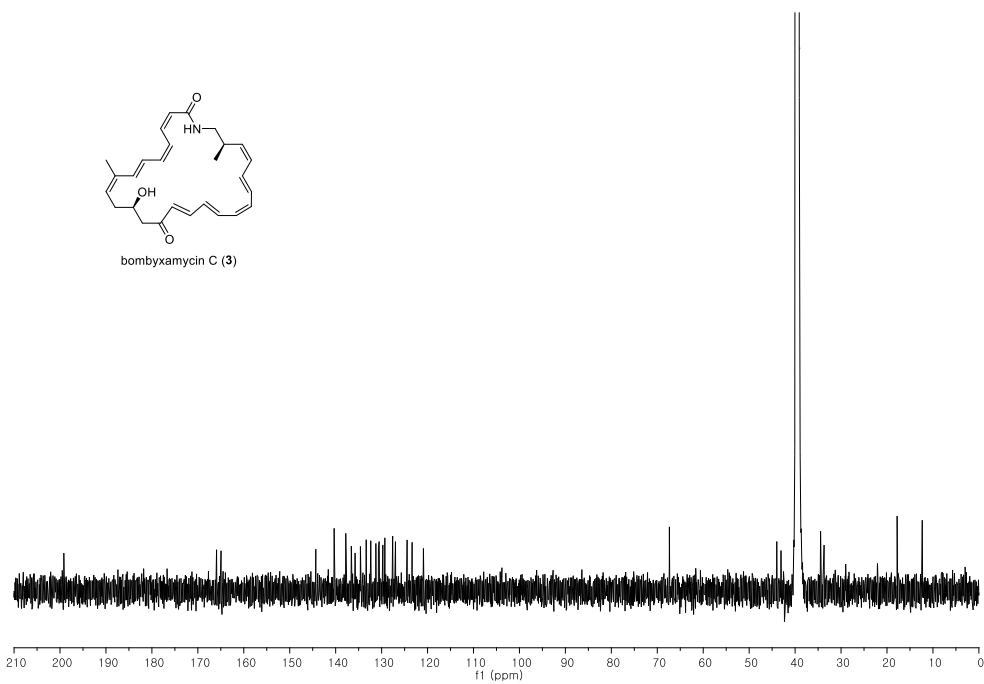


Figure S30. COSY NMR spectrum of bombyxamycin C (**3**) at 500 MHz in DMSO- d_6 .

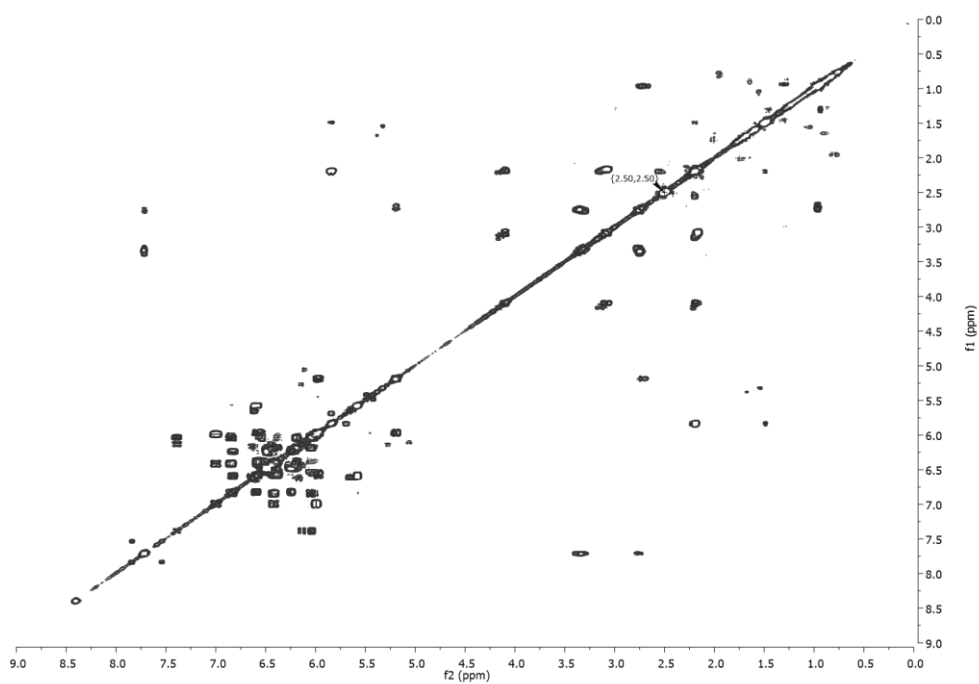


Figure S31. HSQC NMR spectrum of bombyxamycin C (**3**) at 500 MHz in DMSO- d_6 .

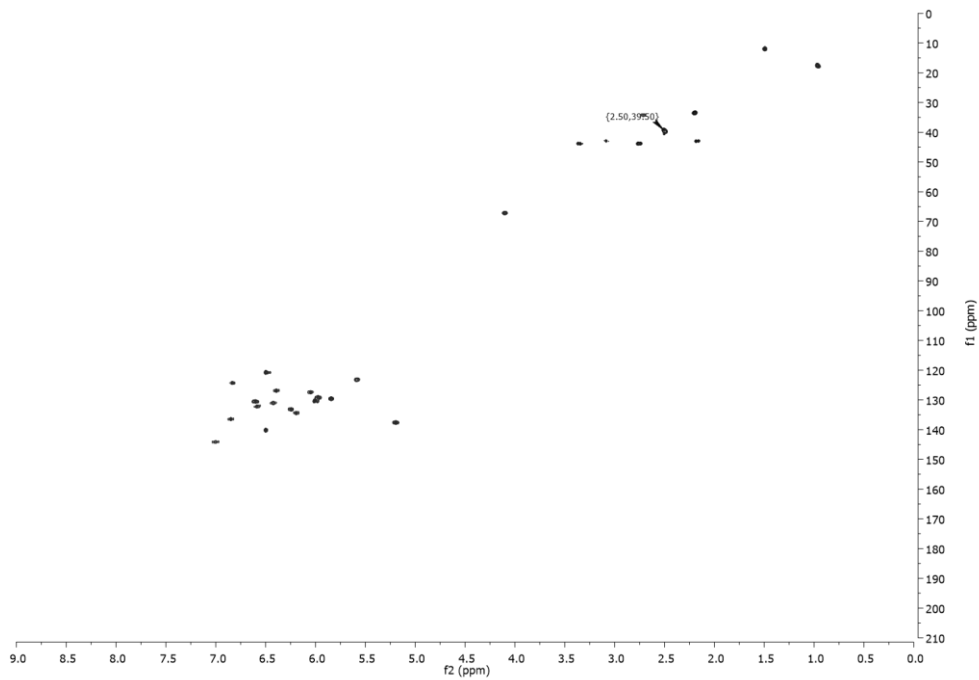


Figure S32. HMBC NMR spectrum of bombyxamycin C (**3**) at 500 MHz in DMSO- d_6 .

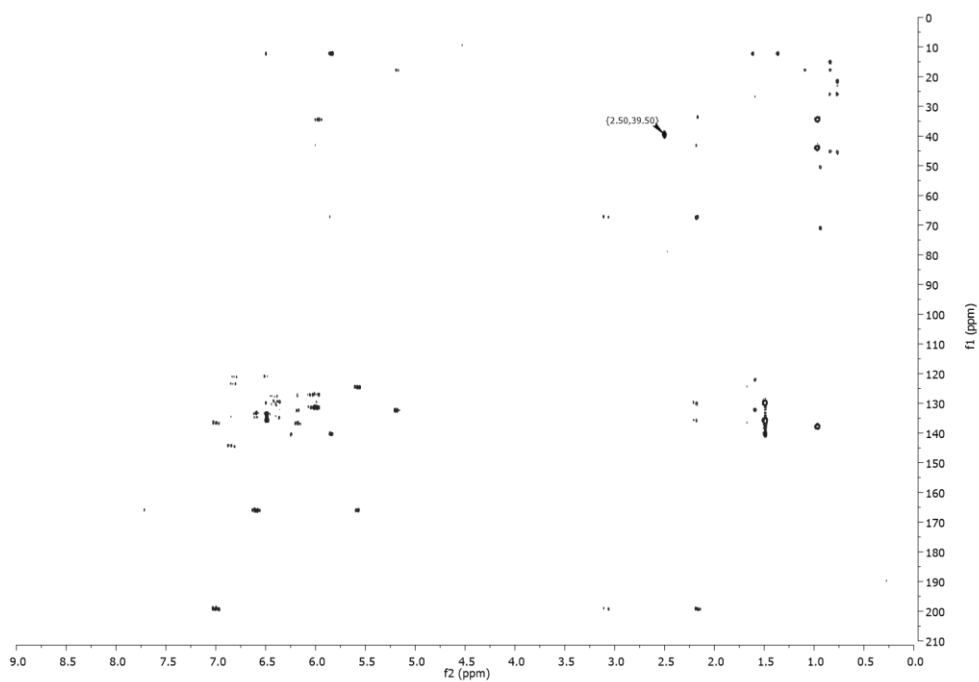
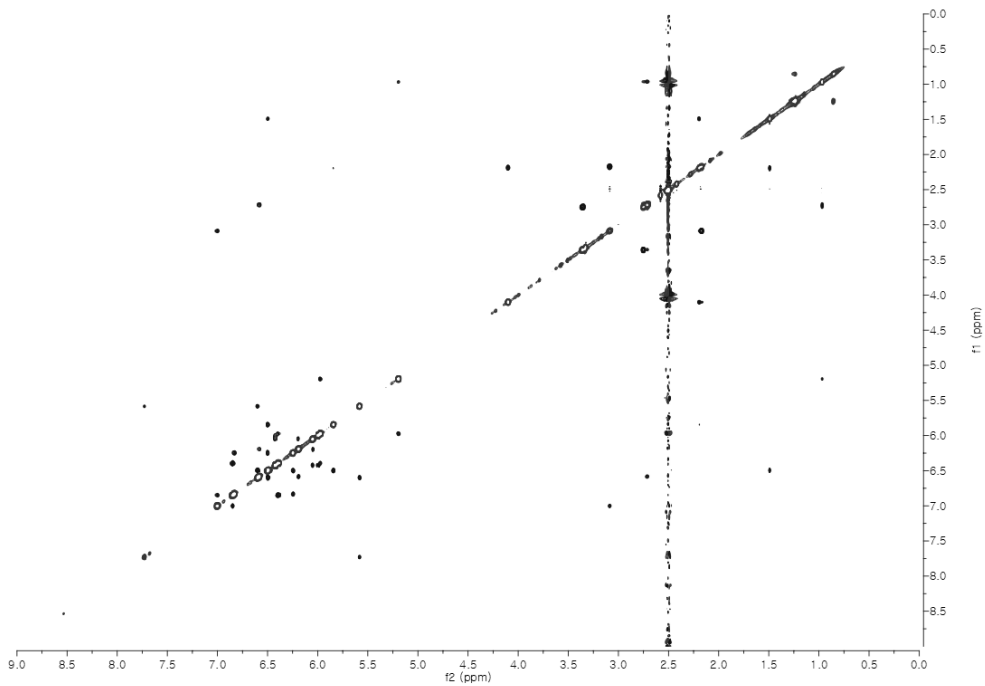


Figure S33. NOESY NMR spectrum of bombyxamycin C (**3**) at 850 MHz in DMSO- d_6 .



S-MTPA ester of **3 (**3a**)**

¹H NMR spectrum (CDCl₃) of the S-MTPA ester of **3** (**3a**). The x-axis represents the chemical shift in ppm, ranging from 0.0 to 9.0. The spectrum shows several peaks, including aromatic signals between 6.0 and 8.5 ppm, a sharp singlet at approximately 4.8 ppm, and aliphatic signals between 0.5 and 4.0 ppm. Integration values are provided below the baseline.

Figure S36. ^1H NMR spectrum of *R*-MTPA ester of **3** (**3b**) at 850 MHz in CD_3OD .

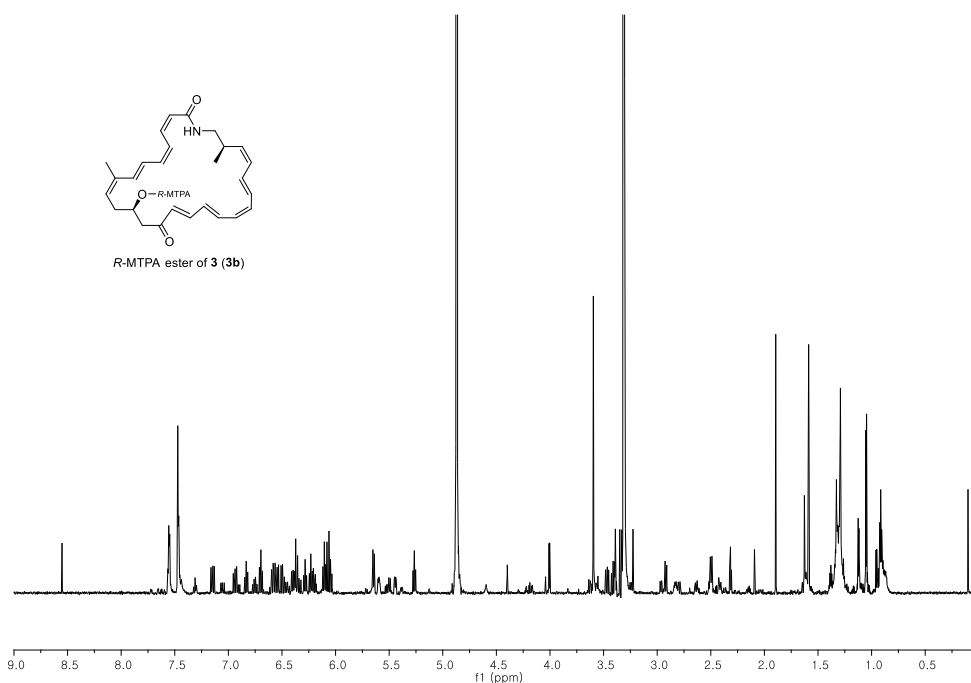


Figure S37. COSY NMR spectrum of *R*-MTPA ester of **3** (**3b**) at 850 MHz in CD_3OD .

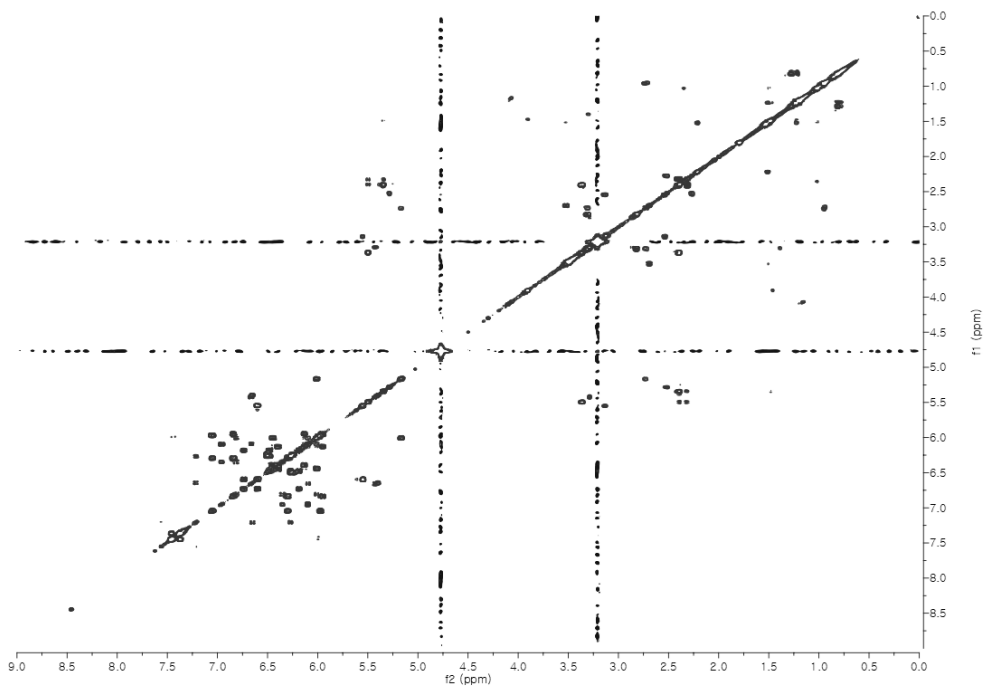


Figure S38. ^1H NMR spectrum of piceamycin (**4**) at 500 MHz in $\text{DMSO}-d_6$.

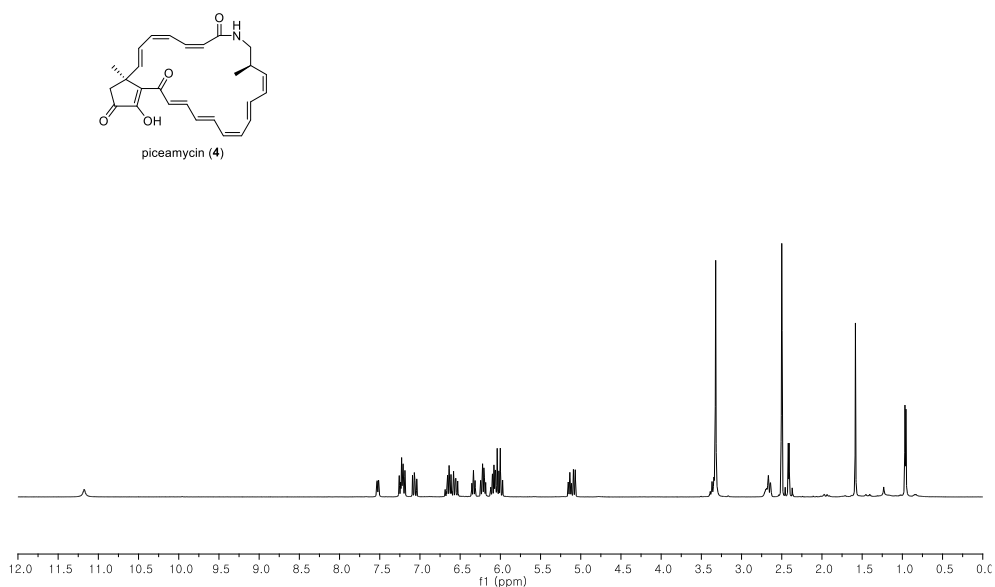


Figure S39. ^{13}C NMR spectrum of piceamycin (**4**) at 212.5 MHz in $\text{DMSO}-d_6$.

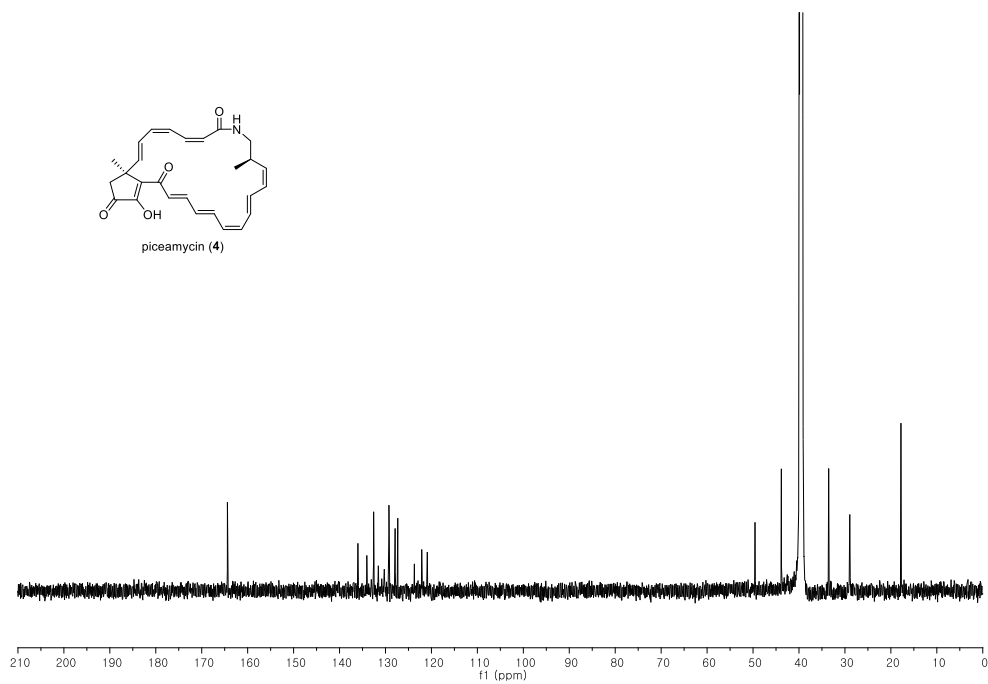


Figure S40. COSY NMR spectrum of piceamycin (**4**) at 500 MHz in DMSO-*d*₆.

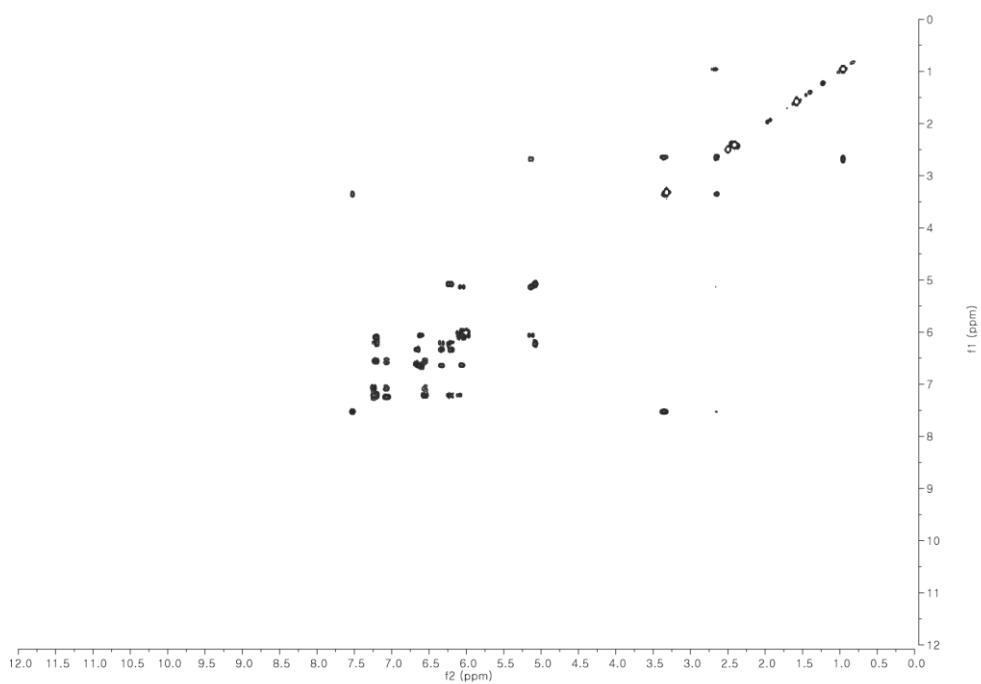


Figure S41. HSQC NMR spectrum of piceamycin (**4**) at 500 MHz in DMSO-*d*₆.

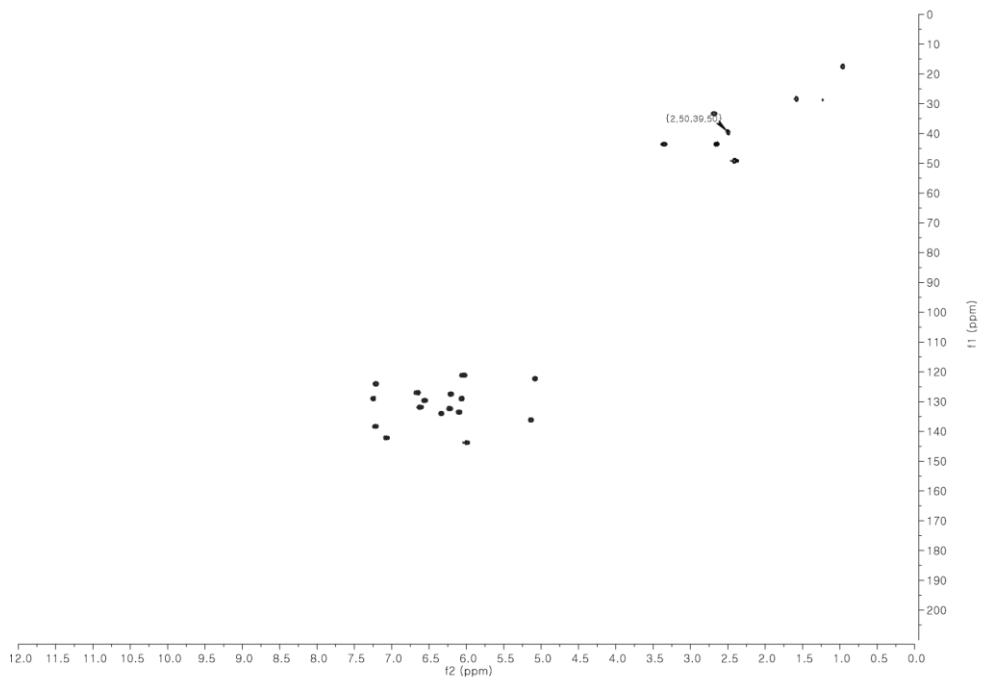


Figure S42. HMBC NMR spectrum of piceamycin (**4**) at 500 MHz in DMSO-*d*₆.

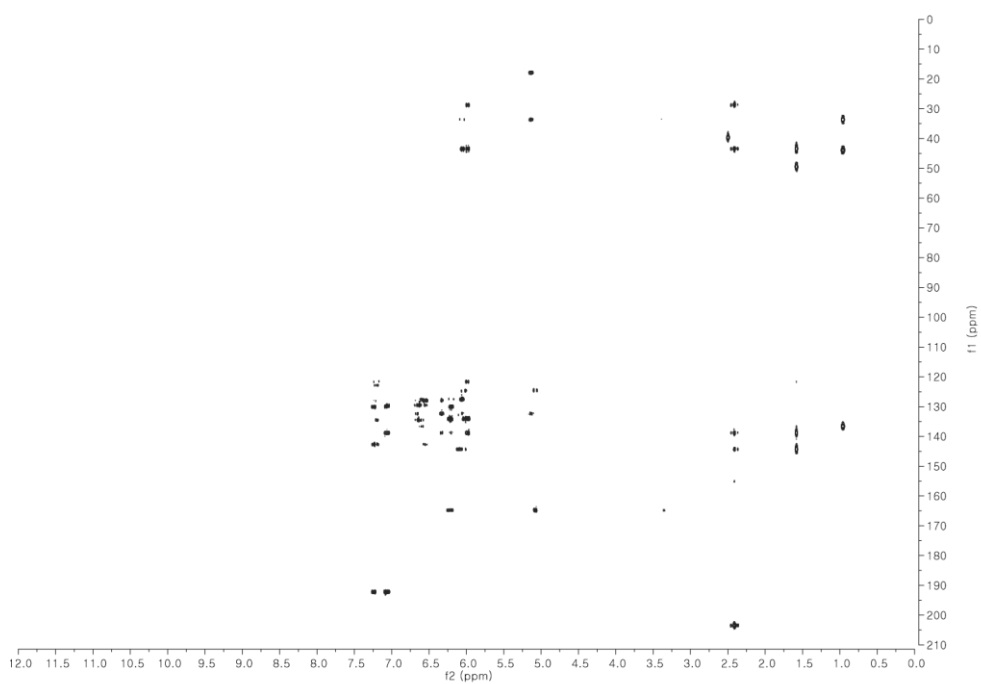


Figure S43. NOESY NMR spectrum of piceamycin (**4**) at 850 MHz in DMSO-*d*₆.

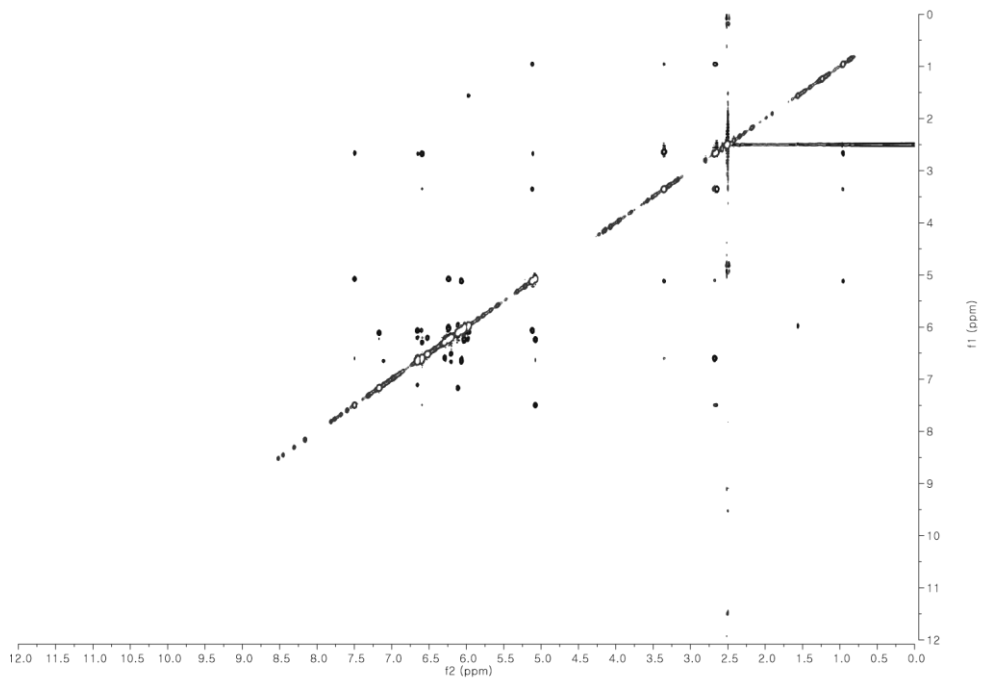


Figure S44. ^1H NMR spectrum of *S*-PGME amide of 2*S*-3-amino-2-methylpropanoic acid (**6**) at 850 MHz in CD_3OD .

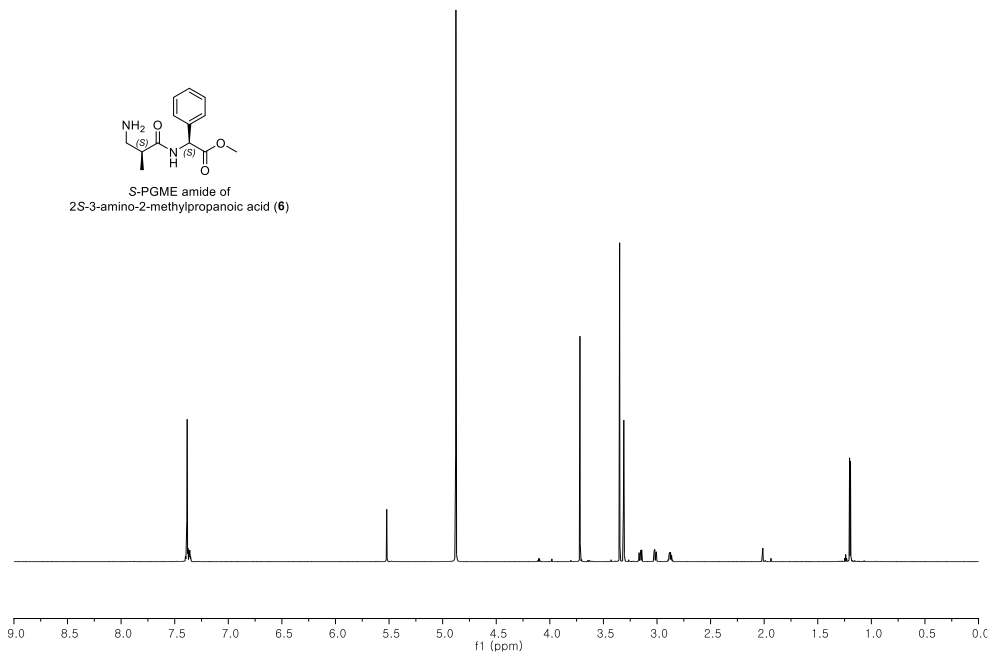
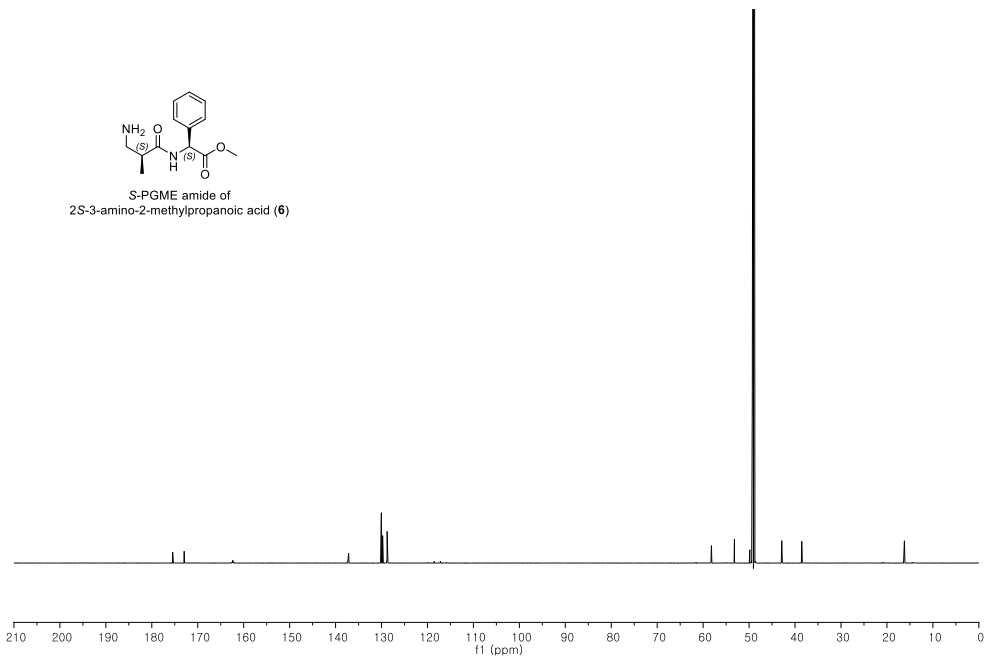


Figure S45. ^{13}C NMR spectrum of *S*-PGME amide of 2*S*-3-amino-2-methylpropanoic acid (**6**) at 212.5 MHz in CD_3OD .



**R-PGME amide of
2*S*-3-amino-2-methylpropanoic acid (**7**)**

¹H NMR spectrum (400 MHz, DMSO-d₆) of **7**. The spectrum shows a broad peak at ~7.4 ppm (NH), a sharp peak at ~5.5 ppm (CH), a large peak at ~4.8 ppm (CH₂), a multiplet at ~3.5 ppm (CH), and several smaller peaks between 2.5 and 3.5 ppm (CH₃ and solvent).

Figure 1 ¹³C NMR spectrum of *R*-PGME amide of 2*S*-3-amino-2-methylpropanoic acid (**7**)

The chemical structure of *R*-PGME amide of 2*S*-3-amino-2-methylpropanoic acid (**7**) is shown above the spectrum. The structure is a dipeptide derivative: *R*-methyl 2-((2*S*-amino-2-methylpropanoate)amido)-3-phenylpropanoate. The spectrum displays peaks corresponding to the various carbon environments in the molecule, including the carbonyl carbons, the chiral centers, the amide nitrogen, the phenyl ring, and the methyl groups.

¹³C NMR spectrum (ppm) showing peaks from 0 to 210 ppm. The spectrum displays several sharp peaks, including a large peak at approximately 172 ppm (likely the carbonyl carbon), and a cluster of peaks between 120 and 140 ppm (likely the aromatic carbons of the phenyl ring). Other peaks are visible in the aliphatic region, including a small peak at approximately 18 ppm (likely the methyl carbon).

Figure S48. ^1H NMR spectrum of *S*-PGME amide of 2*R*-3-amino-2-methylpropanoic acid (**8**) at 850 MHz in CD_3OD .

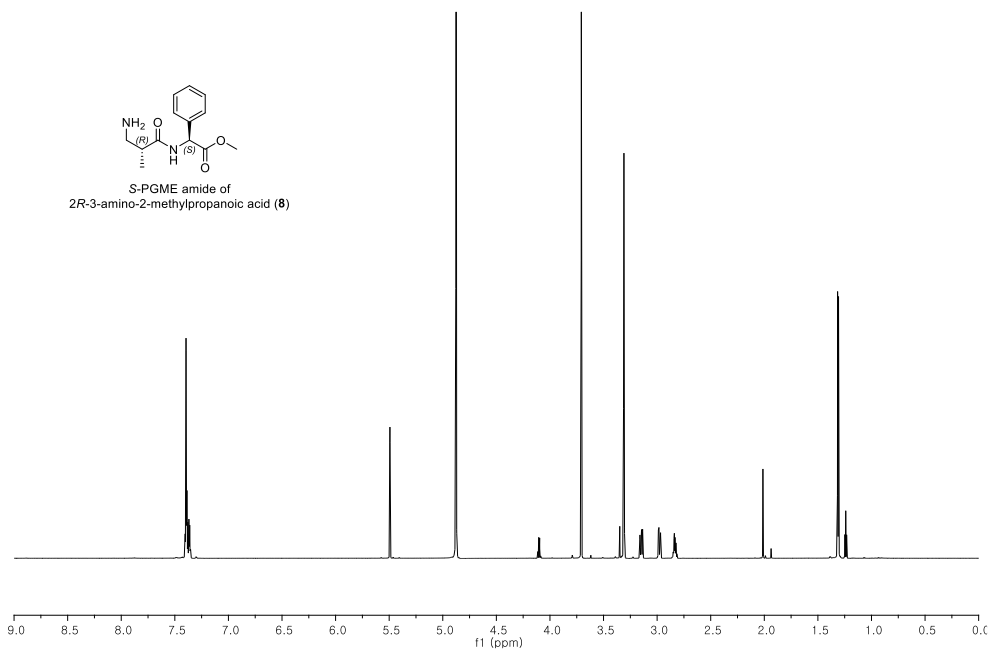


Figure S49. ^{13}C NMR spectrum of *S*-PGME amide of 2*R*-3-amino-2-methylpropanoic acid (**8**) at 212.5 MHz in CD_3OD .

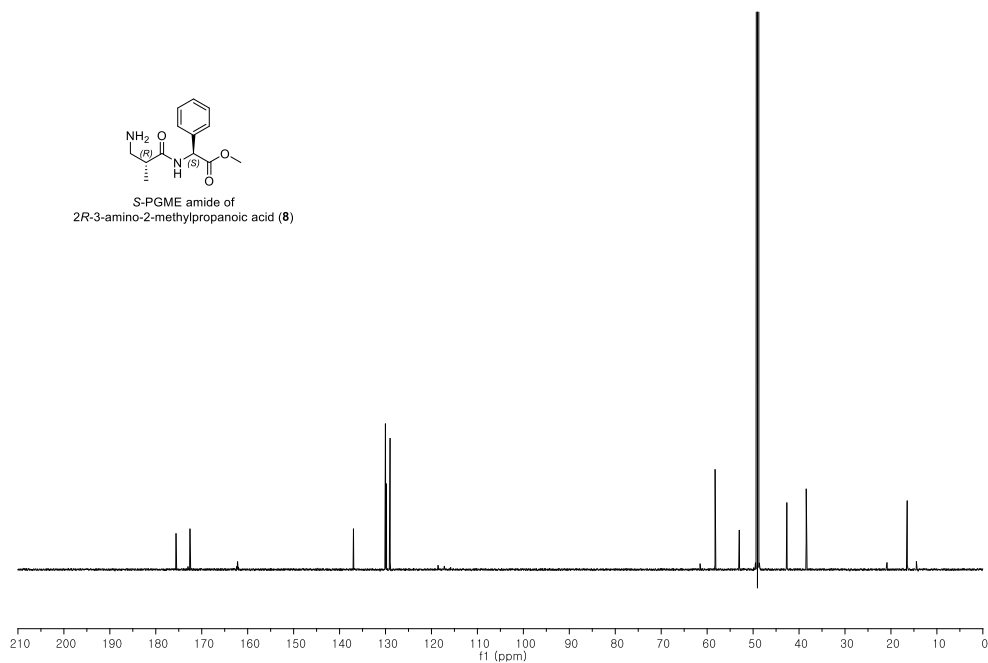


Figure S50. ^1H NMR spectrum of *R*-PGME amide of 2*R*-3-amino-2-methylpropanoic acid (**9**) at 850 MHz in CD_3OD .

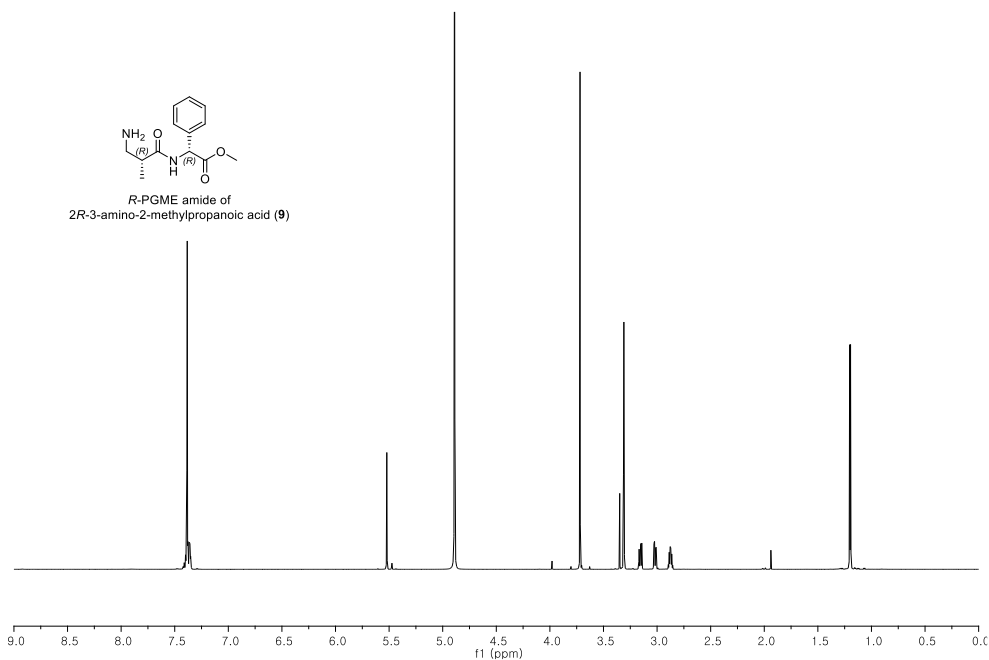


Figure S51. ^{13}C NMR spectrum of *R*-PGME amide of 2*R*-3-amino-2-methylpropanoic acid (**9**) at 212.5 MHz in CD_3OD .

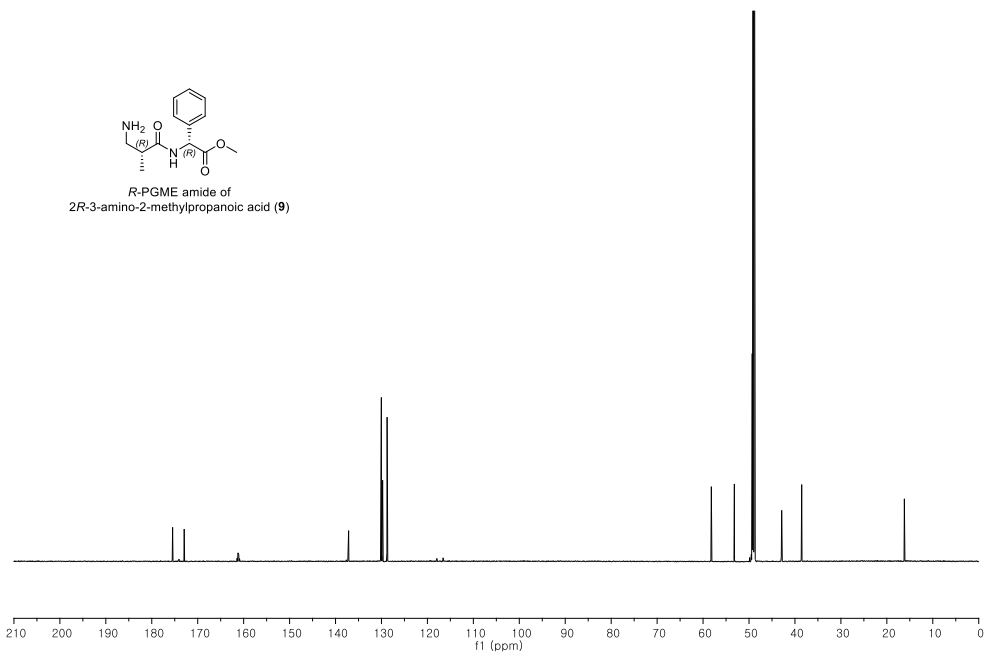


Figure S52. HR-FAB-MS data of bombyxamycin A (1).

[Elemental Composition]
Data : FAB-L481 Date : 13-Mar-2015 17:19 Page: 1
Sample: SD53K 419A
Note : m-NBA
Inlet : Direct Ion Mode : FAB+
RT : 0.10 min Scan#: (2,8)
Elements : C 100/0, H 100/0, N 10/0, O 10/0
Mass Tolerance : 10ppm, 5mmu if m/z < 500, 20mmu if m/z > 2000
Unsaturation (U.S.) : -0.5 - 100.0

Observed m/z	Int%	Err[ppm / mmu]	U.S.	Composition
420.2540	12.7	-6.1 / -2.6	16.0	C 30 H 32 N 2
		+9.9 / +4.2	13.0	C 21 H 28 N 10
		+6.7 / +2.8	12.5	C 23 H 30 N 7 O
		+3.5 / +1.5	12.0	C 25 H 32 N 4 O 2
		+0.3 / +0.1	11.5	C 27 H 34 N O 3
		+9.9 / +4.2	7.5	C 22 H 34 N 3 O 5
		-4.1 / -1.7	4.0	C 14 H 32 N 10 O 5
		+6.7 / +2.8	7.0	C 24 H 36 O 6
		-7.3 / -3.1	3.5	C 16 H 34 N 7 O 6
		-10.5 / -4.4	3.0	C 18 H 36 N 4 O 7
		+2.3 / +1.0	-0.5	C 11 H 34 N 9 O 8

Figure S53. HR-FAB-MS data of bombyxamycin B (2).

[Elemental Composition]
Data : FAB-R916 Date : 11-Dec-2018 14:54 Page: 1
Sample: Bombyxamycin C
Note : m-NBA
Inlet : Direct Ion Mode : FAB+
RT : 2.55 min Scan#: (116,121)
Elements : C 100/0, H 100/0, N 5/0, O 10/0
Mass Tolerance : 20ppm, 5mmu if m/z < 250, 10mmu if m/z > 500
Unsaturation (U.S.) : -0.5 - 50.0

Observed m/z	Int%	Err[ppm / mmu]	U.S.	Composition
450.2284	4.7	-14.2 / -6.4	21.0	C 35 H 30
		+13.7 / +6.2	21.5	C 34 H 28 N
		-2.3 / -1.0	17.5	C 28 H 28 N 5 O
		-5.3 / -2.4	17.0	C 30 H 30 N 2 O 2
		+19.7 / +8.9	17.0	C 31 H 30 O 3
		+3.7 / +1.7	13.0	C 25 H 30 N 4 O 4
		+0.7 / +0.3	12.5	C 27 H 32 N O 5
		-15.3 / -6.9	8.5	C 21 H 32 N 5 O 6
		-18.3 / -8.2	8.0	C 23 H 34 N 2 O 7
		+9.6 / +4.3	8.5	C 22 H 32 N 3 O 7
		+6.7 / +3.0	8.0	C 24 H 34 O 8
		-9.4 / -4.2	4.0	C 18 H 34 N 4 O 9
		+18.6 / +8.4	4.5	C 17 H 32 N 5 O 9
		-12.3 / -5.6	3.5	C 20 H 36 N O 10
		+15.6 / +7.0	4.0	C 19 H 34 N 2 O 10

Figure S54. HR-FAB-MS data of bombyxamycin C (3).

[Elemental Composition]
 Date : 11-Dec-2018 14:41
 Data : FAB-R915
 Sample: Bombyxamycin B
 Note : m-NBA
 Inlet : Direct
 Ion Mode : FAB+
 RT : 0.91 min
 Scan#: (40,46)
 Elements : C 100/0, H 100/0, N 5/0, O 10/0
 Mass Tolerance : 20ppm, 5mmu if m/z < 250, 10mmu if m/z > 500
 Unsaturation (U.S.) : -0.5 - 50.0

Page: 1

Observed m/z	Int%	Err[ppm / mmu]	U.S.	Composition
420.2534	4.1	-7.5 / -3.2	16.0	C 30 H 32 N 2
		+19.2 / +8.1	16.0	C 31 H 32 O
		+2.0 / +0.9	12.0	C 25 H 32 N 4 O 2
		-1.1 / -0.5	11.5	C 27 H 34 N O 3
		-18.3 / -7.7	7.5	C 21 H 34 N 5 O 4
		+8.4 / +3.5	7.5	C 22 H 34 N 3 O 5
		+5.2 / +2.2	7.0	C 24 H 36 O 6
		-11.9 / -5.0	3.0	C 18 H 36 N 4 O 7
		+18.0 / +7.6	3.5	C 17 H 34 N 5 O 7
		-15.1 / -6.4	2.5	C 20 H 38 N O 8
		+14.8 / +6.2	3.0	C 19 H 36 N 2 O 8

Figure S55. HR-FAB-MS data of piceamycin (4).

[Elemental Composition]
 Date : 11-Mar-2019 15:49
 Data : FAB-S214
 Sample: Piceamycin(2)
 Note : m-NBA
 Inlet : Direct
 Ion Mode : FAB+
 RT : 1.91 min
 Scan#: (73,105)
 Elements : C 100/0, H 100/0, N 10/0, O 10/0
 Mass Tolerance : 20ppm, 5mmu if m/z < 250, 10mmu if m/z > 500
 Unsaturation (U.S.) : -0.5 - 50.0

Page: 1

Observed m/z	Int%	Err[ppm / mmu]	U.S.	Composition
432.2174	2.2	-3.3 / -1.4	18.5	C 28 H 26 N 5
		-6.4 / -2.8	18.0	C 30 H 28 N 2 O
		+9.1 / +3.9	15.0	C 21 H 24 N 10 O
		+19.5 / +8.4	18.0	C 31 H 28 O 2
		+6.0 / +2.6	14.5	C 23 H 26 N 7 O 2
		+2.9 / +1.2	14.0	C 25 H 28 N 4 O 3
		-0.2 / -0.1	13.5	C 27 H 30 N O 4
		-13.8 / -6.0	10.0	C 19 H 28 N 8 O 4
		+15.3 / +6.6	10.5	C 18 H 26 N 9 O 4
		-16.9 / -7.3	9.5	C 21 H 30 N 5 O 5
		+12.2 / +5.3	10.0	C 20 H 28 N 6 O 5
		+9.1 / +3.9	9.5	C 22 H 30 N 3 O 6
		-4.5 / -2.0	6.0	C 14 H 28 N 10 O 6
		+6.0 / +2.6	9.0	C 24 H 32 O 7
		-7.6 / -3.3	5.5	C 16 H 30 N 7 O 7
		-10.7 / -4.6	5.0	C 18 H 32 N 4 O 8
		+18.4 / +7.9	5.5	C 17 H 30 N 5 O 8
		-13.8 / -6.0	4.5	C 20 H 34 N O 9
		+15.3 / +6.6	5.0	C 19 H 32 N 2 O 9
		+1.7 / +0.7	1.5	C 11 H 30 N 9 O 9
		-1.4 / -0.6	1.0	C 13 H 32 N 6 O 10

Figure S56. Determining relative configurations of bombyxamycin B (**2**) by interpretation of NOESY correlation data.

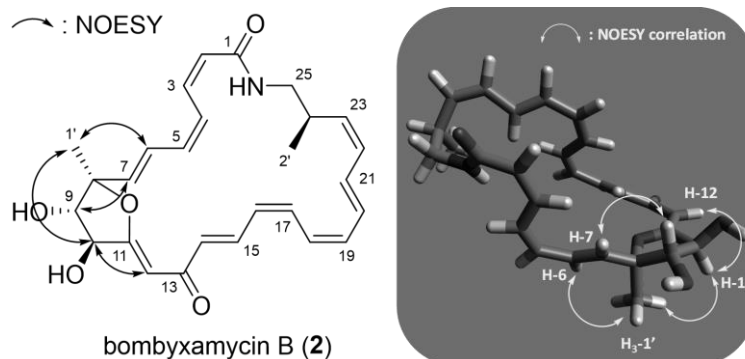


Figure S57. ^1H NMR chemical shifts of *S*- and *R*-PGME amides of **5** (**5a** and **5b**) at 600 MHz in CD_3OD .

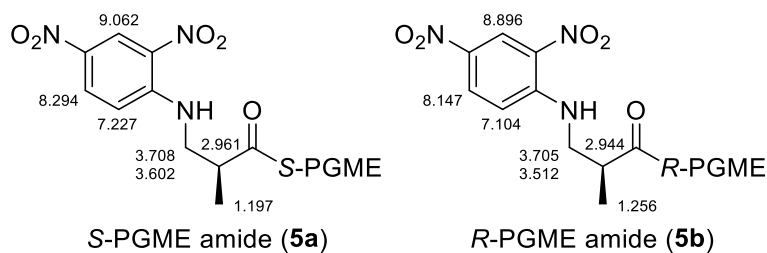


Figure S58. Comparing the retention times of **6**, **8**, and *S*-PGME amide of authentic 2*S*-3-amino-2-methylpropanoic acid (ion extraction for $[M+H]^+$ m/z at 251).

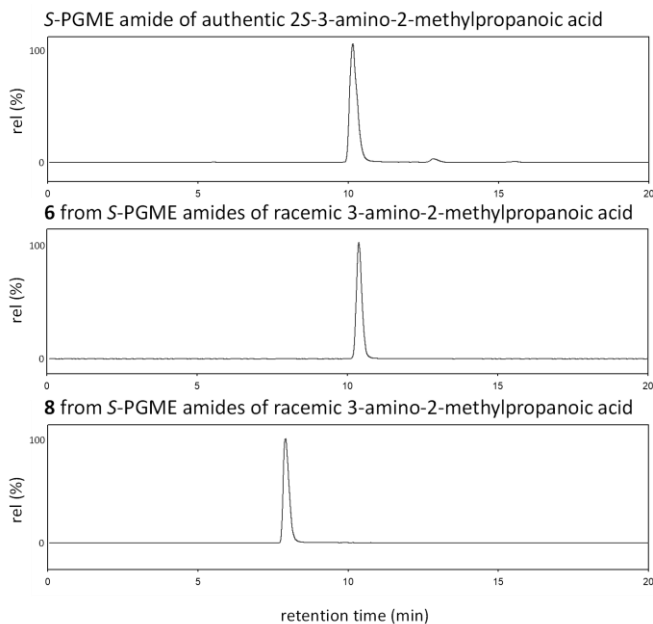


Figure S59. Comparing the retention times of **7**, **9**, and *R*-PGME amide of authentic 2*S*-3-amino-2-methylpropanoic acid (ion extraction for $[M+H]^+$ m/z at 251).

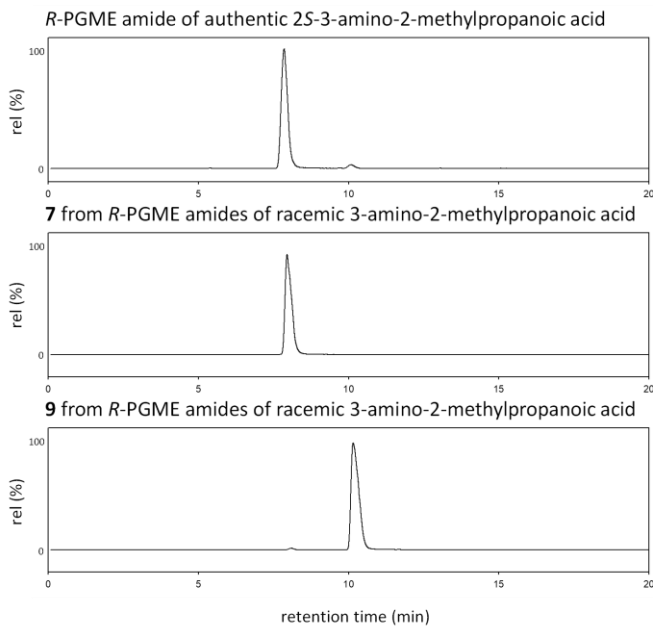


Figure S60. $\Delta\delta_{S-R}$ values in ppm between PGME amides of 3-amino-2-methylpropanoic acids (**6–9**).

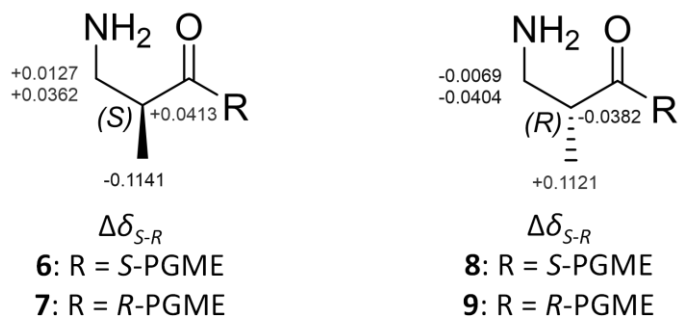


Figure S61. HR-FAB-MS data of 6.

[Elemental Composition]
 Date : 15-Mar-2019 16:58
 Data : FAB-S224
 Sample: S2
 Note : m-NBA
 Inlet : Direct
 RT : 0.28 min
 Elements : C 100/0, H 100/0, N 10/0, O 10/0
 Mass Tolerance : 20ppm, 5mmu if m/z < 250, 10mmu if m/z > 500
 Unsaturation (U.S.) : -0.5 - 50.0
 Ion Mode : FAB+
 Scan#: (1,27)

Observed m/z	Int%	Err[ppm / mmu]	U.S.	Composition
251.1397	100.0	-10.2 / -2.6	10.0	C 16 H 17 N 3
		-15.6 / -3.9	9.5	C 18 H 19 O
		+11.1 / +2.8	6.5	C 9 H 15 N 8 O
		+5.8 / +1.5	6.0	C 11 H 17 N 5 O 2
		+0.4 / +0.1	5.5	C 13 H 19 N 2 O 3
		+16.5 / +4.1	1.5	C 8 H 19 N 4 O 5
		+11.1 / +2.8	1.0	C 10 H 21 N O 6

Page: 1

Figure S62. HR-FAB-MS data of 7.

[Elemental Composition]
 Date : 15-Mar-2019 20:14
 Data : FAB-S225
 Sample: R1
 Note : m-NBA
 Inlet : Direct
 RT : 0.25 min
 Elements : C 100/0, H 100/0, N 10/0, O 10/0
 Mass Tolerance : 20ppm, 5mmu if m/z < 250, 10mmu if m/z > 500
 Unsaturation (U.S.) : -0.5 - 50.0
 Ion Mode : FAB+
 Scan#: (7,18)

Observed m/z	Int%	Err[ppm / mmu]	U.S.	Composition
251.1396	100.0	-10.6 / -2.7	10.0	C 16 H 17 N 3
		-15.9 / -4.0	9.5	C 18 H 19 O
		+10.8 / +2.7	6.5	C 9 H 15 N 8 O
		+5.4 / +1.4	6.0	C 11 H 17 N 5 O 2
		+0.1 / +0.0	5.5	C 13 H 19 N 2 O 3
		+16.1 / +4.0	1.5	C 8 H 19 N 4 O 5
		+10.8 / +2.7	1.0	C 10 H 21 N O 6

Page: 1

Figure S63. HR-FAB-MS data of 8.

[Elemental Composition]
 Date : 15-Mar-2019 16:51
 Data : FAB-S223
 Sample: S1
 Note : m-NBA
 Inlet : Direct
 RT : 0.09 min
 Elements : C 100/0, H 100/0, N 10/0, O 10/0
 Mass Tolerance : 20ppm, 5mmu if m/z < 250, 10mmu if m/z > 500
 Unsaturation (U.S.) : -0.5 - 50.0
 Ion Mode : FAB+
 Scan#: 5

Page: 1

Observed m/z	Int%	Err[ppm / mmu]	U.S.	Composition
251.1399	100.0	-9.3 / -2.3	10.0	C 16 H 17 N 3
		-14.6 / -3.7	9.5	C 18 H 19 O
		+12.1 / +3.0	6.5	C 9 H 15 N 8 O
		+6.8 / +1.7	6.0	C 11 H 17 N 5 O 2
		+1.4 / +0.4	5.5	C 13 H 19 N 2 O 3
		+17.4 / +4.4	1.5	C 8 H 19 N 4 O 5
		+12.1 / +3.0	1.0	C 10 H 21 N O 6

Figure S64. HR-FAB-MS data of 9.

[Elemental Composition]
 Date : 15-Mar-2019 20:19
 Data : FAB-S226
 Sample: R2
 Note : m-NBA
 Inlet : Direct
 RT : 0.35 min
 Elements : C 100/0, H 100/0, N 10/0, O 10/0
 Mass Tolerance : 20ppm, 5mmu if m/z < 250, 10mmu if m/z > 500
 Unsaturation (U.S.) : -0.5 - 50.0
 Ion Mode : FAB+
 Scan#: (6,28)

Page: 1

Observed m/z	Int%	Err[ppm / mmu]	U.S.	Composition
251.1394	100.0	-11.3 / -2.8	10.0	C 16 H 17 N 3
		-16.7 / -4.2	9.5	C 18 H 19 O
		+10.0 / +2.5	6.5	C 9 H 15 N 8 O
		+4.7 / +1.2	6.0	C 11 H 17 N 5 O 2
		-0.7 / -0.2	5.5	C 13 H 19 N 2 O 3
		+15.4 / +3.9	1.5	C 8 H 19 N 4 O 5
		+10.0 / +2.5	1.0	C 10 H 21 N O 6

Figure S65. Chromatographic analysis of (a) *S*-PGME and (b) *R*-PGME amide products of 3-amino-2-methylpropanoic acid from 0.2 mg of **4** (elution order: *R*→*S*; Phenomenex Luna C₁₈(2), 100 × 4.6 mm; 10%–25% CH₃CN–H₂O over 30 min with 0.1% formic acid; flow rate: 0.7 mL/min; ion extraction for [M+H]⁺ *m/z* at 251).

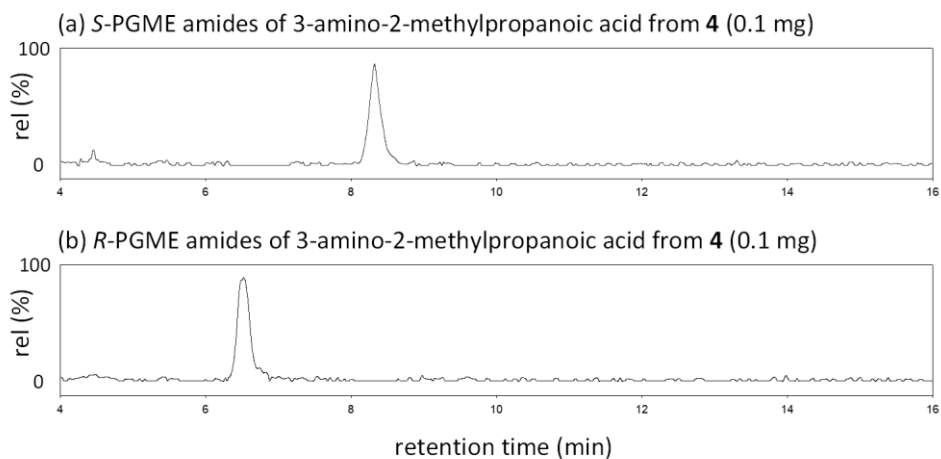


Figure S66. NOESY correlations analysis and energy-minimized model of **4**.

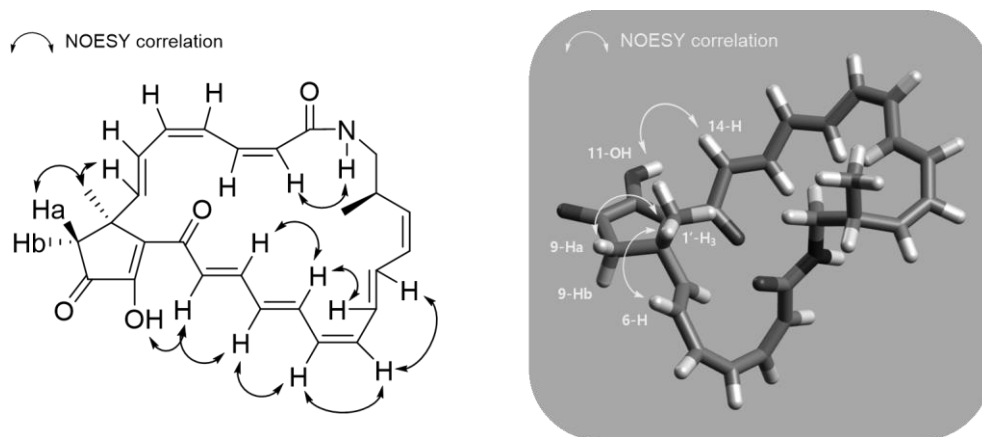


Figure S67. Multiple sequence alignment of KR domains. The boxes indicate conserved motif for an NADP(H) binding site, consensus active motif, and conserved tryptophan instead of Leu–Asp–Asp signature motif. The numbers indicate amino acid positions within sequences and (x)*n* indicates the number of amino acids that separate the active-site residues.

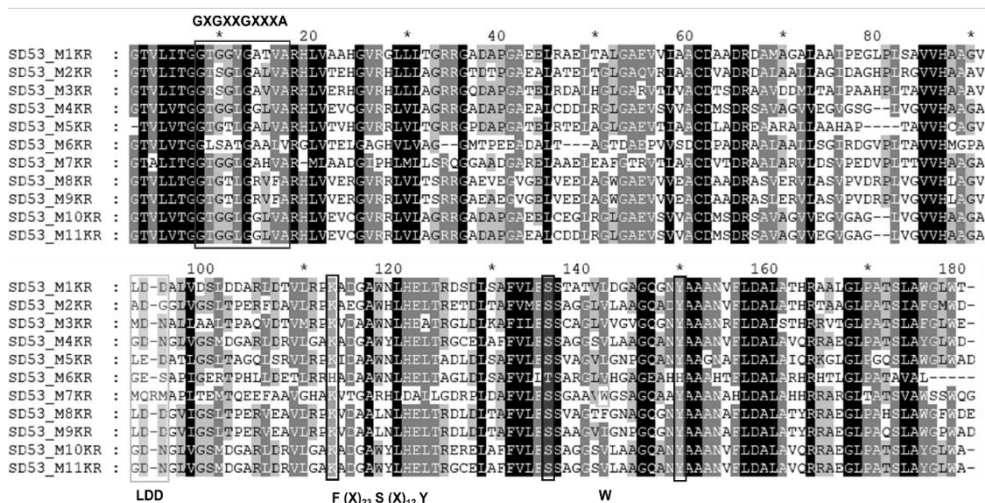


Figure S68. Constuction and verification of *bomK* in-frame deletion in *Streptomyces* sp. SD53. (a) Schematic representation of *bomK* in-frame deletion by homologous recombination. (b) PCR analysis. 1, PCR products (1.741-kb) obtained from wild type strain: 2, PCR products (1.513-kb) obtained from Δ *bomK* mutant; L, DNA ladder.

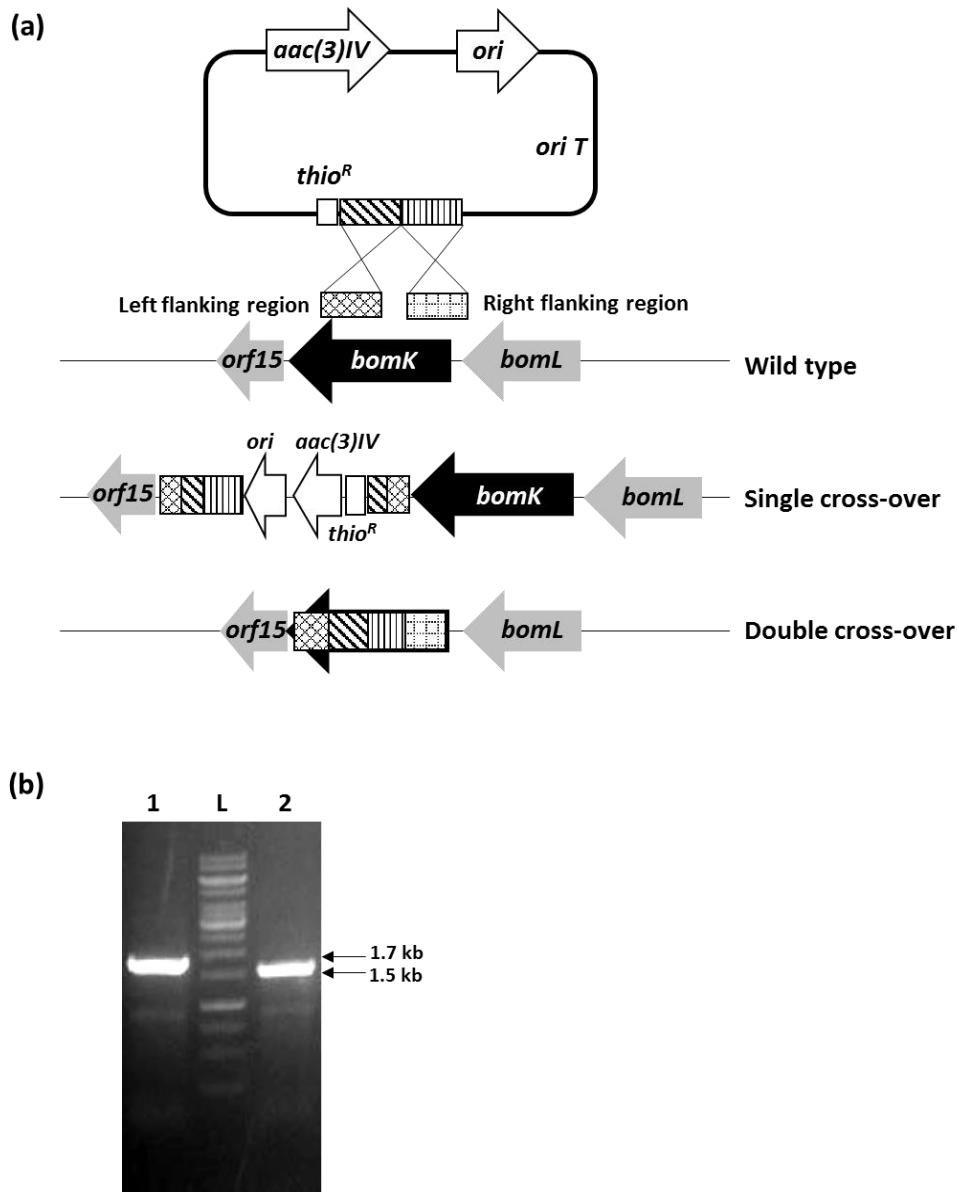


Figure S69. Constuction and verification of *bomN* in-frame deletion in *Streptomyces* sp. SD53. (a) Schematic representation of *bomN* in-frame deletion by homologous recombination. (b) PCR analysis. 1, PCR products (1.945-kb) obtained from wild type strain; 2, PCR products (0.862-kb) obtained from Δ *bomN* mutant; L, DNA ladder.

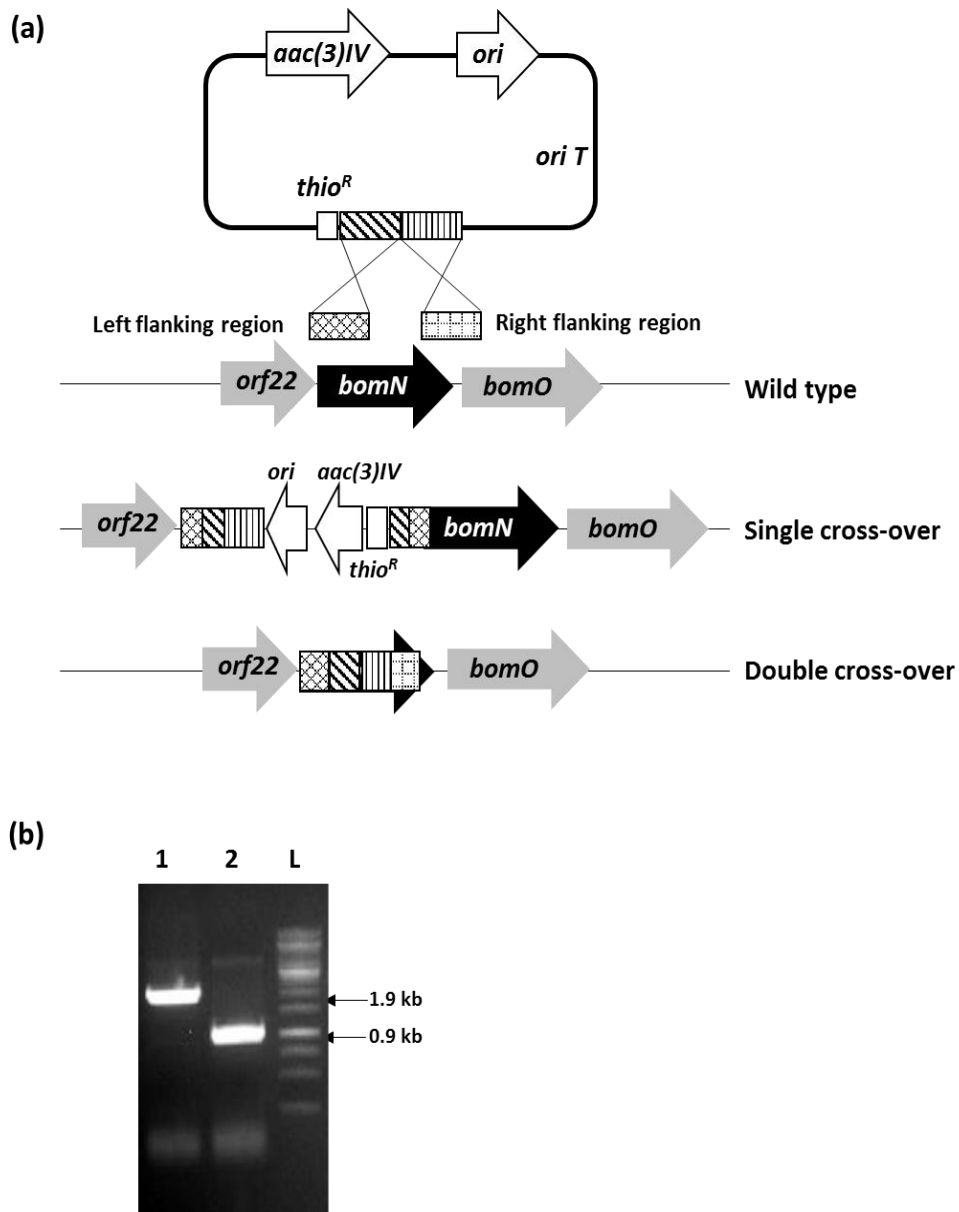


Figure S70. Constuction and verification of *bomO* in-frame deletion in *Streptomyces* sp. SD53. (a) Schematic representation of *bomO* in-frame deletion by homologous recombination. (b) PCR analysis. 1, PCR products (1.610-kb) obtained from wild type strain; 2, PCR products (1.379-kb) obtained from Δ *bomO* mutant; L, DNA ladder.

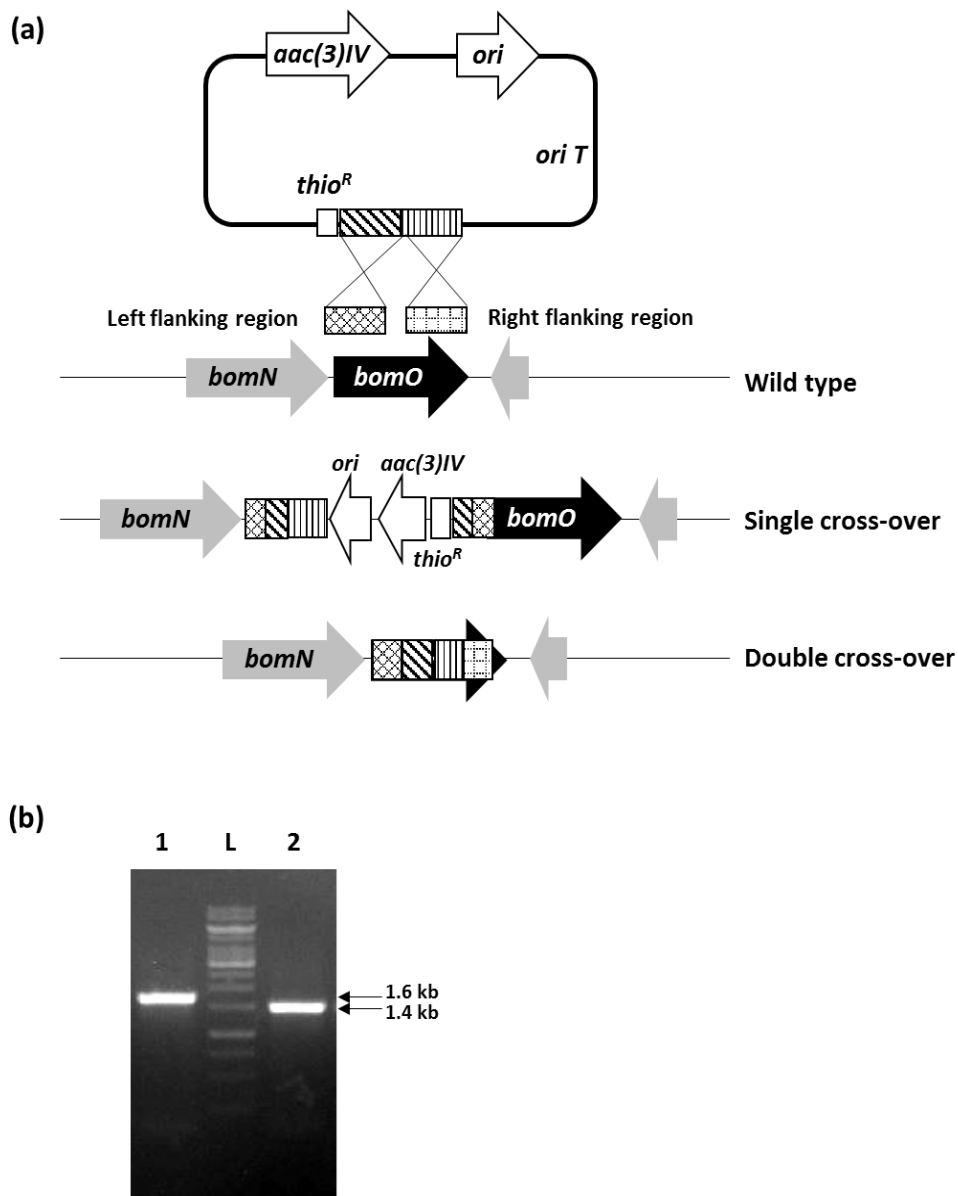


Figure S71. HPLC-ESI-MS/MS chromatograms obtained from the culture of Δ bomN strain selected for $m/z = 450$.

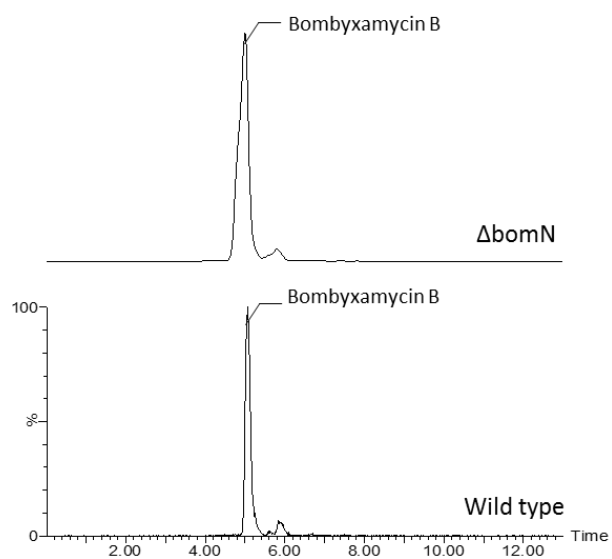


Figure S72. HPLC-ESI-MS/MS chromatograms obtained from the culture of Δ bomO strain selected for $m/z = 450$.

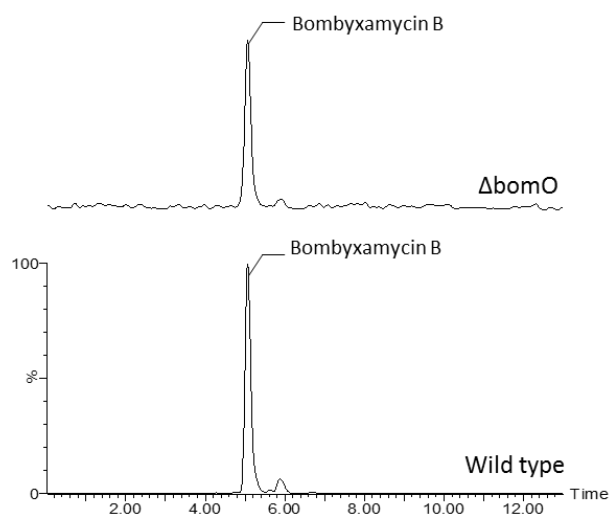


Figure S73. (a) HPLC-ESI-MS/MS chromatograms obtained from the culture of Δ bomK strain selected for $m/z = 420$ and 450, (b) ESI-MS/MS-fragmentation pattern of bombyxamycin A.

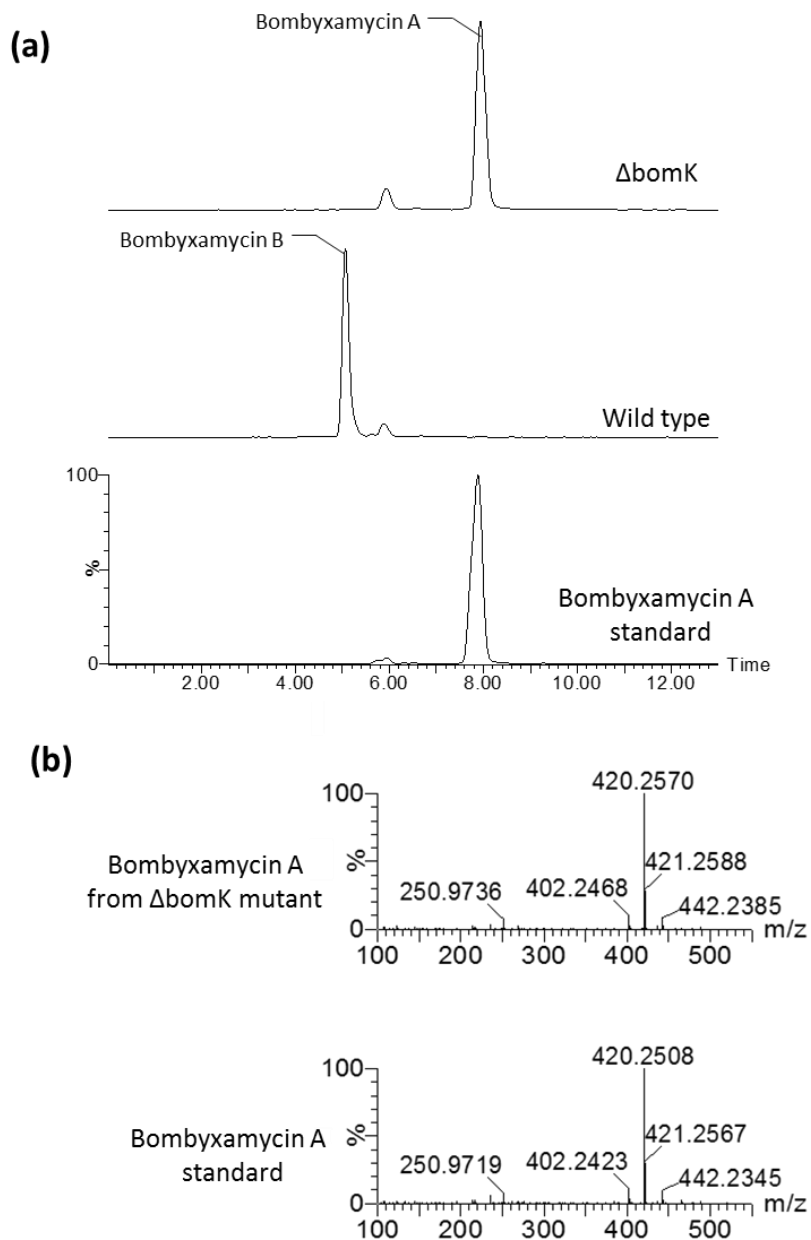


Figure S74. ^1H NMR spectrum of nicrophorusamide A (**10**) at 600 MHz in $\text{DMSO}-d_6$.

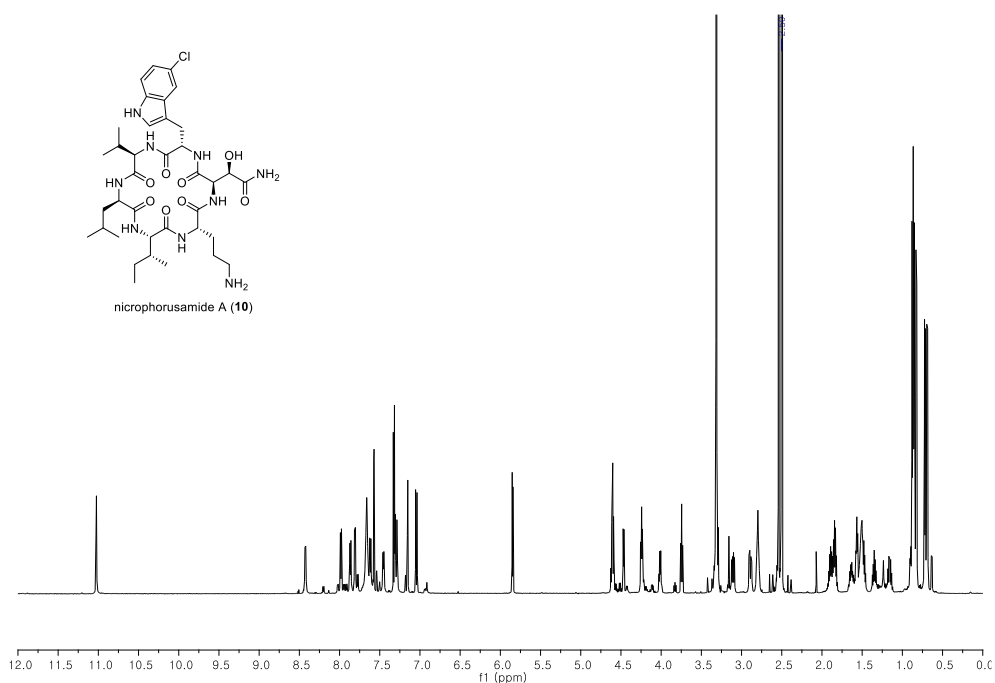


Figure S75. ^{13}C NMR spectrum of nicrophorusamide A (**10**) at 125 MHz in $\text{DMSO}-d_6$.

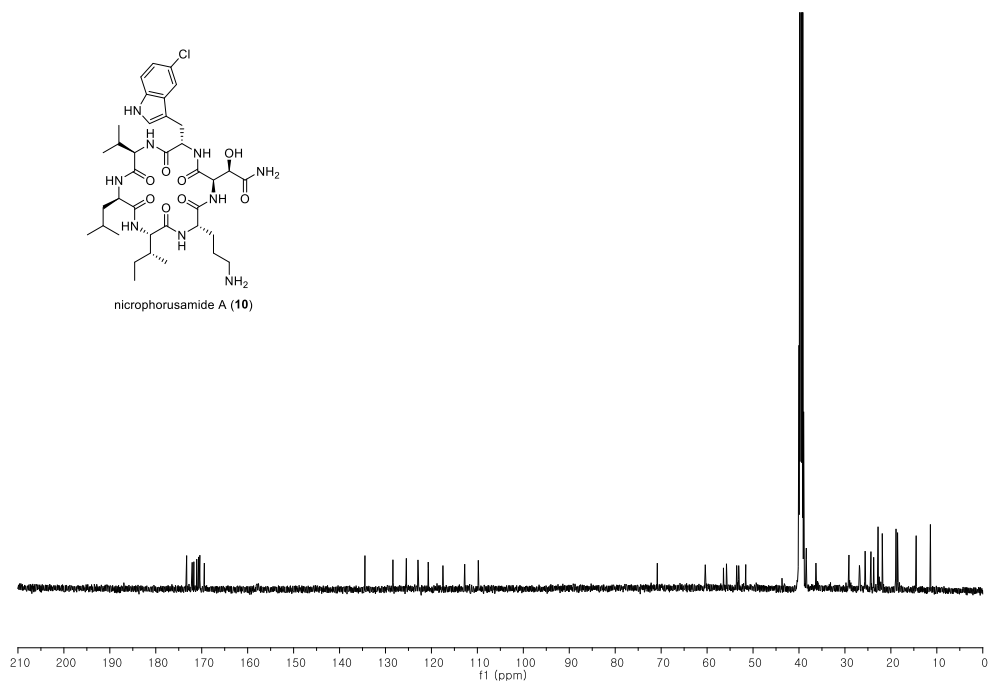


Figure S76. COSY NMR spectrum of microphorusamide A (**10**) at 600 MHz in DMSO-*d*₆.

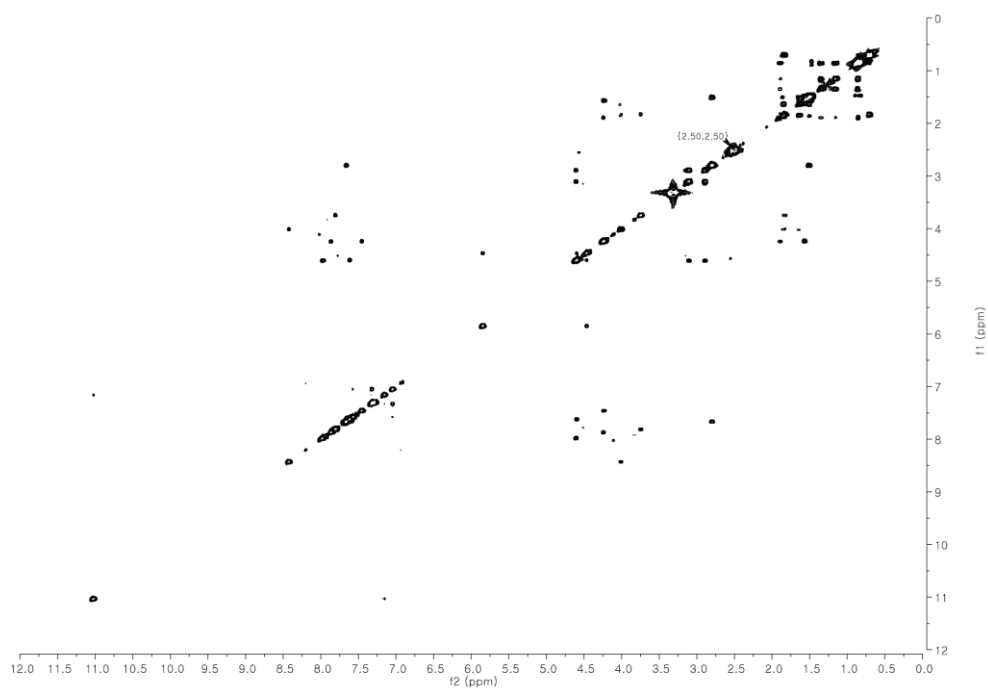


Figure S77. TOCSY NMR spectrum of microphorusamide A (**10**) at 500 MHz in DMSO-*d*₆.

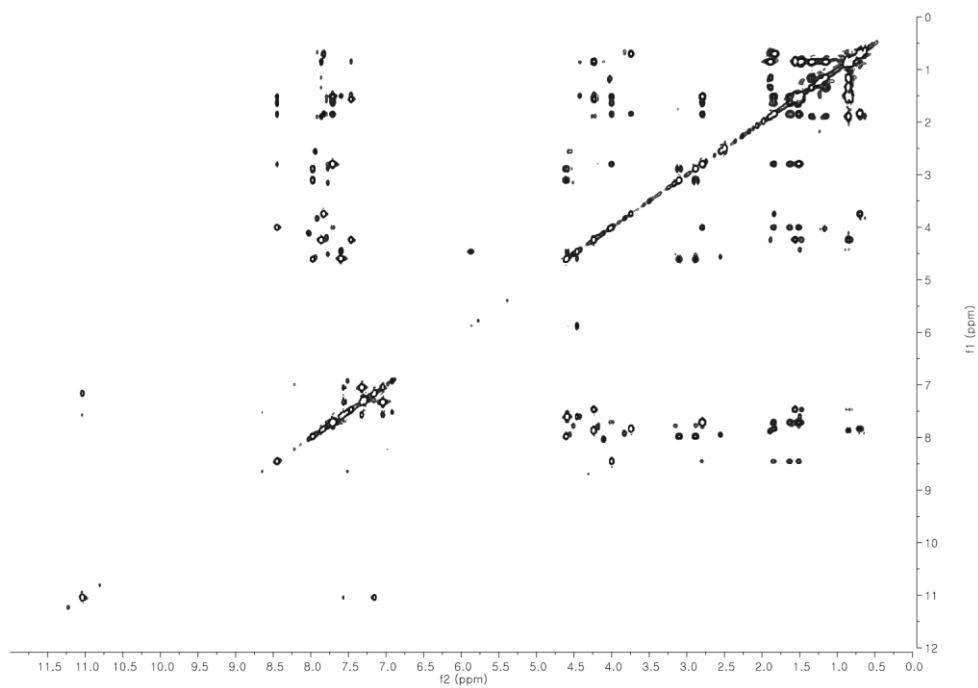


Figure S78. HSQC NMR spectrum of microphorusamide A (**10**) at 500 MHz in DMSO-*d*₆.

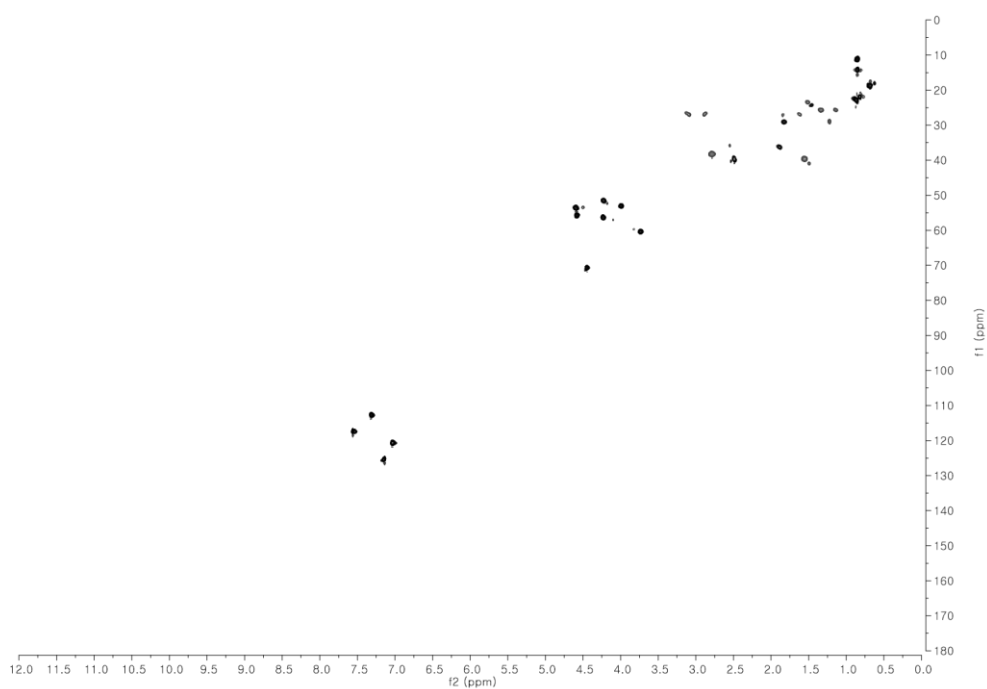


Figure S79. HMBC NMR spectrum of microphorusamide A (**10**) at 500 MHz in DMSO-*d*₆.

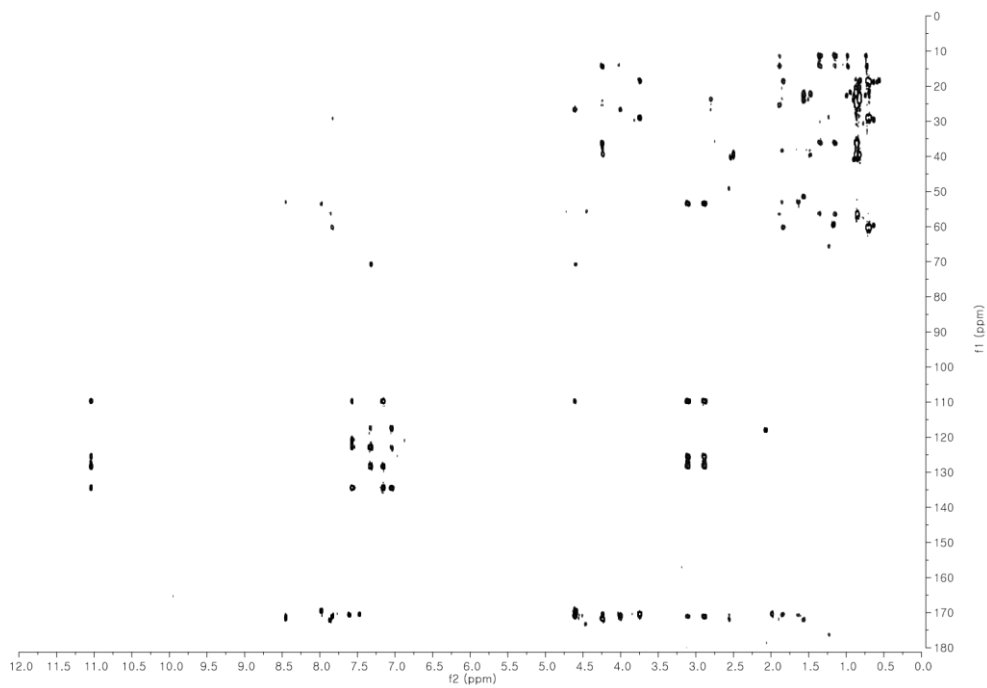


Figure S80. ROESY NMR spectrum of microphorusamide A (**10**) at 500 MHz in DMSO-*d*₆.

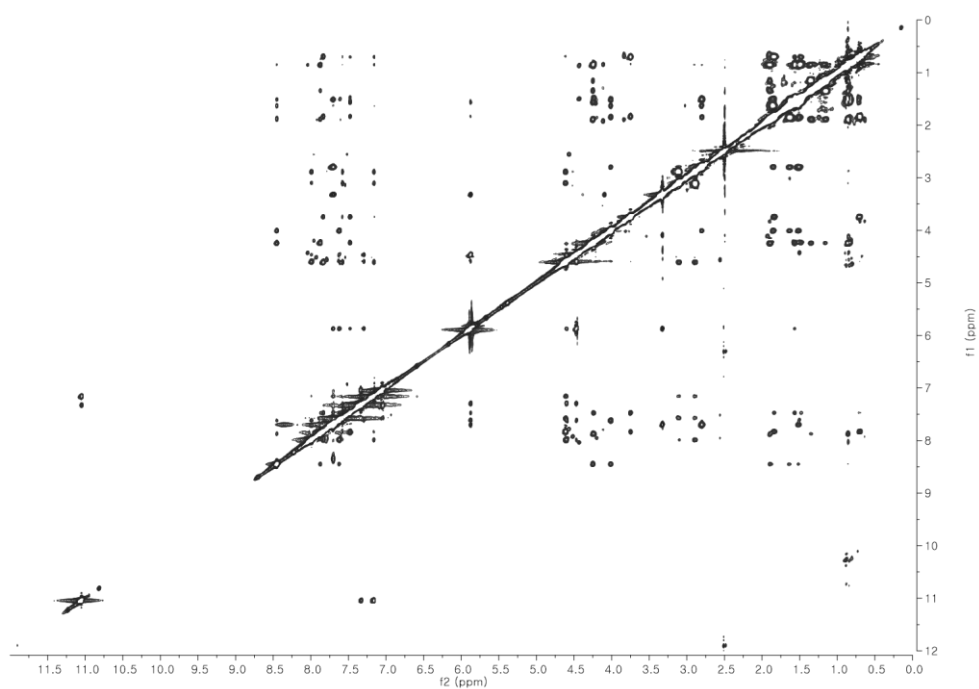


Figure S81. ^1H NMR spectrum of nicrophorusamide B (**11**) at 500 MHz in $\text{DMSO}-d_6$.

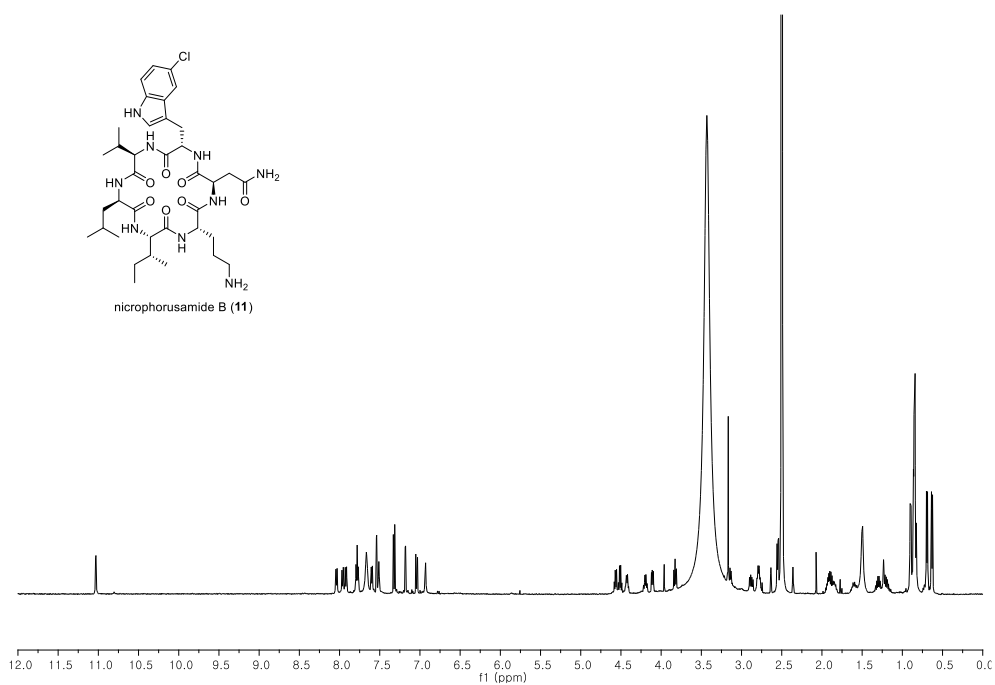


Figure S82. ^{13}C NMR spectrum of nicrophorusamide B (**11**) at 125 MHz in $\text{DMSO}-d_6$.

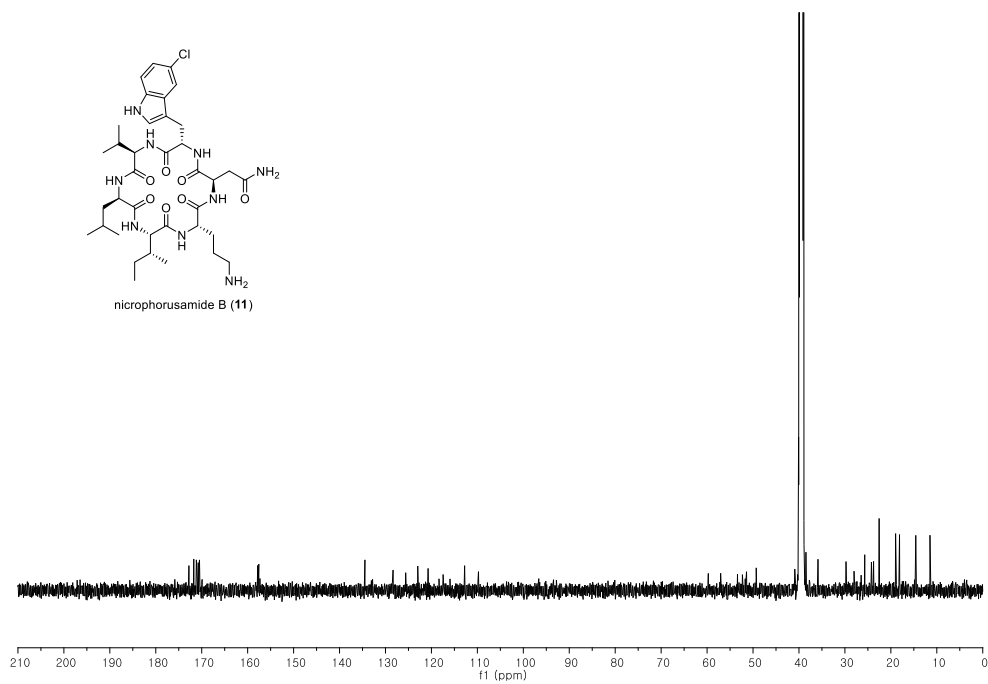


Figure S83. COSY NMR spectrum of nicrophorusamide B (**11**) at 500 MHz in DMSO-*d*₆.

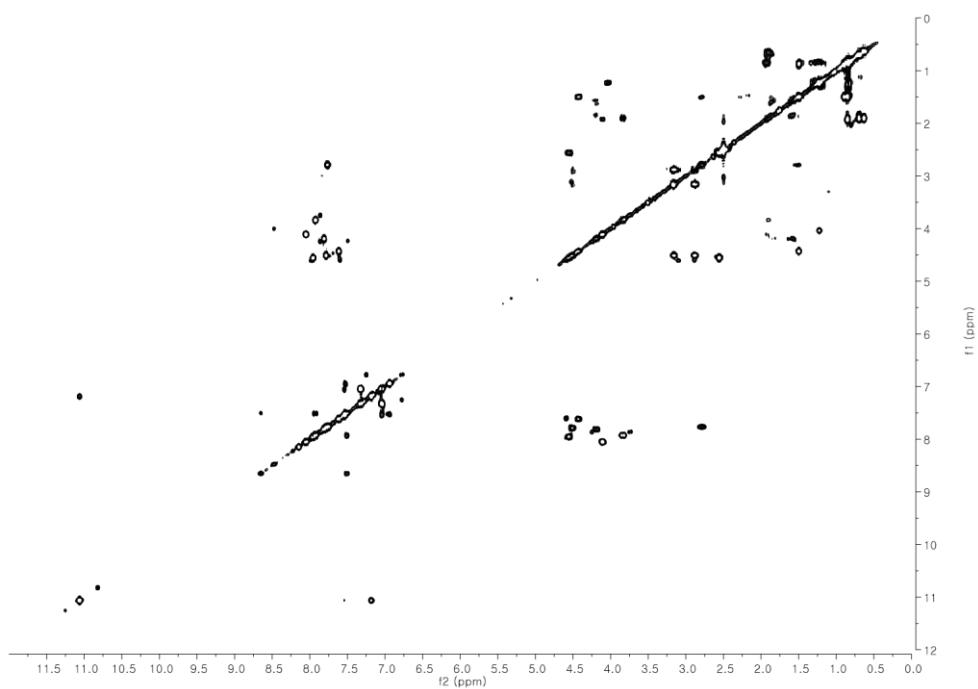


Figure S84. TOCSY NMR spectrum of nicrophorusamide B (**11**) at 500 MHz in DMSO-*d*₆.

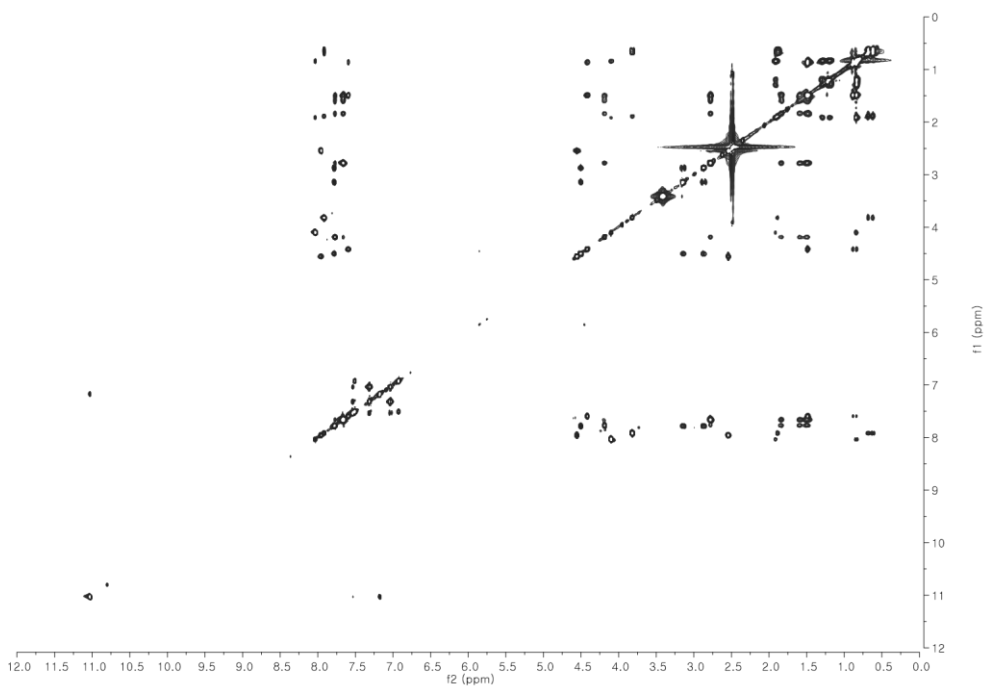


Figure S85. HSQC NMR spectrum of microphorusamide B (**11**) at 500 MHz in DMSO-*d*₆.

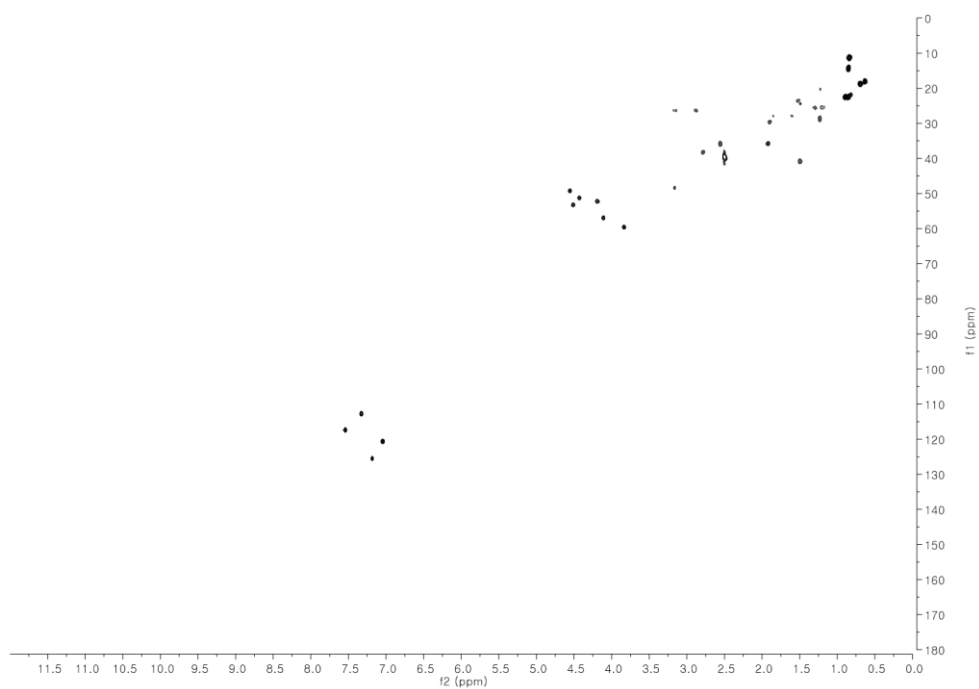


Figure S86. HMBC NMR spectrum of microphorusamide B (**11**) at 500 MHz in DMSO-*d*₆.

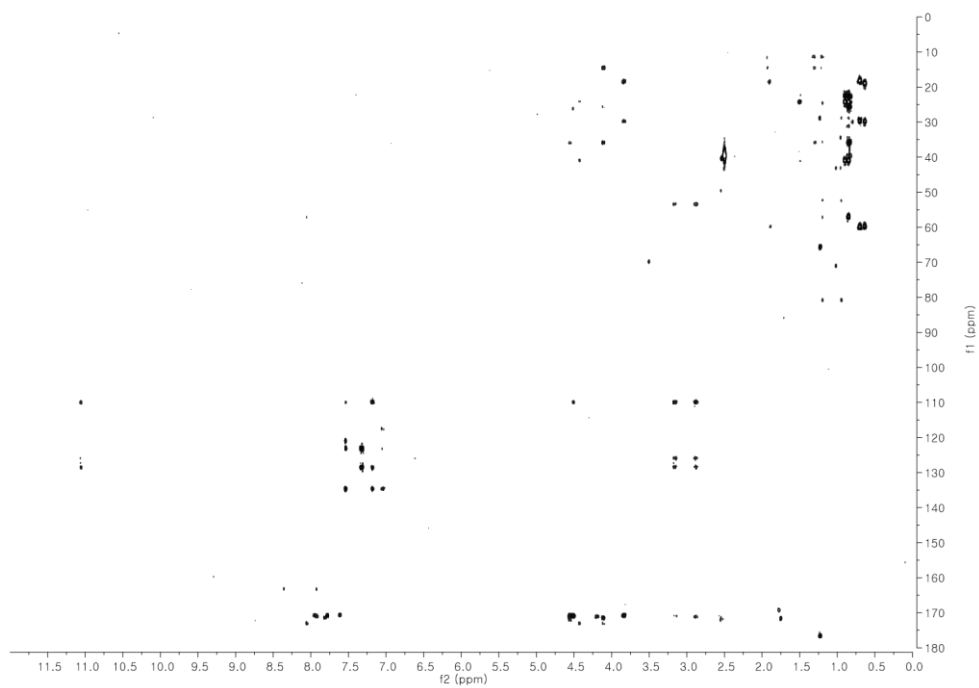


Figure S87. ROESY NMR spectrum of microphorusamide B (**11**) at 500 MHz in DMSO-*d*₆.

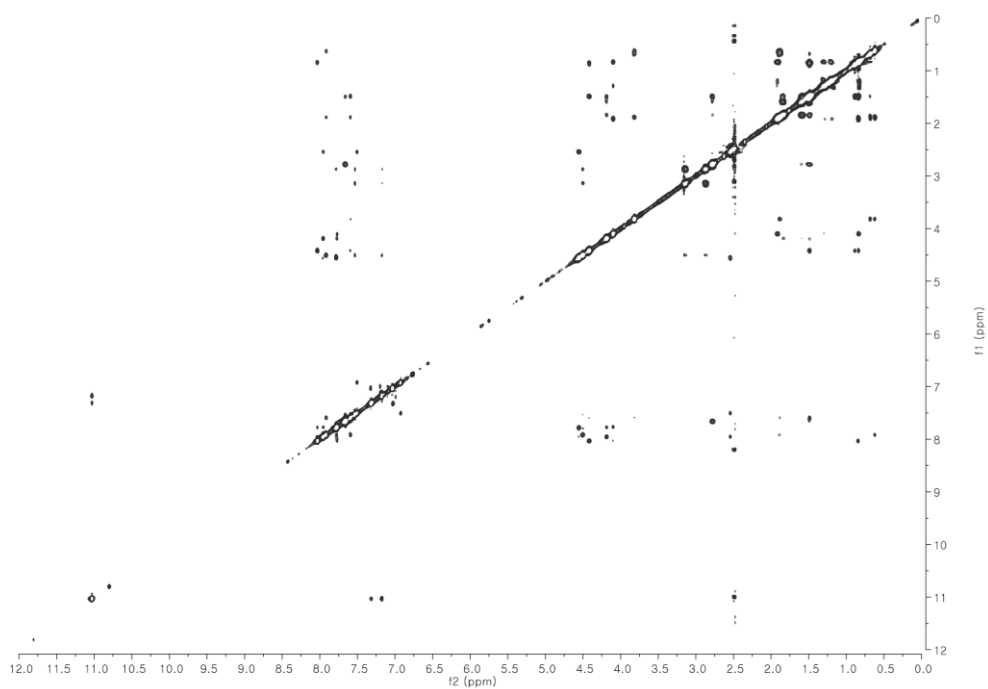


Figure S88. LC/MS analysis of L-FDAA derivatives of amino acids in microphorusamide A (10): (a) valine, (b) isoleucine, (c) leucine, (d) ornithine, (e) β -hydroxyaspartic acid, and (f) 5-chloro-tryptophan.

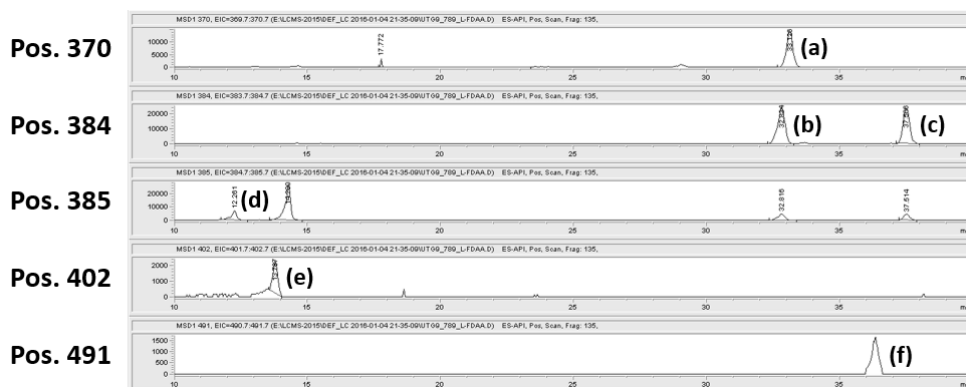


Figure S89. LC/MS analysis of D-FDAA derivatives of amino acids in microphorusamide A (10): (a) valine, (b) isoleucine, (c) leucine, (d) ornithine, (e) β -hydroxyaspartic acid, and (f) 5-chloro-tryptophan.

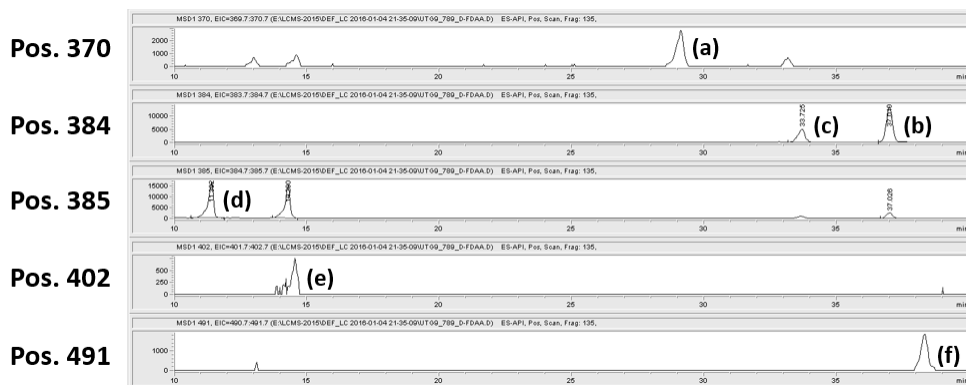


Figure S90. Synthesis of *L-erythro*- β -hydroxyaspartic acid.

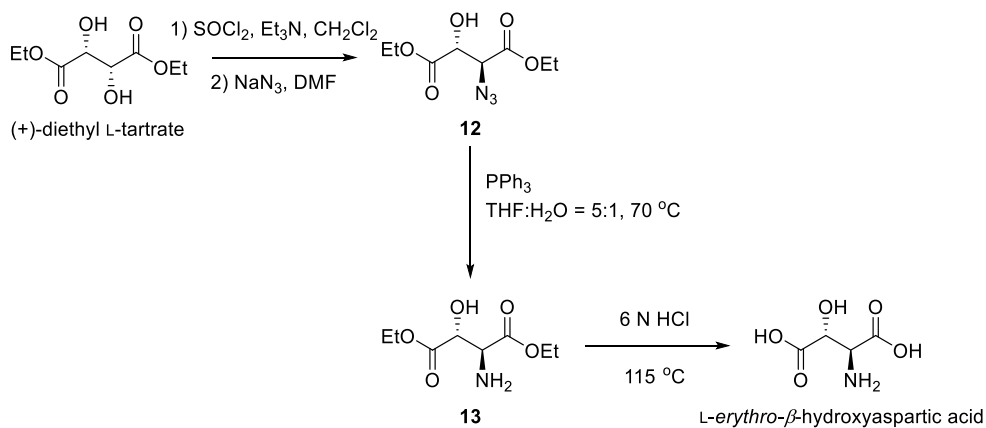


Figure S91. Co-injection experiments to determinate the absolute configuration at the β -carbon of *D*- β -hydroxyasparagine.

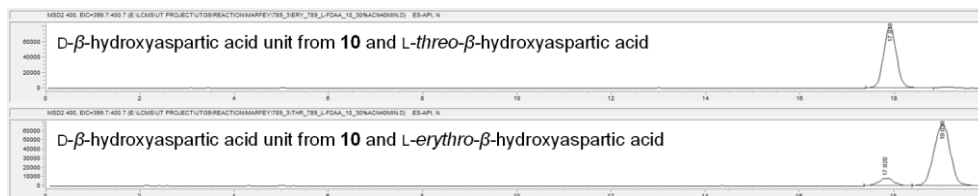


Figure S92. HPLC analysis of GITC derivatives of isoleucine unit in microphorusamide A (**10**) and authentic *L*- / *L-allo*-isoleucine. (detection: UV 210 nm)

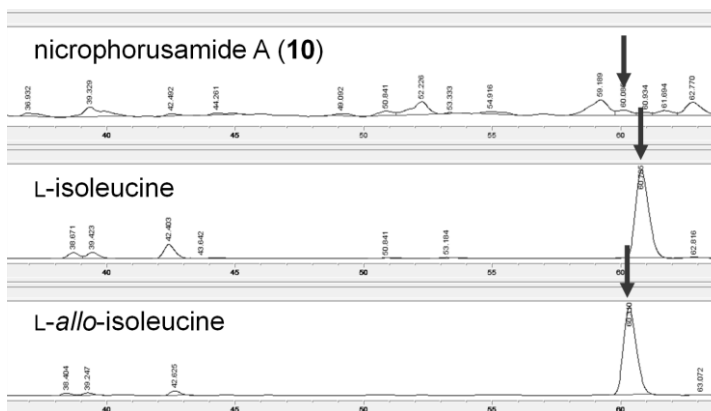


Figure S93. Circular dichroism spectra data of nicrophorusamides A and B (**10** and **11**).

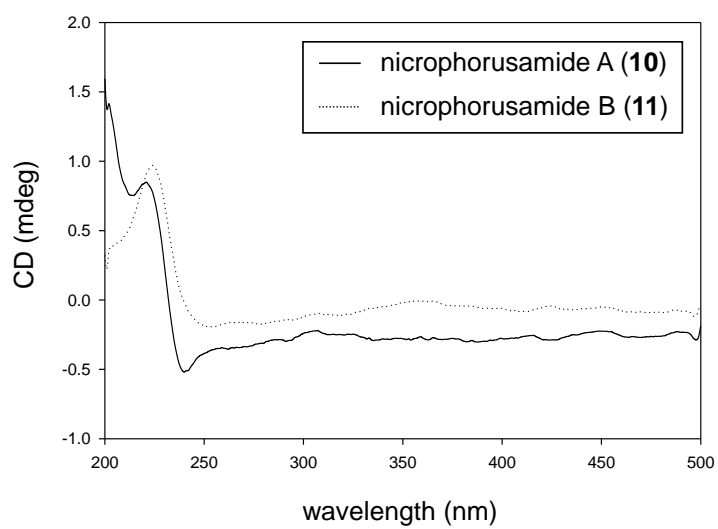


Figure S94. HR-FAB-MS data of microphorusamide A (10).

[Elemental Composition]
 Date : 26-Apr-2017 16:15
 Data : FAB-O838
 Sample: Microphoramide A
 Note : m-NBA
 Inlet : Direct
 RT : 1.38 min
 Elements : C 100/0, H 150/0, Cl 2/0(35Cl 2/0, 37Cl 2/0), N 15/5, O 12/0
 Mass Tolerance : 20ppm, 5mmu if m/z < 250, 10mmu if m/z > 500
 Unsaturation (U.S.) : -10.0 - 100.0

Page: 1

Ion Mode : FAB+
 Scan#: (59,70)

Observed m/z	Int%	Err[ppm / mmu]	U.S.	Composition
790.4022	100.0	+1.5 / +1.2	22.5	C 49 H 58 37Cl 2 N 5
		-6.1 / -4.8	22.0	C 48 H 58 35Cl 37Cl N 6
		+9.8 / +7.7	22.5	C 47 H 56 35Cl 37Cl N 7
		+2.2 / +1.7	22.0	C 46 H 56 35Cl 2 N 8
		-3.8 / -3.0	27.0	C 49 H 53 37Cl N 8
		-11.4 / -9.0	26.5	C 48 H 53 35Cl N 9
		+12.1 / +9.6	27.5	C 48 H 51 37Cl N 9
		+4.5 / +3.6	27.0	C 47 H 51 35Cl N 10
		-9.1 / -7.2	31.5	C 49 H 48 N 11
		+6.8 / +5.4	32.0	C 48 H 46 N 12
		-5.9 / -4.7	19.0	C 41 H 56 37Cl 2 N 12
		+10.0 / +7.9	19.5	C 40 H 54 37Cl 2 N 13
		+2.4 / +1.9	19.0	C 39 H 54 35Cl 37Cl N 14
		-5.2 / -4.1	18.5	C 38 H 54 35Cl 2 N 15
		-11.2 / -8.9	23.5	C 41 H 51 37Cl N 15
		+0.5 / +0.4	21.5	C 48 H 58 35Cl 2 N 5 O
		-5.5 / -4.3	26.5	C 51 H 55 37Cl N 5 O
		+10.4 / +8.2	27.0	C 50 H 53 37Cl N 6 O
		+2.8 / +2.2	26.5	C 49 H 53 35Cl N 7 O
		-10.8 / -8.5	31.0	C 51 H 50 N 8 O
		+5.1 / +4.0	31.5	C 50 H 48 N 9 O
		-7.6 / -6.0	18.5	C 43 H 58 37Cl 2 N 9 O
		+8.3 / +6.6	19.0	C 42 H 56 37Cl 2 N 10 O
		+0.7 / +0.5	18.5	C 41 H 56 35Cl 37Cl N 11 O
		-6.9 / -5.5	18.0	C 40 H 56 35Cl 2 N 12 O
		+9.0 / +7.1	18.5	C 39 H 54 35Cl 2 N 13 O
		+3.0 / +2.4	23.5	C 42 H 51 37Cl N 13 O
		-4.6 / -3.7	23.0	C 41 H 51 35Cl N 14 O
		+11.3 / +8.9	23.5	C 40 H 49 35Cl N 15 O
		-12.5 / -9.9	30.5	C 53 H 52 N 5 O 2
		+3.4 / +2.7	31.0	C 52 H 50 N 6 O 2
		-9.3 / -7.4	18.0	C 45 H 60 37Cl 2 N 6 O 2
		+6.6 / +5.2	18.5	C 44 H 58 37Cl 2 N 7 O 2
		-1.0 / -0.8	18.0	C 43 H 58 35Cl 37Cl N 8 O 2
		-8.6 / -6.8	17.5	C 42 H 58 35Cl 2 N 9 O 2
		+7.3 / +5.7	18.0	C 41 H 56 35Cl 2 N 10 O 2
		+1.3 / +1.0	23.0	C 44 H 53 37Cl N 10 O 2
		-6.3 / -5.0	22.5	C 43 H 53 35Cl N 11 O 2
		+9.6 / +7.6	23.0	C 42 H 51 35Cl N 12 O 2
		-4.0 / -3.2	27.5	C 44 H 48 N 13 O 2
		+11.9 / +9.4	28.0	C 43 H 46 N 14 O 2
		-0.8 / -0.7	15.0	C 36 H 56 37Cl 2 N 14 O 2
		-8.4 / -6.7	14.5	C 35 H 56 35Cl 37Cl N 15 O 2
		-2.7 / -2.1	17.5	C 45 H 60 35Cl 37Cl N 5 O 3
		-10.3 / -8.2	17.0	C 44 H 60 35Cl 2 N 6 O 3
		+5.6 / +4.4	17.5	C 43 H 58 35Cl 2 N 7 O 3
		-0.4 / -0.3	22.5	C 46 H 55 37Cl N 7 O 3
		-8.0 / -6.3	22.0	C 45 H 55 35Cl N 8 O 3
		+7.9 / +6.2	22.5	C 44 H 53 35Cl N 9 O 3
		-5.7 / -4.5	27.0	C 46 H 50 N 10 O 3
		+10.2 / +8.1	27.5	C 45 H 48 N 11 O 3
		-2.5 / -2.0	14.5	C 38 H 58 37Cl 2 N 11 O 3
		-10.1 / -8.0	14.0	C 37 H 58 35Cl 37Cl N 12 O 3
		+5.8 / +4.6	14.5	C 36 H 56 35Cl 37Cl N 13 O 3
		-1.9 / -1.5	14.0	C 35 H 56 35Cl 2 N 14 O 3

-7.8 /	-6.2	19.0	C 38 H 53 37Cl N 14 O 3
+8.1 /	+6.4	19.5	C 37 H 51 37Cl N 15 O 3
-9.7 /	-7.7	21.5	C 47 H 57 35Cl N 5 O 4
+6.2 /	+4.9	22.0	C 46 H 55 35Cl N 6 O 4
-7.4 /	-5.9	26.5	C 48 H 52 N 7 O 4
+8.5 /	+6.7	27.0	C 47 H 50 N 8 O 4
-4.2 /	-3.3	14.0	C 40 H 60 37Cl 2 N 8 O 4
-11.8 /	-9.4	13.5	C 39 H 60 35Cl 37Cl N 9 O 4
+11.7 /	+9.2	14.5	C 39 H 58 37Cl 2 N 9 O 4
+4.1 /	+3.2	14.0	C 38 H 58 35Cl 37Cl N 10 O 4
-3.6 /	-2.8	13.5	C 37 H 58 35Cl 2 N 11 O 4
-9.5 /	-7.5	18.5	C 40 H 55 37Cl N 11 O 4
+12.4 /	+9.8	14.0	C 36 H 56 35Cl 2 N 12 O 4
+6.4 /	+5.0	19.0	C 39 H 53 37Cl N 12 O 4
-1.2 /	-1.0	18.5	C 38 H 53 35Cl N 13 O 4
+1.1 /	+0.9	23.5	C 39 H 48 N 15 O 4
-11.6 /	-9.2	10.5	C 32 H 58 37Cl 2 N 15 O 4
+6.8 /	+5.4	26.5	C 49 H 52 N 5 O 5
-5.9 /	-4.7	13.5	C 42 H 62 37Cl 2 N 5 O 5
+10.0 /	+7.9	14.0	C 41 H 60 37Cl 2 N 6 O 5
+2.4 /	+1.9	13.5	C 40 H 60 35Cl 37Cl N 7 O 5
-5.3 /	-4.2	13.0	C 39 H 60 35Cl 2 N 8 O 5
-11.2 /	-8.9	18.0	C 42 H 57 37Cl N 8 O 5
+10.7 /	+8.4	13.5	C 38 H 58 35Cl 2 N 9 O 5
+4.7 /	+3.7	18.5	C 41 H 55 37Cl N 9 O 5
-2.9 /	-2.3	18.0	C 40 H 55 35Cl N 10 O 5
-0.6 /	-0.5	23.0	C 41 H 50 N 12 O 5
+2.6 /	+2.0	10.5	C 33 H 58 37Cl 2 N 13 O 5
-5.1 /	-4.0	10.0	C 32 H 58 35Cl 37Cl N 14 O 5
+10.9 /	+8.6	10.5	C 31 H 56 35Cl 37Cl N 15 O 5
-7.0 /	-5.5	12.5	C 41 H 62 35Cl 2 N 5 O 6
+9.0 /	+7.1	13.0	C 40 H 60 35Cl 2 N 6 O 6
+3.0 /	+2.4	18.0	C 43 H 57 37Cl N 6 O 6
-4.6 /	-3.7	17.5	C 42 H 57 35Cl N 7 O 6
+11.3 /	+8.9	18.0	C 41 H 55 35Cl N 8 O 6
-2.3 /	-1.8	22.5	C 43 H 52 N 9 O 6
+0.9 /	+0.7	10.0	C 35 H 60 37Cl 2 N 10 O 6
-6.8 /	-5.3	9.5	C 34 H 60 35Cl 37Cl N 11 O 6
+9.2 /	+7.2	10.0	C 33 H 58 35Cl 37Cl N 12 O 6
+1.5 /	+1.2	9.5	C 32 H 58 35Cl 2 N 13 O 6
-4.4 /	-3.5	14.5	C 35 H 55 37Cl N 13 O 6
-12.1 /	-9.5	14.0	C 34 H 55 35Cl N 14 O 6
+11.5 /	+9.1	15.0	C 34 H 53 37Cl N 14 O 6
+3.9 /	+3.0	14.5	C 33 H 53 35Cl N 15 O 6
+9.6 /	+7.6	17.5	C 43 H 57 35Cl N 5 O 7
-4.0 /	-3.2	22.0	C 45 H 54 N 6 O 7
+11.9 /	+9.4	22.5	C 44 H 52 N 7 O 7
-0.8 /	-0.7	9.5	C 37 H 62 37Cl 2 N 7 O 7
-8.5 /	-6.7	9.0	C 36 H 62 35Cl 37Cl N 8 O 7
+7.5 /	+5.9	9.5	C 35 H 60 35Cl 37Cl N 9 O 7
-0.2 /	-0.1	9.0	C 34 H 60 35Cl 2 N 10 O 7
-6.1 /	-4.9	14.0	C 37 H 57 37Cl N 10 O 7
+9.8 /	+7.7	14.5	C 36 H 55 37Cl N 11 O 7
+2.2 /	+1.7	14.0	C 35 H 55 35Cl N 12 O 7
-11.4 /	-9.0	18.5	C 37 H 52 N 13 O 7
+4.5 /	+3.5	19.0	C 36 H 50 N 14 O 7
-8.3 /	-6.5	6.0	C 29 H 60 37Cl 2 N 14 O 7
+7.7 /	+6.1	6.5	C 28 H 58 37Cl 2 N 15 O 7
-10.2 /	-8.0	8.5	C 38 H 64 35Cl 37Cl N 5 O 8
+5.8 /	+4.6	9.0	C 37 H 62 35Cl 37Cl N 6 O 8
-1.9 /	-1.5	8.5	C 36 H 62 35Cl 2 N 7 O 8
-7.8 /	-6.2	13.5	C 39 H 59 37Cl N 7 O 8
+8.1 /	+6.4	14.0	C 38 H 57 37Cl N 8 O 8
+0.5 /	+0.4	13.5	C 37 H 57 35Cl N 9 O 8

Figure S95. HR-FAB-MS data of microphorusamide B (**11**).

[Elemental Composition]
 Date : FAB-0839 Date : 26-Apr-2017 16:22 Page: 1
 Sample: Microphoramide B
 Note : m-NBA
 Inlet : Direct Ion Mode : FAB+
 RT : 1.01 min Scan#: (43,52)
 Elements : C 100/0, H 150/0, Cl 2/0 (35Cl 2/0, 37Cl 2/0), N 15/5, O 12/0
 Mass Tolerance : 20ppm, 5mmu if m/z < 250, 10mmu if m/z > 500
 Unsaturation (U.S.) : -10.0 - 100.0

Observed m/z	Int%	Err [ppm / mmu]	U.S.	Composition
774.4066	17.1	-0.5 / -0.4	21.5	C 48 H 58 35Cl 2 N 5
		-6.6 / -5.1	26.5	C 51 H 55 37Cl N 5
		+9.7 / +7.5	27.0	C 50 H 53 37Cl N 6
		+1.9 / +1.5	26.5	C 49 H 53 35Cl N 7
		-12.0 / -9.3	31.0	C 51 H 50 N 8
		+4.2 / +3.3	31.5	C 50 H 48 N 9
		-8.7 / -6.8	18.5	C 43 H 58 37Cl 2 N 9
		+7.5 / +5.8	19.0	C 42 H 56 37Cl 2 N 10
		-0.3 / -0.2	18.5	C 41 H 56 35Cl 37Cl N 11
		-8.1 / -6.2	18.0	C 40 H 56 35Cl 2 N 12
		+8.2 / +6.3	18.5	C 39 H 54 35Cl 2 N 13
		+2.1 / +1.6	23.5	C 42 H 51 37Cl N 13
		-5.7 / -4.4	23.0	C 41 H 51 35Cl N 14
		+10.5 / +8.2	23.5	C 40 H 49 35Cl N 15
		+2.5 / +1.9	31.0	C 52 H 50 N 6 O
		-10.5 / -8.1	18.0	C 45 H 60 37Cl 2 N 6 O
		+5.8 / +4.5	18.5	C 44 H 58 37Cl 2 N 7 O
		-2.0 / -1.6	18.0	C 43 H 58 35Cl 37Cl N 8 O
		-9.8 / -7.6	17.5	C 42 H 58 35Cl 2 N 9 O
		+6.4 / +5.0	18.0	C 41 H 56 35Cl 2 N 10 O
		+0.3 / +0.3	23.0	C 44 H 53 37Cl N 10 O
		-7.4 / -5.8	22.5	C 43 H 53 35Cl N 11 O
		+8.8 / +6.8	23.0	C 42 H 51 35Cl N 12 O
		-5.1 / -3.9	27.5	C 44 H 48 N 13 O
		+11.2 / +8.7	28.0	C 43 H 46 N 14 O
		-1.8 / -1.4	15.0	C 36 H 56 37Cl 2 N 14 O
		-9.6 / -7.4	14.5	C 35 H 56 35Cl 37Cl N 15 O
		-3.7 / -2.9	17.5	C 45 H 60 35Cl 37Cl N 5 O 2
		-11.5 / -8.9	17.0	C 44 H 60 35Cl 2 N 6 O 2
		+12.5 / +9.7	18.0	C 44 H 58 35Cl 37Cl N 6 O 2
		+4.7 / +3.7	17.5	C 43 H 58 35Cl 2 N 7 O 2
		-1.4 / -1.1	22.5	C 46 H 55 37Cl N 7 O 2
		-9.2 / -7.1	22.0	C 45 H 55 35Cl N 8 O 2
		+7.1 / +5.5	22.5	C 44 H 53 35Cl N 9 O 2
		-6.8 / -5.3	27.0	C 46 H 50 N 10 O 2
		+9.4 / +7.3	27.5	C 45 H 48 N 11 O 2
		-3.5 / -2.7	14.5	C 38 H 58 37Cl 2 N 11 O 2
		-11.3 / -8.8	14.0	C 37 H 58 35Cl 37Cl N 12 O 2
		+12.7 / +9.8	15.0	C 37 H 56 37Cl 2 N 12 O 2
		+4.9 / +3.8	14.5	C 36 H 56 35Cl 37Cl N 13 O 2
		-2.9 / -2.2	14.0	C 35 H 56 35Cl 2 N 14 O 2
		-9.0 / -6.9	19.0	C 38 H 53 37Cl N 14 O 2
		+7.3 / +5.6	19.5	C 37 H 51 37Cl N 15 O 2
		-10.9 / -8.4	21.5	C 47 H 57 35Cl N 5 O 3
		+5.3 / +4.1	22.0	C 46 H 55 35Cl N 6 O 3
		-8.5 / -6.6	26.5	C 48 H 52 N 7 O 3
		+7.7 / +6.0	27.0	C 47 H 50 N 8 O 3
		-5.3 / -4.1	14.0	C 40 H 60 37Cl 2 N 8 O 3
		+11.0 / +8.5	14.5	C 39 H 58 37Cl 2 N 9 O 3
		+3.2 / +2.5	14.0	C 38 H 58 35Cl 37Cl N 10 O 3
		-4.6 / -3.6	13.5	C 37 H 58 35Cl 2 N 11 O 3
		-10.7 / -8.3	18.5	C 40 H 55 37Cl N 11 O 3
		+11.6 / +9.0	14.0	C 36 H 56 35Cl 2 N 12 O 3
		+5.5 / +4.3	19.0	C 39 H 53 37Cl N 12 O 3
		-2.2 / -1.7	18.5	C 38 H 53 35Cl N 13 O 3

+0.1 /	+0.1	23.5	C 39 H 48 N 15 O 3
-12.9 /	-10.0	10.5	C 32 H 58 37Cl 2 N 15 O 3
+6.0 /	+4.6	26.5	C 49 H 52 N 5 O 4
-7.0 /	-5.4	13.5	C 42 H 62 37Cl 2 N 5 O 4
+9.2 /	+7.1	14.0	C 41 H 60 37Cl 2 N 6 O 4
+1.4 /	+1.1	13.5	C 40 H 60 35Cl 37Cl N 7 O 4
-6.3 /	-4.9	13.0	C 39 H 60 35Cl 2 N 8 O 4
-12.4 /	-9.6	18.0	C 42 H 57 37Cl N 8 O 4
+9.9 /	+7.7	13.5	C 38 H 58 35Cl 2 N 9 O 4
+3.8 /	+3.0	18.5	C 41 H 55 37Cl N 9 O 4
-4.0 /	-3.1	18.0	C 40 H 55 35Cl N 10 O 4
+12.3 /	+9.5	18.5	C 39 H 53 35Cl N 11 O 4
-1.6 /	-1.2	23.0	C 41 H 50 N 12 O 4
+1.6 /	+1.3	10.5	C 33 H 58 37Cl 2 N 13 O 4
-6.1 /	-4.7	10.0	C 32 H 58 35Cl 37Cl N 14 O 4
+10.1 /	+7.8	10.5	C 31 H 56 35Cl 37Cl N 15 O 4
-8.1 /	-6.2	12.5	C 41 H 62 35Cl 2 N 5 O 5
+8.2 /	+6.3	13.0	C 40 H 60 35Cl 2 N 6 O 5
+2.1 /	+1.6	18.0	C 43 H 57 37Cl N 6 O 5
-5.7 /	-4.4	17.5	C 42 H 57 35Cl N 7 O 5
+10.5 /	+8.2	18.0	C 41 H 55 35Cl N 8 O 5
-3.3 /	-2.6	22.5	C 43 H 52 N 9 O 5
+12.9 /	+10.0	23.0	C 42 H 50 N 10 O 5
-0.1 /	-0.1	10.0	C 35 H 60 37Cl 2 N 10 O 5
-7.9 /	-6.1	9.5	C 34 H 60 35Cl 37Cl N 11 O 5
+8.4 /	+6.5	10.0	C 33 H 58 35Cl 37Cl N 12 O 5
+0.6 /	+0.5	9.5	C 32 H 58 35Cl 2 N 13 O 5
-5.5 /	-4.3	14.5	C 35 H 55 37Cl N 13 O 5
+10.7 /	+8.3	15.0	C 34 H 53 37Cl N 14 O 5
+3.0 /	+2.3	14.5	C 33 H 53 35Cl N 15 O 5
+8.8 /	+6.8	17.5	C 43 H 57 35Cl N 5 O 6
-5.1 /	-3.9	22.0	C 45 H 54 N 6 O 6
+11.2 /	+8.6	22.5	C 44 H 52 N 7 O 6
-1.8 /	-1.4	9.5	C 37 H 62 37Cl 2 N 7 O 6
-9.6 /	-7.4	9.0	C 36 H 62 35Cl 37Cl N 8 O 6
+6.6 /	+5.1	9.5	C 35 H 60 35Cl 37Cl N 9 O 6
-1.1 /	-0.9	9.0	C 34 H 60 35Cl 2 N 10 O 6
-7.2 /	-5.6	14.0	C 37 H 57 37Cl N 10 O 6
+9.0 /	+7.0	14.5	C 36 H 55 37Cl N 11 O 6
+1.2 /	+0.9	14.0	C 35 H 55 35Cl N 12 O 6
-12.7 /	-9.8	18.5	C 37 H 52 N 13 O 6
+3.6 /	+2.8	19.0	C 36 H 50 N 14 O 6
-9.4 /	-7.3	6.0	C 29 H 60 37Cl 2 N 14 O 6
+6.8 /	+5.3	6.5	C 28 H 58 37Cl 2 N 15 O 6
-11.3 /	-8.8	8.5	C 38 H 64 35Cl 37Cl N 5 O 7
+12.7 /	+9.8	9.5	C 38 H 62 37Cl 2 N 5 O 7
+4.9 /	+3.8	9.0	C 37 H 62 35Cl 37Cl N 6 O 7
-2.9 /	-2.2	8.5	C 36 H 62 35Cl 2 N 7 O 7
-9.0 /	-6.9	13.5	C 39 H 59 37Cl N 7 O 7
+7.3 /	+5.6	14.0	C 38 H 57 37Cl N 8 O 7
-0.5 /	-0.4	13.5	C 37 H 57 35Cl N 9 O 7
+1.9 /	+1.4	18.5	C 38 H 52 N 11 O 7
-11.1 /	-8.6	5.5	C 31 H 62 37Cl 2 N 11 O 7
+5.1 /	+4.0	6.0	C 30 H 60 37Cl 2 N 12 O 7
-2.7 /	-2.1	5.5	C 29 H 60 35Cl 37Cl N 13 O 7
-10.4 /	-8.1	5.0	C 28 H 60 35Cl 2 N 14 O 7
+5.8 /	+4.5	5.5	C 27 H 58 35Cl 2 N 15 O 7
-0.3 /	-0.2	10.5	C 30 H 55 37Cl N 15 O 7
+11.6 /	+9.0	8.5	C 37 H 62 35Cl 2 N 5 O 8
+5.5 /	+4.3	13.5	C 40 H 59 37Cl N 5 O 8
-2.2 /	-1.7	13.0	C 39 H 59 35Cl N 6 O 8
+0.1 /	+0.1	18.0	C 40 H 54 N 8 O 8
-12.9 /	-10.0	5.0	C 33 H 64 37Cl 2 N 8 O 8
+3.4 /	+2.6	5.5	C 32 H 62 37Cl 2 N 9 O 8

Figure S96. ^1H NMR spectrum data of coprisamide C (**14**) at 850 MHz in $\text{DMSO}-d_6$.

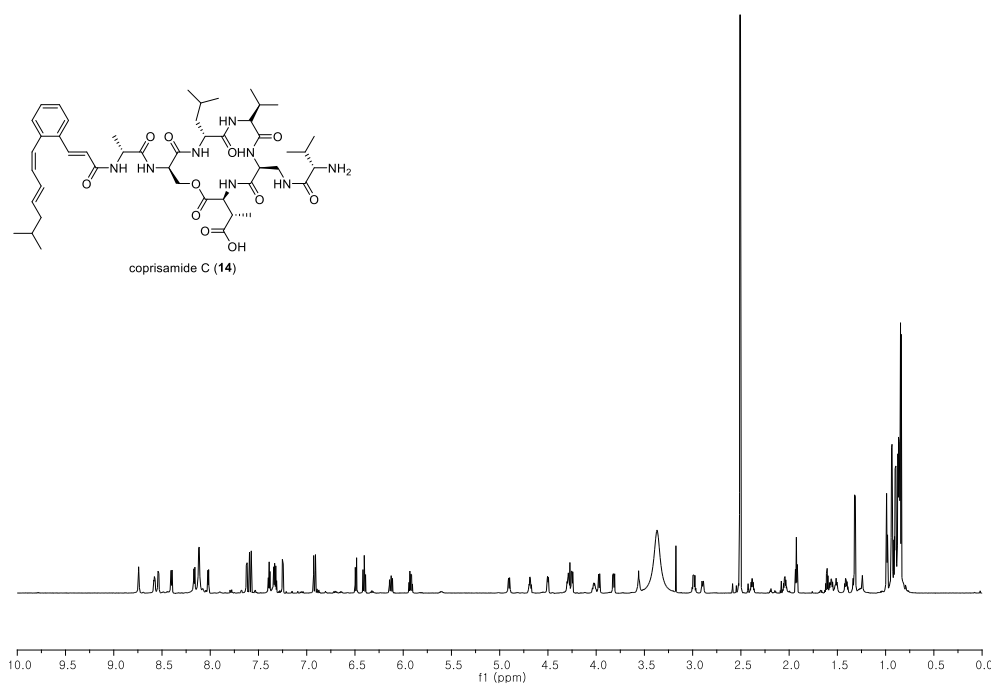


Figure S97. ^{13}C NMR spectrum data of coprisamide C (**14**) at 212.5 MHz in $\text{DMSO}-d_6$.

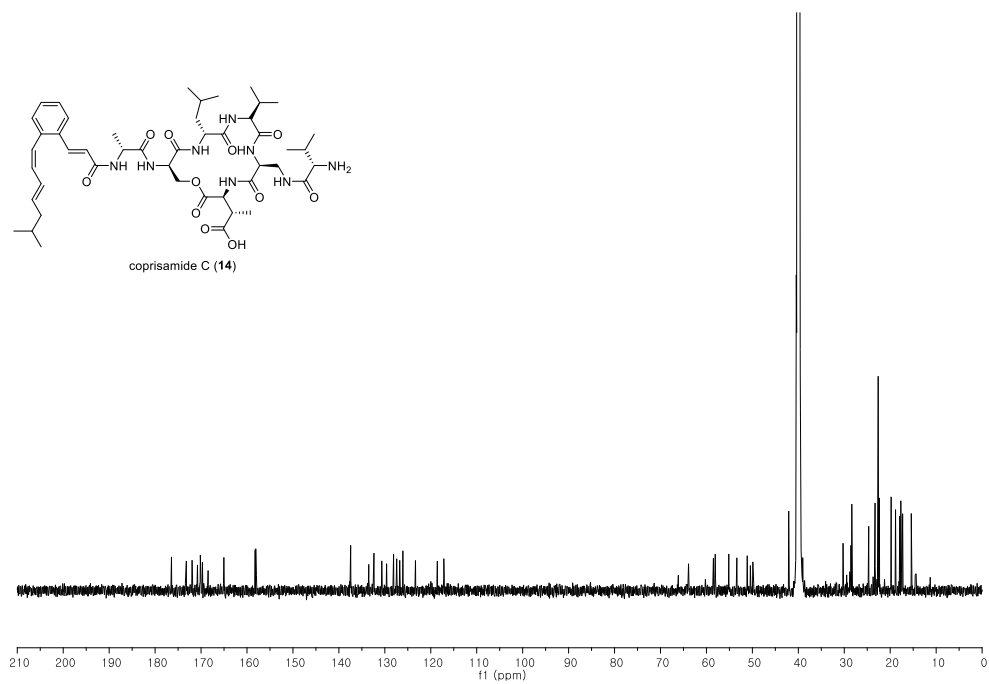


Figure S98. COSY NMR spectrum data of coprisamide C (**14**) at 800 MHz in DMSO-*d*₆.

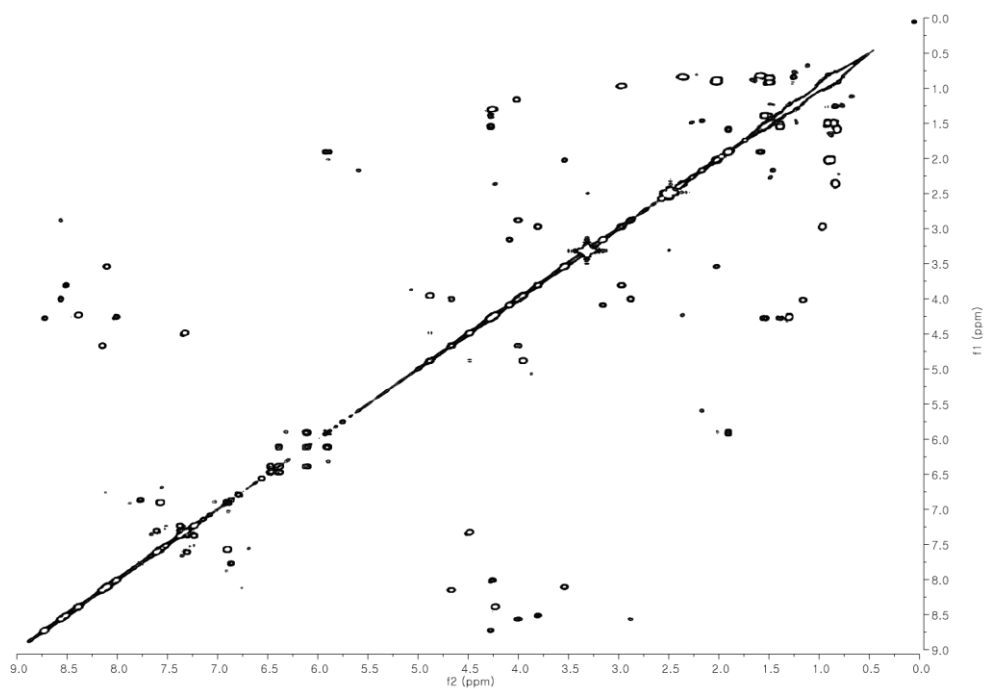


Figure S99. HSQC NMR spectrum data of coprisamide C (**14**) at 800 MHz in DMSO-*d*₆.

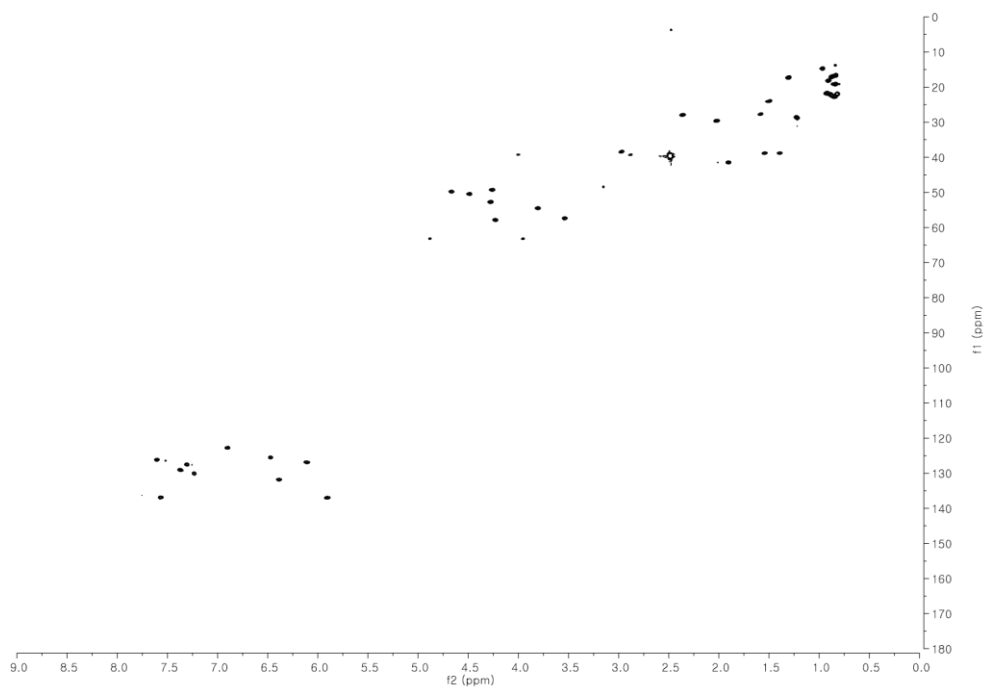


Figure S100. HMBC NMR spectrum data of coprisamide C (**14**) at 850 MHz in DMSO- d_6 .

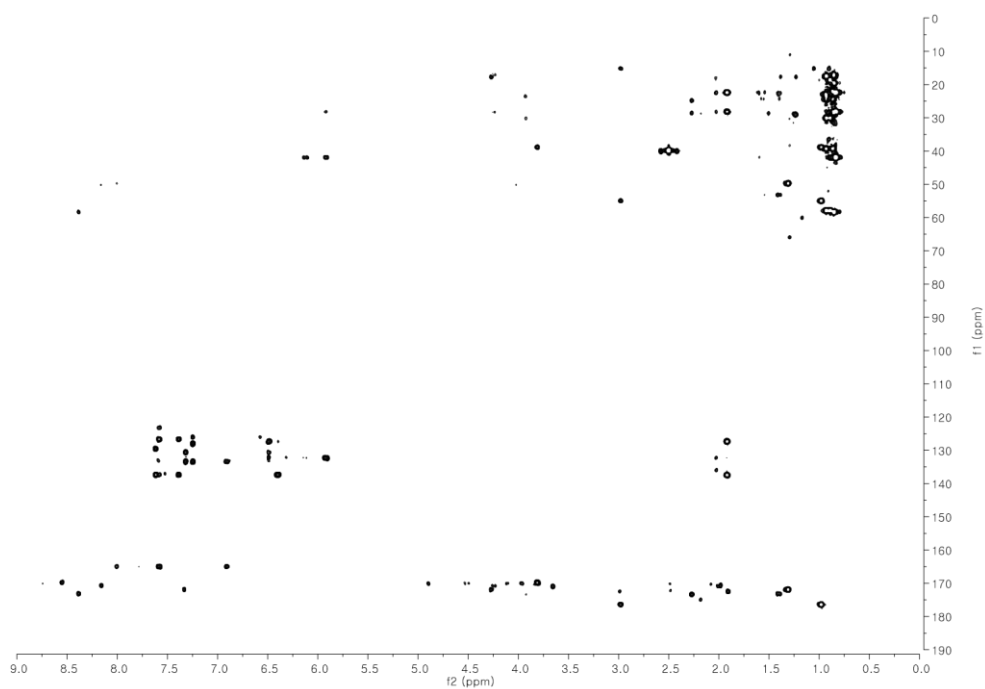


Figure S101. TOCSY NMR spectrum data of coprisamide C (**14**) at 800 MHz in DMSO- d_6 .

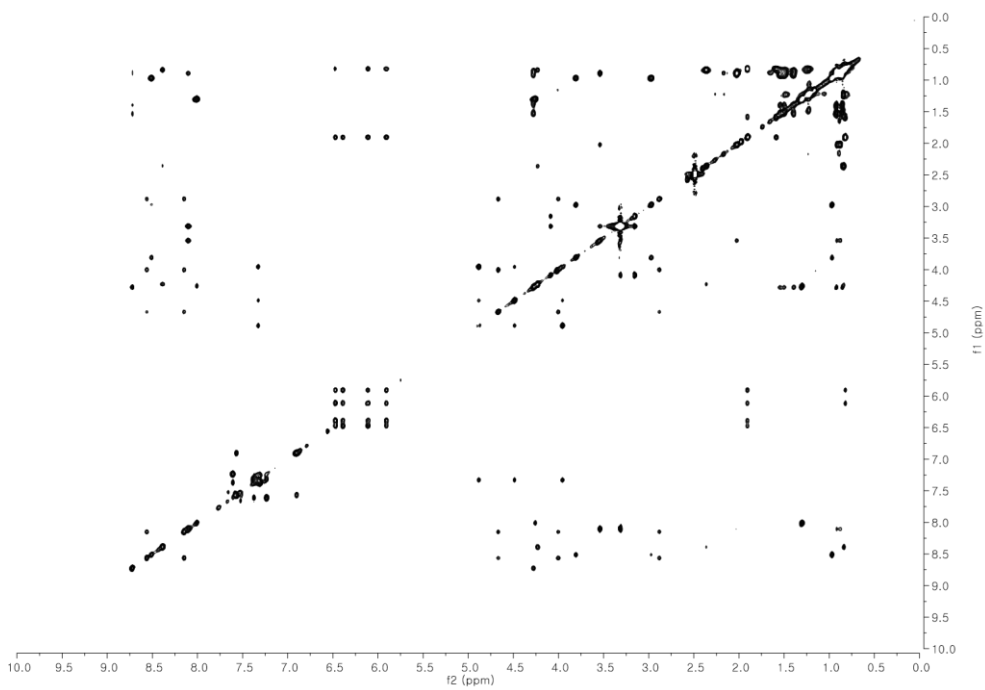


Figure S102. ROESY NMR spectrum data of coprisamide C (**14**) at 800 MHz in DMSO-*d*₆.

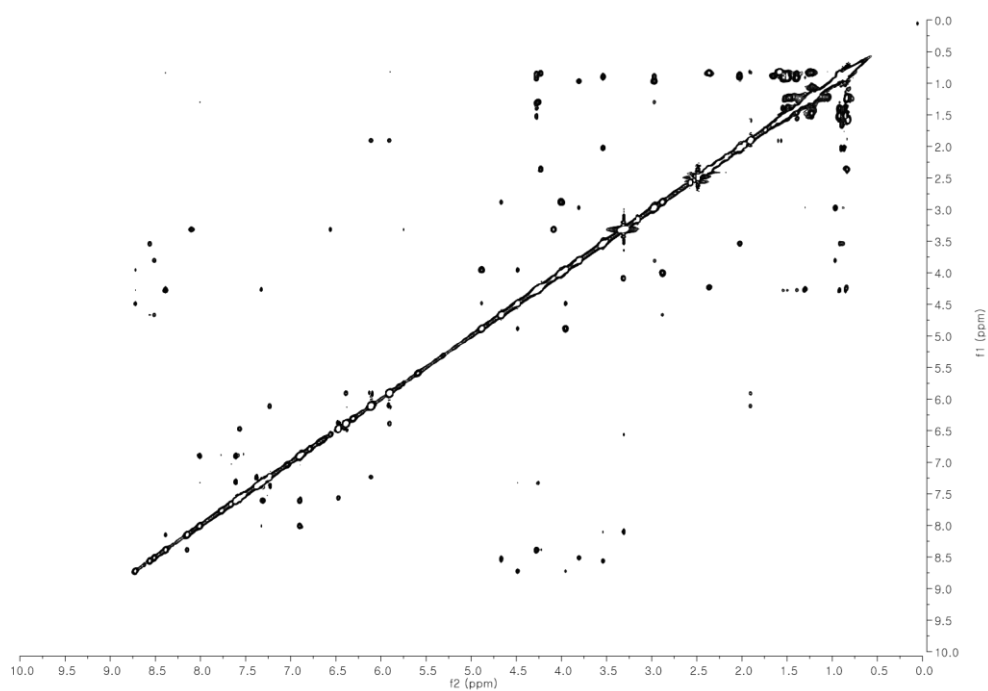


Figure S103. ^1H NMR spectrum data of *S*-PGME amide of **14** (**14a**) at 800 MHz in CD_3OD .

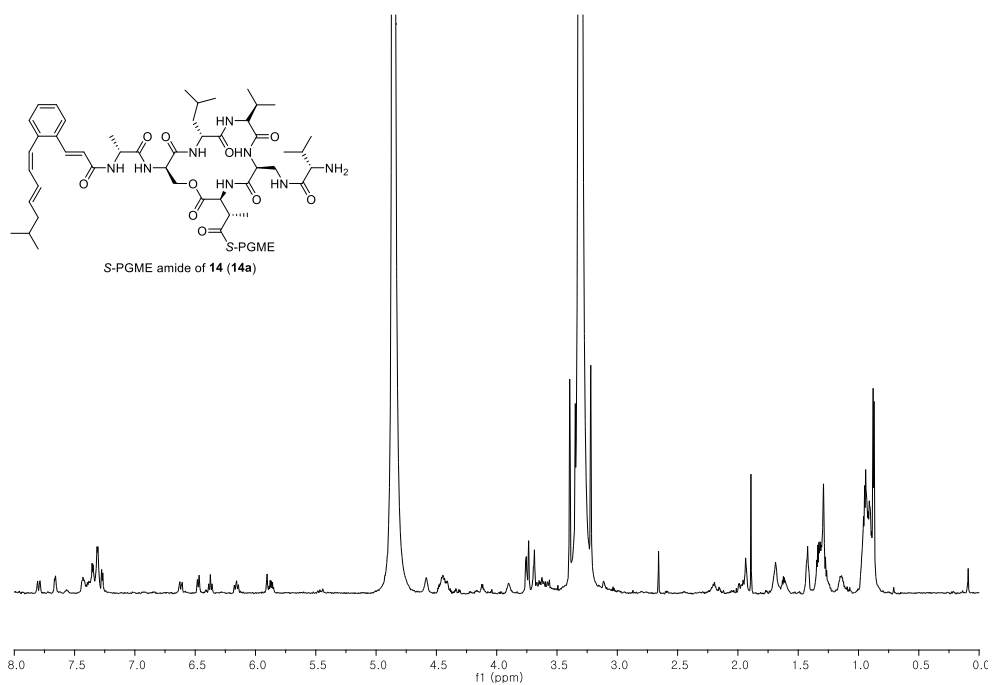


Figure S104. COSY NMR spectrum data of *S*-PGME amide of **14** (**14a**) at 800 MHz in CD_3OD .

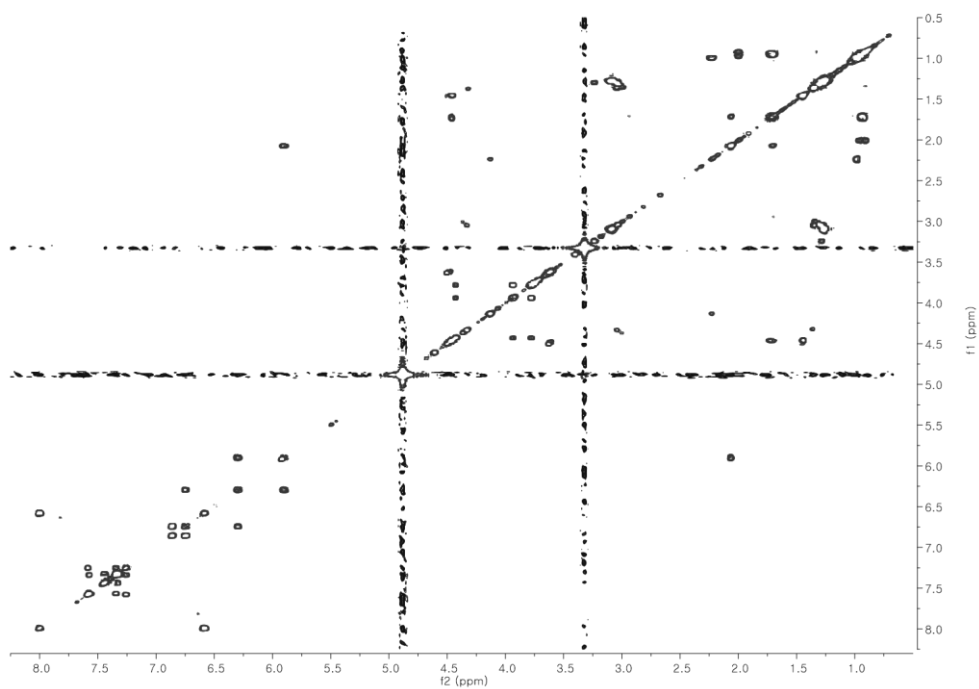


Figure S105. ^1H NMR spectrum data of *R*-PGME amide of **14** (**14b**) at 800 MHz in CD_3OD .

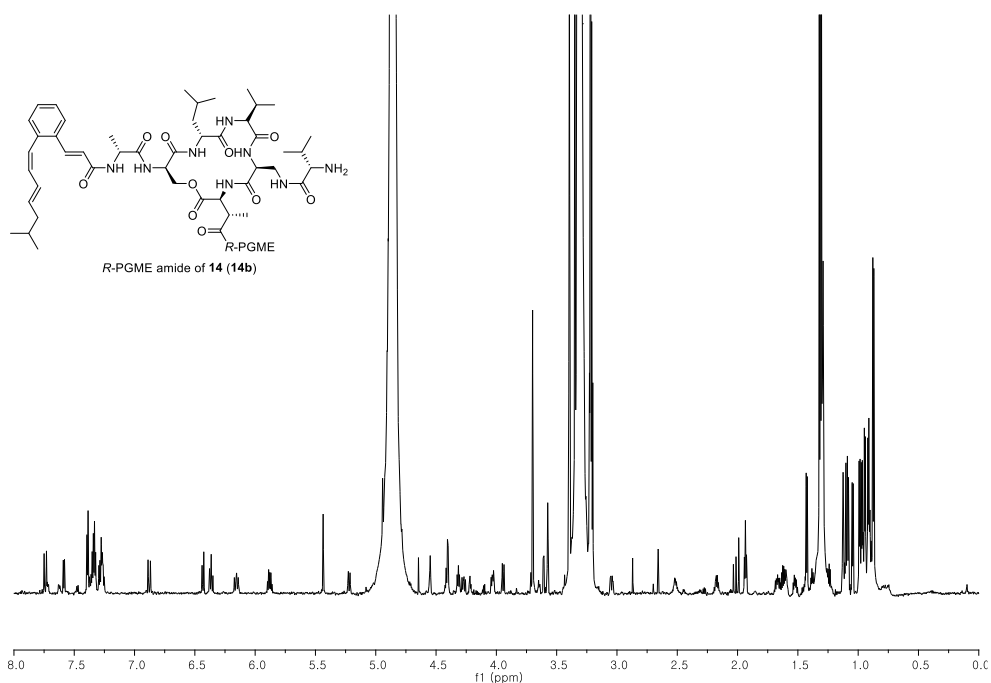


Figure S106. COSY NMR spectrum data of *R*-PGME amide of **14** (**14b**) at 800 MHz in CD_3OD .

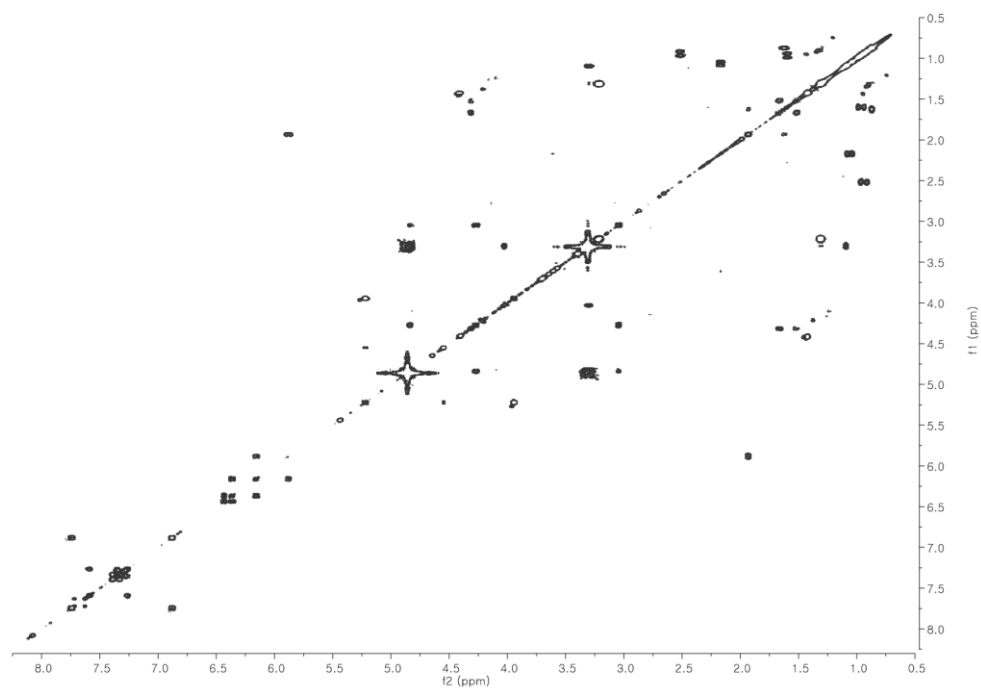


Figure S107. ^1H NMR spectrum data of coprisamide D (**15**) at 800 MHz in $\text{DMSO}-d_6$.

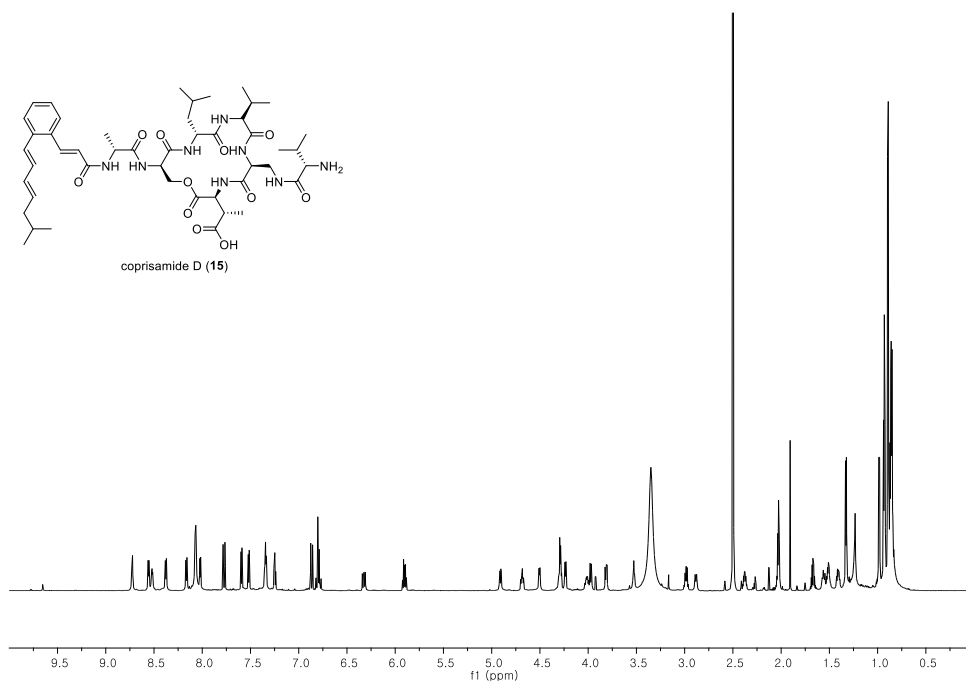


Figure S108. ^1H NMR spectrum data of coprisamide D (**15**) at 200 MHz in $\text{DMSO}-d_6$.

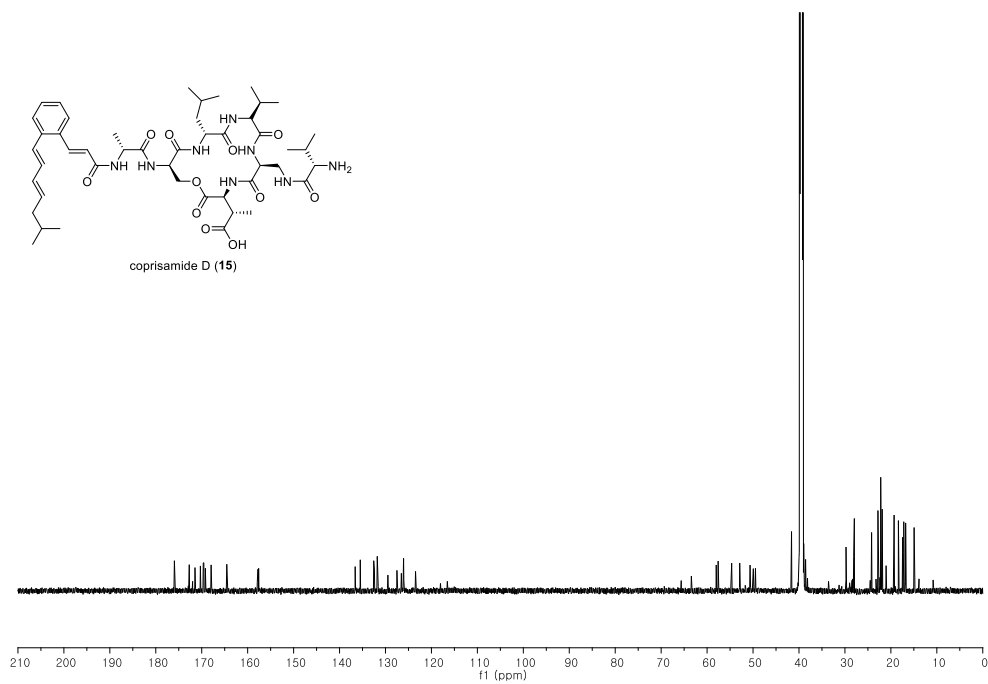


Figure S109. COSY NMR spectrum data of coprisamide D (**15**) at 800 MHz in DMSO- d_6 .

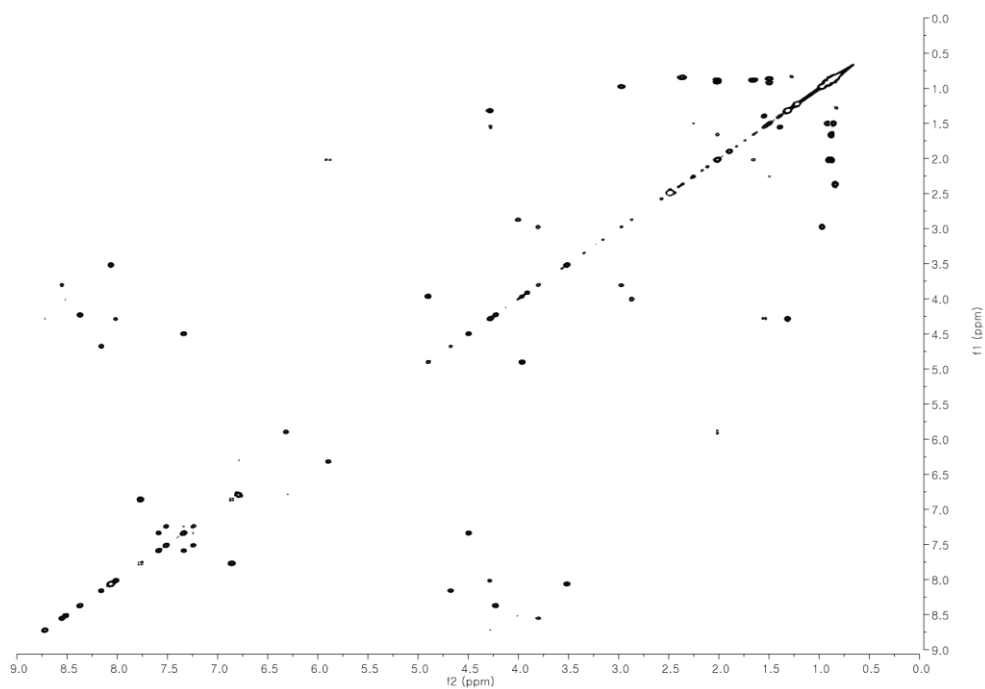


Figure S110. HSQC NMR spectrum data of coprisamide D (**15**) at 800 MHz in DMSO- d_6 .

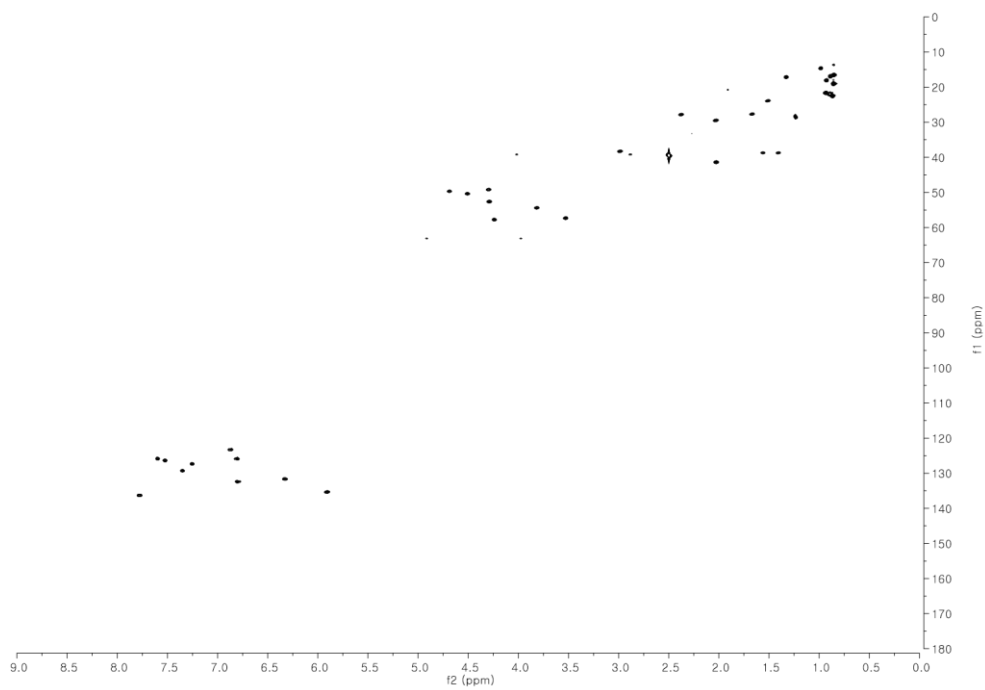


Figure S111. HMBC NMR spectrum data of coprisamide D (**15**) at 800 MHz in DMSO- d_6 .

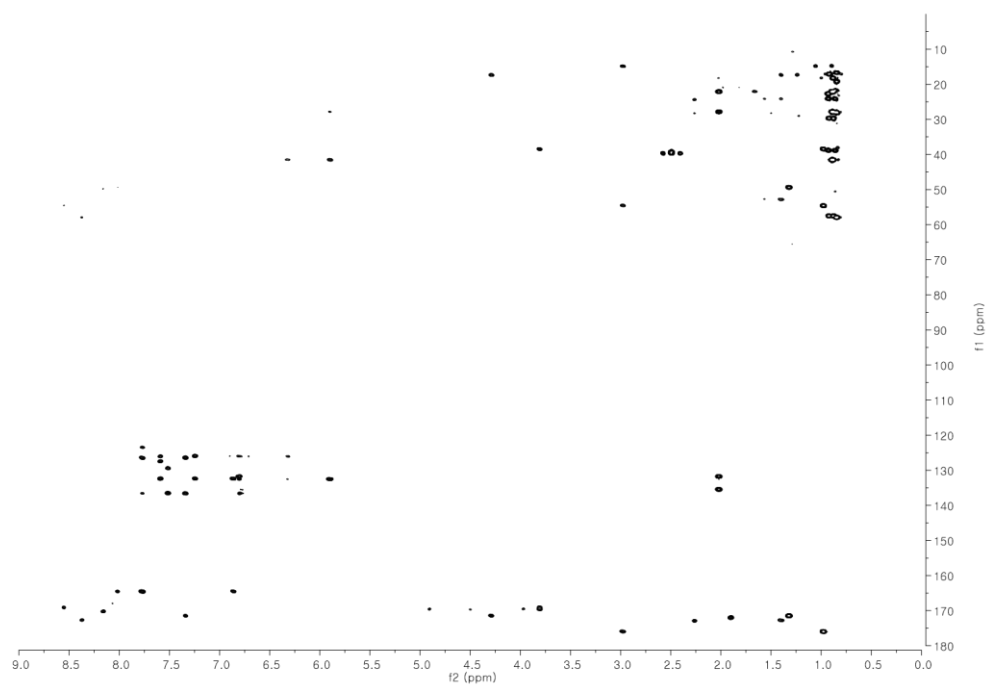


Figure S112. TOCSY NMR spectrum data of coprisamide D (**15**) at 800 MHz in DMSO- d_6 .

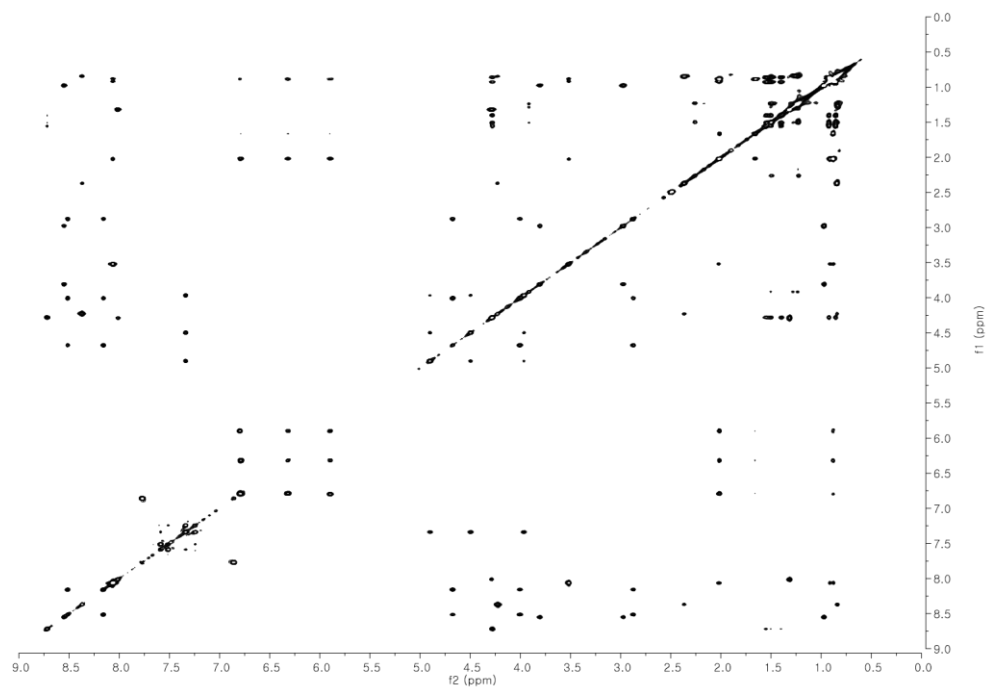


Figure S113. ROESY NMR spectrum data of coprisamide D (**15**) at 800 MHz in DMSO-*d*₆.

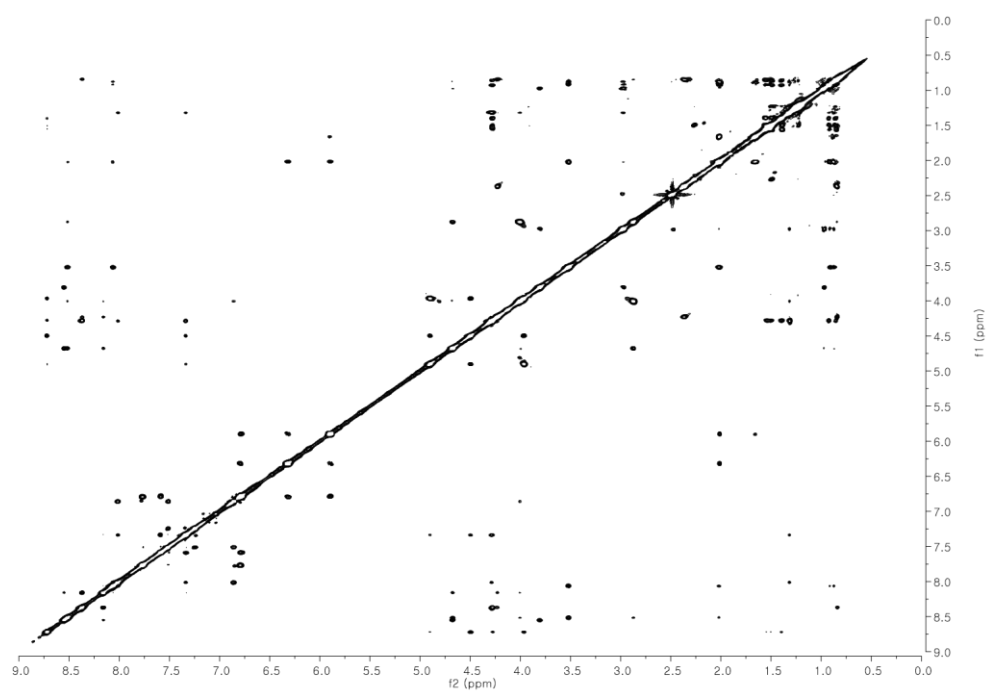


Figure S114. HR-ESI-MS data of coprisamide C (**14**).

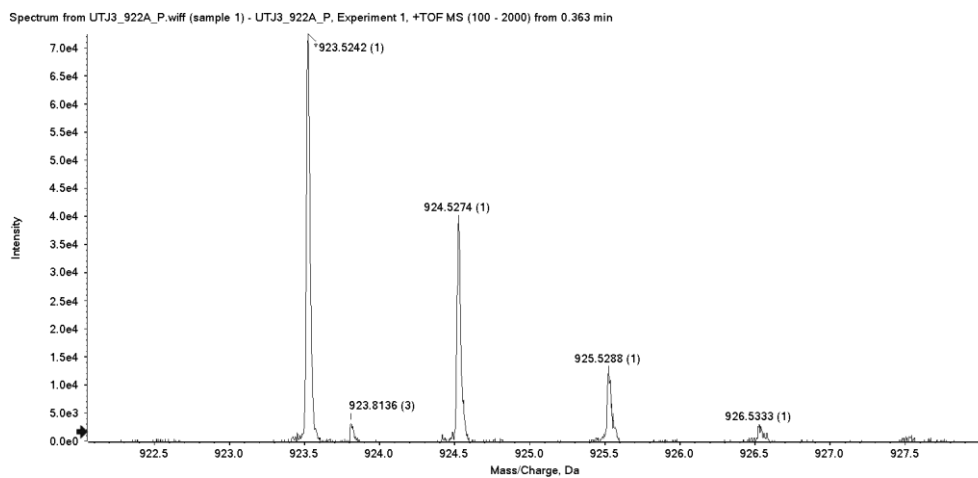


Figure S115. HR-ESI-MS data of coprisamide D (**15**).

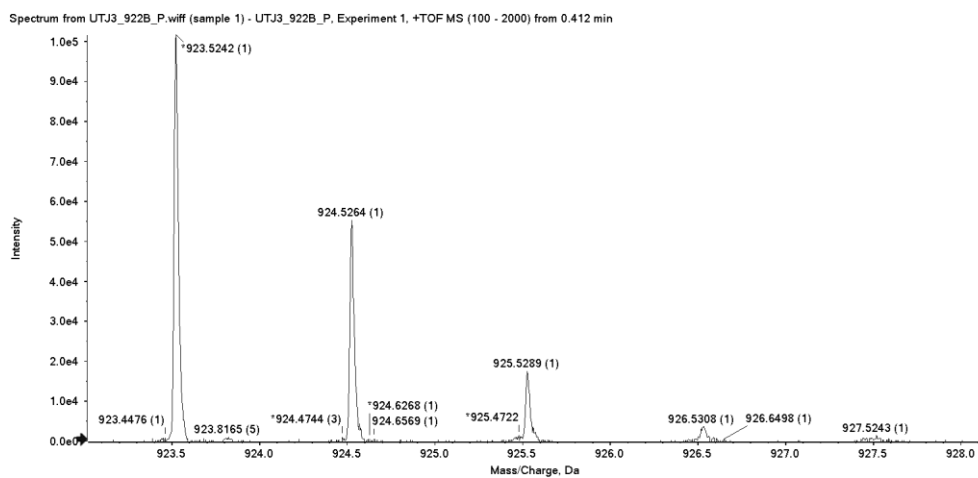


Figure S116. LC/MS chromatogram data of L- and D-FDAA derivatives of the amino acid units in coprisamide C (**14**). (a) β -methyl-aspartic acid, (b) 2,3-diaminopropionic acid (*di*-FDAA), (c) valine, (d) leucine, (e) serine, and (f) alanine.

a) β -methyl-aspartic acid: $[M-H]^-$ m/z at 398



b) 2,3-diaminopropionic acid (*di*-FDAA): $[M-H]^-$ m/z at 607



c) valine: $[M-H]^-$ m/z at 368



d) leucine: $[M-H]^-$ m/z at 382



e) serine: $[M-H]^-$ m/z at 356



f) alanine: $[M-H]^-$ m/z at 340

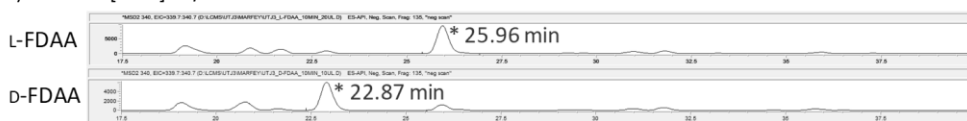


Figure S117. *J*-based configuration analysis of C-2 and C-3 of coprisamide C (**14**).

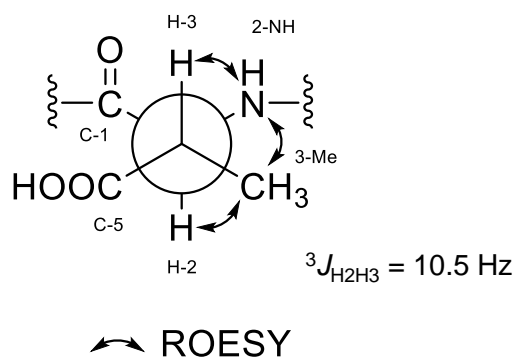


Figure S118. Circular dichroism spectra data of coprisamides C and D (**14** and **15**).

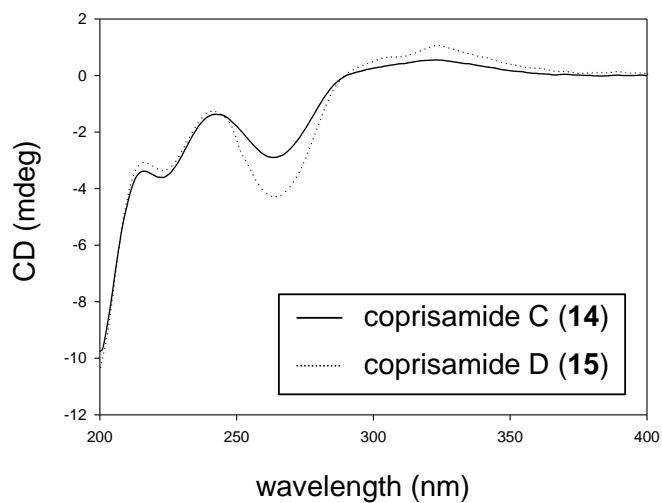
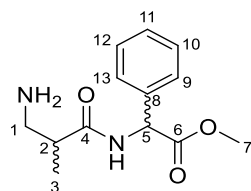


Table S1. ^1H and ^{13}C NMR data for **6–9** in CD_3OD .



6: 2*S*, 5*S* **7:** 2*S*, 5*R*
8: 2*R*, 5*S* **9:** 2*R*, 5*R*

no.	6		7		8		9	
	δ_{C}^a , type	δ_{H}^b , mult, (<i>J</i> in Hz)	δ_{C}^a , type	δ_{H}^b , mult, (<i>J</i> in Hz)	δ_{C}^a , type	δ_{H}^b , mult, (<i>J</i> in Hz)	δ_{C}^a , type	δ_{H}^b , mult, (<i>J</i> in Hz)
1a	42.9, CH ₂	3.1548, dd (12.8, 8.2)	42.7, CH ₂	3.1472, dd (12.8, 8.2)	42.7, CH ₂	3.1480, dd (12.8, 8.2)	42.9, CH ₂	3.1549, dd (12.8, 8.2)
1b		3.0158, dd (12.8, 4.6)		2.9796, dd (12.8, 4.6)		2.9779, dd (12.8, 4.6)		3.0183, dd (12.8, 4.6)
2	38.5, CH	2.8757, m	38.4, CH	2.8344, m	38.4, CH	2.8363, m	38.5, CH	2.8745, m
3	16.2, CH ₃	1.1987, d (7.1)	16.4, CH ₃	1.3128, d (7.1)	16.4, CH ₃	1.3114, d (7.1)	16.2, CH ₃	1.1992, d (7.1)
4	175.4, C		175.6, C		175.6, C		175.4, C	
5	53.2, CH	5.5217, s	53.0, CH	5.4939, s	53.0, CH	5.4931, s	53.2, CH	5.5213, s
6	172.9, C		172.5, C		172.5, C		172.9, C	
7	58.2, CH ₃	3.7186, s	58.3, CH ₃	3.7078, s	58.3, CH ₃	3.7075, s	58.2, CH ₃	3.7187, s
8	137.2, C		137.0, C		137.0, C		137.2, C	
9	130.0, CH		130.0, CH		130.0, CH		130.0, CH	
10	128.8, CH		129.0, CH		129.0, CH		128.8, CH	
11	129.8, CH	7.4025–7.3477, m	129.8, CH	7.4090–7.3501, m	129.8, CH	7.4077–7.3494, m	129.8, CH	7.4241–7.3442, m
12	128.8, CH		129.0, CH		129.0, CH		128.8, CH	
13	130.0, CH		130.0, CH		130.0, CH		130.0, CH	

^a 212.5 MHz, ^b 850 MHz

Table S2. Energy-minimized modeling of **6**.

total energy = -840.68015403485
kinetic energy = 836.36200464106
potential energy = -1677.04215867591

Parameters of Level DFT

DFT settings (functional B3-LYP / gridsize m3)

Geometry optimization options (Energy 10^{-6} Hartree, Gradient norm $|dE/dxyz| = 10^{-3}$ Hartree/Bohr)

Energy minimized coordinates of **6** at the basis set 6-31G for all atoms (Å).

atom	x	y	z	atom	x	y	z
N	-6.062776	0.848977	-0.613960	C	6.984551	10.453200	2.017350
C	-3.730117	2.126166	-1.296358	H	7.633107	3.342679	3.718588
C	-2.085439	3.122449	0.960083	H	9.531663	6.595471	6.501698
H	-2.574488	0.829599	-2.430779	H	9.124215	11.156670	5.421028
H	-4.178811	3.742049	-2.511036	C	5.918471	8.618785	0.438111
C	-3.553030	5.036097	2.585922	H	6.786343	12.439923	1.545265
H	-3.945805	6.740518	1.479037	H	4.855819	9.170701	-1.226112
H	-2.471439	5.594078	4.261606	C	6.643113	1.807808	-1.070476
H	-5.342867	4.213331	3.222846	H	4.525159	4.940554	-2.508185
C	0.290176	4.346875	-0.109003	O	6.408134	-0.253093	0.017212
H	-1.556843	1.487796	2.133499	O	8.540842	2.334656	-2.727551
O	0.201608	6.342028	-1.395226	C	10.435046	0.338834	-3.165163
N	2.520711	3.117756	0.334804	H	11.401468	-0.114456	-1.398587
C	4.915107	4.064308	-0.677723	H	11.733563	1.149033	-4.537543
C	6.158292	6.046933	1.032438	H	9.518228	-1.354216	-3.907139
C	7.456179	5.330628	3.233776	H	2.588258	1.480818	1.319708
C	8.524144	7.166093	4.807578	H	-5.903190	-0.810912	0.318605
C	8.294242	9.732107	4.199780	H	-7.506244	1.940080	-0.007622

Table S3. Energy-minimized modeling of **7**.

total energy = -840.68024294244
kinetic energy = 836.36777780232
potential energy = -1677.04802074476

Parameters of Level DFT

DFT settings (functional B3-LYP / gridsize m3)

Geometry optimization options (Energy 10^{-6} Hartree, Gradient norm $|dE/dxyz| = 10^{-3}$ Hartree/Bohr)

Energy minimized coordinates of **7** at the basis set 6-31G for all atoms (Å).

atom	x	y	z	atom	x	y	z
N	-7.04186	8.729227	-3.38046	C	5.749772	12.80673	0.230417
C	-4.66656	8.792593	-2.00522	H	5.743958	7.038882	-4.30879
C	-3.71539	6.19616	-0.935	H	7.65518	11.08943	-5.67736
H	-4.84693	10.10289	-0.41136	H	7.665678	14.7936	-2.77615
H	-3.20058	9.568145	-3.25112	C	4.678055	10.51839	1.010908
C	-5.62836	5.048434	0.929893	H	5.734244	14.42056	1.496962
H	-5.76468	6.239149	2.617024	H	3.790652	10.36024	2.852218
H	-5.05979	3.14885	1.527677	C	4.999567	3.677032	-0.52942
H	-7.49553	4.907677	0.045877	H	3.270447	5.989381	2.302737
C	-1.18407	6.621326	0.365189	O	4.512449	2.281358	-2.34638
H	-3.46095	4.901849	-2.54381	O	7.060387	3.377793	0.983329
O	-0.99821	7.884235	2.368745	C	8.81459	1.310088	0.34392
N	0.892599	5.613559	-0.79915	H	7.823345	-0.49887	0.39821
C	3.432856	5.952714	0.243145	H	10.27643	1.405887	1.786256
C	4.68294	8.422971	-0.61294	H	9.602315	1.611892	-1.53974
C	5.750912	8.647514	-3.03204	H	0.74087	4.525164	-2.36331
C	6.825494	10.93463	-3.80694	H	-7.06265	7.774442	-5.03507
C	6.830729	13.01851	-2.17484	H	-8.63766	8.529692	-2.35284

Table S4. Energy-minimized modeling of **8**.

total energy = -840.68020713328
 kinetic energy = 836.36564551297
 potential energy = -1677.04585264625

Parameters of Level DFT

DFT settings (functional B3-LYP / gridsize m3)

Geometry optimization options (Energy 10^{-6} Hartree, Gradient norm $|dE/dxyz| = 10^{-3}$ Hartree/Bohr)

Energy minimized coordinates of **8** at the basis set 6-31G for all atoms (Å).

atom	x	y	z	atom	x	y	z
N	-6.55866	3.93827	0.664599	C	5.563617	10.74408	0.456913
C	-3.91923	4.45686	0.117256	H	5.110892	5.739581	5.807127
C	-2.15129	2.087533	-0.12216	H	5.548927	10.27672	6.880315
H	-3.16559	5.693569	1.602749	H	5.841831	13.49423	3.459974
H	-3.79603	5.515607	-1.65804	C	5.325722	8.181703	-0.15366
C	-3.02726	0.314744	-2.25436	H	5.672946	12.14018	-1.04249
H	-5.01412	-0.20306	-1.98639	H	5.202436	7.586706	-2.11164
H	-1.91204	-1.42965	-2.29611	C	6.471166	1.88586	2.724145
H	-2.81378	1.258528	-4.08396	H	5.4157	3.326463	-0.90465
C	0.530572	3.002907	-0.62334	O	5.674796	0.630984	4.534396
H	-2.21021	1.067742	1.689936	O	8.94655	1.960629	2.023165
O	1.141088	4.038504	-2.67225	C	10.75013	0.511874	3.575243
N	2.228384	2.702877	1.303287	H	10.73858	1.220041	5.513689
C	4.844633	3.570474	1.066423	H	12.57344	0.824735	2.678719
C	5.176965	6.362584	1.768383	H	10.2422	-1.48812	3.565554
C	5.245779	7.135306	4.306443	H	1.764607	1.795184	2.920573
C	5.488366	9.696386	4.913121	H	-7.62329	3.244991	-0.75961
C	5.652665	11.50627	2.988688	H	-6.95918	3.177068	2.370722

Table S5. Energy-minimized modeling of **9**.

total energy = -840.68014373373
kinetic energy = 836.36796664395
potential energy = -1677.04811037768

Parameters of Level DFT

DFT settings (functional B3-LYP / gridsize m3)

Geometry optimization options (Energy 10^{-6} Hartree, Gradient norm $|dE/dxyz| = 10^{-3}$ Hartree/Bohr)

Energy minimized coordinates of **9** at the basis set 6-31G for all atoms (Å).

atom	x	y	z	atom	x	y	z
N	-7.11711	2.615939	0.546811	C	5.724258	12.75605	-0.42446
C	-4.71615	3.680532	1.34837	H	6.18641	6.428215	-4.11535
C	-3.26339	5.284796	-0.67606	H	7.845555	10.37258	-6.01911
H	-5.03448	4.889119	2.999385	H	7.555764	14.43446	-3.66299
H	-3.4829	2.132288	1.970612	C	4.79416	10.52957	0.65802
C	-4.84377	7.557344	-1.5711	H	5.577596	14.52485	0.604588
H	-6.69187	6.920734	-2.2538	H	3.88547	10.56716	2.495093
H	-3.90494	8.571685	-3.11301	C	5.598669	3.579698	0.093099
H	-5.12027	8.882309	-0.00493	H	3.656713	6.137589	2.553286
C	-0.78745	6.190099	0.478902	O	5.254365	1.925847	-1.52935
H	-2.86071	4.047666	-2.29926	O	7.631017	3.623123	1.671638
O	-0.73614	7.734472	2.283056	C	9.530865	1.611043	1.350489
N	1.379195	5.171944	-0.49651	H	8.656427	-0.23661	1.63313
C	3.867362	5.827098	0.521661	H	10.94419	1.998228	2.792099
C	4.968573	8.234967	-0.65761	H	10.34708	1.708573	-0.54263
C	6.062885	8.194791	-3.07527	H	1.339071	3.897579	-1.92076
C	6.99518	10.42106	-4.15229	H	-7.06034	1.288274	-0.82634
C	6.831428	12.70642	-2.82676	H	-8.59187	3.817896	0.394966

Table S6. ECD calculation of **4** (8S, 24R).

total energy = -1401.37943822718

kinetic energy = 1395.33958698909

potential energy = -2796.71902521627

Parameters of Level DFT

DFT settings (functional B3-LYP / gridsize m3)

Geometry optimization options (Energy 10^{-6} Hartree, Gradient norm $|dE/dxyz| = 10^{-3}$ Hartree/Bohr)Energy minimized coordinates of **4** (8S, 24R) at the basis set 6-311++G** for all atoms (Å).

atom	x	y	z	atom	x	y	z
C	-20.59184692	-11.53822385	8.18105445	H	-5.58635199	-10.12215196	-7.93249303
C	-21.84588203	-9.47023491	9.72391432	C	-9.53786472	-6.73414742	-8.08301792
C	-20.68227454	-7.04860517	8.92827942	H	-10.22926018	-10.55109496	-7.12562519
C	-18.90235947	-7.40465038	7.06160169	C	-8.81851271	-4.29240334	-7.87269573
C	-18.63074127	-10.22126590	6.34880731	H	-10.31927071	-7.26778070	-9.91378711
H	-22.02647932	-12.60634159	7.13930966	C	-7.66849420	-2.90174307	-5.75851125
H	-19.64907879	-12.87898521	9.44997025	H	-9.00907803	-3.15043721	-9.58463165
C	-19.47596115	-10.70393706	3.63237441	C	-8.63894343	-2.51394293	-3.41378446
C	-15.94185554	-11.22992879	6.91511419	H	-5.90415168	-1.93232985	-6.22664599
C	-18.51335880	-12.43558483	2.04352519	C	-7.37379607	-0.95489432	-1.56062067
C	-19.65371416	-13.11535896	-0.39873456	H	-10.46939018	-3.30129070	-2.92844285
H	-21.15159076	-9.64836650	3.06098546	C	-8.16405924	-0.28643554	0.80290396
H	-16.89344875	-13.56978176	2.60245891	H	-5.59453001	-0.13135798	-2.19361379
C	-20.24879001	-11.60383246	-2.36196029	C	-10.39013975	-0.99038392	2.23477881
H	-20.15691302	-15.10901869	-0.58223669	H	-6.97455635	1.08459981	1.77406710
C	-19.64845928	-8.92845601	-2.79145822	C	-11.87827483	-3.10283260	2.14271785
H	-21.36478006	-12.44088022	-3.88370723	H	-10.89033595	0.38145203	3.69158349
C	-17.38288992	-7.74756772	-2.84790647	C	-13.98594077	-3.34418378	3.84751546
H	-21.26376012	-7.78152155	-3.37325679	H	-11.46229395	-4.65791581	0.86698461
C	-14.86856025	-8.89882179	-2.42030422	C	-15.52613581	-5.37945913	4.19858604
H	-17.36140041	-5.76489420	-3.39918309	H	-14.37928105	-1.71159939	5.04056635
O	-14.45619495	-10.82567980	-1.08958164	C	-17.51411711	-5.21329894	6.11694526
N	-12.91904417	-7.66205185	-3.63776195	H	-15.30089586	-7.12060356	3.13760237
C	-10.31806863	-8.59772238	-3.59504122	O	-18.03833408	-3.04048327	7.09312826
H	-13.32417862	-6.23852088	-4.84650563	O	-23.51200190	-9.74361334	11.34255126
C	-9.20453957	-8.95774507	-6.27612449	O	-21.36510878	-4.85893795	10.00896553
H	-9.10361157	-7.32451900	-2.50252035	H	-20.28484433	-3.49763338	9.19505726
H	-10.36764335	-10.41445463	-2.61207417	H	-15.42076376	-10.78591273	8.86879711
C	-6.38539309	-9.71893610	-6.06652382	H	-14.52361947	-10.40653288	5.65851635
H	-5.27925303	-8.19029809	-5.21208168	H	-15.87025114	-13.28748795	6.69092589
H	-6.17303836	-11.41366499	-4.89277191				

Table S7. ECD calculation of **4** (8*R*, 24*R*).

total energy = -1401.39318623527

kinetic energy = 1395.35927528487

potential energy = -2796.75246152014

Parameters of Level DFT

DFT settings (functional B3-LYP / gridsize m3)

Geometry optimization options (Energy 10^{-6} Hartree, Gradient norm $|dE/dxyz| = 10^{-3}$ Hartree/Bohr)Energy minimized coordinates of **4** (8*R*, 24*R*) at the basis set 6-311++G** for all atoms (Å).

atom	x	y	z	atom	x	y	z
C	14.80500121	9.01970430	-0.97639265	H	13.48975722	-1.41922510	-19.47100267
C	12.09047235	9.70185616	-1.52817187	C	13.43395276	2.05560867	-15.63468271
C	10.63842574	7.34109034	-1.75841061	H	13.35957464	-1.91700508	-14.74455174
C	12.08484535	5.27434475	-1.29752308	C	11.08695197	2.71100113	-14.85768095
C	14.83743765	6.05489178	-0.64883316	H	14.57297968	3.51492406	-16.55030145
H	15.48307606	9.99321203	0.72058484	C	9.25486480	1.10667336	-13.56940690
H	16.00999920	9.63489422	-2.54706892	H	10.45296660	4.63218188	-15.25135981
C	16.54100265	4.82851749	-2.61738974	C	6.73400763	1.61043682	-13.51633994
C	15.55210711	5.33603608	2.09346911	H	9.93750504	-0.61213725	-12.66934179
C	18.85765258	3.81753200	-2.31717399	C	4.81470088	0.06689780	-12.27973934
C	20.18470970	2.52663586	-4.38360214	H	6.03850073	3.20831900	-14.62257519
H	15.72698299	4.78823223	-4.51056438	C	4.89376598	-0.91041706	-9.89406320
H	19.83102600	3.94305483	-0.50719067	H	3.12370222	-0.30728777	-13.39734024
C	19.11466893	0.78798714	-5.94657134	C	6.70839597	-0.23551130	-7.97434477
H	22.17200646	2.99400661	-4.65446113	H	3.37377225	-2.17339849	-9.31939584
C	16.63825650	-0.35820978	-5.53077377	C	6.89312024	-1.35226737	-5.65599429
H	20.23774806	0.05645551	-7.50760688	H	7.98847365	1.30992300	-8.42435551
C	15.23055639	-1.73754953	-7.16510775	C	8.58352589	-0.50036529	-3.68175456
H	15.90804532	-0.18609701	-3.61530213	H	5.78168180	-3.04197549	-5.27028647
C	15.65605444	-2.21310456	-9.88849275	C	9.37668806	1.92745090	-3.35273904
H	13.57003978	-2.70659026	-6.44995973	H	9.27623210	-1.90553459	-2.34493143
O	14.97031810	-4.25385852	-10.90494864	C	11.33974516	2.58206706	-1.51684056
N	16.73191922	-0.30804200	-11.29591956	H	8.57081854	3.44842399	-4.46458634
C	17.11814516	-0.60528628	-14.01834200	O	12.52388135	0.92128311	-0.26935664
H	16.99559349	1.40157755	-10.49422169	O	11.10460422	11.82087121	-1.82968956
C	14.63778537	-0.52974719	-15.59181569	O	8.13592887	7.47887330	-2.38059307
H	18.41832423	0.87901582	-14.65133952	H	7.66597233	9.27761478	-2.53175459
H	18.02491349	-2.43849269	-14.33591945	H	14.24338797	6.23174336	3.42539617
C	15.21681127	-1.38468719	-18.33248834	H	17.46532978	5.99194606	2.54339682
H	16.03851264	-3.28644071	-18.34059671	H	15.44578760	3.29224322	2.34344146
H	16.55959593	-0.09530112	-19.25190883				

Table S8. Deduced function of ORFs in the bombyxamycin biosynthetic gene cluster from *Streptomyces* sp. SD53.

gene	size [bp] (aa)	putative function	best match	
			organism / GenBank	identity [%] / similarity [%] (residues)
<i>bomA</i>	1566 (521)	monooxygenase	<i>Streptomyces</i> sp. ATexAB-D23 / WP_018553609.1	99 (514) / 99 (517)
<i>orf1</i>	204 (67)	unknown	<i>Streptomyces</i> sp. ATexAB-D23 / WP_078622609.1	99 (67) / 99 (67)
<i>orf2</i>	1650 (549)	long-chain-fatty-acid-CoA ligase	<i>Streptomyces</i> sp. ATexAB-D23 / WP_078622610.1	99 (542) / 99 (544)
<i>orf3</i>	843 (280)	2-amino-4,5-dihydroxy-6-one-heptanoic acid-7-phosphate synthase	<i>Streptomyces</i> sp. ATexAB-D23 / WP_018553612.1	99 (278) / 100 (280)
<i>orf4</i>	1119 (372)	3-dehydroquinate synthase II family protein	<i>Streptomyces</i> sp. ATexAB-D23 / WP_018553613.1	99 (371) / 99 (371)
<i>bomB</i>	1239 (412)	monooxygenase	<i>Streptomyces</i> sp. ATexAB-D23 / WP_026249982.1	97 (389) / 97 (390)
<i>bomR1</i>	609 (202)	LuxR family transcriptional regulator	<i>Streptomyces</i> sp. MUSC 125 / KIE27929.1	95 (191) / 96 (195)
<i>orf5</i>	1431 (476)	unknown	<i>Streptomyces</i> sp. ATexAB-D23 / WP_037710561.1	98 (452) / 98 (454)
<i>orf6</i>	2121 (706)	ATP-binding protein	<i>Streptomyces</i> sp. ATexAB-D23 / WP_051094646.1	99 (701) / 99 (704)
<i>orf7</i>	2304 (767)	unknown	<i>Streptomyces</i> sp. ATexAB-D23 / WP_018553618.1	99 (757) / 99 (761)
<i>orf8</i>	675 (224)	RES domain-containing protein	<i>Streptomyces</i> sp. ATexAB-D23 / WP_018553619.1	98 (219) / 98 (221)
<i>orf9</i>	258 (85)	unknown	<i>Capnocytophaga</i> sp. oral taxon 326 / WP_009412250.1	40 (18) / 55 (25)
<i>bomR2</i>	390 (129)	XRE family transcriptional regulator	<i>Streptomyces</i> sp. ATexAB-D23 / WP_026249984.1	100 (129) / 100 (129)

<i>orf10</i>	1194 (397)	unknown
<i>bomR3</i>	2139 (712)	SARP family transcriptional regulator
<i>bomR4</i>	2673 (890)	LuxR family transcriptional regulator
<i>orf11</i>	849 (282)	metallophosphoesterase
<i>orf12</i>	771 (256)	4'-phosphopantetheinyl transferase superfamily protein
<i>bomR5</i>	906 (301)	transcriptional regulator
<i>bomR6</i>	690 (229)	TetR family regulator for fatty acid degradation FadQ
<i>bomR7</i>	444 (147)	cold-shock protein
<i>bomC</i>	933 (310)	L-amino acid amidase
<i>bomP1</i>	11217 (3738)	PKS (KS-AT-DH-KR-ACP-KS-AT-DH-KR-ACP-TE)
<i>bomP2</i>	10734 (3577)	PKS (KS-AT-DH-KR-ACP-KS-AT-DH-KR-ACP)
<i>bomP3</i>	4872 (1623)	PKS (KS-AT-KR-ACP)
<i>bomP4</i>	10602 (3533)	PKS (KS-AT-DH-KR-ACP-KS-AT-DH-KR-ACP)
<i>bomD</i>	237 (78)	acyl carrier protein (ACP)
<i>orf13</i>	903 (300)	transposase
<i>bomE</i>	1551 (516)	long-chain-fatty-acid-CoA ligase

<i>Streptomyces</i> sp. ATexAB-D23 / WP_026249985.1	97 (384) / 97 (388)
<i>Streptomyces</i> sp. ATexAB-D23 / WP_018553622.1	97 (692) / 98 (699)
<i>Streptomyces</i> sp. ATexAB-D23 / WP_078622613.1	99 (885) / 99 (888)
<i>Streptomyces</i> sp. ATexAB-D23 / WP_018553624.1	97 (274) / 97 (276)
<i>Streptomyces</i> sp. ATexAB-D23 / WP_018553625.1	96 (247) / 97 (249)
<i>Streptomyces</i> sp. ADI92-24 / RPK43204.1	85 (182) / 89 (193)
<i>Streptomyces</i> sp. NRRL S-1824 / WP_030971278.1	87 (167) / 94 (182)
<i>Streptomyces</i> sp. ATexAB-D23 / WP_026249986.1	98 (144) / 98 (145)
<i>Streptomyces</i> sp. ATexAB-D23 / WP_018553629.1	99 (309) / 100 (310)
<i>Streptomyces</i> sp. ATexAB-D23 / WP_018555433.1	99 (77) / 98 (77)
<i>Streptomyces</i> sp. ATexAB-D23 / WP_018555432.1	99 (297) / 99 (299)
<i>Streptomyces</i> sp. ATexAB-D23 / WP_018555431.1	99 (511) / 99 (512)

<i>orf14</i>	1596 (531)	transporter
<i>bomR8</i>	762 (253)	TetR family transcriptional regulator
<i>bomF</i>	1203 (400)	FAD-dependent oxidoreductase
<i>bomP5</i>	5214 (1737)	PKS (KS-AT-DH-KR-ACP-KS-AT-DH-KR-ACP)
<i>bomP6</i>	16308 (5435)	PKS (ACP-KS-AT-DH-KR-ACP-KS-AT-DH-KR-ACP-KS-AT-DH-KR-ACP)
<i>bomG</i>	1362 (453)	methyiaspartate mutase
<i>bomH</i>	501 (166)	glutamate mutase sigma subunit 2
<i>bomI</i>	1263 (420)	diaminopimelate decarboxylase
<i>bomJ</i>	1536 (511)	long-chain-fatty-acid-CoA ligase
<i>orf15</i>	195 (64)	ferredoxin
<i>bomK</i>	1230 (409)	cytochrome P450 hydroxylase
<i>bomL</i>	864 (287)	sugar phosphate isomerase/epimerase
<i>bomM</i>	948 (315)	ACP S-malonyltransferase
<i>orf16</i>	1611 (536)	acyl-CoA carboxylase subunit beta
<i>orf17</i>	234 (77)	unknown
<i>bomR9</i>	765 (254)	Type II thioesterase

<i>Streptomyces</i> sp. ATexAB-D23 / WP_018555430.1	99 (530) / 100 (531)
<i>Streptomyces</i> sp. CEV 2-1 / ROQ82949.1	93 (234) / 96 (242)
<i>Streptomyces</i> sp. ATexAB-D23 / WP_018555428.1	98 (393) / 98 (395)
<i>Streptomyces</i> sp. ATexAB-D23 / WP_018551423.1	98 (444) / 98 (448)
<i>Streptomyces</i> sp. CEV 2-1 / WP_123461760.1	88 (146) / 89 (149)
<i>Streptomyces</i> sp. ATexAB-D23 / WP_018551425.1	99 (416) / 99 (417)
<i>Streptomyces</i> sp. ATexAB-D23 / WP_018551426.1	99 (509) / 99 (509)
<i>Streptomyces</i> sp. ATexAB-D23 / WP_018551427.1	100 (64) / 100 (64)
<i>Streptomyces</i> sp. ATexAB-D23 / WP_018551428.1	99 (408) / 100 (409)
<i>Streptomyces</i> sp. ATexAB-D23 / WP_018551429.1	99 (286) / 99 (286)
<i>Streptomyces</i> sp. ATexAB-D23 / WP_018551430.1	99 (286) / 100 (288)
<i>Streptomyces</i> sp. ATexAB-D23 / WP_018551431.1	99 (532) / 99 (533)
<i>Streptomyces</i> sp. ATexAB-D23 / WP_106435480.1	96 (54) / 100 (56)
<i>Streptomyces</i> sp. ATexAB-D23 / WP_018551433.1	98 (248) / 98 (251)

<i>orf18</i>	270 (89)	unknown	<i>Streptomyces</i> sp. ATexAB-D23 / WP_018551434.1	100 (89) / 100 (89)
<i>orf19</i>	1518 (505)	histidine kinase	<i>Streptomyces</i> sp. ATexAB-D23 / WP_018551435.1	97 (409) / 98 (495)
<i>orf20</i>	444 (147)	roadblock LC7 family protein	<i>Streptomyces</i> sp. ATexAB-D23 / WP_018551436.1	99 (146) / 100 (147)
<i>orf21</i>	363 (120)	unknown	<i>Streptomyces</i> sp. ATexAB-D23 / WP_018551437.1	99 (119) / 99 (119)
<i>orf22</i>	633 (210)	ATP-binding protein	<i>Streptomyces</i> sp. LaPpAH-199 / SDD49948.1	92 (194) / 95 (201)
<i>bomN</i>	1350 (449)	cytochrome P450 hydroxylase	<i>Streptomyces</i> sp. ATexAB-D23 / WP_018551439.1	99 (445) / 99 (447)
<i>bomO</i>	1248 (415)	cytochrome P450 hydroxylase	<i>Streptomyces</i> sp. ATexAB-D23 / WP_086023908.1	99 (394) / 99 (397)

Table S9. Bacterial strains and plasmids used in this study.

strain/vector	relevant characteristics	reference
bacterial stains		
<i>Escherichia coli</i>		
DH5α	Host for general cloning	New England Biolabs
ET12567/pUZ8002	Donor strain for intergeneric conjugation between <i>E. coli</i> and <i>Streptomyces</i>	
<i>Streptomyces</i>		
SD53	Wild type bombyxamycins-producing strain	This study
ΔbomK	Mutant of SD53 with an in-frame deletion of <i>bomK</i> , produce 2 in YPM media	This study
ΔbomN	Mutant of SD53 with an in-frame deletion of <i>bomN</i> , produce 2 in YPM media	This study
ΔbomO	Mutant of SD53 with an in-frame deletion of <i>bomO</i> , does not produce 2 in YPM media	This study
plasmid		
pGEM-Teasy	PCR fragment cloning vector	Promega
pKC1139	High-copy-number temperature-sensitive <i>E. coli-Streptomyces</i> shuttle vector	
pΔbomK	Deletion plasmid with in-frame deletion of 228-bp internal <i>bomK</i> fragment	This study
pΔbomN	Deletion plasmid with in-frame deletion of 1,083-bp internal <i>bomN</i> fragment	This study
pΔbomO	Deletion plasmid with in-frame deletion of 231-bp internal <i>bomO</i> fragment	This study

Table S10. Primers used in this study.

primer sequence	5' to 3' (restriction site underlined)	restriction enzyme
bomK-LF	AAA <u>GCTAGC</u> CCGCAGCAGTACGAGATCGGACT	NheI
bomK-LR	AAA <u>TCTAGA</u> CAGATGCTCGTCCGCATGCAGCT	XbaI
bomK-RF	AAA <u>TCTAGA</u> GTCGACGGCCTGGCCCGACAGTT	XbaI
bomK-RR	AAA <u>AAGCTT</u> CCCAACGCCGGTCTGCTCATCGA	HindIII
bomN-LF	AAA <u>GCTAGC</u> TGATGTTCTGTACCGTTCCGGCT	NheI
bomN-LR	AAA <u>TCTAGA</u> CGGCGTGCTCATGAGGACT	XbaI
bomN-RF	AAA <u>TCTAGA</u> CAGGACCCGGCCCGGCTGATCA	XbaI
bomN-RR	AAA <u>AAGCTT</u> TGATTCGGTACGCGACCTGGCGTT	HindIII
bomO-LF	AAA <u>GCTAGC</u> TCGGCAACCGCTCCACCTGGCATT	NheI
bomO-LR	AAA <u>TCTAGA</u> CTCGACCACGTCCGACCAGCTCGCCTT	XbaI
bomO-RF	AAA <u>TCTAGA</u> GCACCCCTGGCCCGCCTGGAGA	XbaI
bomO-RR	AAA <u>AAGCTT</u> GGTAACAGGCCGCAGCAGGGAACCA	HindIII

Table S11. LC/MS analysis of L- and D-FDAA derivatives of the amino acids in microphorusamide A (**10**).

amino acid	t_{RL} (min)	t_{RD} (min)	elution order	Δt (min)
5-chloro-tryptophan	36.4	38.3	L→D	1.9
valine	33.1	29.1	D→L	-4.0
leucine	37.5	33.7	D→L	-3.8
isoleucine	32.8	37.0	L→D	4.2
ornithine	12.3	11.4	D→L	-0.9
β -hydroxyaspartic acid	13.8	14.6	L→D	0.8

$$\Delta t = t_{RD} - t_{RL}$$

Table S12. Energy minimized coordinates of microphorusamide A (**10**) at the basis set def-SVP for all atoms (Å).

atom	x	y	z	atom	x	y	z	atom	x	y	z
N	-3.0148	-0.1348	0.0435	N	4.9958	-0.6705	-2.1095	C	-5.6214	1.5924	-0.0735
C	-4.3060	-0.5321	-0.5301	O	3.4296	0.4248	-0.8694	H	-6.5301	2.0077	0.3909
C	-1.8538	-0.1673	-0.6612	C	2.3086	-7.3164	-0.1275	H	-4.7626	2.1491	0.3365
C	-0.5817	0.1584	0.1272	H	2.1796	-5.8804	1.5056	H	-5.6667	1.8053	-1.1529
N	0.4847	-0.6376	-0.4431	C	3.7271	-7.7520	0.2813	C	-5.4835	-0.1664	1.7406
C	1.3931	-1.2815	0.3244	H	1.6080	-8.1074	0.1863	H	-6.3907	-0.4146	-0.1843
C	2.2873	-2.3027	-0.4057	H	2.2466	-7.2433	-1.2262	H	-6.4159	0.2046	2.1953
N	2.0747	-3.5711	0.2864	C	-2.4070	-6.6794	2.5400	H	-4.6604	0.3779	2.2381
C	2.2612	-4.7638	-0.3169	H	-2.0179	-4.5695	2.2946	H	-5.3918	-1.2376	1.9615
C	1.8009	-5.9984	0.4813	C	-2.1895	-8.0390	1.8589	H	0.4149	-0.8181	-1.4394
N	0.3446	-5.9752	0.6048	H	-2.7822	-8.1395	0.9322	H	1.7647	-3.5188	1.2561
C	-0.2656	-5.5524	1.7474	H	-2.4917	-8.8645	2.5202	H	-0.2300	-6.1079	-0.2204
C	-1.8039	-5.4975	1.7412	H	-1.1317	-8.1980	1.5987	H	-3.0962	-6.0287	0.1277
N	-2.3790	-5.3693	0.4044	C	-3.8847	-6.4115	2.8927	H	-2.9849	-1.9360	-2.0815
C	-2.3481	-4.1510	-0.2166	H	-1.8366	-6.6788	3.4844	H	-2.9424	-0.1465	1.0552
C	-3.1401	-3.9822	-1.5418	C	-4.4862	-7.3899	3.9044	O	-4.9504	-2.7752	0.2104
N	-3.6066	-2.6035	-1.6179	H	-4.4978	-6.4165	1.9727	O	-1.8043	-0.4163	-1.8647
C	-4.3521	-2.0801	-0.5989	H	-3.9636	-5.3863	3.2931	O	1.4755	-1.1621	1.5378
C	1.1521	2.3886	-1.8660	H	-4.5340	-8.4193	3.5145	O	2.7110	-4.8474	-1.4667
N	0.9811	3.0745	-3.0504	H	-5.5137	-7.0948	4.1704	O	0.3459	-5.2551	2.7626
C	-0.3243	3.4998	-3.1533	H	-3.8958	-7.4135	4.8360	O	-1.6693	-3.2326	0.2164
C	-1.0045	3.0538	-1.9811	C	-4.2384	-5.0275	-1.8057	H	5.2692	0.1662	-2.6096
C	-0.0398	2.3454	-1.1719	H	-2.3716	-4.0800	-2.3273	H	5.4660	-1.5576	-2.2513
C	-0.9725	4.2324	-4.1558	C	-5.0243	-4.8407	-3.1181	H	3.9984	-3.6322	-1.3684
C	-2.3231	4.5255	-3.9871	H	-4.9457	-5.0104	-0.9619	C	-0.2640	1.6844	0.1583
C	-3.0013	4.0904	-2.8291	H	-3.7658	-6.0276	-1.8319	H	-0.6942	-0.1723	1.1715
C	-2.3688	3.3655	-1.8257	C	-6.1546	-5.8750	-3.2037	C	4.8614	-6.7737	-0.0468
H	-0.4412	4.5686	-5.0503	H	-6.7691	-5.7203	-4.1052	H	3.9400	-8.7170	-0.2124
H	-2.8676	5.0917	-4.7445	H	-6.8217	-5.8156	-2.3284	H	3.7443	-7.9587	1.3681
H	-2.9282	3.0458	-0.9458	H	-5.7533	-6.9030	-3.2491	N	4.7837	-5.5760	0.7855
Cl	-4.7097	4.4845	-2.6630	C	-4.1295	-4.9006	-4.3631	H	5.8296	-7.3118	0.0401
H	1.7102	3.2552	-3.7266	H	-5.4845	-3.8379	-3.0810	H	4.7719	-6.4636	-1.1003
C	3.7910	-1.9212	-0.4144	H	-4.7290	-4.7972	-5.2819	H	5.2506	-4.7748	0.3615
H	1.9634	-2.4312	-1.4515	H	-3.5946	-5.8652	-4.4247	H	5.1880	-5.7313	1.7083
C	4.0429	-0.5953	-1.1560	H	-3.3772	-4.0956	-4.3782	H	2.1157	1.9580	-1.5930
O	4.5882	-2.9574	-0.9586	C	-5.4997	0.0926	0.2252	H	0.6346	1.7876	0.7857
H	4.0884	-1.7453	0.6362	H	-4.3079	-0.1557	-1.5650	H	-1.0840	2.1888	0.6970

Table S13. Energy minimized coordinates of microphorusamide B (**11**) at the basis set def-SVP for all atoms (Å).

atom	x	y	z	atom	x	y	z	atom	x	y	z
N	-3.1729	-0.1331	-0.2161	O	4.1260	0.4093	0.4708	H	-6.2376	2.4871	-1.0882
C	-4.4007	-0.4893	-0.9327	C	1.7099	-6.1639	-1.8386	H	-4.4891	2.3628	-0.8159
C	-1.9276	-0.4708	-0.6459	H	2.3007	-5.8692	0.2455	H	-5.1913	1.7724	-2.3389
C	-0.7904	-0.0363	0.2771	C	3.1213	-6.5392	-2.3185	C	-5.8472	0.6122	0.9032
N	0.3337	-0.9276	0.0896	H	1.1243	-7.0950	-1.7567	H	-6.4566	0.0024	-1.0562
C	1.2946	-1.0391	1.0375	H	1.2202	-5.5329	-2.6000	H	-6.7550	1.2166	1.0596
C	2.5079	-1.9088	0.6435	C	-1.7677	-6.9449	2.6158	H	-5.0300	1.1445	1.4232
N	2.1713	-3.3191	0.5740	H	-1.6438	-4.7916	2.4531	H	-5.9966	-0.3675	1.3751
C	1.8893	-3.9251	-0.6085	C	-1.6364	-8.2219	1.7715	H	0.4363	-1.3683	-0.8242
C	1.6045	-5.4418	-0.4899	H	-2.4617	-8.3286	1.0434	H	2.1031	-3.8752	1.4260
N	0.2568	-5.6089	0.0607	H	-1.6629	-9.1202	2.4059	H	-0.5296	-5.5687	-0.5777
C	-0.0133	-5.5687	1.3884	H	-0.6878	-8.2442	1.2122	H	-2.8254	-6.3142	0.2440
C	-1.5003	-5.6607	1.7937	C	-3.1127	-6.8492	3.3619	H	-3.1290	-2.3694	-1.8342
N	-2.4130	-5.4934	0.6714	H	-0.9615	-6.9547	3.3695	H	-3.2741	0.1172	0.7613
C	-2.8327	-4.2480	0.2721	C	-3.3691	-7.9740	4.3681	O	-5.6335	-2.3552	0.0598
C	-3.7018	-4.2116	-1.0137	H	-3.9396	-6.8140	2.6287	O	-1.7123	-1.0394	-1.7133
N	-3.9320	-2.8313	-1.3964	H	-3.1432	-5.8808	3.8905	O	1.2279	-0.4826	2.1287
C	-4.7395	-1.9852	-0.6846	H	-3.4608	-8.9584	3.8816	O	1.7911	-3.3188	-1.6686
C	1.6457	1.7166	-1.4638	H	-4.3047	-7.7968	4.9221	O	0.8568	-5.4753	2.2489
N	1.9122	2.0514	-2.7746	H	-2.5536	-8.0431	5.1081	O	-2.4702	-3.2348	0.8418
C	0.7361	2.3568	-3.4214	C	-4.9711	-5.0858	-0.9151	H	5.0231	1.2465	2.6359
C	-0.3172	2.1992	-2.4722	H	-3.0622	-4.6370	-1.8073	H	4.5922	-0.1701	3.5445
C	0.2867	1.7863	-1.2268	C	-5.9105	-5.0254	-2.1334	C	-0.3980	1.4661	0.0698
C	0.4919	2.7590	-4.7409	H	-5.5336	-4.7925	-0.0184	H	-1.1207	-0.1336	1.3239
C	-0.8240	3.0128	-5.1181	H	-4.6572	-6.1390	-0.7815	C	4.1093	-5.3859	-2.5258
C	-1.8700	2.8575	-4.1839	C	-7.1442	-5.9022	-1.8815	H	3.0120	-7.0771	-3.2765
C	-1.6419	2.4578	-2.8728	H	-7.8627	-5.8249	-2.7137	H	3.5683	-7.2686	-1.6159
H	1.3054	2.8692	-5.4629	H	-7.6678	-5.6046	-0.9584	N	4.5933	-4.8660	-1.2456
H	-1.0584	3.3347	-6.1341	H	-6.8668	-6.9670	-1.7823	H	4.9255	-5.7388	-3.1921
H	-2.4772	2.3441	-2.1812	C	-5.2160	-5.4106	-3.4456	H	3.6001	-4.5629	-3.0517
Cl	-3.5193	3.1790	-4.7141	H	-6.2563	-3.9818	-2.2229	H	5.0956	-3.9887	-1.3814
H	2.8333	2.0599	-3.1912	H	-5.9279	-5.3909	-4.2869	H	5.2572	-5.5180	-0.8248
C	3.6588	-1.6616	1.6150	H	-4.7974	-6.4322	-3.3941	H	2.4593	1.4470	-0.7889
H	2.8145	-1.6059	-0.3673	H	-4.3984	-4.7174	-3.6986	H	0.2661	1.7119	0.9117
C	4.1697	-0.2255	1.5150	C	-5.5664	0.4696	-0.6016	H	-1.3068	2.0792	0.1907
H	3.3440	-1.8848	2.6464	H	-4.1631	-0.3900	-2.0042	H	4.4872	-2.3436	1.3590
N	4.7359	0.2737	2.6468	C	-5.3586	1.8434	-1.2526				

Table S14. LC/MS analysis of L- and D-FDAA derivatives of the amino acids in coprisamide C (**14**).

amino acids	t_{RL} (min)	t_{RD} (min)	elution order	Δt_R (min)
β -methyl-aspartic acid	20.96	22.47	L→D	-1.51
2,3-diaminopropionic acid (<i>di</i>)	33.94	34.72	L→D	-0.78
valine	29.21	33.13	L→D	-3.92
leucine	38.01	33.57	D→L	4.44
serine	18.35	17.69	D→L	0.66
alanine	25.96	22.87	D→L	3.09

$$\Delta t = t_{RD} - t_{RL}$$

Table S15. Deduced putative functions of ORFs in the coprisamides biosynthetic gene cluster (*cpr* cluster) from *Micromonospora* sp. UTJ3.

gene	size [bp] (aa)	putative function	best match		
			organism	GenBank	identity [%] / similarity [%] (residue)
orf1	6075 (2024)	glucose/arabinose dehydrogenase, beta-propeller fold	<i>Micromonospora pattaloongensis</i>	SDY94410.1	80 (1523) / 88 (1678)
orf2	708 (235)	hypothetical protein SAMN05444365_104252	<i>Micromonospora pattaloongensis</i>	SDY94386.1	68 (162) / 73 (175)
orf3	501 (166)	hypothetical protein Pflav_002560	<i>Phytohabitans flavus</i>	BCB73846.1	55 (94) / 66 (115)
orf4	549 (182)	hypothetical protein	<i>Micromonospora</i> sp. CB01531	WP_073836516.1	89 (161) / 93 (169)
cprR1	783 (260)	AfsR/SARP family transcriptional regulator	<i>Micromonospora viridifaciens</i>	WP_089006817.1	95 (246) / 96 (252)
cprR2	681 (226)	response regulator transcription factor	<i>Micromonospora viridifaciens</i>	WP_089006818.1	92 (209) / 95 (216)
cprR3	1086 (361)	histidine kinase-, DNA gyrase B-, and HSP90-like ATPase	<i>Micromonospora viridifaciens</i>	SCF03543.1	86 (291) / 92 (311)
orf5	570 (189)	DUF3995 domain-containing protein	<i>Micromonospora viridifaciens</i>	WP_089006820.1	88 (166) / 92 (175)
cprA	1209 (402)	beta-ketoacyl-[acyl-carrier-protein] synthase family protein	<i>Micromonospora viridifaciens</i>	WP_089006821.1	94 (379) / 96 (387)
cprB	1122 (373)	hypothetical protein	<i>Micromonospora narathiwatensis</i>	WP_091192145.1	89 (333) / 92 (346)
cprC	1128 (375)	beta-ketoacyl synthase	<i>Micromonospora viridifaciens</i>	WP_089009981.1	93 (340) / 95 (350)
cprD	924 (307)	beta-ketoacyl synthase, N-terminal domain	<i>Micromonospora narathiwatensis</i>	SBT41149.1	88 (269) / 89 (276)
orf6	816 (271)	alpha/beta hydrolase	<i>Micromonospora narathiwatensis</i>	WP_091192147.1	84 (230) / 88 (242)
orf7	903 (300)	hypothetical protein	<i>Micromonospora</i> sp. CB01531	WP_073836475.1	93 (279) / 96 (289)
cprE	720 (239)	2-hydroxychromene-2-carboxylate isomerase	<i>Micromonospora viridifaciens</i>	SCF03634.1	91 (218) / 94 (227)
orf8	945 (314)	beta-ketoacyl-ACP synthase III	<i>Micromonospora narathiwatensis</i>	WP_091192150.1	98 (308) / 99 (313)
cprF	990 (329)	cysteine synthase A	<i>Micromonospora narathiwatensis</i>	SBT41168.1	95 (312) / 96 (319)
cprG	1023 (340)	2,3-diaminopropionate biosynthesis protein SbnB	<i>Micromonospora viridifaciens</i>	WP_089006827.1	92 (313) / 95 (326)
orf9	963 (320)	ATP-binding cassette domain-containing protein	<i>Micromonospora narathiwatensis</i>	WP_091192153.1	94 (302) / 97 (312)
orf10	789 (262)	ABC transporter permease	<i>Micromonospora tulbaghiae</i>	WP_091416752.1	90 (236) / 93 (246)
cprH	9213 (3070)	NRPS (C-A-PCP-E-C-A-PCP-E)			
cprI	14979 (4992)	NRPS (C-A-PCP-E-C-A-PCP-C-A-PCP-C-A-PCP-TE)			
orf11	234 (77)	MbtH family protein	<i>Micromonospora</i> sp. CB01531	WP_073836465.1	96 (74) / 96 (74)
cprJ	738 (245)	3-oxoacyl-[acyl-carrier-protein] reductase	<i>Micromonospora narathiwatensis</i>	WP_091192162.1	96 (235) / 99 (243)
cprK	414 (137)	3-hydroxyacyl-ACP dehydratase	<i>Micromonospora viridifaciens</i>	WP_089006835.1	88 (121) / 92 (127)
cprL	483 (160)	beta-hydroxyacyl-ACP dehydratase	<i>Micromonospora viridifaciens</i>	WP_089006836.1	96 (154) / 98 (158)
cprM	258 (85)	acyl carrier protein	<i>Micromonospora narathiwatensis</i>	SBT41212.1	99 (84) / 100 (85)
orf12	870 (289)	alpha/beta fold hydrolase	<i>Micromonospora</i> sp. MP36	WP_148802794.1	82 (237) / 86 (249)
orf13	624 (207)	2-hydroxychromene-2-carboxylate isomerase	<i>Micromonospora viridifaciens</i>	SCF03829.1	92 (191) / 95 (198)
cprN	444 (147)	hypothetical protein	<i>Micromonospora</i> sp. CB01531	WP_073836459.1	92 (131) / 92 (132)
cprO	1317 (438)	methylaspartate mutase	<i>Micromonospora narathiwatensis</i>	WP_091192171.1	90 (392) / 93 (406)
orf14	549 (182)	GNAT family N-acetyltransferase	<i>Micromonospora</i> sp. CB01531	WP_073836455.1	79 (143) / 80 (146)
orf15	732 (243)	hypothetical protein	<i>Micromonospora</i> sp. CB01531	WP_073836454.1	61 (149) / 71 (176)
orf16	732 (243)	hypothetical protein	<i>Micromonospora</i> sp. CB01531	WP_073836453.1	69 (174) / 78 (198)

cprR4	975 (324)	LuxR family transcriptional regulator
orf17	657 (218)	hypothetical protein D9V44_09755
orf18	1176 (391)	FtsX-like permease family protein
orf19	675 (224)	ABC transporter ATP-binding protein
orf20	867 (288)	hypothetical protein
orf21	492 (163)	hypothetical protein
orf22	411 (136)	hypothetical protein
orf23	726 (241)	hypothetical protein
orf24	300 (99)	hypothetical protein
orf25	198 (65)	hypothetical protein DSY84_08510, partial
cprR5	1227 (408)	PucR family transcriptional regulator
orf26	1083 (360)	ferredoxin reductase
orf27	1143 (380)	acyl-CoA desaturase
orf28	1125 (374)	glycosyltransferase
orf29	1065 (354)	glycosyltransferase family 2 protein
orf30	1368 (455)	glycosyltransferase involved in cell wall biosynthesis
orf31	1599 (532)	glycosyltransferase
orf32	1839 (612)	CocE/NonD family hydrolase
orf33	402 (133)	hypothetical protein
cprR6	747 (248)	GntR family transcriptional regulator
orf34	237 (78)	hypothetical protein
orf35	180 (59)	hypothetical protein
orf36	426 (141)	hypothetical protein
orf37	459 (152)	hypothetical protein
cprR7	552 (183)	MarR family transcriptional regulator
orf38	576 (191)	NADPH-dependent F420 reductase
orf39	906 (301)	dioxygenase
orf40	309 (102)	hypothetical protein
orf41	309 (102)	hypothetical protein
orf42	1089 (362)	hypothetical protein
orf43	501 (166)	GNAT family N-acetyltransferase
orf44	2529 (842)	FtsX-like permease family protein
orf45	786 (261)	ABC transporter ATP-binding protein
orf46	132 (43)	hypothetical protein GA0070214_103168
orf47	306 (101)	cation transporter
orf48	813 (270)	MBL fold metallo-hydrolase
cprR8	1137 (378)	helix-turn-helix transcriptional regulator
orf49	483 (160)	polyketide cyclase
orf50	600 (199)	TIGR03086 family protein

<i>Streptomyces</i> sp. SID1034	MYV90803.1	59 (193) / 73 (238)
<i>Actinobacteria</i> bacterium	TDB36787.1	37 (67) / 48 (89)
<i>Streptomyces</i> sp. SID13031	WP_164600285.1	44 (170) / 61 (240)
<i>Actinoplanes xinjiangensis</i>	WP_109592884.1	57 (127) / 70 (156)
<i>Streptomyces</i> sp. SID13031	WP_164600287.1	50 (137) / 63 (176)
<i>Streptomyces</i> sp. SID13031	WP_164600288.1	46 (70) / 61 (93)
<i>Streptomyces</i> sp. SID13031	WP_164600289.1	50 (55) / 69 (77)
<i>Streptomyces</i> sp. TRM68348	WP_149827260.1	42 (97) / 55 (127)
<i>Amycolatopsis xylanica</i>	WP_091298931.1	38 (28) / 56 (42)
<i>Candidatus Marinimicrobia</i> bacterium	RTZ98766.1	42 (19) / 55 (25)
<i>Micromonospora</i> sp. MP36	WP_148802766.1	92 (375) / 94 (385)
<i>Micromonospora viridifaciens</i>	WP_089006841.1	92 (332) / 95 (343)
<i>Micromonospora</i> sp. CB01531	WP_073837639.1	95 (357) / 98 (371)
<i>Micromonospora</i> sp. MP36	WP_148802757.1	88 (321) / 91 (333)
<i>Micromonospora narathiwatensis</i>	WP_091192182.1	88 (313) / 93 (330)
<i>Micromonospora narathiwatensis</i>	SBT41262.1	86 (387) / 91 (408)
<i>Micromonospora</i> sp. CB01531	WP_073837636.1	89 (469) / 94 (500)
<i>Micromonospora</i> sp. CB01531	WP_073837634.1	83 (505) / 90 (547)
<i>Kribbella</i> sp. VKM Ac-2575	WP_133980112.1	65 (74) / 78 (90)
<i>Micromonospora</i> sp. RV43	WP_047891300.1	85 (211) / 92 (230)
<i>Micromonospora purpureochromogenes</i>	WP_088962506.1	66 (50) / 81 (62)
<i>Micromonospora</i> sp. MP36	WP_148798040.1	90 (53) / 93 (55)
<i>Micromonospora</i> sp. MW-13	WP_128763569.1	86 (83) / 91 (89)
<i>Micromonospora</i> sp. NEAU-HG-1	WP_161689758.1	88 (129) / 91 (135)
<i>Micromonospora viridifaciens</i>	WP_089006856.1	93 (155) / 95 (160)
<i>Micromonospora viridifaciens</i>	WP_089006857.1	91 (174) / 95 (183)
<i>Micromonospora viridifaciens</i>	WP_089006858.1	94 (283) / 95 (288)
<i>Micromonospora narathiwatensis</i>	WP_157739868.1	77 (79) / 89 (91)
<i>Micromonospora kangleipakensis</i>	WP_130337791.1	68 (65) / 81 (78)
<i>Micromonospora</i> sp. MP36	WP_148800373.1	89 (324) / 92 (336)
<i>Micromonospora viridifaciens</i>	WP_089006862.1	85 (141) / 89 (149)
<i>Micromonospora</i> sp. MP36	WP_148798029.1	90 (762) / 95 (800)
<i>Micromonospora viridifaciens</i>	WP_089006864.1	94 (245) / 96 (253)
<i>Micromonospora chaitiyaphumensis</i>	SCE90600.1	83 (33) / 92 (37)
<i>Micromonospora</i> sp. AP08	WP_148425917.1	78 (68) / 82 (72)
<i>Kribbella</i> sp. VKM Ac-2571	WP_133782969.1	77 (204) / 89 (237)
<i>Nocardia yamanashiensis</i>	WP_067716089.1	68 (249) / 81 (298)
<i>Micromonospora terminaliae</i>	WP_154226311.1	89 (143) / 94 (151)
<i>Micromonospora</i> sp. CB01531	WP_073835090.1	88 (166) / 93 (175)

cprR9	3120 (1039)	predicted ATPase	<i>Micromonospora rhizosphaerae</i>	SCL27761.1	85 (883) / 88 (916)
orf51	1092 (363)	putative flavoprotein involved in K ⁺ transport	<i>Micromonospora viridifaciens</i>	SCF04413.1	90 (313) / 92 (321)
orf52	198 (65)	heavy-metal-associated domain-containing protein	<i>Micromonospora rhizosphaerae</i>	WP_091342501.1	82 (53) / 87 (57)
orf53	3255 (1084)	copper-translocating P-type ATPase	<i>Micromonospora viridifaciens</i>	WP_089009989.1	90 (977) / 93 (1016)
orf54	714 (237)	spermidine synthase	<i>Micromonospora narathiwatensis</i>	WP_091192205.1	96 (228) / 97 (232)
orf55	1014 (337)	zinc-binding dehydrogenase	<i>Micromonospora eburnea</i>	WP_091117958.1	95 (321) / 97 (330)
orf56	609 (202)	class I SAM-dependent methyltransferase	<i>Micromonospora viridifaciens</i>	WP_089006869.1	90 (180) / 93 (187)
orf57	672 (223)	methyltransferase domain-containing protein	<i>Micromonospora narathiwatensis</i>	WP_091192212.1	93 (186) / 96 (193)
orf58	1314 (437)	PLP-dependent aminotransferase family protein	<i>Micromonospora narathiwatensis</i>	WP_091192216.1	89 (389) / 92 (404)
orf59	1299 (432)	MFS transporter	<i>Micromonospora narathiwatensis</i>	WP_091192218.1	89 (383) / 90 (391)
orf60	393 (130)	DUF2267 domain-containing protein	<i>Micromonospora</i> sp. AMSO31t	WP_151462435.1	87 (109) / 93 (118)
cprP	359 (1152)	AMP-binding protein	<i>Micromonospora viridifaciens</i>	WP_089006881.1	89 (1037) / 92 (1075)
orf61	3138 (1045)	alpha/beta fold hydrolase	<i>Micromonospora</i> sp. MP36	WP_148797997.1	83 (864) / 87 (914)

Abstract in Korean

나비목, 딱정벌레목 곤충으로부터 분리된

장내미생물이 생산하는 생리활성 이차대사물질의 발견

신연혁

서울대학교 약학대학 대학원

천연물과학전공

미생물 유래 천연물의 연구는 지난 수 십 년간 신약 개발 과정에 있어 지속적으로 중요한 역할을 수행하여 왔다. 2012 년 발표된 통계 자료에 따르면, 현재까지 발견된 70,000 여종의 미생물 유래 신규 천연 화합물 중 450-500 종의 물질이 신약으로 개발되었으며, 이는 합성 화합물의 신약 개발 비율보다 높은 신약개발 비율을 보여준다. 특히 박테리아로부터 유래된 천연물의 경우 약 5.7%가 생리활성적으로 뛰어나다고 판단되는데, 이는 곰팡이 (1.5%)나 동물 (1.6%), 식물 (0.9%)로부터 유래된 천연물에 비하여 3 배 이상 높은 결과이다. 뿐만 아니라 2015 년, William C. Campbell 과 Satoshi Omura 가 토양 방선균 *Streptomyces avermitilis*로부터 avermectin 을 발견함으로써 노벨상 생리의학상 부문을 수상하였고, 이는 신약 개발에 있어 박테리아 유래 천연물의 연구가 현재까지도 나타내고 있는 중요성을 시사하였다.

곤충은 지구상에서 가장 큰 종 다양성을 보유하고 있는 동물군으로, 그만큼 다양한 서식 환경을 장내 미생물 혹은 공생 미생물에게 제공한다. 이러한 서식 환경의 다양성은 장내미생물의 종 다양성으로 연결되며, 결과적으로 미생물 유래 천연물의 다양성으로 연결된다. 이와 같은 이유로, 곤충 미생물이 생산하는 생리활성 이차대사물질의 연구를 진행하였고, 나비목에 속하는 누에와 딱정벌레목에 속하는 김정송장벌레, 넓정송장벌레의 장내 미생물을 분리, 해당 미생물들이 생산하는 신규 이차대사물질의 구조 규명 연구를 진행하였다.

1. 누에에서 분리된 *Streptomyces* sp. 균주가 생산하는 세포독성 활성의 거대환락탐 계열 물질 연구

곤충 공생 미생물은 지난 10 년간 중요한 천연물 발굴원으로 인식되어 왔다. 곤충 중 가장 큰 목을 차지하고 있는 딱정벌레 (Coleoptera)로부터 다양한 종류의 신규 천연물이 발굴되어 왔다. 하지만 딱정벌레와 마찬가지로 곤충의 종 다양성 중 큰 부분을 차지하고 있는 나비목 (Lepidoptera) 곤충 유래 미생물의 경우 거의 연구가 진행되지 않았다. 이러한 관점에 착안하여 나비목에 속하는 누에 (*Bombyx mori*)의 장내미생물의 연구를 진행하였다. 누에나방은 나비목에 속하는 곤충으로, 산업적으로도 중요한 역할을 수행하는 곤충이다. 4-5 령 누에의 장으로부터 분리된 방선균 균주인 *Streptomyces* sp. SD53 균주로부터 신규 물질인 bombyxamycins A-C 와 기지 물질인 piceamycin 을 분리하였다. 분리된 미생물의 배양과 추출, LC/MS 분석을 이용한 화학적 프로파일링을 통하여 해당 균주가 생산하는 이차대사물질의 존재를 확인할 수 있었고, 분광학적 분석 방법을 통하여

해당 4 종 물질의 평면구조가 26 개 원소로 이루어진 고리구조를 포함하는 거대한락탐 물질이라는 것을 밝힐 수 있었다 (Figure 1). 언급된 4 종 물질의 절대 입체구조는 다단계 화학 반응 (Figure 2)과 분광학적 분석 방법, 크로마토그래프 법, 그리고 ECD (electronic circular dichroism) 계산을 통하여 확인할 수 있었다. 뿐만 아니라 기존의 복잡하고 시간 소모가 큰 3-amino-2-methylpropanoic acid 으로부터 유래된 절대 입체구조의 규명 과정을 단순화한 방법을 제시하여, piceamycin 의 절대 입체구조 규명 과정에 적용하였다. 또한 해당 방선균 균주의 전체 유전자 염기서열 분석을 진행하여 bombyxamycins와 piceamycin 의 생합성 유전자군 (biosynthetic gene cluster)을 확인할 수 있었고, 시작 모핵 (3-amino-2-methylpropanoic acid)의 생합성 과정, bombyxamycins A 와 C 로부터 각각 bombyxamycin B 와 piceamycin 이 생합성 되는 post-PKS modification 과정을 확인하였다 (Figure 3). 대표 물질인 bombyxamycin A 와 piceamycin 의 경우 인간 병원성을 나타내는 특정 그람 양성균인 *Streptococcus aureus* 와 그람 음성균인 *Proteus hauseri* 와 *Salmonella enterica* 에 대하여 훌륭한 항박테리아 활성을 나타냈다. 특히 piceamycin 의 경우 그람 양성균에 속하는 병원성 균주 *Enterococcus faecalis* 와 *Enterococcus faecium*, 그리고 누에의 병원성 균주인 *Bacillus thuringiensis* 의 성장을 억제하는 활성이 추가적으로 확인되었다. 이와 더불어 bombyxamycins A 와 C, piceamycin 의 경우 대부분의 인간 암세포주에 대하여 항암활성을 나타내었다.

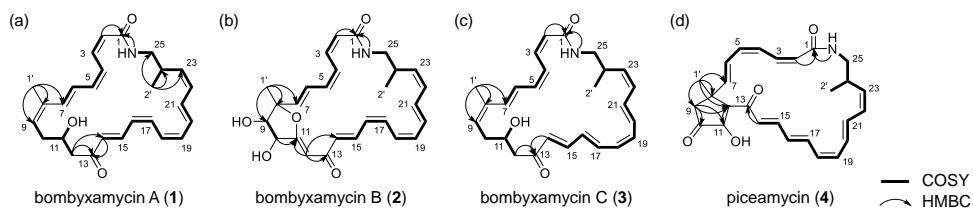


Figure 1. Key COSY and HMBC correlations for constructing the planar structures of (a) bombyxamycins A, (b) bombyxamycin B, (c) bombyxamycin C, and (d) piceamycin.

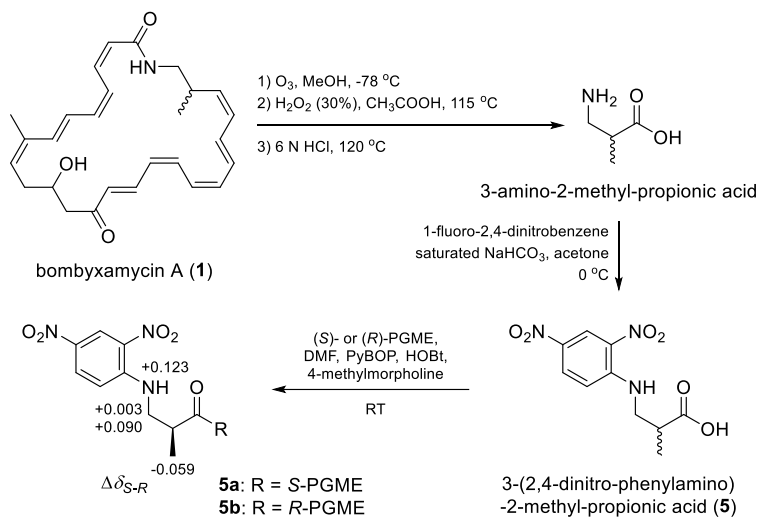


Figure 2. Chemical reactions for the identification of the absolute configuration at C-24 of bombyxamycin A.

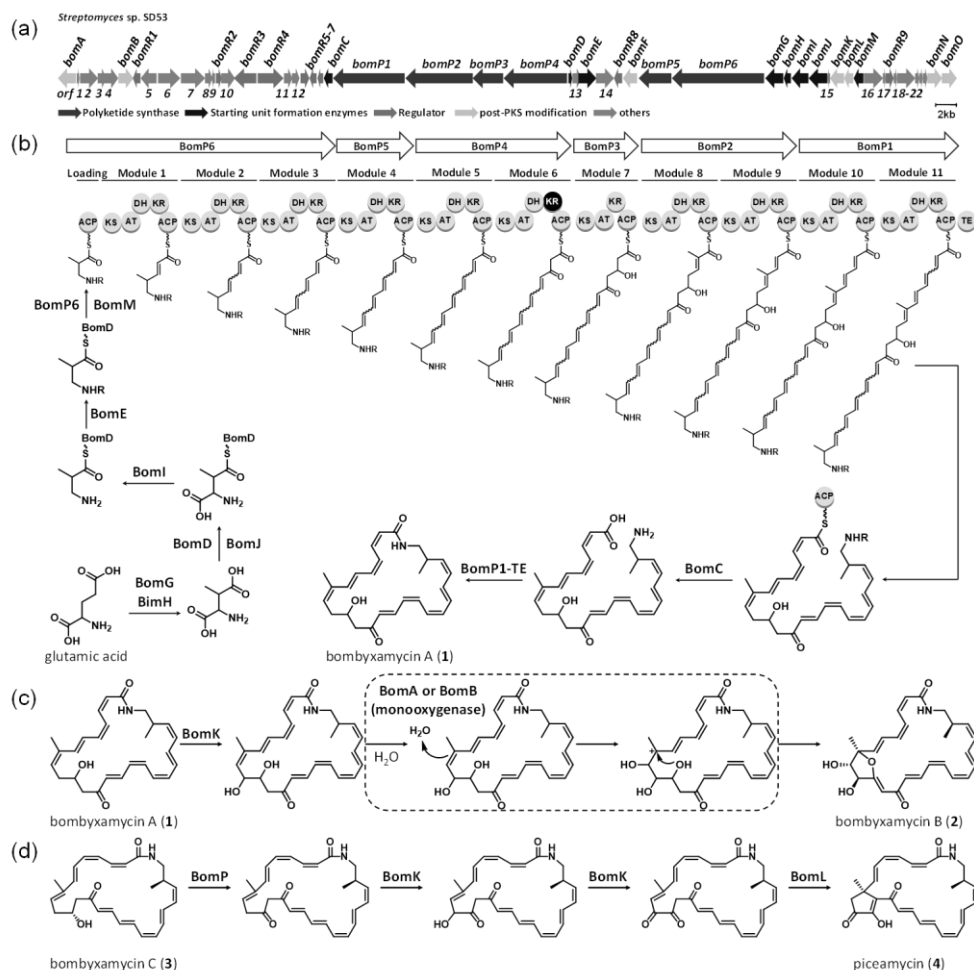


Figure 3. (a) Biosynthetic gene cluster for bombyxamycins A–C and piceamycin. (b) Schematic representation of predicted biosynthetic procedure for bombyxamycin A. Domains within each module are represented by circles. The black circle indicates a domain that is predicted from the final structure and deletions in the active sites to not be active. KS, ketoacyl synthase; AT, acyl transferase; DH, dehydratase; KR, keto reductase; ACP, acyl carrier protein; TE, thioesterase. (c) The proposed biosynthetic pathway for producing bombyxamycin B from bombyxamycin A. (d) Predicted post-PKS modification pathway for piceamycin from bombyxamycin C.

2. 검정송장벌레에서 분리된 *Microbacterium* sp. 균주가 생산하는 항박테리아 활성의 염소계 고리형 펩타이드 계열 물질 연구

송장벌레는 딱정벌레목 (Coleoptera)에 속하는 곤충으로, 죽은 짐승의 시체를 먹이 및 서식지로 삼고 그곳에 알을 낳아 번식한다. 이러한 그들의 생태학적 특성으로 인하여, 송장벌레들은 필연적으로 병원성 세균들에 노출되는 경우가 많아진다. 이처럼 그들의 생태학적 특징과 더불어, 해당 곤충이 장내미생물 혹은 공생미생물을 활용하여 외부의 병원성 미생물로부터 자신들을 보호할 것이라는 가설에서 착안하여 연구를 진행하였다. 경기도 과천시 서울대공원 부근 매봉산에서 채집된 검정송장벌레 (*Nicrophorus concolor*) 개체로부터 장내미생물의 분리를 진행하였고, 이 과정 중 분리된 희소 방선균 *Microbacterium* sp. UTG9 균주의 배양 과정에서 신규 화합물 nicrophorusamides A 와 B 를 발견 및 연구하였다. 해당 균주의 소규모 배양 및 추출, 추출물의 LC/MS 분석 과정에서 해당 균주가 생산하는 이차대사물질의 존재를 확인할 수 있었다. 해당 물질들의 자외선 스펙트럼분석을 통하여 indole 모핵을 포함하는 구조임을 확인할 수 있었다. 또한 질량 스펙트럼의 분석 과정에서 동위원소 패턴이 관찰되었음을 통하여, 해당 물질들이 하나의 염소원자 (Cl)를 포함하고 있다는 사실을 추가적으로 확인하였다. 해당 2 종 신규물질의 ^1H 와 ^{13}C NMR 및 COSY, HSQC, HMBC, ROESY, TOCSY NMR 등 2 차원 NMR 스펙트럼 자료를 기반으로 고리형 펩타이드 구조의 물질이라는 것을 확인할 수 있었다 (Figure 4). 대표 물질인 nicrophorusamide A 의 절대 입체구조를 규명하기 위하여 산성 가수분해 반응과 화학반응을 통한 유도체화 반응, 그리고 해당 반응 물질들의 크로마토그래피 분석이 진행되었고, 이를 바탕으로 각 아미노산 모핵에

존재하는 절대 입체구조를 모두 규명할 수 있었다. Nicrophorusamide B 의 경우 nicrophorusamide A 물질과의 CD 스펙트럼 비교와 생합성적으로 유사성을 바탕으로 동일한 절대 입체구조를 가질 것이라고 추론되었다. Nicrophorusamide A 물질은 인간 병원성 그람 양성균인 *Streptococcus aureus*, *Enterococcus faecalis*, *Enterococcus faecium* 에 대하여 항박테리아 활성을 나타내었고, 그람 음성균에 해당하는 *Salmonella enterica* 균주에 대한 성장억제활성 또한 확인되었다 (Table 1). 또한 분자 구조 모델링을 통하여 nicrophorusamide A 가 수소결합을 통한 추가적인 고리구조를 갖는다는 것을 확인하였고, 이 고리 구조가 항박테리아 활성에 있어 중요한 역할을 수행할 것이라고 추론할 수 있었다 (Figure 5).

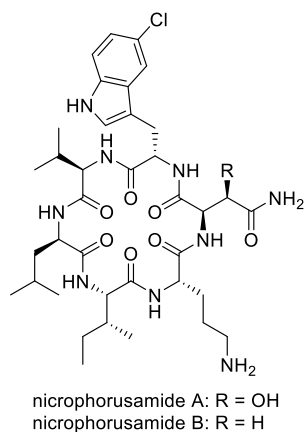


Figure 4. Chemical structures of nicrophorusamides A and B.

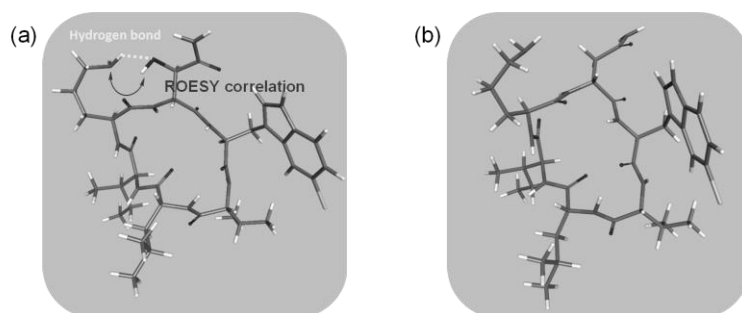


Figure 5. Energy minimized conformations of nicrophorusamides A and B: (a) nicrophorusamide A, (b) nicrophorusamide B.

Table 1. Inhibitory activities of nicrophorusamides A and B against bacterial strains.

	MICs ($\mu\text{g/mL}$)				
	Gram-positive			Gram-negative	
	<i>S. aureus</i>	<i>E. faecalis</i>	<i>E. faecium</i>	<i>S. enterica</i>	<i>E. coli</i>
nicrophorusamide A	8	16	16	16	>128
nicrophorusamide B	64	128	128	>128	>128
ampicillin	0.13	0.5	0.25	0.13	8

3. 넓적송장벌레에서 분리된 *Micromonospora* sp. 균주가 생산하는 cinnamic acid 포함

고리형 펩타이드 계열 물질 연구

넓적송장벌레는 딱정벌레목 (Coleoptera; Silphidae; Silphinae)에 속하는 곤충으로써, 기존에 연구된 검정송장벌레 (Nicrophorinae)와는 다른 아과 (subfamily)에 속하는 곤충이다. 해당 곤충 역시 부패한 동물의 시체를 탐지하여 그것을 먹이로 삼아 서식하는 곤충으로 알려져 있다. 이들 역시 그들의 서식 습성에 따라 필연적으로 다양한 병원성 미생물에 노출될 가능성이 크고, 그만큼 공생미생물을 활용한 방어체계를 구성할 가능성이 크다고 판단하여 연구를

진행하였다. 서울특별시 관악구 관악산에서 채집된 넓적송장벌레의 장으로부터 희소 방선균 *Micromonospora* sp. UTJ3 균주를 분리하였고, 해당 균주가 생산하는 신규 펩타이드 계열 물질인 coprisamides C와 D를 발견하였다. 해당 물질들의 구조는 UV, MS 자료와 더불어 ^1H , ^{13}C , COSY, HSQC, HMBC, ROESY, TOCSY NMR 등 분광학적 자료의 종합적인 분석을 통하여 규명되었고, 변형된 아미노산 유닛을 다수 포함하는 펩시펩타이드 계열의 물질 구조임을 확인하였다 (Figure 6). 해당 물질들의 절대 입체구조는 advance Marfey's method 의 적용과 PGME 를 이용한 화학반응, 그리고 생성된 반응물의 NMR 스펙트럼 분석을 통하여 확인할 수 있었다. Coprisamide C의 경우 병원성 결핵 세균인 *Mycobacterium tuberculosis* mc² 6230 균주에 대하여 성장 억제 활성을 나타내었다 (Figure 7). 또한, 해당 균주의 총 유전체 분석을 통하여 해당 물질들의 생산에 관여하는 생합성 유전자군과 생합성 경로를 확인할 수 있었고, 추가적으로 해당 물질들에 포함되어 있는 cinnamic acid 모핵과 특이 아미노산 (β -methyl aspartic acid, 2,3-diaminopropionic acid)의 생합성 과정을 확인할 수 있었다 (Figure 8).

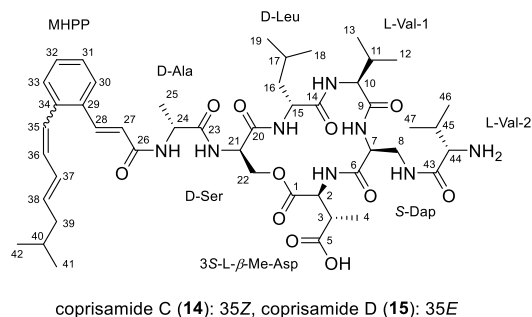


Figure 6. Chemical structures of coprisamides C and D.

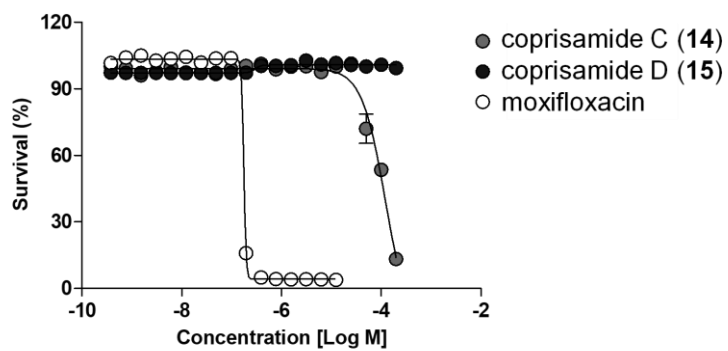


Figure 7. Dose response curve of coprisamides C and D against *Mycobacterium tuberculosis* mc² 6230. Moxifloxacin was used for positive control.

Publication List

Papers

1. **Shin, Y.-H.**; Kang, S.; Byung, W. S.; Jeon, C.-W.; Beom, J. Y.; Hong, S.; Lee, J.; Shin, J.; Kwak, Y.-S.; Lee, S. K.; Oh, K.-B.; Yoon, Y. J.; Oh, D.-C. Absolute configuration and antibiotic activity of piceamycin. *Journal of Natural Products*, **2020**, *83*, 277–285.
2. Byun, W. S.; Kim, S.; **Shin, Y.-H.**; Kim, W. K.; Oh, D.-C.; Lee, S. K. Antitumor activity of ohmyungsamycin A through the regulation of the Skp2-p27 axis and MCM4 in human colorectal cancer cells. *Journal of Natural Products*, **2020**, *83*, 118–126.
3. Kim, E.*; **Shin, Y.-H.***; Kim, T. H.; Byun, W. S.; Cui, J.; Du, Y. E.; Lim, H.-J.; Song, M. C.; Kwon, A. S.; Kang, S. H.; Shin, J.; Lee, S. K.; Jang, J.; Oh, D.-C.; Yoon, Y. J. Characterization of the ohmyungsamycin biosynthetic pathway and generation of derivatives with improved antituberculosis activity. *Biomolecules*, **2019**, *9*, 672–686. ***co-first author**
4. **Shin, Y.-H.**; Beom, J. Y.; Chung, B.; Shin, Y.; Byun, W. S.; Moon, K.; Bae, M.; Lee, S. K.; Oh, K.-B.; Shin, J.; Yoon, Y. J.; Oh, D.-C. Bombyxamycins A and B, cytotoxic macrocyclic lactams from an intestinal bacterium of the silkworm *Bombyx mori*. *Organic Letters* **2019**, *21*, 1804–1808.
5. Rischer, M.; Lee, S. R.; Eom, H. J.; Park, H. B.; Vollmers, J.; Kaster, A.-K.; **Shin, Y.-H.**; Oh, D.-C.; Kim, K. H.; Beemelmans, C. Spirocyclic cladosporicin A and cladosporiumins I and J from a Hydractinia-associated *Cladosporium sphaerospermum* SW67. *Organic Chemistry Frontiers* **2019**, *6*, 1084–1093.
6. Choi, B.-K.; Park, S.-Y.; Choi, D.-K.; Shin, B.; **Shin, Y.-H.**; Oh, D.-C.; Lee, H.-S.; Lee, H.-S.; Lee, Y.-J.; Lee, J. S.; Lee, J. H.; Shin, H. J. Streptoglycerides A–D with a rare 6/5/5 tricyclic ring skeleton from a marine actinomycete. *Streptomyces* species. *Organic Letters* **2018**, *20*, 6037–6040.
7. Kim, D.; Lee, E.; Lee, J.; Leutou, A.; **Shin, Y.-H.**; Choi, B.; Hwang, J.; Hahn, D.; Choi, H.; Chin, J.; Cho, S.; Hong, Y.; Ko, J.; Seong, C.; Maloney, K.; Oh, D.-C.; Yang, I.; Hwang,

- H.; Nam, S.-J. Antartin, a cytotoxic zizaane-type sesquiterpenoid from a *Streptomyces* sp. isolated from an antarctic marine sediment. *Marine Drugs* **2018**, *16*, 130.
8. Hur, J.; Jang, J.; Sim, J.; Son, W. S.; Ahn, H.-C.; Kim, T. S.; **Shin, Y.-H.**; Lim, C.; Lee, S.; An, H.; Kim, S.-H.; Oh, D.-C.; Jo, E.-K.; Jang, J.-C.; Lee, J.; Suh, Y.-G. Conformationally-enabled total syntheses of ohmyungsamycins A and B and structural revision of ohmyungsamycin B. *Angewandte Chemie International Edition* **2018**, *57*, 3069–3073.
9. **Shin, Y.-H.**; Bae, S.; Sim, J.; Hur, J.; Jo, S.-I.; Shin, J.; Suh, Y.-G.; Oh, K.-B.; Oh, D.-C. Nicrophorusamides A and B, antibacterial chlorinated cyclic peptides from a gut symbiont of the carrion beetle *Nicrophorus concolor*. *Journal of Natural Products* **2017**, *80*, 2962–2968.
10. Kim, T. S. *; **Shin, Y.-H.** *; Lee, H.-M. *; Kim, J. K.; Choe, J. H.; Jang, J.-C.; Um, S.; Jin, H. S.; Komatsu, M.; Chan, G.-H.; Chae, H.-J.; Oh, D.-C.; Jo, E.-K. Ohmyungsamycins promote antimicrobial responses through autophagy activation via AMP-activated protein kinase pathway activation. *Scientific Reports* **2017**, *7*, 3431. ***co-first author**

Patents

1. Oh, D.-C.; Shin, J.; Oh, K.-B.; **Shin, Y.-H.**

Macrocyclic lactam-based derivative compound, production method therefor, and use thereof.

PCT International Application WO2018/110799 A1, July 21, 2018.

2. Oh, D.-C.; **Shin, Y.-H.**; Jo, E.-K.; Lee, H.-M.; Kim, T.-S.; Kim, W.

Pharmaceutical composition for preventing or treating mycobacterium species infection and method using the same.

United States Patent Application Publication US2018/0221437 A1, August 9, 2018.

3. Oh, D.-C.; Shin, J.; Oh, K.-B.; **Shin, Y.-H.**

Macrocyclic lactam-based derivative compound, production method therefor, and use thereof.

Korean Patent Application Publication KR10-1911892 B1, October 19, 2018.

4. Oh, D.-C.; **Shin, Y.-H.**; Jo, E.-K.; Lee, H.-M.; Kim, T.-S.; Kim, W.

Pharmaceutical composition for preventing or treating mycobacterium species infection and method using the same.

Korean Patent Application KR10-2019-0007083 A, January 14, 2019.



5. Oh, D.-C.; Du, Y. E.; **Shin, Y.-H.**; Shin, J.; Yoon, Y. J.; Kim, E.


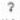



Method of the selective and high yield production of ohmyungsamycin A.


Korean Patent Application KR10-2019-0055745, May 13, 2019.

**Permissions for Republication of the
Published Paper in Thesis**

*Reproduced from [Shin, Y.-H.; Beom, J. Y.; Chung, B.; Shin, Y.; Byun, W. S.; Moon, K.; Bae, M.; Lee, S. K.; Oh, K.-B.; Shin, J.; Yoon, Y. J.; Oh, D.-C. Bombyxamycins A and B, cytotoxic macrocyclic lactams from an intestinal bacterium of the silkworm *Bombyx mori*. *Organic Letters* **2019**, *21*, 1804–1808.]

 Home
  Help
  Email Support
  Sign in
  Create Account



Bombyxamycins A and B, Cytotoxic Macrocyclic Lactams from an Intestinal Bacterium of the Silkworm *Bombyx mori*
 Author: Yarn-Hyerk Shin, Ji Yoon Beom, Beomkoo Chung, et al
 Publication: *Organic Letters*
 Publisher: American Chemical Society
 Date: Mar 1, 2019
 Copyright © 2018, American Chemical Society

PERMISSION/LICENSE IS GRANTED FOR YOUR ORDER AT NO CHARGE



This type of permission/license, instead of the standard Terms & Conditions, is sent to you because no fee is being charged for your order. Please note the following:

- Permission is granted for your request in both print and electronic formats, and translations.
- If figures and/or tables were requested, they may be adapted or used in part.
- Please print this page for your records and send a copy of it to your publisher/graduate school.
- Appropriate credit for the requested material should be given as follows: "Reprinted (adapted) with permission from (COMPLETE REFERENCE CITATION). Copyright (YEAR) American Chemical Society." Insert appropriate information in place of the capitalized words.
- One-time permission is granted only for the use specified in your request. No additional uses are granted (such as derivative works or other editions). For any other uses, please submit a new request.


[BACK](#)
[CLOSE WINDOW](#)

© 2018 Copyright - All Rights Reserved | Copyright Clearance Center, Inc. | Privacy statement | Terms and Conditions
 Comments? We would like to hear from you. E-mail us at customerscare@copyright.com

*Reproduced from [Shin, Y.-H.; Kang, S.; Byung, W. S.; Jeon, C.-W.; Beom, J. Y.; Hong, S.; Lee, J.; Shin, J.; Kwak, Y.-S.; Lee, S. K.; Oh, K.-B.; Yoon, Y. J.; Oh, D.-C. Absolute configuration and antibiotic activity of piceamycin. *Journal of Natural Products*, **2020**, 83, 277–285.]

[Home](#)
[Help](#)
[Email Support](#)
[Sign in](#)
[Create Account](#)



Absolute Configuration and Antibiotic Activity of Piceamycin
 Author: Yern-Hyerk Shin, Saeyoon Kang, Wroong Sub Byun, et al
 Publication: *Journal of Natural Products*
 Publisher: American Chemical Society
 Date: Feb 1, 2020
 Copyright © 2020, American Chemical Society

PERMISSION/LICENSE IS GRANTED FOR YOUR ORDER AT NO CHARGE



This type of permission/license, instead of the standard Terms & Conditions, is sent to you because no fee is being charged for your order. Please note the following:






- Permission is granted for your request in both print and electronic formats, and translations.
- If figures and/or tables were requested, they may be adapted or used in part.
- Please print this page for your records and send a copy of it to your publisher/graduate school.
- Appropriate credit for the requested material should be given as follows: "Reprinted (adapted) with permission from (COMPLETE REFERENCE CITATION). Copyright (YEAR) American Chemical Society." Insert appropriate information in place of the capitalized words.
- One-time permission is granted only for the use specified in your request. No additional uses are granted (such as derivative works or other editions). For any other uses, please submit a new request.


[BACK](#)
[CLOSE WINDOW](#)

© 2020 Copyright - All Rights Reserved | Copyright Clearance Center, Inc. | Privacy statement | Terms and Conditions
 Comments? We would like to hear from you. E-mail us at customerservice@copyright.com

*Reproduced from [Shin, Y.-H.; Bae, S.; Sim, J.; Hur, J.; Jo, S.-I.; Shin, J.; Suh, Y.-G.; Oh, K.-B.; Oh, D.-C. Nicrophorusamides A and B, antibacterial chlorinated cyclic peptides from a gut symbiont of the carrion beetle *Nicrophorus concolor*. *Journal of Natural Products* **2017**, *80*, 2962–2968.]

 Home
  Help
  Email Support
  Sign In
  Create Account



Nicrophorusamides A and B, Antibacterial Chlorinated Cyclic Peptides from a Gut Bacterium of the Carrion Beetle *Nicrophorus concolor*
 Author: Yern-Hyerk Shin, Suhyun Bae, Jaehoon Sim, et al
 Publication: *Journal of Natural Products*
 Publisher: American Chemical Society
 Date: Nov 1, 2017
 Copyright © 2017, American Chemical Society

PERMISSION/LICENSE IS GRANTED FOR YOUR ORDER AT NO CHARGE

This type of permission/license, instead of the standard Terms & Conditions, is sent to you because no fee is being charged for your order. Please note the following:

- Permission is granted for your request in both print and electronic formats, and translations.
- If figures and/or tables were requested, they may be adapted or used in part.
- Please print this page for your records and send a copy of it to your publisher/graduate school.
- Appropriate credit for the requested material should be given as follows: "Reprinted (adapted) with permission from [COMPLETE REFERENCE CITATION]. Copyright (YEAR) American Chemical Society." Insert appropriate information in place of the capitalized words.
- One-time permission is granted only for the use specified in your request. No additional uses are granted (such as derivative works or other editions). For any other uses, please submit a new request.

[BACK](#)
[CLOSE WINDOW](#)

© 2020 Copyright - All Rights Reserved | Copyright Clearance Center, Inc. | [Privacy statement](#) | [Terms and Conditions](#)
 Comments? We would like to hear from you. E-mail us at customerscare@copyright.com

Acknowledgements

감사의 글

2020 년 8 월이 되면 저는 서울대학교를 졸업을 합니다. 대학생으로 이 학교에 입학하여 인생의 3 할을, 10 년이 넘는 기간을 이곳에서 보냈습니다. 짧다고 할 수는 없는 시간이지요. 그동안 덕분에 소중한 인연들을 만날 수 있었고, 많은 것을 보고 배웠습니다. 그래도 아직도 철부지 대학생인 것 같은 제가, 이제 곧 박사학위를 받고 대학원 졸업을 코앞에 두고 있다는 것을 생각하니 스스로도 많이 어색합니다. 또 정든 이 학교를 이제는 떠나야 한다는 사실에 아쉬운 마음이 큼니다.

실험실 생활이 마냥 행복했다고 하면 거짓말이겠지요. 돌이켜 생각해보면 힘들었던 순간들이 많았습니다. 포기하고 싶었던 순간들도 있었고, 더이상 버티지 못할 것 같은 순간들도 있었습니다. 하지만 그만큼 행복했던 추억들이 있어서 이겨낼 수 있었습니다. 처음으로 균주 분리에 성공하였을 때, 첫 물질을 분리하여 구조를 풀었을 때, 첫 논문이 나왔을 때, 대학원 생활에서 얻을 수 있는 보람이라는 것을 느낄 수 있었습니다. 돌이켜 생각해보면 이러한 추억과 보람들이 저를 박사졸업까지 이끌어 준 것 같습니다. 먼저 졸업하신 선배님들도 저와 비슷하셨을 것이라 생각합니다.

제가 이렇게 무사히 박사학위를 받을 수 있었던 것은, 부족한 저에게 하나부터 열까지 가르쳐 주신 오동찬 교수님 덕분입니다. 교수님께서는 학문적인 것뿐만 아니라 인격적인 부분에서도 많은 배움을 얻을 수 있었습니다. 연구에 있어서 부족한 부분이 많았던 저에게 항상 격려의 말씀을 해 주셨고, 졸업

이후에도 세계적으로 인정받는 실험실의 박사후연구원 지원을 도와 주셨습니다. 교수님 밑에서 박사학위를 밟을 수 있었던 것이 제 인생에 있어 가장 큰 행운이었던 것 같습니다. 감정표현에 서툴러 한번도 제대로 말씀드린 적은 없지만, 교수님 감사합니다. 교수님이 없으셨다면 지금의 저도 없었겠지요. 앞으로 교수님의 명성에 해가 가지 않도록 훌륭한 연구자로 성장하도록 하겠습니다.

저는 화학과 그리 친한 사람은 아니었습니다. 때문에 대학원을 시작할 때에만 하더라도 화학과 관련된 지식이 많이 부족하였고, 흥미도 없었습니다. 하지만 신종헌 교수님의 수업을 듣고 화학에 흥미가 생길 수 있었습니다. 교수님께서 훌륭하게 설명해주신 영향도 있지만, 학문을 대하는 교수님의 자세에서 많은 것을 배울 수 있었습니다. 1, 2 학년때 들었던 신종헌 교수님의 수업으로 저의 6 년간 연구를 무사히 진행할 수 있었습니다. 앞으로의 연구 생활에서도 저에게 큰 힘이 될 것 같습니다. 교수님께서 가르쳐 주신 지식과 학문을 향한 열정을, 저도 다음 세대에 전달할 수 있도록 최선을 다하겠습니다.

박사학위 심사 발표는 제 인생에서 가장 긴장되고 떨렸던 발표였습니다. 저보다 훨씬 더 먼저 학위를 받으시고, 지금은 교수라는 자리에 계신 분들께 제 능력을 평가를 받는 자리임에 매우 긴장되었습니다. 발표가 끝나고 마무리되었을 때, 인준서에 도장을 받았을 때, 교수님들께서 해 주신 축하한다는 말씀에 저도 모르게 울컥하였습니다. 바쁘신 와중에도 시간을 내어 박사학위 심사에 참석해주신 이상국 교수님, 이지연 교수님, 그리고 심상희 교수님께 감사드립니다. 뿐만 아니라 생합성 관련 연구에서 항상 많은 도움과 조언을 주신 윤여준 교수님과, 생리활성 탐색 과정에서 많은 도움을 주신 오기봉 교수님께도 감사드립니다.

학위 과정을 밟는 6 년이라는 시간 동안 가장 많은 시간을 보낸 사람들은 바로 실험실 식구들이었습니다. 제가 긴 실험실 생활을 버틸 수 있었던 것은 선후배님들 덕분입니다. 본래 성격이 예민하고 날카로워 같이 지내기 어려웠음에도 불구하고 항상 다정하게 대해줘서 고맙습니다. 또한 기쁘고 즐거운 일이 있을 때도, 슬프고 힘든 일이 있을 때에도 같이 있어준 실험실 가족들 덕분에 큰 힘을 얻을 수 있었습니다. 모두들 하고 있는 일들과 하고자 하는 일들이 잘 마무리될 수 있기를 바라고, 이후에 각자의 자리에서 다시 만날 수 있으면 좋겠습니다.

제가 학업에만 정진할 수 있었던 것은 저를 믿고 지지해준 가족들이 있었기 때문입니다. 가족들이 없었다면 저는 이 학위를 절대 받지 못하였을 것입니다. 10 년이 넘는 기간 동안 학생으로 남아있는 저를 끝까지 지원해주신 부모님께 감사드립니다. 이제까지는 걱정만 끼쳐드리는 철부지 아들이었지만, 앞으로는 어엿한 아들로 성장하겠습니다.

끝으로, 학위 과정 동안 연구에 도움을 주셨던 교수님들과 선후배님들, 저의 마음의 짐을 나누어 준 친구들, 많은 분들께 이 자리를 빌려 감사말씀드립니다. 앞으로는 독립적인 과학자로서, 자랑스러운 선후배로서, 어엿한 아들로써 발전하도록 하겠습니다. 감사합니다.

신연혁 올림.